FLUID FLOW DIVERSION

BY GUIDE VANES IN MITER BENDS

by
St. Anthony Falls Hydraulic Laboratory
University of Minnesota

Project Report No. 8

Submitted by
Lorenz G. Straub
Director

Prepared by
Edward Silberman

April 1949

Prepared for the
David Taylor Model Basin
Department of the Navy
Washington, D. C.

Bureau of Ships Contract NObs-34208
Task Order 3

COPY NO.20

P R E F A C E

Under Contract NObs-34208 between the University of Minnesota and the Bureau of Ships, Department of the Navy, the St. Anthony Falls Hydraulic Laboratory has conducted a research program on flow diversion for the David Taylor Model Basin. The work was performed under Task Orders 1 and 3 of the above contract. The program has included a review of the literature on flow diversion [1]*, a study of flow diversion by radius elbows [2] , a model study of a guide vane cascade for a proposed water tunnel [17] , and, finally, a more general study of flow diversion by guide vanes in miter bends which is the subject of the present report. The research undertaken by the above contract has now been completed.

The present work was supervised and the report written by Edward Silberman. Feng Hsiao, assisted principally by T. D. Chen and Alexander P. Rodionov, was responsible for obtaining and plotting the experimental data. Polly Canfield assisted in preparation of the manuscript. Alvin G. Anderson and Mr. Hsiao have reviewed the manuscript. Many other members of the Laboratory Staff assisted in such details as photography, drafting, and assembling the experimental apparatus.

The program was under the general direction of Dr. Lorenz G. Straub, Director of the St. Anthony Falls Hydraulic Laboratory.

---

* Numbers in brackets refer to corresponding numbers in the Bibliography, pp. 178-179

S Y N O P S I S

A search of existing literature revealed several papers dealing with experimental investigations of specific vaned turns and others which approached the problem analytically. None of these, however, outlined general criteria for design and performance of guide vane cascades in miter bends which would be applicable to new installations. Such criteria have been established in this paper.

It has been found that for any given deflection angle of the flow and shape of vane, there exists a critical ratio of vane spacing to chord length. Below the critical ratio the flow from the trailing edges of the vanes is sensibly parallel to the trailing edge tangents and no change in inclination of the vanes is required with changes in spacing-chord ratio. Above the critical ratio, the inclination of the vanes (measured by the stagger angle) must be increased for each increase in spacing-chord ratio until stalling occurs. If the stagger angle is too small for a given spacing-chord ratio, the flow is underturned and if it is too large, the flow is overturned. The critical spacing-chord ratio is dependent on the maximum camber, thickness, and location of maximum camber of the vane shape. Numerical values are given in the body of the report. Optimum spacing-chord ratio and stagger angle for a given cascade occur when minimum resistance is obtained. The optimum spacing-chord ratio is at or slightly above the critical value. Optimum values for several cascades are given in Table VIII of the report.

When a guide vane cascade with a limited number of vanes is installed in a miter bend a turn is produced which may be a product of the cascade and bend walls acting together. Such a combination is generally undesirable because it results in a disturbed velocity and pressure distribution behind the cascade. Criteria are given in the report for controlling the design of the bend walls and for determining whether the cascade alone is producing the turn.

This research has not answered all the questions regarding design of guide vane cascades for miter bends, but it has established a framework into which the answers may be fitted. Fields for further worthwhile research are outlined in this paper.

C O N T E N T S

FLUID FLOW DIVERSION BY GUIDE VANES IN MITER BENDS

I. INTRODUCTION

A. General

Bends that do not distort the velocity profile are required for water and wind tunnel design and frequently for other purposes. An ordinary elbow causes a maldistribution of both pressure and velocity downstream from the elbow, and usually results in excessive head loss [1,2] *. The use of guide vanes will improve the pressure and velocity distribution downstream from a bend, and the resulting head loss may be of the same order of magnitude as the optimum loss for an ordinary bend. A search of existing literature, however, shows that there is a lack of reliable information on the design criteria for guide vane bends. It is the purpose of this paper to make a thorough study of the application of guide vanes to flow diversion.

A number of works on this subject and the closely related subjects of pump and compressor blade design have already been published. Considerable success has attended the theoretical pump and compressor blade studies. Recent articles by Spannhake [3] and Marcinowski [4] review these fields and include numerous references. Abstracts of some of the papers referred to by Spannhake and Marcinowski appear in a separate bibliographical report [1] . In general, the final results of the pump and compressor work are not directly applicable to the guide vane problem for the following reasons:

1. Many of the analyses are limited by approximations to small deflection angles associated with pump and compressor blades.

2. Usually thin profiles are investigated and even when thick profiles are considered, the growth of the boundary layer and separation are neglected.

3. Results that have been obtained lack experimental verification.

The methods used in the pump and compressor work are useful, however, in their application to guide vanes.

Other work has dealt with the guide vane problem directly. Most of this has been primarily experimental in nature and will be reviewed critically

* Numbers in brackets refer to corresponding numbers in the Bibliography.

in Part III of this paper. Abstracts of some guide vane papers may also be found in the Bibliography [1] .

Several satisfactory guide vane applications have been made as a result of the previous work. Some questions still unanswered or only partially answered are:

1. What is the general relation between guide vane shape, size, spacing, and angular setting to produce a given flow diversion?

2. What combination of the above features will produce a given flow diversion with small loss of head?

3. How can vibration or cavitation be avoided?

4. What is the influence of such factors as Reynolds number and turbulence on the performance of guide vanes?

5. What is the effect on the vane performance of structural supports between vanes, or of inserts such as shafts through the vanes?

6. How do confining walls influence the vanes?

7. Is there a difference in performance between guide vanes in a uniform stream and those in a nonuniform stream?

8. What are the similarity criteria for vane installations?

It is proposed to consider these questions and others relating to guide vanes, first by logical reasoning, then by reference to existing data, and finally by obtaining necessary new experimental data.

B. Definition of Terms

The principal terms used in this paper are defined in Table I and some of these terms are indicated in Fig. 1. Several terms of local importance are not given in Table I, but these as well as all others are defined where they first occur. The guide vanes taken together are termed a "cascade of vanes."

TABLE I

Definitions

Cascade axis	Straight line drawn through the centers of pressure of all vane profiles in the cascade

Center of pressure	Assumed point of application of the resultant pressure on a vane profile, determined by the intersection of the resultant of the external pressures with the mean line. (The mean line in the practical case may be taken as the line lying halfway between the pressure and suction surfaces of the profile.)
b	Width of duct
c	Vane chord; the chord line is tangent to the leading and trailing edges of the profile of the vane
C_L	Coefficient of lift of a single airfoil at infinite aspect ratio
C_R	Dimensionless reaction coefficient for a vane profile corresponding to the coefficient of lift of an airfoil $C_R = \frac{R}{c \frac{\rho W^2}{2}}$
d	Depth of duct
D	Distance along centerline of duct
g	Acceleration of gravity
H	Total head
H_s	Static head
k	C_R/C_L
ℓ	Span of a guide vane
ℓ/s	Aspect ratio of the space between vanes
n	Number of guide vanes in a cascade
P	Resultant pressure on a vane per unit span
R	Reaction on a vane per unit span
Re	Reynolds number, $\frac{W_1 c}{\nu}$. (Reynolds number based on duct depth, d, is also used locally in the text.)
s	Vane spacing measured along the cascade axis between centers of pressure
s/c	Spacing-chord ratio
t	Maximum thickness of a vane profile
u	Velocity component parallel to the duct walls
$\vec{U}$	Vectorial mean velocity through a cascade of vanes (magnitude U)
$\vec{W_1}$	Velocity of approaching flow (magnitude W_1)
$\vec{W_2}$	Velocity of departing flow (magnitude W_2)
$\vec{W}$	Velocity of equal approaching and departing flows (magnitude W)
y_m	Maximum camber of the mean line of a profile
α	Angle of attack measured between chord line and U, ($\alpha = \theta - \beta$)
α_1	Angle of attack measured between chord line and W_1 ($\alpha_1 = \theta - \beta_1$)

β, β_1, β_2	Angles measured counterclockwise between the cascade axis and the directions of U, W_1, and W_2, respectively
Γ	Circulation about a vane profile
Δ	Deflection angle through which the flow is to be turned $\Delta = \beta_2 - \beta_1$
ζ	Bend loss coefficient. Per cent of entrance velocity head which is lost in the bend
θ	Stagger angle measured counterclockwise from the cascade axis to the vane chord
ρ	Density of fluid
ν	Kinematic viscosity of fluid
ϕ	Flow-off angle measured between the tangent to the mean line at the trailing edge of a vane and the direction of W_2 shown positive in Fig. 1.

The subscript 1 refers to the space preceding a cascade and the subscript 2 to the space following it. A line over a quantity denotes the mean value of that quantity and an arrow over a symbol denotes a vector.

II. MECHANICS OF FLOW DIVERSION

A. General

At first flow diversion may be considered as a purely two-dimensional problem. The two-dimensional viewpoint will be maintained throughout the major portion of Part II of this paper. A stream-flow diversion may be caused by applying suitable forces to the stream. In a river bend or pipe elbow, the forces are applied at external fluid boundaries. In a flow diversion by guide vanes the forces are applied at a number of internal boundaries (and possibly at external boundaries also). If a diversion is made only by external boundaries, the forces must be applied over a considerable area of wall in order to reach all the fluid particles in the stream. Since force is applied to a stream as pressure, the pressure and the velocity distribution are altered both upstream and downstream from a bend. This is a common phenomenon. If sufficient internal boundaries are used in a bend, the total force is applied to the stream in small increments and each particle is quickly turned; the diversion is accomplished in a short space and no maldistribution of pressure results beyond this short distance either side of the diversion. If a diversion is produced by a combination of internal and external boundaries, some disturbance will occur both upstream and downstream, depending on the relative force exerted by each boundary. Frequently the loss resulting from

the generation of vortexes is reduced by the better velocity distribution from the use of guide vanes so that there is no resultant increase in resistance for the bend. In any event, additional resistance due to the internal boundaries may be kept at a minimum by proper design and placement of the vanes.

If a diversion is to be made with the least possible disturbance to the pressure and velocity distribution, it would appear that a large number of vanes with small spaces between vanes (infinitesimal s/c in Fig. 1) should be used so that the turning force may be applied most directly to each fluid particle. If the diversion is to be made with reasonably small resistance, however, a smaller number of vanes (larger s/c) would have to be used to prevent excessive skin friction. Furthermore, in the design of a miter bend, the smaller the number of vanes, the less is the initial cost. These factors make it desirable to use as large a spacing-chord ratio (s/c) as will effectively produce the desired results. Other factors affecting the maximum value of s/c are the maximum permissible load on each vane for structural reasons, and the minimum permissible aspect ratio (ℓ/s) of the space between vanes to avoid secondary currents.

With infinitesimal s/c, fluid particles can be expected to follow the guide vane surfaces exactly since there is no other possible course. In this case a cascade could be made to produce a desired flow diversion simply by orienting its vanes so that the tangents to their trailing edges would point in the downstream flow direction. The shape of the vanes would be immaterial. With finite s/c, however, when consideration is given to the behavior of the boundary layer, it is apparent that the bulk of the fluid particles cannot be expected to follow exactly the guide vane surfaces. (Unless some attention is given to vane design the fluid particles may not even follow the surfaces closely, and the equivalent of stalling in an airfoil will occur.) If the value of s/c is sufficiently large, the fluid particles may be seen to leave the trailing edge of a vane in cascade at some angle ϕ with the trailing edge tangent (Figs. 1 and 24). When this occurs, it is necessary to increase the stagger angle θ of the vanes in order to obtain the desired diversion. The required increase in θ is not necessarily equal to ϕ but depends on the changes in the boundary layer as θ is increased. If the increase in θ is insufficient, the flow will be underturned (Fig. 24c) but if θ is increased excessively, the flow will be overturned (Fig. 24g). The design of a guide vane cascade reduces to a selection of profile shape, s/c, and θ, which together

will produce the desired flow diversion with a small number of vanes and a reasonable resistance. The above factors, profile shape, s/c and θ, are known as the cascade characteristics.

B. Forces on a Guide Vane

The force required of guide vanes to divert a fluid stream through a given angle may be determined quite readily from momentum considerations. For example, consider a 90° miter bend in a duct of constant width b and great depth with fluid flow steady, uniform, and axial of velocity W, both before and after the bend. The flow of momentum at any cross section is then ρbW^2 per unit depth where ρ is the fluid density. This flow must be annihilated in the direction approaching the bend and re-created in the direction leaving the bend. Assuming that there is no pressure drop, the required force in each direction is equal to the change of momentum in that direction of ρbW^2. The resultant force acting along the miter line is $\sqrt{2}\ \rho bW^2$. Disregarding the walls and assuming this force is to be carried by n equally spaced guide vanes, the reaction per vane per unit depth must be $\frac{\sqrt{2}b}{n}\ \rho W^2$. Since $\frac{\sqrt{2}b}{n}$ is equivalent to the spacing s of the n vanes, the reaction per vane per unit depth is

$$R = 2s\ \left(\frac{\rho W^2}{2}\right) \tag{1}$$

This reaction is produced by pressure differences on the vane surfaces.

A coefficient of reaction (analogous to the coefficient of lift of an airfoil) may be defined from dimensional considerations as

$$C_R = \frac{R}{c\ \frac{\rho}{2} W^2}$$

where c is the chord length of a vane. It should be noted that the reaction acts along the miter line (disregarding drag) and not normally to W, the approaching velocity. Combining Eq. (1) with the definition for C_R,

$$C_R = 2\ s/c \tag{2a}$$

The value of C_R determined by Eq. (2a) will be termed the required C_R.

If a cascade of guide vanes is to produce a flow diversion without external assistance, each vane must develop the reaction given by Eq. (1) with a line of action along the miter line. If, because of their stagger angle or for some other reason, the vanes develop more or less reaction than that given by Eq. (1), the flow will be overturned or underturned. If the bend is confined by the walls of a miter elbow and the flow is underturned, the walls

must provide assistance to produce the total required turning force. If the flow is overturned by the vanes, the walls must resist the turn. In either event there will be some pressure and velocity maldistribution, and the properties of an ordinary radius elbow may be exhibited to some degree.

If the velocity across the duct width is not uniform and resistance is not considered, the width may be subdivided into a number of stream tubes, each containing one vane, in which the velocity may be considered uniform. Again the force per vane per unit depth is given by Eq. (1), but $\underline{W}$ is now the velocity of approach before each vane. For velocity nonuniform in depth, Eq. (1) may be applied to elementary lengths of vane span to determine the vane load; however, this may be done only if the velocity remains essentially axial and if the velocity gradient in depth is not excessive. In both cases the velocity distribution would be unchanged by the cascade. In either of the above cases Eq. (2a) yields a constant required C_R for constant s/c; theoretically, there is no need to change the cascade characteristics to accommodate a variable velocity profile.

It must be recognized that there is a pressure drop along the vanes resulting from a combination of skin drag and form drag. There is additional pressure drop in the vane wakes resulting from the viscous dissipation of the wake vortexes and there is also pressure drop from duct wall resistance. To introduce the pressure drop in the previous illustration, it is assumed that the approaching flow has a uniform pressure p_1 and the departing flow a uniform pressure p_2, so that $(p_1 - p_2) = \Delta p = \frac{\zeta}{100} \frac{\rho W^2}{2}$ where ζ is the per cent of entrance velocity head lost in the cascade. In the direction of approaching flow, the fluid force to be annihilated is $F_1 = \rho b W^2 + h_1 b \Delta p$ per unit depth where h_1 is a fraction less than unity, representing the portion of the pressure drop occurring in the F_1 direction. In the direction of the departing flow, $F_2 = \rho b W^2 - h_2 b \Delta p$ per unit depth must be created where h_2 is also a fraction less than unity, representing the portion of the pressure drop along the vane occurring in the F_2 direction. Furthermore, $h_1 + h_2 < 1$ since the total pressure drop includes some loss in the wakes. The resultant force for a 90° deflection may be written

$$F = \sqrt{2}\ b\ \rho W^2 \sqrt{1 + \zeta/2\ (h_1 - h_2) + \zeta^2/8\ (h_1^2 + h_2^2)}$$

Since $F_2 < F_1$, the resultant force acts not along the miter line, but along a line that makes an angle of less than 45° with the approaching flow. If the diversion is to be made by $\underline{n}$ equally spaced guide vanes, the required reaction

per vane per unit depth is given closely by Eq. (1), since $|h_1 - h_2| < 1$ and ζ is about 10 or 20 per cent for a normal cascade. Hence, except for line of action, the required guide vane reaction in an ideal and in a real fluid differ by less than 5 per cent if the cascade has reasonably small resistance.

In experimental work, measurements of the pressure distribution on a guide vane are frequently made in place of the actual reactions. It is useful to note that the component vane reaction which resists F_1 is produced by the sum of the integrated measured pressures and the skin drag on the vane in the direction of F_1. The component vane reaction which creates F_2 is produced by the difference of the integrated measured pressures and the skin drag on the vane in the direction of F_2. The form or pressure drag is already included in the measured pressures. Figure 2 indicates these relationships. The skin drag is small compared to the reactions and has probably been exaggerated in Fig. 2. The resultant of the measured pressures on the vane surfaces (indicated by $\underline{P}$ in Fig. 2) may, because of the resistance, act more nearly parallel to the miter line, and it may be slightly larger or smaller than the actual vane reaction. Equation (1) should give the required resultant pressure per vane in a practical case to the same approximation as it gives the required reaction.

The preceding reasoning may be extended readily to ducts other than those having 90° deflections. It may also be extended to ducts with contracting or diverging cross sections. These extensions will not be made by the momentum method in this paper.

C. The Flow Field of a Guide Vane Cascade

From another viewpoint, a flow diversion may be looked upon as a purely potential flow problem. The theoretical flow has been obtained by several different methods. Those holding the most promise for future applications to guide vanes are the methods of Garrick [5] and Mutterperl [6]. Both of these methods permit the eventual transformation of a cascade of arbitrary profiles and the space surrounding the profiles into a single circle and the space surrounding it. Garrick's method involves a preliminary transformation of the profile in cascade to a nearly circular profile. Mutterperl's method involves a preliminary transformation to an equivalent cascade of straight lines. The Mutterperl transformation is more readily handled and offers a better approach to the inverse problem of finding a cascade to fit

required conditions of deflection and spacing-chord ratio. A simpler process, applicable only to Joukowski-like profiles, has been developed by Merchant [7] in which the basic flow occurs about a row of ovals, and also by Weinig [8] in which the basic flow occurs about a single circle. Both the Garrick and Mutterperl methods depend on Weinig's development.

Another potential flow approach to the problem consists of replacing each vane profile with a single vortex or a row of vortexes, and in determining the streamline pattern due to a uniform flow superimposed on these vortexes. Thick profiles may be provided for in the system by a suitable distribution of sources and sinks as was done by Ackeret [9] . Thin profiles may be obtained by transforming profiles with known characteristics from a rectilinear streamline pattern to the curvilinear field of the vortexes and uniform flow as was done by Krober [10] . None of these potential flow methods has been applied to the guide vane problem in this paper because of the labor involved, the difficulty of allowing for boundary layer development, and the uncertainty of the end results. It is believed desirable, however, to consider the general characteristics of the flow field about a cascade, and to that end there follows an analysis of the flow field created by a line of rectilinear vortexes in a uniform stream. No attention is given to the details of flow about individual profiles.

In Fig. 3a an infinite row of rectilinear vortexes is shown, each of circulation Γ , spaced at equal distances s along the y-axis in a fluid otherwise at rest. The vortexes will produce a velocity $v = \pm \frac{\Gamma}{2s}$ parallel to the y-axis at a great distance each side of the axis [11] . If Γ and s are both reduced together toward zero so that the velocity v is maintained constant, the distance either side of the y-axis at which this velocity obtains becomes quite small in a real fluid, and when in the limit a vortex sheet on the y-axis exists, $v = \pm \frac{\Gamma}{2s}$ immediately adjacent to the axis.

If the row of vortexes is superimposed on a uniform flow of velocity U making an angle $\beta = 90^\circ$ with the row as in Fig. 3a, the two flows will be added. At some distance each side of the y-axis, the resulting velocities will be $\vec{W}_1 = \vec{U} + \frac{\Gamma}{2s}$ and $\vec{W}_2 = \vec{U} - \frac{\Gamma}{2s}$, added vectorially. As a result of the superposition, the new flow will be turned through an angle Δ where $\tan \frac{\Delta}{2} = \frac{\Gamma}{2sU}$ or $\sin \frac{\Delta}{2} = \frac{\Gamma}{2sW_1}$. $\vec{W}_1$ and $\vec{W}_2$ are equal in magnitude and differ in direction only. $\vec{U}$ is the vectorial mean of $\vec{W}_1$ and $\vec{W}_2$.

To produce a given deflection Δ in an originally uniform flow of velocity $\vec{U}$, it is necessary only to arrange for a series of rectilinear vortexes of proper strength and spacing along an axis normal to $\vec{U}$. The required strength of the vortexes is

$$\Gamma = 2sU \tan \frac{\Delta}{2} = 2sW_1 \sin \frac{\Delta}{2} \qquad (3)$$

W_1 is the magnitude of the resulting velocity of the fluid approaching the turn. By making s smaller, and thus reducing Γ, the given deflection Δ is accomplished in a smaller space. In order to confine the flow, two neutral streamlines, each crossing the y-axis midway between two vortexes, may be chosen as lateral boundaries (Fig. 3a). These would have to be frictionless, of course. On such boundaries the velocities (and, therefore, the pressures) will be equal at corresponding points and there will be no external reaction.

In a real fluid, the circulation required by Eq. (3) may be produced by using guide vanes. In accordance with the Kutta-Joukowski condition for finite velocity at the sharp trailing edge of a profile, a given circulation may be obtained by properly adjusting the angle of attack or stagger angle of the profile. Of course, the details of the flow, including the shape of the boundary streamlines near the cascade, are different for the guide vane profiles than for the rectilinear vortexes first considered, but the overall effect is the same. According to the Kutta-Joukowski theorem, on each profile which develops the circulation given by Eq. (3), the reaction is $R = \rho \Gamma U = 2s \sin\Delta \frac{\rho W_1^2}{2}$ per unit depth. Theoretically, R acts normally to the direction of $\vec{U}$. Basing C_R on the approach velocity W_1, as before, rather than on U,

$$C_R = 2\, s/c \sin\Delta \qquad (2b)$$

When $\Delta = 90^\circ$, Eq. (2b) reduces to Eq. (2a). It is apparent that a vane profile which produces the required circulation also develops the required C_R.

The circulation may be considered distributed along the vanes in proportion to the local reaction or pressure difference between the suction and pressure surfaces of the vanes. The center of circulation, which corresponds to the vortex center of Fig. (3a), is then located at the center of pressure and the vortex axis and cascade axis are identical. But the vortex axis in Fig. (3a) is the miter line of the bend and, therefore, the cascade axis of a guide vane cascade should be located along the miter line of the bend.

The angle of attack of a vane in cascade is the angle between the chord and the direction of $\vec{U}$, $\alpha = \theta - \beta$ in Fig. 1. If β is fixed, α varies

linearly with θ, and when s/c approaches infinity ($\Delta \to 0$) α is seen to be the angle of attack as defined for an ordinary airfoil. Using the approach velocity $\vec{W}_1$ as the reference velocity, the angle of attack becomes $\alpha_1 = \theta - \beta_1$. This angle is also sometimes used as the definition of angle of attack for vanes in cascade because it is more readily measured than α. If β_1 is fixed, α_1 varies linearly with θ, and also becomes equal to the angle of attack for ordinary airfoils when s/c approaches infinity.

Krober [10] made use of the rectilinear vortex pattern of Fig. (3a) to develop guide vane profiles semiempirically following a method evolved by Betz. One vortex was removed and the potential flow net in the vicinity of the absent vortex was developed. A single thin airfoil of known properties was then transformed by plotting from its normal rectilinear flow net to the curvilinear flow net to obtain a thin guide vane. It was assumed that the guide vane profiles would produce approximately the same flow net as occurs in the vicinity of the missing vortex. The transformation was also based on the assumption that the circulation (or reaction) distribution would be the same on the thin vane as on the thin airfoil and that the total circulation must be that given by Eq. (3). Experimentally, after some manipulation of the original transformation, Krober found an adjustment in stagger angle of $2\frac{1}{2}^\circ$ was necessary in his transformed guide vane to produce the design deflection of 90°. Krober's experiments are discussed in Part III.

For reference, in Appendix I the previous analysis has been extended to the situation where the vortex axis and direction of uniform flow are not mutually perpendicular ($\beta \neq 90^\circ$). This situation is represented in Fig. 3b and corresponds to a flow diversion in a miter elbow with an expansion ($\beta < 90^\circ$) or with a contraction ($\beta > 90^\circ$).

D. Critical Values of s/c

For a thin, slightly cambered profile used in a cascade in an ideal fluid, it can be shown [3] that the developed C_R is a function of the angle of attack, the stagger angle, and the spacing-chord ratio, or $C_R = f_1(\alpha, \theta, s/c)$. For the same profile used single ($s/c \to \infty$) at infinite aspect ratio, the coefficient of lift is a function of the angle of attack only, or $C_L = f_2(\alpha)$. Frequently C_R is written as kC_L where k is a dimensionless factor and C_L may be the actual or theoretical value of the lift coefficient of a single airfoil or other shape. It is seen that $k = f_3(\theta, s/c)$. Theoretical values

of $\underline{k}$ for flat plates have been worked out by Weinig [8] as well as others, and are reproduced in Fig. 4. (The curves applying to specific values of θ in Fig. 4 apply also to the supplementary angles.) These results are generally assumed to hold for thin vanes and small deflection angles. Partial verification has been obtained by Shimoyama [12] . Of course, $\underline{k}$ approaches unity when s/c approaches infinity regardless of θ or the vane shape, and remains closely equal to unity down to approximately s/c = 2 or 3. For smaller values of s/c, $\underline{k}$ is generally less than unity because, as s/c is reduced, the zero lift direction of the profile is changed, requiring less circulation to satisfy the Kutta-Joukowski condition at the trailing edge and producing less reaction. Finally, when $s/c \to 0$, both the circulation and reaction per vane of finite chord approach 0 and $k \to 0$. It may be seen from Fig. 4 that $\underline{k}$ becomes directly proportional to s/c for flat plates at values of s/c less than approximately 0.5. From $s/c \approx 2.0$ to $s/c \approx 0.5$, $\underline{k}$ decreases less rapidly than s/c. (It may also be noted from Fig. 4 that for $\theta = 90^\circ$, $\frac{dk}{d\theta}$ is very small. This would indicate that there is some latitude in stagger angle to obtain the correct turn if θ is near 90°). It must be remembered that the theoretical curves of Fig. 4 give no consideration to boundary layer development, cavitation, or stalling.

For thick, cambered profiles the expression for C_R should be written: $C_R = f_4 (\alpha, \theta, s/c, t/c, \frac{y_m}{c})$ where $\underline{t}$ is the maximum thickness of the profile, and y_m is the maximum camber of its mean line. For profiles of not too large camber, Leiblein [13] has shown: $C_R = kC_1 + k_1 \frac{y_m}{c} + k_2\, t/c + k_3 \delta$ where δ is the included angle between the tangents to the upper and lower surfaces at the trailing edge of the profile and k_1, k_2 and k_3 are constants for given values of s/c and θ. Leiblein gives values which may be used to determine k_1, k_2, and k_3 for certain theoretical profiles. The constants are all positive except for k_1 when θ is less than 15° to 40°, depending on s/c. Hence the tendencies of increasing camber, increasing thickness, and increasing trailing edge angle are to increase the developed C_R at normal stagger angles. It is interesting to observe from Leiblein's data that with $\theta = 90^\circ$, k_2 and k_3 are both zero, but $k_1 \frac{y_m}{c}$ must be of the same order of magnitude as kC_L. Between $\theta = 70^\circ$ and $\theta = 110^\circ$, k_1 changes little, k_2 obtains some importance, but is small, while k_3 is still negligible. It should be possible to extend these results qualitatively to profiles of large camber like those normally encountered in guide vanes. (It may be noted that boundary layer growth should have a similar effect on the developed C_R as an increase in thickness.)

In a flow through a cascade of thin vanes of any shape at infinitesimal s/c in an ideal fluid, β_2 will be determined by the direction of the trailing edges of the vanes. Thus it is possible to adjust θ so that with a fixed inflow a certain value of Δ will be obtained. As s/c is increased by increasing $\underline{s}$, $\underline{k}$ (Fig. 4) will increase in almost direct proportion to s/c at first, and the developed C_R of the vane ($C_R = kC_L$) will increase in almost direct proportion to s/c. Also, by Eq. (2b), the required C_R to maintain the above value of Δ increases in proportion to s/c. Therefore, as s/c is increased, there will be little or no change in the value of Δ or of β_2 at first. The angle ϕ (Fig. 1) will remain zero. (From the viewpoint of boundary layer theory, this can be true only if there is no separation with increasing s/c. Actually, there will be some differences in velocity immediately behind the vanes as a result of boundary layer growth and wake development, but at small s/c these differences will be ironed out in the flow and their average effect will be sensibly zero.)

As s/c is increased to the point where $\underline{k}$ is no longer nearly proportional to s/c, the developed C_R becomes smaller than the required C_R for the required value of Δ and it is no longer possible to make this turn without increasing the developed C_R. For this value of s/c, the developed C_R may be increased in one or more of the following ways: C_L may be increased by increasing α_1 (or increasing θ since $\alpha_1 = \theta - \beta_1$ and β_1 is fixed); $\underline{k}$ may be increased by increasing or decreasing θ depending on whether θ is greater than or less than 90°; and finally the profile may be changed by increasing $\frac{y_m}{c}$ or t/c or the trailing edge angle. If $\theta \geq 90^\circ$ the required value of Δ may be maintained by increasing θ ; but then ϕ becomes larger than zero since the trailing edge pointed originally in the β_2 direction. If, on the other hand, Δ is maintained by increasing the camber or thickness while maintaining the tangent at the trailing edge in the β_2 direction, ϕ will remain equal to zero until s/c is still further increased. (In a real fluid, the velocity profiles immediately behind the vanes probably become quite distorted as s/c is increased, but as long as no separation occurs the average value of ϕ at some distance downstream should remain sensibly zero.)

The preceding argument leads to the conclusion that in an ideal fluid a cascade of vanes whose trailing edge tangents point in the downstream direction, will give a desired turn for a certain critical value of s/c and for all smaller values. The critical value of s/c at which the cascade ceases

to produce the required turn increases principally with increasing camber and also increases with thickness when $\theta > 90^{\circ}$. These critical values of s/c must be determined by experiment with typical cascades. Of course, in a real fluid neither the camber nor thickness may be made excessively large. If either becomes too large, a value of s/c will be reached at which separation or even stalling occurs, and the vanes will fail to develop the required C_R before the critical value of s/c is reached. The critical value of s/c is not necessarily the best design value, as will become apparent later. It may still be useful to use a slight positive value of ϕ, permitting some separation, and thus reduce the number of vanes per cascade by using an s/c larger than critical.

E. Resistance

Head loss caused by a bend containing a guide vane cascade is defined in the usual manner as the loss in a given length of duct containing the bend less the loss in the same length of straight duct, when both lengths are measured along the centerline of the duct. The length chosen must extend for a sufficient distance each side of the bend to include all disturbances to the flow. In a properly designed guide vane bend, the additional head loss is confined almost entirely to the region of the guide vanes and the wakes since the flow is otherwise undisturbed both before and after the vanes. In a guide vane cascade which does not make the proper turn without assistance from the walls, the additional loss may occur not only in the region of the guide vanes, but also downstream where the flow pattern has been changed. In the following discussion it will be assumed that the entire additional head loss takes place in the region of the cascade. The head loss in a cascade may be looked upon as the sum of the losses of the individual vanes including their wakes, plus a possible additional loss near the confining walls where the flow must be disturbed; the loss near the walls will be disregarded at present.

Individual vane resistance is determined by the growth of the boundary layer along the vane and its dissipation in the wake. Weske [14] has studied vane drag analytically and experimentally for cascades of symmetrical profiles at $\theta = 0^{\circ}$ and $C_R = 0$ (no deflection). He concludes that the drag under the above conditions at moderate values of s/c can be computed with sufficient approximation from the momentum equation of the turbulent boundary layer, assuming a constant skin friction. He also points out that the drag from

momentum transfer in the wake is likely to be quite large for very small s/c where the wake is relatively thick. Weske's experimental work was conducted with cascades of NACA 0012 profiles of 15-in. chord in a wind tunnel at high, but unspecified, Reynolds number. His plotted curves of profile drag against s/c show a nearly constant value of drag from $s/c = \infty$ (the value for a single profile) to $s/c \approx 0.7$. The drag then increases slowly to $s/c \approx 0.5$ and more rapidly to $s/c \approx 0.3$. Above the latter value the drag increases abruptly. An experimental investigation by Kirschmer [15] using nonstreamlined, rectangular grating bars in water showed that the head loss in the bars increased logarithmically with the ratio of thickness to spacing, t/s. Whether the decrease in spacing-chord ratio, s/c, or the decrease in cross section of the flow passage as measured by the increase in t/s is the more important factor is difficult to say. Weske's data when plotted against t/s also give a nearly logarithmic curve.

These data for undeflected flow are not directly applicable to highly cambered guide vanes. Generally, a single guide vane profile tested in a wind tunnel would show a very large resistance caused by large-scale separation. In a cascade at finite s/c where the constraint of the adjacent vanes would prevent separation, the resistance for the same profile should be materially less. Qualitatively, the resistance of a guide vane profile might be expected to follow a course such as this: At small s/c the resistance would be large because of the relative space occupied by the boundary layer and wake. As the s/c is increased the resistance would drop progressively (but at a decreasing rate because of the thickening of the boundary layer) until the critical value of s/c is reached, or until large-scale separation occurs. After the critical s/c is passed, increasing separation would increase the profile resistance until finally large-scale separation would involve a large increase in resistance.

Parallel reasoning shows that for a cascade in a fixed bend the overall head loss should decrease at first with increasing s/c, both because individual vane resistance decreases and because the number of vanes decreases. If large-scale separation occurs before the critical value of s/c is reached, then the head loss will abruptly increase at this point and the cascade will fail to make the required turn. If large-scale separation does not occur, the head loss should continue to fall to the critical value of s/c. Beyond this point it may either increase or decrease (depending upon the relative effects

of increasing profile resistance and decreasing number of vanes) until large-scale separation does occur and the head loss begins to climb rapidly. For greatest overall efficiency it would appear that a guide vane cascade should be designed to operate at that value of s/c which occurs near the end of the region of small resistance. This may occur above the critical value of s/c for well-designed vanes. It would not be advisable to operate too close to the region of large-scale separation because, as noted later, changes in Reynolds number or stream turbulence could cause a marked change in both deflection and resistance.

Other factors influencing boundary layer growth and separation in addition to those already discussed are: the stagger angle θ, which partially determines the restraint on the streamlines at the trailing edges of the vanes; the relative retardation of the flow for nonuniform cross sections $\frac{W_2}{W_1}$, which influences the pressure gradient in the boundary layer; the shape of the passage between the vanes which also influences the pressure gradient; the shape of the vane profile; the smoothness of entry at the leading edge of the profile; and, of course, Reynolds number, stream turbulence, and surface roughness. The separate influence of these other factors will not be considered in detail at this time except to note that as $\frac{W_2}{W_1}$ becomes smaller, it becomes increasingly difficult to avoid large-scale separation at moderate values of s/c. This does not mean that a miter bend in combination with a diffusing flow is impossible, but such a combination may be expected to involve large energy losses. It may also be noted that after the bend is fixed and the vane profile selected, leaving only the values of s/c and θ to be determined, these additional factors will have very little importance. In making an initial selection of a vane profile for a given bend, some idea of the effect of profile shape and θ ($\theta = \beta_1 + \alpha_1$) may be obtained from the work on single airfoils [16]. However, excessive refinements in such factors as profile shape are not warranted until such time as the influence of the main factors in deflection and resistance are better understood.

F. Reynolds Numbers and Other Factors

It is to be expected that Reynolds number, turbulence, and surface roughness may have an effect on resistance and deflection of a guide vane

cascade since each has an effect on the boundary layer. For instance, a cascade operating below the critical s/c ($\phi = 0$) at a high Reynolds number may operate with $\phi \neq 0$ at a lower Reynolds number as a result of boundary layer separation at the trailing edge. Large-scale turbulence and rough surface, of course, may have the same effect as high Reynolds number. Since most cascades must operate over a range of Reynolds numbers, it becomes desirable to select cascade characteristics which show a minimum change with Reynolds number, or else to use such a large chord that the Reynolds number will always be above a certain minimum. Characteristics which will perform the first mission are not known without additional experimentation. In any event, the selected characteristics should produce a minimum positive pressure gradient on the convex surface of the vanes which are selected. Some data regarding the minimum Reynolds number are given in Part III and other data have been obtained in the present experiments. No measurements of the effect of turbulence or roughness on guide vanes have been recorded and none were contemplated in the present investigation.

It was previously shown that for an ideal fluid a variable velocity in the plane of the bend would have no effect on deflection angle. If the effect of Reynolds number is considered, however, then this statement may no longer be true. If a cascade is installed in the pointed velocity distribution following a diffuser, the vane Reynolds number will be at a maximum near the center and may be considerably less near the outside vanes. It is therefore possible for different parts of the flow to be turned differently. Furthermore, since the resistance at the center is greatest, there must also be a tendency for the flow to be redistributed radially from the center vane. One way to overcome the possible adverse effect of a pointed velocity distribution would be to increase the chord length of the vanes in inverse proportion to the velocity while maintaining s/c constant. This would involve manufacturing difficulties in a practical installation, however. Another method is to use vanes showing small changes in deflection and resistance with Reynolds number. A still better way, where practicable, is to avoid variable velocity distribution altogether. There is at present little information on the effect of variable velocity distribution.

Another factor likely to affect guide vane performance is the aspect ratio of the space between the vanes (ℓ/s). The space between vanes is very

similar to the curved space in a radius elbow. It has been shown [1,2] that if the aspects ratio is equal to or greater than approximately five, the secondary vortexes generated in a radius elbow are localized and rapidly damped out, and the resistance is materially decreased. Observations described later show that the secondary vortexes in the space between guide vanes do exist, but they are confined to the regions near the ends of the vanes if ℓ/s is large enough. It is, therefore, desirable to maintain $\ell/s \geq 5$ in choosing the ratio, s/c and the chord length, c.

Even with large aspect ratio the secondary vortexes tend to have a minor adverse effect on the guide vanes by increasing the local velocity and decreasing the minimum pressure on the convex sides of the vanes near the ends. This tends to cause local separation or even cavitation. With a safe cavitation index the small vortexes near the ends of the vanes should give little concern.

The dimensions and shape of the vanes are important in designing a guide vane elbow, not only because they determine the flow process, but also because they determine the structural strength and natural period of vibration of the vanes. Structurally, the section modulus of the vane cross section about an axis normal to the line of the reaction must be great enough to resist the bending moments created by the reaction. Since the reaction per unit length of the vanes, and hence the bending moment, is proportional to s (Eq.1) and the section modulus for a given profile is approximately proportional to c, the maximum flexural stress in a given vane is approximately proportional to s/c. With the combinations of s/c and camber ordinarily employed in guide vanes, there is generally no structural problem even in a fluid as heavy as water unless the vanes have very great length.

Vibration of all or part of a vane is a common phenomenon on many existing guide vane structures. Neither the natural frequency of vanes in a given fluid, nor the frequency of forces tending to produce vibration can be determined with certainty prior to operating a given installation, but it is possible to estimate the possibility of resonance. Logical methods of eliminating vibration and increasing strength of guide vanes are to increase the vane thickness, to use stiffeners between the vanes, or both. If strength is not a problem, a change in natural frequency of the vanes by changing end fastening conditions or chord length may be all that is required. An analysis of strength and natural frequency of one of the thick vanes investigated in

this report may be found in a previous project report [17] , and a strength analysis of one of the thin vanes of this report is given in Appendix II of this paper.

Stiffening plates or struts tend to have the effect of reducing the aspect ratio ℓ/s of the space between the vanes. However, if this ratio is maintained at five or more, the struts should have no worse effect on the cascade than the original vortexes near the end walls. Some experiments with plate stiffeners are mentioned in Part III and other experiments with strut stiffeners are conducted as a part of this investigation.

D. Wall Effects

In Section C, it was observed that inasmuch as corresponding neutral streamlines were chosen as boundaries (as in Fig. 3, for instance), there would be no disturbance to the flow and no force on the boundaries. In introducing guide vane profiles to produce circulation, the streamline pattern produced by the rectilinear vortexes is supplanted by a new streamline pattern characteristic of the guide vanes. It is still possible to select neutral corresponding streamlines as boundaries so that there will be no force on the boundaries (neglecting drag). However, it is unlikely that the boundaries could be made to follow such streamlines exactly in a practical installation.

If boundaries are selected which do not correspond with the theoretical boundaries, there will be a net pressure and resulting force on the boundaries. In other words, the boundaries will affect the turn. If the boundaries correspond to streamlines other than the neutral ones, there will be no disturbances to the flow as a whole, but there may be a net pressure on the boundaries in the vicinity of the vanes. If the boundaries cut across the theoretical streamline pattern of the guide vane profiles, as they usually do, the entire flow picture around the vanes will be changed, at least in the vicinity of the boundaries.

It is apparent that in designing a guide vane cascade an effort should be made to have the boundaries in the plane of the bend follow a pair of neutral corresponding streamlines. However, the greater the relative number of vanes in the bend, the more closely the conditions for an infinite number of vanes are approached, and the less likely it is that a disturbance near the

boundaries will affect the interior of the flow. Thus, the larger the number of vanes in a cascade, the less exact the boundary shape need be. In other words, to fit a guide vane cascade to a given bend it is better, from the point of view of boundary effects, to have a small spacing and small chord to produce a given s/c than to have a large spacing and large chord.

The theoretical boundaries for a given cascade may be determined mathematically and more rapidly by graphical construction of the flow net between the vanes. No attempt was made in the analysis on page 9 to determine the local flow patterns in the vicinity of the vanes. Smooth curves of the approximate shape of the vane mean line connected to tangents parallel to the two flow directions, generally make satisfactory boundaries. These should be located about one-half vane space from the end vanes of the cascade to correspond with the theoretically neutral streamlines.

If the boundaries are located a full space from the end vanes, as they are in many installations, the net pressure to be expected on the boundaries is not determinable without a complete analysis of the flow patterns. Since the two boundaries together cannot have the exact shape of one vane profile (particularly near the nose of a vane), the resultant pressure on the boundaries cannot be expected to equal that of one vane in the interior of the flow. As an estimate, it may be said that the boundaries in this situation will carry from zero to one times the theoretical load on one vane. But if the boundaries do not carry the load of one vane, then each vane must carry more than the load given by Eq. (1). If the boundaries carried zero load, the vanes would have to carry $\frac{n+1}{n}$ times the load given by Eq. (1) where n is the number of vanes. With walls a full space away from the end vanes each vane must carry a load between the latter value and that given by Eq. (1). If, on the other hand, the walls are less than approximately one-half space from the closest vanes, the walls will tend to resist the turn and the vanes will again have to carry somewhat more than the load given by Eq. (1). In any event, the sum of the loads carried by the vanes and the walls must equal the total change in pressure plus momentum through the cascade. If the number of vanes is large enough, the effect of the walls on Eq. (1) may be disregarded.

The foregoing discussion has assumed that the angle of deflection for which the cascade is designed is the same as the angle of deflection of the boundaries in the plane of the bend. This is not necessarily the case

in practice, principally because of deficiencies in cascade design. It has already been noted that if the cascade is designed for a smaller deflection than the walls, the resulting guide vane reactions will be too small and the walls must assist the turn. If the cascade is designed for a greater deflection than the walls, the resulting guide vane reactions will be too large and the walls must resist the turn. The resulting maldistribution of pressure appears at the walls, but unlike that for imperfect boundary shape, it should be noticeable at some distance both upstream and downstream of the bend, for the walls must provide some turning force for each of the fluid particles.

It should also be considered whether the cross-sectional shape of the duct has any influence on cascade performance. As already mentioned, the principal requirement in this respect must be to maintain the aspect ratio in the space between vanes (l/s, or vane span divided by spacing) large enough to assure largely two-dimensional flow. If this requirement is met, the effects produced near the ends of the vanes by three-dimensional flows, although they exist, may be conveniently disregarded. Also, if the velocity gradient in the direction of vane span is assumed to be small (as is the case in a normal turbulent profile), the three-dimensional effects from this cause may also be disregarded. It must be assumed that the Reynolds number is of constant order of magnitude across the cascade; this will be true for a normal turbulent profile and constant vane chord. Under these circumstances, the proportions of a rectangular duct will have no bearing on the performance of a properly designed cascade. A circular, or other shaped, duct has a varying wall effect depending on the space between the end vanes and the walls, but this has little influence on the interior of the fluid. A properly designed cascade should show little, if any, influence due to duct shape.

If the cascade is not designed to produce the same deflection as the walls, as often happens in practice, then the shape of the duct may become quite important to performance. This is true because of the effect the walls must have in assisting the turn. In every plane parallel to the plane of the bend, the force not carried by the vanes must be transmitted to the walls. In a rectangular duct this force would be approximately equal on all planes, but in a duct of circular, octagonal, or similar shape, the forces transmitted to the walls would vary on different planes. The force would be greater near midspan where the number of vanes is large than near the ends of the spans where vanes are few. Thus, there would be an unbalance in wall pressure spanwise of

the vanes which could result in the creation of secondary currents to add to an already disturbed pressure and velocity distribution.

H. Similarity and Performance Criteria for Guide Vane Cascades

It appears that dynamic similarity should be obtained between two cascades in an infinite fluid if the cascade characteristics and Reynolds numbers are identical, and if fluid turbulence and relative vane roughness are identical or of such values that they may be disregarded. In a confined fluid, when a small number of vanes make wall effects important, there is a question whether the above conditions are sufficient, or whether similarity can be obtained at all. The test for dynamic similarity between two cascades is that they should produce identical deflections and resistances. The deflection angle and the resistance associated with given cascade characteristics will be defined as the cascade performance. The performance of an infinite cascade can be judged immediately by noting the direction of flow and total energy content of the fluid at some distance each side of the cascade. This is not true of a cascade confined in lateral boundaries, since the eventual flow direction is predetermined by the boundaries and may be partially influenced by them. Consequently, a basis for judging confined cascade performance must be established.

The previous analysis shows that, theoretically, a properly designed cascade installed in a bend should exhibit the following properties:

1. Each vane will develop the C_R given by Eq. (2b) if the number of vanes is great enough.

2. The flow streamlines approaching and leaving the vanes must be parallel to the walls except possibly for a very short distance each side of the vanes.

3. The energy, pressure, and velocity distribution before and after the cascade will be identical, except in the immediate vicinity of the walls.

4. The aggregate energy loss in the bend will not be excessive, and the entire excess loss caused by the vanes will be confined to the region of the vanes and the short distance downstream in which the wake vortices are dissipated.

5. The lateral walls will carry between zero and one times the load of one vane, depending on the shape and location of the walls.

The pressure unbalance which determines this load will be confined to the region of the cascade. Elsewhere, normal pressure gradients must exist along the walls.

Before proceeding with the investigation, it is proposed to limit the number of variables in order to maintain the present program within workable bounds. Therefore, only deflections which involve neither contraction nor expansion (ducts of constant cross section) will be considered in this paper. Furthermore, to limit the possible number of profile shapes and to furnish a basis for comparing profiles previously investigated, all shapes will be arbitrarily classified by reference to their maximum camber, maximum thickness, and location of maximum camber. A system similar to the NACA four-digit series [18] will be used for this purpose. This will avoid the necessity of creating a new family system immediately. Maximum camber will generally be over 9 per cent; therefore, it is proposed to use two digits where necessary for maximum camber, placing the two digits in parentheses. For example, a (21)515 profile has a 21 per cent maximum camber, located at 50 per cent of the chord from the leading edge, and a maximum thickness of 15 per cent of the chord. This system is proposed purely as a mechanical system of description; it does not propose to take advantage of existing single airfoil data.

It should be noted that many of the theoretical methods for analyzing cascades previously mentioned [5, 6, 7, 8, 10] produce useful families of profiles. It is a laborious procedure to obtain these, however, and until the effects of such important factors as the three above have been analyzed, it is just as well to neglect the exact shape of the profile.

III. ANALYSIS OF PREVIOUS EXPERIMENTAL WORK

A. Experiments by Klein, Tupper, and Green

It is proposed to review basic experimental work by Klein, Tupper, and Green [19], the Ordnance Research Laboratory of Pennsylvania State College [20], Collar [21], Krober [10], and Harris and Fairthorne [22]. These are the principal investigations involving turns of constant cross section.

Klein, Tupper, and Green [19] used a bend in a rectangular duct carrying air. The duct was 18 in. wide by 36 in. deep. The bend was confined by the channel walls so that Δ was 90°. The vane shapes used are shown in

Fig. 5, which was taken directly from the original paper. Vane chords were 6 in. long for the majority of the tests. The experiments measured the cascade performance for various combinations of profile shape, s/c and θ. (Klein, Tupper, and Green use the term gap-chord ratio which is to be multiplied by $\sqrt{2}$ to obtain s/c. All of the data have been converted to s/c in this paper.)

Figures 6, 7, and 8, taken from the same reference, show the velocity distribution about two and one-half chord lengths downstream from the closest vane, when the input velocity profile was fairly flat. The inside of the bend is at the bottom of each figure. Figures 9 and 10, also taken from the same source, illustrate the pressure drop across the corner as influenced by s/c and θ, respectively. (Note especially that the mean pressure drop rather than total head loss is given here, and that several feet of duct approaching and leaving the corner are included. When the cascade does not make the correct turn, the mean pressure drop may be a very poor measure of loss and Figs. 9 and 10 cannot be accepted literally in those cases.) Reynolds number was about 2×10^5 based on the vane chord and mean approach velocity W_1. Another series of experiments was made with vane no. 4 and with a smaller chord at s/c = 0.47 and $\theta = 90^\circ$ so that Re = 3.5×10^4. An increase of approximately one-third in corner pressure drop was noted at the lower Reynolds number.

Klein, Tupper, and Green also noted the effect of continuous plate spacers or stiffeners between the vanes. The spacers caused a three-dimensional swirl which persisted for some distance downstream, but no further measurements of its effect were made. Klein, Tupper, and Green conclude that design of vanes for 90° confined miter bends need not be elaborate, since any reasonable vane will give a fairly good turn and small resistance.

It is interesting to carry the interpretation of the results obtained by Klein, Tupper, and Green a little further. Doing so tends to lend verification to some of the analysis in Part II. Vanes no. 1, 2, 3, and 4 form a series of thin vanes of constant chord and decreasing maximum camber from 50 per cent for no. 1 to 21 per cent for no. 4. Number 5 is similar to a Göttingen section and has no. 4 for its mean line so that nos. 4 and 5 form a series of varying thickness. For all of these vanes except no. 5, $\phi = 0^\circ$ when $\theta = 90^\circ$ if the vanes make the proper turn. (In terms of the NACA four-digit series, these vanes are approximately: no. 5-(21)515; no. 4-(21)500; and no. 3-(30)500.)

In Fig. 8, vane no. 4 is seen to produce a satisfactory turn for s/c = 0.25 at $\theta = 90^{\circ}$, but the turn becomes progressively worse as s/c is increased until at s/c = 0.60 and 0.71 (Fig. 6), separation occurs at the inside wall at the measuring station. In Fig. 9 it may be noted that the additional pressure drop accompanying a poorer turn above s/c = 0.25 is apparently compensated by the reduced number of vanes to s/c = 0.46, but thereafter the poor turn and increased separation on the vanes multiply the loss. Number 4 would probably produce a satisfactory turn at a value of θ somewhat greater than 90° with s/c between 0.25 and 0.46. Vane no. 3 which has a higher camber than no. 4 (approximately 30 per cent) still produces a satisfactory turn at s/c = 0.71 for $\theta = 90^{\circ}$ (Fig. 6), and it may be assumed that it would produce a satisfactory turn at all lower values of s/c. In Fig. 9 an increase in s/c for vane no. 3 is seen to be accompanied by a reduced pressure drop until s/c = 0.71 and an increased pressure drop thereafter. Vanes no. 1 and 2 which have still higher camber than no. 3 could be expected to produce satisfactory turns to even higher values of s/c except that, as explained in Part II of this paper, the equivalent of stalling occurs when a certain value of s/c is exceeded. From Fig. 9 it would appear that stalling occurred in vane no. 2 at $s/c \approx 0.60$ and in vane no. 1 below any value of s/c that was tested. Of this series of thin vanes no. 3 appears to be the most useful since it produces a satisfactory turn with the least number of vanes and with reasonably slight resistance.

Vane no. 5, which is the thickened version of no. 4, does not produce a satisfactory turn at $\theta = 90^{\circ}$ in any of the data shown. In Fig. 6 it is seen that no. 5 produces a better turn than no. 4 at s/c = 0.71, and it may be inferred that it would produce a satisfactory turn at $\theta = 90^{\circ}$ and some value of s/c greater than 0.25, the critical value for no. 4. In Fig. 7 it is seen that no. 5 also produces a satisfactory turn at s/c = 0.53 and $\theta = 100^{\circ}$. At the latter value of θ and s/c the pressure drop has increased as may be seen in Fig. 10, probably because of separation and a thickened wake. It appears desirable to use no. 5 at a value of s/c less than 0.53 to obtain the best performance.

A pressure diagram for the central vane of a cascade of vanes, no. 5 at $\theta = 90^{\circ}$ and s/c = 0.71, is reproduced in Fig. 11 (it is the only pressure diagram published in the Klein, Tupper, and Green report). Planimetry of the area of this diagram indicates that the developed $C_R \approx 0.87$. By Eq. (2a),

the required $C_R = 2\ s/c = 1.42$. This confirms the previous conclusion that the flow is underturned.

B. Experiments by the Pennsylvania State Ordnance Research Laboratory

The Ordnance Research Laboratory at Pennsylvania State College [20] made measurements on a cascade of vanes the profiles of which were taken from the Klein, Tupper, and Green no. 5 vane with modifications to obtain uniform surface curvature. The vanes were tested in cascade using $\theta = 90^\circ$, and two values of s/c: 0.53 and 1.06 (gap-chord = 0.375 and 0.75). The vanes were of constant chord, 1.48 inches; the number of vanes was varied to obtain the change in s/c. The duct was a 10-in. diameter pipe with a 90° miter bend; water was used as a fluid. The input velocity profile was rather pointed because a diffuser preceded the bend. Reynolds numbers up to 1.8×10^5 based on the vane chord and the maximum approach velocity were used.

Velocity profiles were obtained downstream from the center vane. With s/c = 1.06, the downstream velocity was so badly disturbed that reversed flow occurred near the inside of the bend. With s/c = 0.53 the distribution was improved, but even here the flow was underturned. At some distance downstream the velocity made an angle of about 6° with the pipe axis. The Pennsylvania State paper concludes that the vane stagger angle should be increased about 1° for s/c = 0.53 to give a proper turn. No further check was made of the recommended setting; it is doubtful that this change in θ would be sufficient in view of the small rate of change of $\underline{k}$ with θ at $\theta = 90^\circ$ (page 12 and Fig. 4). (It was stated in the discussion of the Klein, Tupper, and Green no. 5 vane that a value for θ of about 100° was required to give a correct turn at s/c = 0.53 and these cascades are nearly dynamically similar.)

Figure 11, taken from the Pennsylvania State College paper, is a plot of pressures obtained near the center of the central vane of the cascade. (It also includes a plot of pressures obtained by Klein, Tupper, and Green on their no. 5 vane. Positive pressure was not measured for gap-chord = 0.75.) The Pennsylvania State College paper reports that planimetry of the pressure diagram for s/c = 0.53 yields a loading five per cent in excess of the theoretical loading determined by momentum. (The required C_R for this turn is $2 \times 0.53 = 1.06$ and the developed C_R from the Pennsylvania State College data is 1.115.) From these data it appears that the vanes are carrying slightly more load than required for the turn, causing the flow to be overturned. This

deduction is contradictory to the one previously reached both in the Pennsylvania paper and in the discussion of the Klein, Tupper, and Green paper on page 25. As a matter of fact, this vane at s/c = 0.53 appears to develop a larger C_R than the Klein, Tupper, and Green vane does at the larger value of s/c of 0.71 and at the same Reynolds number. The discrepancy is attributed to the pointed diffuser velocity distribution or possibly to experimental error, showing the need for further investigation of the effect of velocity distribution on guide vane performance.

Pressure drop measurements were also made for these cascades. From these measurements the vane resistance was estimated at 0.15 $W_1^2/2g$ plus or minus 0.05 for the cascade with s/c = 0.53, and at less than 0.28 $W_1^2/2g$ for the cascade with s/c = 1.06. There is great possibility for error in these estimates because the kinetic energy factor had to be estimated both upstream and downstream of the cascade, and because losses not caused by the cascade were included.

C. Experiments by Collar

Collar [21] diverted the flow from a rectangular duct (15 in. high by 12 in. wide) in a wind tunnel by a series of vanes so that the discharge was unconfined. (He also made measurements by confining the discharge.) Three vane forms were tested, each for a fixed value of θ determined so that the approach velocity was approximately in the direction of the tangent to the vane mean line at the leading edge. The profiles are shown in Fig. 12. The passages between the vanes were of nearly uniform cross section. Each cascade was placed so that $\beta_1 = 45^\circ$. The deflection angle Δ and the resistance were measured. Results are given in Table II. The loss was determined as the change in total head before and behind the vanes (no duct loss was included). This loss is given in the table as a percentage of the entrance velocity head. Reynolds number, which is based on the chord length and approach velocity W_1, was varied by changing W_1.

Collar also changed the cross section of the approach duct to an octagonal shape and found no change in performance of section B vanes from that in the original rectangular duct. (He also investigated vanes for making a 90° turn with an expansion of area; however, that part of his investigation is outside the immediate field of this paper.) In connection with Table II, it should be observed that since β_1 is fixed, β is equal to 90° only if

$\Delta = 90^\circ$ (see Fig. 3b and Appendix I). For $\Delta = 82^\circ$ and $\beta_1 = 45^\circ$, for instance, $\beta \approx 83^\circ$, and $\frac{W_2}{W_1} = 0.885$; the flow is considerably retarded, and the loss as measured by Collar may include the velocity head change caused by retarding the flow.

TABLE II

Collar's Data [21]

Reynolds No.	(Approx.)	5×10^4	9×10^4	1.4×10^5	1.8×10^5
Section A	Δ°	82.1	88.5	90.8	90.0
s/c = 0.51	Loss, %	36	16	12	11
$\theta = 90^\circ$					
Section B	Δ°	91.1	89.9	89.0	88.7
s/c = 0.49	Loss, %	13	11	10	9
$\theta = 90^\circ$					
Section C	Δ°	90.4	89.0	88.7	88.6
s/c = 0.56	Loss, %	10	7	6	5
$\theta = 100^\circ$					

Collar's sections A, B, and C correspond very roughly to NACA (23)519, (28)515, and (24)(4.5)18 vanes, respectively. Section C is derived from section B by rounding off the nose. The cascade of section A vanes is most like the cascade of Klein, Tupper, and Green no. 5 vanes. At a Re of approximately 2×10^5, the principal differences are that the former consists of vanes having about a 2 per cent larger camber and a 4 per cent larger thickness and its s/c is 0.51 compared with 0.53 for the latter. These differences are apparently sufficient to cause the section A vanes to operate at $\phi \approx 0^\circ$ while the no. 5 vanes operate at $\phi > 0^\circ$. Comparing section C and section A, camber and thickness are almost the same, but the point of maximum camber is shifted forward in C to maintain shockless entry and the convex surface of the vane has less curvature in C than in A. The resistance is materially decreased by this change, indicating that the shape of vane C is preferable to that of vane A.

Collar's data indicate that changing Reynolds number, at least up to 1.8×10^5 for the profiles tested, affects both the deflection angle and the resistance. It appears that the boundary layer of section A at $Re = 5 \times 10^4$ may have separated completely, probably as a laminar layer. Turbulence in the boundary layer, which accompanies increasing Reynolds numbers, seems to restore the boundary layer to the surface and to reduce ϕ to approximately zero, after which ϕ gradually increases again with Reynolds number as the turbulent boundary layer tends to separate at the trailing edge. The other two sections lie entirely in the range of ϕ increasing with Re. The vane surfaces are apparently smooth as the resistance continues to decrease with increasing Re; the increase in ϕ is so small that no separation loss is incurred.

D. Experiments by Krober

Krober [10] made measurements in confined turns in a square duct 200 mm on a side. Air was the fluid in these tests. Deflection angles used were $\Delta = 90^\circ$, 60°, 45°, and 30° and multiple deflection angles of $\Delta = 2 \times 90^\circ$, $2 \times 45^\circ$, and $3 \times 60^\circ$. In the multiple cascades, a minimum of approximately two chord lengths separated the closest vanes. Only one profile was studied for each Δ except for a minor change in profile for $\Delta = 90^\circ$; θ was varied only slightly for each experiment. For $\Delta = 90^\circ$, both a square and a round duct section were used. The experiments were directed principally toward evaluating a thin profile derived by transformation from an airfoil profile. Krober's profiles are shown in Fig. 13; they have been numbered for convenience in reference. His results are given in Table III. In the table, head loss is determined as the difference in average total head before and behind the vanes and straight duct loss is subtracted. Head loss is given as a percentage of the entrance velocity head. The value of θ is for the minimum head loss; other values of θ were apparently tried but results were not published.

Krober quotes Reynolds number as 4×10^4 but it appears that, based on the vane chord for $\Delta = 90^\circ$ and approach velocity W_1, approximately 1×10^5 is more appropriate. The paper contains diagrams of velocity and pressure distribution downstream of the vanes in the experiments pertaining to the first two lines of Table III. These all show a fairly uniform distribution for the values of θ given in Table III, but Krober notes that minimum energy loss and best downstream distribution do not necessarily occur simultaneously.

TABLE III

Krober's Data [10]

Δ	Shape of Duct	Vane	s/c	θ	Head Loss, %
90°	Square	1	0.47	101 1/2°	13.4
90°	Square	1 slightly modified	0.47	100°	13.8
90°	Circular	1	0.47	101 1/2°	13.6
60°	Square	2	0.54	98°	14.6
45°	Square	3	0.685	100 3/4°	14.2
30°	Square	4	0.96	97 1/2°	10.0
2 x 90°	Square	1	0.47	101 1/2°	26.0
2 x 45°	Square	3	0.685	100 3/4°	26.6
3 x 60°	Square	2	0.54	98°	30.4

Krober also tested the no. 1 vane in an unconfined turn and found that $\theta = 101\frac{1}{2}^\circ$ gives $\Delta = 90^\circ$ for s/c = 0.47. Threads on the trailing edges of the vanes were used to find the angle β_2. $\phi \approx 5^\circ$ for this value of θ. The reaction was not measured in the unconfined turn, but one of the no. 1 vanes was equipped with a double wall and the pressure distribution was obtained at several values of θ for s/c = 0.47. Planimetry of the pressure curves and resolution of the resulting pressure on a line of action along the cascade axis (in accordance with the argument at the end of Section B, page 8) gives the following values for the developed C_R:

$$\theta = 99\tfrac{1}{2}^\circ,\ C_R \approx \frac{0.875}{\cos 9\frac{1}{2}^\circ} = 0.888$$

$$\theta = 101\tfrac{1}{2}^\circ,\ C_R \approx \frac{0.926}{\cos 11\frac{1}{2}^\circ} = 0.945$$

$$\theta = 103\tfrac{1}{2}^\circ,\ C_R \approx \frac{0.945}{\cos 13\frac{1}{2}^\circ} = 0.973$$

For s/c = 0.47, the required C_R is 2 x 0.47 = 0.94. This is in agreement with the use of $\theta = 101\frac{1}{2}^\circ$ for the proper turn angle.

Attention should be directed to the fact that the tangent to the leading edge of the Krober vanes was approximately parallel to the approach velocity W_1. It may also be observed that the circular and square ducts gave nearly the same vane resistance; this can be attributed to the fact that the cascade was exactly designed for these turns. The Krober vane no. 1 is roughly an NACA (29)400 profile.

E. Experiments by Harris and Fairthorne.

Harris and Fairthorne [22] installed a test cascade in a nozzle in a wind tunnel. A fixed reversing cascade located approximately two chord lengths behind the test cascade was used to maintain the flow within the original tunnel. The effective working section was approximately 2 ft sq. In the experiments, the stagger angle θ, the approach angle β_1, and the spacing-chord ratio s/c were varied for a fixed vane shape. The profile is an RAF airfoil on a circular arc mean line of 45° central angle and corresponds nearly to an NACA (10)510 (Fig. 14). Measurements were made of Δ (by measuring β_2), the mean total head loss, and the reaction on one vane (using a balance). All measurements were made on or behind the central vane of the test cascade.

Since both β_1 and θ varied independently in these experiments, β varied and $\frac{W_2}{W_1}$ varied. In Table IV below, data for $\frac{W_2}{W_1}$ approximately equal to unity ($\beta \approx 90^\circ$) have been extracted from a longer table published in the original paper. The stagger angle for all values in Table IV is $\theta = 90.5^\circ$ (the profile chord is taken as the line connecting the centers of curvature of the leading and trailing edges). Reynolds number is about 0.9×10^5 based on vane chord and approach velocity W_1. Head loss is given as a percentage of the approach velocity head. Columns (1) through (6) are taken from the original paper and columns (7), (8), (9), and (10) are computed from the data in the previous columns. (β is determined from the relations in the footnote to Appendix I.) The column headings have been altered from those of the original table in order to use symbols introduced in this paper. Equation (2b) was used in computing column (9) and Fig. 1 was used in determining values for column (10). If straight line interpolation between the first two lines of Table IV is permissible, it is seen that at s/c = 0.5, $\beta_1 = 72.5^\circ$, $\Delta = 35^\circ$ and $\beta = 90^\circ$.

TABLE IV

Extract of Harris and Fairthorne Data [22]

(1)	(2)	(3)	(4)	(5)	(6)	(7)	(8)	(9)	(10)
s/c	β_1	Δ	$\frac{W_2}{W_1}$	Head Loss %	Measured $\frac{C_R}{2\ s/c}$	β	Developed C_R	Required C_R	ϕ
0.5	67.5°	40°	0.999	4.4	0.666	87°	0.666	0.625	5°
0.5	77.5°	30°	1.054	5.0	0.536	92 3/4°	0.536	0.513	5°
1.0	77.5°	24°	1.017	2.2	0.448	89 1/2°	0.896	0.810	11°
1.5	77.5°	21°	1.010	1.4	0.362	88°	1.086	1.064	14°

In interpreting the results of Harris and Fairthorne, it must be mentioned that the reversing cascade was not identical in all details with the test cascade in each instance. Since only two chord lengths separated the two, some of the results may have been influenced by an upstream effect of the reversing cascade. This effect was probably small.

With reference to Table IV, comparison of columns (8) and (9) shows fair agreement between the C_R developed by the vanes and the required C_R, although the developed C_R appears to be 10 per cent too large in one instance. The differences may possibly be due to the small number of vanes in the cascade. All of the cascades are being used at values of s/c greater than the critical value. The last three lines of the table clearly show the dependence of the angle ϕ on the value of s/c since the other cascade characteristics are fixed in this series. It is seen that Δ for a cascade may be increased by decreasing s/c, but this is done at the cost of increased resistance even though ϕ is decreased by the changes. A comparison between the first two lines of Table IV shows that Δ may also be increased by increasing the developed C_R, in this instance, by increasing $\alpha = (\theta - \beta)$. The resistance decreases for the larger value of Δ because the streamlines approach the vanes almost along the tangent at the leading edge.

F. Summary of Previous Experimental Work

In Table V, the data for several of the various vane profiles used in the experiments just described have been collected. Obviously some of the data are estimated from data in the original papers.

TABLE V

Summary of Previous Experimental Work

(1)	(2)	(3)	(4)	(5)	(6)	(7)	(8)	(9)	(10)	(11)
Δ Degree	Vane	Approx. NACA Profile	s/c	θ for Proper Turn, Degree	Critical s/c	Approx. % Head Loss Corresponding to (5)	ϕ Degree	Approx. Re x 10^{-5}	Duct Shape	Approach Velocity Profile
90	K, T & G No. 3	(30)500	0.71	90	0.71	23*#	0	2	Rect.	Flat
90	K, T & G No. 4	(21)500	0.25	90	0.25	20*#	0	2	Rect.	Flat
90	K, T & G NO. 5	(21)515	0.53	100	< 0.53	27*#	Approx. 5	2	Rect.	Flat
90	Penn. State	(21)515	0.53	90	< 0.53	15± *	Approx. 5	1.8	Round	Very Pointed
90	Collar, A	(23)519	0.51	90	> 0.51	11	0 %	1.8	Square %	Flat
90	Collar, B	(28)515	0.49	90	> 0.49	11	0	0.9	Square % and Octagonal	Flat
90	Collar, C	(24)(4.5)18	0.56	100	> 0.56	10	0	0.5	Square %	Flat
90	Collar, C	(24)(4.5)18	0.56	100	< 0.56	5	1.4	1.8	Square %	Flat
90	Krober, No. 1	(29)400	0.47	101½	< 0.47	13½	5.5	1	Round & Square	Flat
30	Krober, No. 4	8400	0.96	97½	< 0.96	10	Approx. 4	1	Square	Flat
35	Harris & Fairthorne	(10)510	0.5	90½	< 0.5	5	Approx. 5	0.9	Square %	Flat

* Based on mean pressure drop
\# Includes considerable duct
% The turn was unconfined

Some conclusions to be drawn from examination of Table V and from the previous paragraphs of this section are:

1. If an ideal velocity and pressure distribution upstream and downstream from the vanes is not required, but only a reasonably small resistance is the objective, then, as was concluded by Klein, Tupper, and Green, guide vanes are relatively insensitive to changes in shape, stagger angle θ, and spacing-chord ratio s/c.

2. If the velocity and pressure distribution are important, the turn should be made by a cascade which satisfies the criteria of Part II, Section H. Some suitable vanes may be found in Table V for the values of Δ given there.

3. The existence of a critical value of s/c, below which value a cascade will make a required turn with the angle $\phi \approx 0^{\circ}$ is confirmed. Depending upon the shape of the vane, the minimum resistance may occur at or above the critical value of s/c.

4. In confirmation of the reasoning in Part II, Section D, it is worth noting that Δ may be increased by increasing the developed C_R, or by decreasing s/c (at least to a certain point). The developed C_R may be increased by one or more of the following steps:

(a) Increasing the camber of the profile

(b) Increasing the thickness of the profile (for favorable θ)

(c) Increasing α or θ. This is frequently the only practicable step after a cascade and bend have been constructed, but it may increase the resistance.

5. The shape of the duct does not appear to affect the performance of a properly designed cascade, at least if the entrance velocity profile is fairly flat (uniform velocity approaching the cascade).

6. The type of entrance velocity profile (or the kinetic energy distribution) appears to have an effect on the performance of an improperly designed cascade in circular ducts. (See the Pennsylvania State College experiments, Part III, Section B.)

7. There is some change in both deflection angle and resistance for a given cascade with changing Reynolds number, at least

below Re = 2 x 10^5 and at values of s/c near to and above the critical. There may exist an optimum profile for minimum change of angle and resistance with Reynolds number.

8. The principal factors contributing to small resistance are: relatively large s/c, ϕ approximately equal to zero, and smooth flow near the leading edge.

9. The shape of the passage between vanes does not appear to have a separate, measurable effect on either deflection or resistance as long as the aspect ratio of the passage is maintained large enough.

IV. EXPERIMENTAL PROGRAM

A. Objective

The experimental program to be undertaken is designed to extend the reasoning of Part II and to supplement the previous experimental work which was summarized in Table V. Basically, it is proposed to investigate the relation between cascade characteristics and cascade performance for families of related cascades. It is also intended to examine such subsidiary points as the effect on cascade performance of changes in scale and in Reynolds number, of changes in velocity profile approaching the cascade, and of the placement of stiffeners between the vanes. Incidentally, it will be necessary to verify experimentally the criteria for a properly designed cascade, as given in Part II, Section H. To permit a thorough investigation, the deflection angle will be confined to 90° for these experiments.

B. The Test Installation

The experimental apparatus was designed to make use of test bend facilities and instrumentation already available from a set of experiments on radius elbows. This apparatus was previously described in greater detail in Project Report No. 5 of the St. Anthony Falls Hydraulic Laboratory [2]. In order to receive the test cascades, the apparatus was fitted with a transparent, lucite, 90° miter bend. A photograph of the test installation is reproduced in Fig. 15, and two views of the miter bend are shown in Fig. 16.

Details of the miter bend and connecting tangents are shown in Fig. 17. Except at the corner, the inside cross section is 6 in. square. The

inside wall at the corner is made on a $1\frac{1}{2}$ in. radius and the outside wall on a $2\frac{1}{2}$-in. radius. The cross section of the duct was held to the 6-in. size in order to obtain large flow velocities within the discharge limitations. The radii at the corners were constructed as approximations of the boundary streamlines for the first type of vane to be tested; unfortunately, since the walls were not readily changeable, the same boundaries had to serve for all vanes.

The elbow was used in the test installation with the bend horizontal. The entrance to the upstream tangent of the elbow was bolted to a plate on the end of a 12-in. diameter supply pipe. A 6-in. square hole was centered in the plate to match the cross section of the lucite pipe. Bolts through this plate served to hold a bell-mouthed nozzle and a distributor ring inside the 12-in. pipe. The nozzle provided a uniform flow at the entrance, and the distributor ring was used in conjunction with a supply of compressed air to inject dye or air bubbles into the flow.

Many holes were provided in the test bend and connecting tangent to serve in mensuration. The holes were of two types: the first of 1/4-in. diameter to permit insertion of a pitot cylinder in order to obtain total head and direction measurements, and the second of 1/16-in. diameter to serve as piezometer taps. The piezometer holes were all carefully rounded to 1/64-in. radius on the inside to remove burrs. The holes were organized into one measuring station before and three measuring stations after the bend, each station consisting of five 1/4-in. holes and six 1/16-in. holes on each face of the square duct. The measuring stations are labeled D-D, K-K, M-M, and P-P in Fig. 17. In addition to the regular measuring stations, several other piezometer holes were provided in the walls. Also, two rotating disc measuring stations, one immediately before and one immediately after the bend, were provided to give access to the bend region with the pitot cylinder. A set of four piezometer holes, one in each face of the duct, located 12 in. upstream of Station D-D and connected to each other, served as a reference station to which all head readings were referred. Suitable plugs were provided to close any or all of the holes when they were not in use.

The top and bottom surfaces of the bend were provided with holes to receive vane trunnions and set screws for holding the vanes in place. The original holes (Fig. 17) provided for five vanes in the bend with approximately a full space between each end vane and the adjacent wall, but these holes were later changed in number and location to accommodate different

cascade arrangements. Subsequent to drawing Fig. 17, the set-screw holes were slotted to permit adjustment of the stagger angle.

Details of the test installation are shown in Fig. 18. Fluid is supplied to the test bend by a 12-in. diameter supply pipe. Air from a large capacity blower and water from the Mississippi River are available as fluids. Regulating valves in the 12-in. line are about 40 ft upstream from the elbow with about 30 ft of straight 12-in. pipe between the valves and elbow. A long honeycomb in the straight pipe further rectifies the flow before it reaches the test bend.

Discharge from the downstream tangent of the elbow is led through a diffuser and a short length of 12-in. diameter pipe into a vertical pipe. The top leg of this vertical pipe is open at the top and serves as a pressure regulator for maximum pressure on the lucite pipe. The lower leg of the vertical pipe, fitted with a tailwater regulating valve, leads to a calibrated measuring flume.

A maximum water flow of 4.5 cu ft per sec and a maximum air flow of 1800 cu ft per min may be taken through the test bend. Water flow is limited by the capacity of the measuring flume; air flow is limited by the capacity of the blower. No significant variation in flow, either water or air, occurred during the progress of a run in the experimental apparatus.

C. The Experimental Cascades

Several related guide vane cascades were designed to be tested in the experimental elbow. The cascades consisted of seven basic shapes, each of which was used at two or more spacing-chord ratios (s/c). Since the NACA four-digit series was used to define the principal shape parameters, the exact four-digit shape was used for several of the profiles. The combinations of shape and s/c which were used are defined in Table VI. For each shape, it was intended to make s/c small enough to establish the behavior of the cascade below the critical value of s/c and large enough to reach the point of rapidly increasing resistance. This was not possible in every case because of the limitations of apparatus and of time.

The seven vane shapes are shown in Fig. 19 and photographs of two are reproduced in Figs. 20 and 21. Coordinates of the vane surfaces are given in Table VII, except for the type I vane, the dimensions of which are included in Fig. 22.

TABLE VI

Test Cascades

Vane Shape	s/c							
	Series		Group					
Type I (21)515 approx.			0.48 / 10 & 10A		0.41 / 110	0.36 / 210	0.32 / 310	
Type II (17)315 approx.					0.45 / 20	0.385 / 120		
(21)315			0.50 / 30		0.43 / 130			
(21)300			0.50 / 40			0.375 / 240	0.333 / 40L & 340	0.285 / 140L
(30)300		0.60 / 160S	0.50 / 60		0.43 / 160			
(30)400		0.60 / 170S	0.50 / 70	0.467 / 370S	0.43 / 170		0.333 / 370	
(30)500	0.70 / 80SA	0.60 / 180S	0.525 / 280S					

S - Vane chord = 2.02 in. L - Vane chord = 4.25 in. A - One half space between end vanes and walls

TABLE VII

Vane Shape Data

Shape (and other data)	y, % Chord Upper	Lower	X, % chord	y, % Chord Upper	Lower	Shape (and other data)
Type II	+6.5	0.0	0	+5.5	0.0	(21)315
Approx. (17)315	8.7	-0.7	1.25	8.5	-0.5	L.E. Rad:
L.E. Rad: 3.5% chord	10.2	-1.1	2.5	10.8	-0.3	2.5% chord
Slope of Mean Line	13.7	0.0	5.0	14.5	+1.5	
	16.2	+2.5	7.5	17.5	3.2	Slope of Mean Line
	19.6	3.6	10.0	20.1	4.8	
	21.2	6.0	15.0	24.0	8.0	
	23.0	7.5	20.0	26.65	10.8	
L.E: $\frac{dy}{dx} = -1.73$	23.7	9.1	25.0	28.0	12.7	L.E: $\frac{dy}{dx} = -1.4$
	24.2	9.8	30.0	28.5	13.6	
T.E: $\frac{dy}{dx} = 0.49$	22.8	10.2	40.0	28.0	13.5	T.E: $\frac{dy}{dx} = 0.6$
	21.2	9.6	50.0	26.1	12.8	
	18.3	8.6	60.0	23.3	11.5	
	14.5	6.5	70.0	19.1	9.5	
	10.0	4.5	80.0	13.9	7.0	
	5.5	2.0	90.0	7.5	4.25	
	3.3	0.5	95.0	4.0	+1.8	
	1.0	-1.0	100.0	+0.5	-0.3	

TABLE VII - Continued

Shape (and other data)	y, % Chord Upper	y, % Chord Lower	X, % Chord	y, % Chord Upper	y, % Chord Lower	Shape (and other data)
(30)300 Slope of Mean Line: L.E: $\frac{dy}{dx} = -2.0$ T.E: $\frac{dy}{dx} = 0.858$	0 2.44 4.79 9.16 13.12 16.66 22.50 26.66 29.16 30.00 29.39 27.55 24.49 20.00 14.70 7.96 4.14 0		0 1.25 2.5 5.0 7.5 10 15 20 25 30 40 50 60 70 80 90 95 100	0 1.71 3.35 6.41 9.19 11.67 15.73 18.67 20.40 21.00 20.55 19.32 17.13 14.13 10.28 5.56 2.89 0		(21)300 Slope of Mean Line: L.E: $\frac{dy}{dx} = -1.4$ T.E: $\frac{dy}{dx} = 0.6$
(30)400 Slope of Mean Line: L.E: $\frac{dy}{dx} = -1.5$ T.E: $\frac{dy}{dx} = 1.0$	0 1.84 3.63 7.03 10.20 13.12 18.28 22.50 25.78 28.12 30.00 29.16 26.66 22.50 16.66 9.16 4.79 0		0 1.25 2.5 5.0 7.5 10 15 20 25 30 40 50 60 70 80 90 95 100	0 1.48 2.42 5.70 8.32 10.80 15.30 19.20 22.50 25.20 28.80 30.00 28.80 25.20 19.20 10.80 5.70 0		30(500) Slope of Mean Line: L.E: $\frac{dy}{dx} = -1.2$ T.E: $\frac{dy}{dx} = 1.2$

Each run in an experimental series, involving a particular combination of vane and s/c, was identified by one number from a group of ten. Series were identified by the specific number group into which the runs fell. Thus, all runs for the cascade of (21)315 vanes at s/c = 0.5 were numbered between 30 and 39. These data are designated the 30 series group. In Table VI, the series group under which data may be found for each combination of vane and s/c is given. Numbers are assigned so that those between 10 and 89 indicate that six vane spaces were used in the elbow, those between 110 and 189 indicate that seven vane spaces were used, numbers between 200 and 300 indicate that eight spaces were used, and numbers between 300 and 400 indicate that nine spaces were used. The letter A following the number indicates that the spaces were distributed so that approximately one-half vane space or less occurred between the end vanes and the adjacent walls instead of a full space as was used in the other runs.

The seven basic shapes are obtained by progressive variation of one shape factor at a time: maximum thickness, maximum camber, or location of maximum camber. Therefore, all of these shapes are closely related. They are also related in a general way to previously tested vanes because all have been defined in terms of the NACA four-digit system.

The first two vane shapes listed in Table VI are not exact NACA four-digit series shapes. The type I vane is an approximate duplication of the Klein, Tupper, and Green no. 5 vane, using circular arc surfaces similar to the Collar section C. The type II vane was developed by conformal transformation using the Krober method [10] from an NACA 23012 air-foil (five-digit) in rectilinear flow.

Several chord lengths were used, but one set of each of the vane shapes except the type II and the (30)500 was built on a chord length of $2\sqrt{2}$ inches. To study similarity and to obtain the larger values of s/c, a set of each of the (30)300, (30)400, and (30)500 vanes was built on a 2.02-in. chord and a set of (21)300 vanes was built on a $3\sqrt{2}$-in. chord. Experimental series on vanes with the 2.02-in. chord are designated by the letter S in Table VI; those on vanes with the $3\sqrt{2}$-in. chord are designated by the letter L. All vanes have a span of 6 inches. Six to eight vanes of each shape were required in order to make a complete cascade at the smallest value of s/c for that shape.

The vanes were supported by trunnions which fitted into the trunnion holes in the miter bend. The stagger angle for each cascade could be adjusted by rotating the vanes about their trunnions. Once set, the stagger angle was fixed by set screws which protruded through the bend walls and screwed into the vanes. The stagger angle could be set and measured to the closest $1/2^{\circ}$.

D. Construction Details of the Vanes

The thin vanes were made of 16-ga. sheet brass. First they were formed roughly on a sheet metal break, then hammered to final shape on a short wooden form. At each end two 1/2-in. sections of 5/16-in. diameter brass rod were soldered to the vane, drilled and tapped, to receive the trunnion screws and set screws. The fairness of the vane surface was thus destroyed near the ends of the vanes, but the disturbance was sufficiently localized so that overall results should hardly be affected. Figure 21 is a photograph of one of the thin vanes, a (30)300 shape.

The thick vanes were cast of "Cerrobend," a low melting point alloy. Each vane was cast about a sheet brass core in the shape of its mean line. All inserts, including trunnions and copper tubes for piezometer taps, were soldered to the core before casting, and the core itself was pierced with holes to give good bond. Castings were made in forms of molding plaster, surfaced with shellac and dusted with carbon black. Figure 20 is a photograph of one of the thick vanes, the type I. Figure 22 is a construction drawing of this vane.

All vanes, both thick and thin, were carefully checked against accurate templets, and surface irregularities were eliminated by building up with solder and by filing and rubbing with emery cloth. The surface roughness of all the vanes was approximately equal to that of commercial sheet brass.

Certain vanes of each of the thick vane shapes were cast with internal pressure tubes. These tubes permitted the drilling of 1/32-in. piezometer holes for determining the surface pressures. The internal tubes were extended through the trunnions to the outside of the elbow. The connections between trunnion and vane were made by a jack-like arrangement of short pieces of hypodermic needle sweated into copper tubes in the trunnions. A tight joint was obtained by fitting the other ends of the needles into the copper tubes in the vanes and coating the space between the needles with rubber cement (Fig. 20).

E. Procedure

The experimental program consisted essentially of the following operations:

1. One of the cascades described in Table VI was installed in the elbow at an arbitrary stagger angle. When thick vanes were used, those with piezometer holes were placed nearest the center of the cascade.

2. A water or air flow which would produce a predetermined Reynolds number was started through the cascade.

3. Measurements were made of total head, flow direction, and static head at station D-D before the cascade, at stations K-K, M-M, and occasionally at station P-P after the cascade. Measurements were also made of the static head at the wall piezometers around the bend shown in Fig. 17 and on the vane surfaces of the thick vanes. Visual and photographic observations of the flow phenomenon were made at this time.

4. Measurements were reduced and analyzed using the criteria of Part II, Section H.

5. A better stagger angle was selected if necessary, and the above steps were repeated until it was possible to select cascade characteristics which would actually produce a 90° turn for each cascade. In general, the stagger angle was changed by about 2° between runs in each series so that the correct value of the stagger angle would be bracketed if not reached exactly in two or three trials.

For some series groups, several trials were required for each shape and s/c in order to determine the proper stagger angle. Not all runs resulted from trials for proper stagger angle, however. Several runs were made at constant stagger angle and at varying Reynolds numbers. One run involved a distorted entrance velocity profile; three others were made with stiffeners between vanes. The normal Reynolds number* was 1.5×10^5 and the normal fluid was water. Reynolds numbers varying from 0.6 to 4.0×10^5 were used, and air was used as a fluid occasionally.

*Reynolds number $= \frac{cW_1}{\nu}$ where c is the vane chord, W_1 is the approach velocity and ν is the kinematic viscosity.

For the most part, spacing-chord ratio was altered by changing the number of vanes in the bend, since each set of vanes was of fixed chord. Some changes in spacing-chord ratio were made by substituting vanes of new chord lengths; the exact combinations are indicated by the series group number in Table VI. No matter how many vanes were used, the trunnions were always placed on the same trunnion line (Fig. 17). The trunnion line was not identical with the cascade axis, however. The axis was much closer to the miter line of the bend, but its location varied somewhat with variation in the location of the center of pressure of the individual vanes. The differences may be seen in the data presented in the next section.

F. Experimental Data

As indicated in the previous section, data were obtained both from head and direction measurements and from visual and photographic observation. Internal measurements in the duct before and after the bend were made with a 1/4-in. diameter pitot cylinder, which gave total head and direction of flow. The pitot cylinder is a tube provided with two piezometer holes about 80° apart in a diametral plane near midspan. The holes are connected to opposite ends of the tube so that the head on either hole may be read independently. By rotating the cylinder until the head on the two holes balances, the direction of flow may be read on a suitable scale; then the total head may be read by turning one of the holes into the flow. These cylinders and their use are described in detail in a separate paper [23] . Static head measurements were made only on the walls and vane surfaces using the prepared piezometer taps.

All heads were read on differential manometers. A 100-in. U-tube manometer using a water-air interface was provided for large head, and a 6-in. water-air interface micromanometer was provided for small head readings. The micromanometer was essentially a U-tube fitted with micrometer depth gages graduated to 0.001 inch. All head readings were referred to the reference station upstream from station D-D through the U-tube manometers. Use of this reference system eliminated possible errors caused by small transitory changes in pressure or velocity on the entire system.

In order to make total head and direction readings with the Pitot cylinder, the duct cross section at each station was divided into twenty-five 1-in. squares, twenty 1 x 1/2-in. rectangles, and four 1/2-in. squares.

This division is shown in Fig. 17. The readings with the cylinder were made at the centers of each of these elementary areas, except the 1/2-in. squares, by inserting the cylinder through appropriate holes in the walls. The 1/2-in. squares were entirely neglected on the assumption that excessive readings were obtained by placing the cylinder at the centers of the 1 by 1/2 in. end rectangles, and that the two effects were counterbalancing. Static heads at the centers of these elementary areas were obtained by interpolation from the walls where the readings were made. The interpolation of static heads and neglect of corner squares was justified by work previously done in a similar situation with a radius elbow [2] .

After reduction of the readings, a true velocity and true total head were obtained at the center of each elementary area. For plotting purposes the velocity was resolved into three components, one longitudinal (normal to the cross section) and the other two at right angles to each other within the cross section. The mean longitudinal velocity at each station was determined by integration using the formula $\bar{u} = \frac{\Sigma u \Delta A}{\Sigma \Delta A}$, where $\bar{u}$ is the mean longitudinal velocity in a cross section, u is the local longitudinal velocity at the center of an elementary area, and ΔA is the elementary area. The mean total head at each station was also computed, using the formula $\bar{H} = \frac{\Sigma H u \Delta A}{\Sigma u \Delta A}$, where $\bar{H}$ is the mean total head at a station, H is the local total head at the center of an elementary area, and the other quantities are as defined above.

All data were finally reduced to dimensionless form for plotting purposes. Velocities were divided by the mean flow velocity for the cross section and plotted as $\frac{u}{\bar{u}}$; total heads and static heads were divided by the dynamic head corresponding to the mean flow velocity and plotted as $\frac{H}{\bar{u}^2/2g}$ and $\frac{Hs}{\bar{u}^2/2g}$, respectively. Total head and velocity data were plotted for study in cross-sectional diagrams similar to Figs. 45 to 53, but such figures are not reproduced for all runs. Instead, velocity and total head traverses at mid-depth have been replotted from the more complete diagrams and are presented in Figs. 26 to 44. It may be noticed in the velocity diagrams that $\bar{u}$ is not constant at consecutive stations, apparently defying the equation of continuity. The small differences are due to experimental error, but the larger ones result from deliberate changes in velocity to maintain a constant Reynolds number as the temperature of the fluid changed.

Wall pressure variation measured in the plane of the bend at mid-depth is plotted in Figs. 55 to 75. These figures also contain representative bottom wall pressures obtained in the rotating discs before and after the vanes. Vane surface pressure distribution measured in the plane of the bend at mid-depth for the thick vanes is plotted in Figs. 77 to 87. The vane surface pressures are for a composite vane using readings from the two or three vanes closest to the center of the cascade. Since all pressures are given with respect to the pressure at the reference station, the vane stagnation pressure is plotted as the velocity head in the center of the duct, at station D-D less the straight pipe loss from the reference station to the leading edge of the vanes. Wall and vane pressure data were also obtained in planes nearer the ends of the vanes; samples of these data are plotted in Figs. 65, 73, and 78. Some data for the 10 series group are not presented in this report but were presented in a special report dealing with the type I vane at s/c = 0.48 [17].

The mean total head gradient for each run, plotted in dimensionless form, may be found in Figs. 88 to 101. Broken lines on these latter figures show the straight pipe energy gradient which is determined from the formula $\frac{h_f}{\bar{u}^2/2g} = \lambda \frac{D}{d}$ where h_f is the loss in head in the length D of duct of depth d. λ is given by $\frac{1}{\sqrt{\lambda}} = 2 \log Re\sqrt{\lambda} - 0.8$ for smooth, circular pipes, where Re is the Reynolds number based on pipe size. This straight pipe loss is only an approximation of the true loss, but it checks very closely with the pressure drop between the reference station and station D-D (in which region there is only a small change in kinetic energy). With $Re = 3 \times 10^5$, which is the most common value for the duct in these experiments, $\lambda = 0.0145$.

On both the wall pressure and vane pressure diagrams, the pressures have been integrated to give the wall and vane reactions respectively. The wall reactions are given on the wall pressure diagrams (Figs. 55 to 75) in units of the stagnation pressure per foot of depth where the stagnation pressure is based on the mean velocity at mid-depth at station D-D. The wall reaction is determined by integration in a plane at mid-depth completely around a boundary consisting of imaginary walls across stations D-D and K-K and the actual duct walls between those stations. Vane pressure diagrams (Figs. 77 to 87) show the developed C_R for each thick vane and the center of pressure for some vanes; C_R is based on the mean velocity at mid-depth at station D-D.

In one instance, velocity measurements in air were made immediately behind a cascade of vanes using a hot wire anemometer. The data obtained are plotted in Fig. 54. The hot wire was a 0.001-in. tungsten wire 1/4 in. long supported on nickel electrodes. The wire was placed in the plane of the bend at mid-depth and was rotated in its plane until a maximum reading was obtained. The wire was operated on the constant temperature principle; it had been previously calibrated, but the calibration curve had to be extrapolated in order to obtain the plotted values in Fig. 54.

In another group of experiments, some data were taken in the vaned turns of the bends of a model water tunnel. These bends used cascades of type I vanes at $s/c = 0.48$, $\theta = 100^{\circ}$. Representative velocity traverses are given in Figs. 102 and 103. Other data for the tunnel bends are cited in a previous project report [17].

Various schemes of visual and photographic observations were used in different series. Both still and motion pictures were obtained. In water flows, most success was had with air bubbles which were introduced along the bottom of the duct at the distributor ring previously described. At the usual working velocities, the bubbles rose to mid-depth by the time they reached the bend. Figures 23a and 24 were obtained by this means. Lighting in Fig. 24 was by two 300-watt spot lights located just beyond the plane of the bubbles, making angles of about 105° with the camera axis. In Fig. 25a air bubbles are shown being used to delineate boundary effects. Figures 23e and 23f illustrate another technique in water, that of spreading aluminum powder in SAE 30 oil on the walls and vanes.

Two techniques were used successfully with air flows. One was the attachment of threads to the vane and wall surfaces and the suspension of threads in the stream by fine wires. The other was the introduction of colored water to the boundary layer to observe boundary layer effects on the vanes. Figures 23b, 23c, 23d, and 25b illustrate these techniques.

V. ANALYSIS

A. General Observations

Some general facts about flow through cascades in bends may be obtained from casual observations of the photographs and data. That the velocity, total head, and pressure distribution behind a guide vane bend are much

better than that behind a favorable bend without guide vanes may be seen by comparing some of the figures of this report with corresponding figures in a previous report on radius elbows [2] . Even when the guide vanes are not set at the correct stagger angle, the improvement over the bend without guide vanes is quite marked.

In Fig. 24 the effect of the cascade on the two-dimensional flow approaching and leaving the bend may be observed. This figure concerns the cascades of type I vanes, but similar flow patterns were obtained with comparable variations in the other cascades. In the photographs straight streamlines are represented accurately by the air bubble paths, but when the streamlines are curved, the air bubble paths are more curved because of the effect of centrifugal forces on the lighter weight air bubbles. It may easily be seen that only one spacing-chord ratio for each stagger angle gives a turn in which the streamlines approaching and leaving the bend are straight. Small changes in stagger angle produce perceptible changes in streamline curvature. These changes are manifest in the plotted velocity profiles downstream from the cascade, and in all of the other data as well. It should be noted from Fig. 24 that underturning produces a streamline pattern tending toward that normally found in a radius elbow, with high velocity near the inside of the bend. Overturning tends to produce the opposite streamline pattern with high velocity near the outside of the bend. The more the stagger angle differs from its correct value, the more pronounced these trends become.

Figure 24 also indicates that the distance between the walls and the closest vanes is not too important from the viewpoint of making the correct turn. The spacing-chord ratio is constant in Figs. 24a, 24b, and 24c, but in Fig. 24b there is approximately one-half space between the end vanes and walls while in the other two there is a full space. Yet these three photographs make as continuous a group as either Figs. 24d, 24e, and 24f or Figs. 24g, 24h, and 24i, neither of which has had a change in end conditions. The same conclusion may be reached in Fig. 45 by comparing run 10 with run 10A.

Another factor in velocity distribution is apparent in Figs. 23b, 23d, 23f, and Fig. 25. The walls at the ends of the vanes induce a three-dimensional effect somewhat similar to the double spiral which occurs in a radius elbow. Since in these experiments the aspect ratio is moderately large and the vane surface is of short length, the spirals do not penetrate to mid-depth, and the flow is purely two dimensional in most of that region. At the

inside wall where the wall surface continues further, the spirals penetrate somewhat more toward mid-depth as may be seen from Fig. 23f. The formation of the spirals has been explained in a previous project report [2] . The spiral phenomena in guide vanes has been discussed previously by Klein, Tupper, and Green [19] .

Using observations of threads, air bubbles and dyed liquid as guides, the general form of the boundary streamlines has been sketched in Fig. 104. The pronounced overturning of the layer near the top and bottom boundaries is characteristic of all the vanes tested and is shown photographically in Fig. 25. However, this is a very narrow layer, about 1/4 in. thick, just downstream from the vanes, as shown by the hot wire anemometer readings in Fig. 54. The overturned layer persists for some distance downstream as may be recognized in the measurements at stations K-K and M-M, but it has generally disappeared at station P-P. The contrary effect of underturning occurs at about two vane spaces toward mid-depth from each end wall and near only the inside wall. This is the approximate depth to which the spirals penetrate. The underturning is small but recognizable in the measurements at station K-K for most runs; it is not definitely recognizable at station M-M except in a few instances. The overall turning effect of the guide vane cascades in these experiments is a composition of the normal two-dimensional turn and the overturning and underturning resulting from the three-dimensional effects.

It is apparent that if the aspect ratio of the spaces between the vanes were made much smaller than in this experiment (about four or smaller) the double spirals would affect the entire flow and no reasonable measurements could be had. On the other hand, by making the aspect ratio larger the two-dimensional flow may be made to govern throughout most of the bend.

Inspection of the various velocity distribution diagrams in Figs. 26 to 53 shows that the distribution downstream from the cascade is appreciably different from that upstream. A part of the difference is caused by normal boundary layer growth along the walls between measuring stations. Another part may be attributed to the failure of the elbow walls, particularly the inside walls, to follow the cascade streamline pattern. The remainder is a result of the three-dimensional effects just discussed. That close uniformity of the velocity distribution exists in the two-dimensional region just downstream from the vanes is seen in the hot wire data, Fig. 54.

An interesting comparison is drawn in Fig. 46 for the cascade of (21)300 vanes at s/c = 0.333. The total head and velocity distribution is smoother behind the cascade of long chord vanes than behind the cascade of normal chord vanes, the vane Reynolds number remaining constant. A similar comparison could have been made between run 370s and runs 73 or 170 for the (30)400 vanes where the cascade of normal chord vanes gives a smoother distribution than a cascade of short chord vanes. The reason for this is not immediately apparent; it would seem that other factors being fixed as they are in these experiments, a smaller chord would produce a larger aspect ratio and larger relative number of vanes, which in turn would result in a reduction in three-dimensional effects and in a smoother distribution. Possibly the scale of turbulence produced by the vanes has a bearing on the matter. Another comparison of similar type is found in Fig. 49 for the type I vanes. Although in this figure the two runs have different cascade characteristics, the result of the comparison is the same as that for the other runs.

In using the cascade of type I vanes at s/c = 0.48 in a large water tunnel bend, for which velocity data are plotted in Fig. 102, some improvement in smoothness of distribution over that in the small experimental bend is noticeable. Velocity distribution for the same cascade in the experimental elbow may be found in Fig. 45. The improvement may be attributed to the reduction in three-dimensional effects resulting from the increased aspect ratio and decreased importance of the walls.

B. Stagger Angle and Trailing Edge Angle

The criteria stated on page 22 were used to select the run with the correct stagger angle for each cascade. At first only those runs involving uniform approach velocity and the Reynolds number of approximately 1.5×10^5 were considered in this process. Interpolation between runs was resorted to when no single run gave the correct stagger angle. In some cases, choosing the correct stagger angle was a matter of compromise between the values indicated by the several criteria, and in those cases the error in stagger angle may be as large as 1° or $1\frac{1}{2}^\circ$. In most cases, however, the maximum error in stagger angle probably does not exceed $1/2^\circ$ since this is the sensitivity of most of the tests. The validity of the reasoning, which led to the criteria on page 22, is verified by the coordination obtained between the several criteria, especially in view of the small number of vanes used in each cascade.

Applying the criteria of Part II, Section H to the experimental data involved the following steps:

1. The first and easiest application was to observe air bubbles in water approaching and leaving the vanes in the plane of the bend near mid-depth as shown in Fig. 24. Although photographs like Fig. 24 were not made in each case, the bubbles were observed for every run. This test was sensitive to about the closest two degrees without photographs and probably to the closest degree with photographs.

2. The wall pressures at the mid-depth plane (Figs. 55 to 75) were examined next since of all measured data they could be most readily obtained. If, in accordance with the criterion, the normal pressure gradient for pipe flow appeared to exist on both sides of the cascade, this was evidence of having obtained almost the correct stagger angle. This test was particularly sensitive upstream from the cascade. A change in stagger angle of only $1/2^{\circ}$ caused a recognizable change in the pressure distribution. Figure 62 of the (21)300 vane at $s/c = 0.333$ for which the correct stagger angle was determined to be 104°, may be examined as an example. This test gave reasonable results even when the elbow wall shape was unsuitable for the vane profile.

The wall reaction on the fluid at the mid-depth plane as found by integration of the wall pressures was considered in conjunction with examination of the wall pressure distribution. According to the criterion, the wall reaction should be between zero and one times the required reaction on one vane at the correct stagger angle. The integrated wall reaction is given in the pressure diagrams and the required vane reaction is given by Eq. (1). Inspections of the integrated values show that in all but a few cases this criterion agrees with the other criteria. The discrepancies might be attributed to very poor wall shape at the turn or to small errors in setting the stagger angle of the outer vanes.

3. Criterion of vane reaction was applied to thick vanes where vane surface pressures were available. Since the velocity was distributed almost uniformly across the width of the channel, the vanes must be loaded equally when the cascade has the proper stagger angle. On this basis, the pressure at corresponding points on all the vanes

must be the same. Figure 76, taken from an earlier report [17], is a representative comparison of this type. Similar comparisons were made for other runs by inspection of the original data which are not presented here. This test was very sensitive, so much so that in a few cases no reasonable results could be obtained because of small discrepancies in location of piezometer taps on adjacent vanes.

The developed C_R of the thick vanes is given in the vane pressure diagrams (Figs. 77 to 87) and may be compared with the required C_R (= 2 s/c). Because of wall effects discussed in Part II, Section G, the agreement is not satisfactory for the cascades with a small number of vanes.

4. The next criterion involves examination of the velocity and total head distribution downstream of the cascade. Consideration of the two-dimensional region near mid-depth is not entirely sufficient for this purpose as was explained on page 48. However, it was considered unduly laborious to reproduce all the original data; therefore, the mid-depth distributions are contained in Figs. 26 to 44. For the small number of vanes per cascade used in these experiments, this test is not very sensitive because the walls are relatively important. Even so, once the correct stagger angle has been determined by other means, comparison of the velocity and energy distributions readily verifies the determination. In this connection, Fig. 47 for the (30)500 vane is a good comparison of slightly overturned and correctly turned flow. The correct stagger angle for this cascade was determined to be 95°.

5. The last criterion is also quite sensitive in most cases. It involves examination of the energy loss gradient (Figs. 88 to 101). In the energy diagrams it is apparent that in most cases one stagger angle gives a rate of energy loss between stations K-K and M-M or P-P that is about the same as the loss in a straight pipe, and that the others give a greater rate of loss in this region. Obviously that one stagger angle is the correct one since it is the only one which has not appreciably disturbed the flow. (The effect of stagger angle or angle of attack on individual vane resistance is indicated approximately by the rate of energy loss between stations D-D and K-K.)

In Fig. 105, the stagger angle determined as described above has been plotted against spacing-chord ratio for each cascade tested at the Reynolds number of 1.5×10^5. For each vane shape, these plotted points have been connected by a straight line or lines showing the variation of θ with s/c. The breaks in the lines apparently occur at the critical value of s/c and any reduction in s/c below this value requires no further change in θ. All of the points for each shape fall on the same line regardless of chord length or arrangement of spaces between the end vanes and walls. The curves show clearly that above the critical s/c, an increase in s/c must be accompanied by an increase in θ; the rate of increase in θ is about 1° to $1\frac{1}{2}^\circ$ for a one-tenth increase in s/c for the thin vanes, and as much as 3° or 4° for the thick ones. The cascade characteristics given in Fig. 105 should be applicable for design purposes for cascades of vanes of the shapes given at the Reynolds number of 1.5×10^5 regardless of scale.

The data of Fig. 105 have been replotted in Fig. 106a as curves of trailing edge angle ϕ against s/c. The values of ϕ have been determined by applying to the values of θ the angle β_2, which is fixed at 135° in these experiments, and the angle of the tangent at the trailing edge of the vanes which is given in Table VII. The critical s/c, where it has been reached, is seen to occur at $\phi = 0^\circ$ except in the case of the (30)500 vane where $\phi = 10^\circ$. Since only three points were obtained on the curve for (30)500 vanes, the result might be attributed to experimental error or to other unexplained causes.

Three points for cascades of vanes somewhat similar to those used in these experiments have been selected from the experiments reviewed in Part III, and have also been plotted in Fig. 106a. The data for these points have been obtained from Table V. The Klein, Tupper, and Green no. 5 vane which is closely related to the type I vane yields a point which falls nearly on the prolongation of the type I vane line and the Krober vane, which is closely related to the (30)400 vane, falls nearly on the (30)400 vane line. However, the Klein Tupper, and Green no. 3 vane does not agree at all with the curve for the (30)500 vane which it most closely resembles. The former vane is composed of a circular arc with two equal tangents while the latter is made up of two parabolic arcs. Consequently, even though both have the same maximum camber and location of maximum camber, they are of considerably different shape, which may account for the difference in results as explained later. The other two vanes are more closely related to those tested in this program.

Comparing the cascades of thick vanes in Fig. 106a it is apparent that the change from the type I vane (approximately a (21)515 shape) to the (21)315 vane has moved the critical s/c from about 0.38 to about 0.43, and has reduced the rate of change of θ with s/c. This change must be attributed to the moving of the location of maximum camber toward the nose in the (21)315. The change from the type II vane (approximately a (17)315 shape) to the (21)315 vane has produced almost the same change in the critical s/c but the change must now be attributed to the increase in camber of the (21)315. The change from the type I vane to the type II has scarcely influenced the curves of Fig. 106a, indicating that the larger camber in the former and the location of maximum camber nearer the nose in the latter are counterbalancing effects. Further comparisons may be made with the thick Collar vanes, data for which appear in Table V, Part III; with more camber than the experimental vanes the Collar vanes appear to have a still higher critical s/c.

A comparison of thick and thin vanes in cascade is given by the (21)300 and (21)315 curves. Apparently thickness has practically no effect on ϕ or θ since the curves are so nearly alike. This was to be expected from the discussion in Part II, Section D where it was noted that thickness should have only a small effect on the developed C_R of a vane when $\theta \approx 90^\circ$. A comparison of the (21)300 vanes with the (30)300 vanes shows the effect of maximum camber. Apparently an increase in maximum camber reduces the critical s/c, but this is in opposition to the conclusions previously reached and confirmed in Part III, Section A. The apparent discrepancy is explained by the following reasoning: With a cascade of vanes made up of circular arc and tangent sections like those used by Klein, Tupper, and Green, the camber of the vanes may be increased without changing the directions of the tangents at the leading and trailing edges as may be seen in Fig. 5 (so long as the camber is 21 per cent or more). This is not true of parabolic arc sections as may be seen in Fig. 19. Thus, for a cascade of (21)300 vanes of circular arc section, the s/c being equal to the critical value, the camber could be increased to form a cascade of (30)300 vanes without changing the direction of the trailing edge tangent or affecting the conditions of flow at the leading edge, and the s/c could be increased above the previous critical without increase in ϕ. However, with parabolic arc sections, as soon as a change from (21)300 to (30)300 vanes is made, both the direction of the trailing edge tangent and the flow conditions at the leading edge are changed. To make ϕ equal to zero for the cascade of parabolic (30)300 vanes, a change in θ of about 10° from

its value for the parabolic (21)300 vanes would be required, but this would completely alter the symmetry of the two cascades. Thus there is no true basis for comparison between these parabolic vanes; circular arcs rather than parabolic sections would have been better in order to make a comparison of the effect of camber. The failure shown in Fig. 106a of the cascade of (30)500 vanes to give the same ϕ value at the same s/c as the cascade of Klein, Tupper, and Green no. 3 vanes may now be explained on the same basis.

A comparison of the effect of moving the location of maximum camber forward is obtained from the series of cascades made up of (30)500, (30)400 and (30)300 vanes. Moving the maximum camber forward reduces ϕ and apparently would produce a larger critical value of s/c. This same conclusion was previously reached in comparing the thick vane cascades and also in the review of previous experimental work in Part III.

C. Cascade Resistance

The loss due to the bend has already been defined as the total head loss around the bend less the loss due to an equivalent length of straight duct. It will be written $\zeta \frac{\bar{u}^2}{2g}$. For each cascade ζ is given by the difference in ordinates between the theoretical straight duct-loss curve and the actual loss curve for that cascade in the energy diagrams, Figs. 88 to 101. For uniformity, ζ has been measured at station M-M for all of the cascades in these experiments. Measurements which include station P-P indicate that for the correct stagger angle, there is little if any change in ζ beyond station M-M.

The experimental values of ζ have been plotted against s/c in Fig. 106b for each cascade at its correct stagger angle, at a Reynolds number of approximately 1.5×10^5. Original data are represented in the figure by the points without asterisks. Where interpolated values of the stagger angle were used, ζ was taken from the data for the stagger angle closest to the interpolated one. For this reason, some points may be in error by two or three per cent in ζ, but for the majority of the points the error should not exceed one per cent. Unlike the stagger angle data, there appears to be a variation in head loss for fixed cascade characteristics when the chord length or distance between the outside vanes and the walls is changed. The code introduced in connection with Table VI has been used in Fig. 106b to distinguish the data for different chord lengths and wall conditions. Thus, the letters L and

S indicate vanes with 4.25-in. and 2.02-in. chords, respectively, while the remaining vanes have the normal chord of approximately 2.83 inches. The letter A represents a cascade located in the bend so that the end vanes are quite near the walls as opposed to the usual location of a full space between the end vanes and walls.

According to the definition, ζ is not the excess loss due to cascade resistance alone. It includes losses from three-dimensional effects and also from poor velocity distribution at the inside and outside walls of the bend. It could be expected, therefore, that the additional losses would decrease with improving flow conditions produced by increasing aspect ratio and increasing relative number of vanes. This trend is apparently confirmed in comparing the ζ values for the cascade of type I vanes at s/c = 0.48 in these experiments, with the loss of the same cascade in the water tunnel experiments whose velocity distribution is given in Fig. 102. The value of ζ for the water tunnel cascade at a Reynolds number of about 1.4×10^5 is only 0.085 ± 0.02. This is materially less than the corresponding value of ζ for these experiments. On the other hand, two values of ζ for a cascade of (21)300 vanes at s/c = 0.333, one for a long chord and one for a normal chord, and two values of ζ for a cascade of (30)400 vanes at s/c = 0.467, one for a normal chord and one for a short chord, indicate the opposite trend. For these cascades, decreasing the chord and thereby increasing both the aspect ratio and the relative number of vanes has resulted in an apparent 20 per cent increase in loss at constant Reynolds number. On page 49 it was noted that decreasing the chord length resulted in poorer velocity and total head distribution and this probably accounts for a part of the additional head loss.

The discrepancy in head loss data at any given s/c is also partially attributable to the small number of vanes in the cascade and to the consequent importance of the boundary conditions. If 10 ducts similar to the experimental duct are placed side by side so as to make a duct of great width, and if a cascade of type I vanes, for example, at s/c = 0.48 is installed in this wide duct, there will be more vanes in the cascade than there would be in 10 cascades like those used in series 10 in the ratio 6/5 and there will be the same number as in 10 cascades like those used in series 10A. Hence, series 10 cascades have less surface area and less skin friction than series 10A cascades and also less area and skin friction than a cascade of the same spacing-chord ratio with many more vanes. It would appear, then, that series

10A gives the correct resistance for a much larger cascade than the one tested, and that series 10 resistance should be increased by approximately the above fraction to make it comparable to a larger cascade. This is true except for the increased resistance due to three-dimensional effects cited in the previous paragraph. Since most of the data recorded in Fig. 106b have been obtained for series like series 10, with nearly a full space between each end vane and wall, and since the resistance is probably high anyway because of three-dimensional effects, the value of ζ for series 10A has been reduced to a value comparable to series 10 by multiplying by 5/6. The resulting agreement is seen to be fair in Fig. 106b where the corrected point is identified by an asterisk. A similar correction has been applied to series 80SA for the (30)500 vane. In the case of the long and normal chord vanes of the (21)300 shape, the corrective fractions are 6/5 and 10/9, respectively; for the normal and short chord vanes of the (30)400 shape they are about 6/5 and 10/9, respectively. These corrections bring the two values closer together in each case and the remaining discrepancy is probably accounted for by the increase in resistance accompanying a decrease in chord length described in the previous paragraph. For purposes of estimating the relative values of ζ and the trends of these values for the experiments, all data have been reduced to the loss corresponding to the normal chord length. To accomplish this the measured ζ values have been arbitrarily increased or reduced, as the case may be, by 20 per cent from the other chord-length data. For the reasons just outlined, the values of ζ for the three additional points plotted in Fig. 106a are not directly comparable to those in these experiments and are not plotted in Fig. 106b.

For each vane shape and size, the points in Fig. 106b have been connected by straight lines to give the variation of ζ with s/c. Heavy lines have been used with original data and lighter lines with corrected data. The trend indicated by these lines shows clearly an abrupt decrease in ζ with increasing s/c until the critical value has been reached or exceeded and then a gradual increase in ζ with continued increase in s/c. Had the values of s/c been carried high enough to produce stalling, a more rapid increase in ζ would occur. The optimum cascade performance at each shape occurs near the point of minimum resistance. Estimated cascade characteristics for optimum performance for each of the shapes tested in this program are given in Table VIII, as closely as the data permit. These data are for a vane chord length

of approximately 3 in. used in a small cascade where both the duct walls and vane surfaces are smooth and the vane Reynolds number is about 1.5×10^5.

TABLE VIII

Cascade Characteristics for Optimum Performance

Vane Shape	s/c	θ, Degree	Relative ζ % (Approx.)
Type I	0.36 to 0.48	97 to 100	13
Type II	0.45	112	10
(21)315	0.50	105	11
(21)300	0.37 to 0.50	104 to 105	21
(30)300	0.52	99	21
(30)400	0.53	97.5	16
(30)500	0.55	95	16

It is interesting to observe that increased camber in thin vanes increased the optimum s/c and probably also decreased the resistance. The curves are not defined well enough to draw general conclusions as to the effect of shifting the location of maximum camber, but it appears that the (30)300 vane is less effective than either the (30)400 or (30)500. It also appears that moving the maximum camber location forward in the thick vanes as well as increasing the camber, was effective in increasing the optimum s/c and decreasing resistance. Decreasing resistance is caused at least in part by improved flow conditions near the leading edge resulting from the changes in camber and location of maximum camber as may be seen in Fig. 107.

The ζ values obtained with cascades in this miter bend may be compared with those in a radius elbow of the same cross section having a radius ratio (radius of curvature of the centerline of the duct divided by breadth of the duct) of two. An investigation of the latter elbow was previously reported [2] . At a duct Reynolds number of 4×10^5 (compared to 3×10^5 and 4.5×10^5 for the duct for most of the present experiments) ζ for the radius elbow was about 10.4. It must be noted, though, that the radius ratio of two is probably somewhat smaller than the optimum radius ratio and that for the most favorable radius ratio a value of ζ of approximately nine might have been

obtained. It may be concluded that properly designed guide vane cascades will give losses of about the same order of magnitude as the best radius elbow for the same duct.

D. Vane and Wall Pressure Distribution

Examination of the diagrams for pressure distribution on the vanes (Figs. 77-87) shows that the most favorable pressure gradients on the convex surfaces of the vanes occur for the type II vane at s/c = 0.45 (Figs. 82 and 83) and for the (21)315 vane at s/c = 0.5 (Fig. 86). These are the same cascades which give the smallest head losses.

As already noted, all wall and vane reaction computations were based on data obtained at the mid-depth plane. These data should be compared with those taken nearer the end walls to determine the influence of three-dimensional effects. Such a comparison of wall pressure data has been made for run 370 in Fig. 69 and for run 21 in Fig. 73. The comparison in Fig. 69 is typical of all runs at a duct Reynolds number of 3.0×10^5 and higher (vane Reynolds number of 1.5×10^5 and higher in most cases). At 1/2 in. from the end wall the side wall pressure distribution is very much the same as at mid-depth in spite of three-dimensional effects. The comparison in Fig. 73 is more typical of the runs at smaller Reynolds numbers and shows more important although still relatively small differences at 1/2 in. from the end walls.

A similar comparison for vane pressure distribution for the type I vane may be had from run 2 (Fig. 77) in which the pressure taps are at mid-depth and runs 1, 4, and 6 (Fig. 78), in which the pressure taps are approximately 3/8 in. from one end of the vanes. (It should be noted that these runs do not apply to the correct stagger angle for the cascade, but they are nevertheless informative.) At vane Reynolds numbers of about 1.5×10^5 and higher, the pressure distribution near the ends is very similar to that at mid-depth, but at lower Reynolds numbers, there is a decided decrease in vane load at 3/8 in. from the end. As the Reynolds number decreases, the duct boundary layer penetrates further from the ends of the vanes and produces the changes that have been observed. These data, together with that on page 48 on secondary current formation, indicate that at duct Reynolds numbers above 3×10^5 and vane Reynolds numbers above 1.5×10^5, the end effects can be practically disregarded and the vanes and walls may be assumed to be uniformly loaded from end to end. Even at considerably lower Reynolds numbers this is probably true.

As already observed, the vane loading of the thick vanes at the mid-depth plane as given in Figs. 77 to 87 does not agree with the theoretical value. In some of these figures the stagger angle is not the correct one for that cascade, and the discrepancy is accounted for by the unequal load distribution between vanes and the influence of the walls. For the remainder, the discrepancy is probably caused by the failure of the walls to carry the load of one vane so that the excess load must be divided among the small number of vanes in the cascade, as explained in Part II. As a check on the experimental data, the combined reaction of all the vanes (obtained by multiplying the reaction on the central vane by the number of vanes) and the walls was compared with the estimated change in pressure plus momentum through the cascade, and the agreement was found to be within 10 per cent except for the 110 and 130 series. The developed C_R of the thick vanes is not useful as a criterion of flow because of the discrepancies in vane loading. The wall reaction criterion is much more dependable with so few vanes.

A knowledge of the pressure distribution on the vanes is useful when determining the velocity and pressure which corresponds to incipient cavitation. The vane pressure diagrams, Figs. 77 to 87, give the distribution for the thick vanes. For the type I vane, the best anticavitation setting appears to be $s/c = 0.41$ and $\theta = 98^\circ$ where the maximum negative pressure is roughly $1.2\,\rho\,\frac{W_1^2}{2}$ below the local static pressure. For the (21)315 vane, $s/c = 0.50$ and $\theta = 105^\circ$ give a maximum negative dynamic pressure of about $1.3\,\rho\,\frac{W_1^2}{2}$, and about the same value is obtained with the type II vane at $s/c = 0.45$ and $\theta = 112^\circ$. As in the case of ordinary airfoils, the point of maximum negative pressure moves toward the nose with increasing θ or angle of attack.

Pressure distribution and the value of the maximum negative pressure on the thin vanes cannot be judged too well from the data for the thick vanes. However, a comparison of wall pressure readings on the inside wall of the bend for the (21)300 and (21)315 vanes indicates that the maximum negative pressures on a thin vane are less than on a thick vane, probably because of reduced restriction of the passage by the thin vanes. This statement is based on a comparison between run 40, (Fig. 61) and run 31, (Fig. 60) for the (21)300 and (21)315 vanes at $s/c = 0.50$ and $\theta = 105^\circ$. There is likely to be another negative pressure peak on the thin vanes near the leading edge, unless smooth flow is obtained at that point. The geometry of flow for the (21)300 vanes

at $\theta = 105^{\circ}$ (Fig. 107) indicates that the stagnation streamline would have to approach the leading edge on the concave side so that smooth flow would not be obtained. For the (30)500 vanes at $\theta = 95^{\circ}$ (s/c = 0.5 to 0.6), however, the leading edge tangent is in line with the approaching flow and smooth flow without a high negative peak is probably obtained.

By plotting the pressure distribution on the thick vanes on a line normal to the chord, integrating the pressure, and combining this result with the integrated pressure from Figs. 77 to 87, the line of action of the resultant pressure was obtained. The line of action is plotted in the diagrams of vane pressure distribution, Figs. 77 to 87, for several of the runs. The center of pressure for the type I vanes in cascade is just over 35 per cent of the chord from the leading edge, while that for the type II and (21)315 vanes is more nearly 30 per cent. With one or two exceptions, the lines of action are nearly parallel to the miter line, a result anticipated in Part II, Section B.

E. Effects of Reynolds Number and Scale Effect

The preceding analysis, for the most part, has been confined to that data obtained at a vane Reynolds number of about 1.5×10^5. It was tacitly assumed that on this basis similarity between the various runs would be obtained. That similarity was obtained, at least insofar as stagger angle is concerned, was shown on page 52. A further proof of similarity is contained in Fig. 48 for runs 41 and 42 for the (21)300 vane. Air and water, respectively, were used as fluids in these runs. A constant vane Reynolds number of 1.5×10^5 was used, and constant cascade characteristics were used (although the stagger angle was not the correct one for the cascade). The two runs are seen to produce almost identical velocity patterns; they also produce the same head loss as may be seen in Fig. 95 and the same pressure distribution on the walls around the bend. Runs 2 and 3 for the type I vane using water and air, respectively, at constant Reynolds number and constant cascade characteristics (but again the incorrect stagger angle) are also practically identical in all respects. This may be seen in Figs. 26, 55, 77, and 88.

On the other hand, it was pointed out on page 54 that there is a variation of ζ with chord length, the Reynolds number and all cascade characteristics being constant. It is seen that if the vane Reynolds number and fluid viscosity are constant and the chord length decreases, the velocity of

flow, and hence the duct Reynolds number in a fixed bend must increase. However, the increase in duct Reynolds number could not be expected to produce the increase in ζ shown by the data; the opposite should be the case. The variation in ζ may be attributable to the scale of the turbulence generated by the vanes as pointed out previously. In any event, the smaller values of ζ appear to accompany the smoother flow. It was also noted that, other things being equal, ζ would vary with the size of the bend. These considerations lead to the conclusion that to obtain complete similarity between two cascades, the cascades and the flow must be identical in every respect, except possibly when the two cascades each have long chords and a large number of vanes. If exact resistance values are not too important, as is frequently the case, similarity may be obtained between two cascades by using identical cascade characteristics and vane Reynolds numbers, regardless of chord length or number of vanes.

As the vane Reynolds number changed from the constant value of 1.5×10^5, some changes in the performance of the cascades were noticeable. The Reynolds number runs were made on the thick vanes only, so that the effect on vane pressure distribution, as well as the other effects, could be studied. Series 10 and 310 for the type I vanes, 20 and 120 for the type II vanes, and 30 and 130 for the (21)315 vanes contained runs at Reynolds numbers other than 1.5×10^5. All of the Reynolds number runs, except those for the 30 series, were made at constant stagger angle equal or nearly equal to the correct stagger angle at $Re = 1.5 \times 10^5$. For the 30 series, a high Reynolds number run, run 32, was made at a stagger angle 2.5° less than that corresponding to the correct angle at $Re = 1.5 \times 10^5$.

Figure 50 contains the total head and velocity distribution diagrams for the cascade of type I vanes at $s/c = 0.32$ at a low and at a high Reynolds number, runs 312 and 314, respectively. These may be compared with run 311 (Fig. 49) at the same cascade characteristics and the normal Reynolds number of 1.5×10^5. This comparison, together with those for wall and vane pressure distribution and for energy loss (Figs. 57, 72, 81, and 90), show that neither the low nor the high Reynolds number runs give perfect performance. Run 314, the high Reynolds number run, is quite like run 311, the medium Reynolds number run, but it does not satisfy the energy loss criterion (Fig. 90). Run 312, the low Reynolds number run, does not give as smooth a velocity and total head distribution as run 311, and it develops both a high wall loading

and a higher vane loading at the mid-depth planes. The higher loadings at mid-depth may be explained by the fact that the boundary layer penetrates more toward mid-depth resulting in lower loading at the vane ends as explained previously. It may be concluded that for the type I vanes at s/c = 0.32, $\theta = 97^{\circ}$ is close to the correct stagger angle for all Reynolds numbers between 0.7 and 3.0×10^5, although the smoothness of the flow is more disturbed at the lower Reynolds number. The disturbance to the smoothness may be a duct wall effect which would be eliminated in a large installation.

A similar comparison for the type I vane cascade at s/c = 0.48 leads to the same results; namely, that stagger angle is not affected by Reynolds number changes within the range of the tests, although the high and low Reynolds number runs do not satisfy all of the criteria quite as well as the medium Reynolds number run. For the type II vane cascades, discrepancies very similar to those just described also occur, but again no change is warranted in stagger angle within the range of Reynolds numbers that were tested. For the (21)315 vane cascade at s/c = 0.43 there are no detectable discrepancies between Reynolds number runs within the range from 0.7 to 4.0×10^5. For the (21)315 cascade at s/c = 0.50, a high Reynolds number run (run 32) at a smaller stagger angle than the correct one for the medium Reynolds number shows definite underturning, although the energy grade line criterion appears to be satisfied (Fig. 94). The general conclusion to be drawn from these runs is that the stagger angle setting within the range of Reynolds numbers from about 0.6×10^5 to about 4.0×10^5 is a constant. This conclusion is in disagreement with Collar's results given in Table II, Part II where a variation of turning angle with Reynolds number is shown. However, it should be observed that the variation in turning angle as measured by Collar is fairly small to begin with; also, the variation is not necessarily equal to the change required in θ for a constant turning angle, so that the actual change in θ with Reynolds number for constant turning angle in Collar's experiments may be within the limits of error of the present experiments. The variation is small enough, in any event, to be disregarded in most practical installations.

In Fig. 108 the variation of ζ with Reynolds number has been plotted for the cascades just discussed. The similarity in pattern for each vane shape, regardless of the spacing-chord ratio, is striking. For all the cascades there appears to be a general decrease in resistance to a point near $Re = 1.5 \times 10^5$, but beyond this point while the resistance of the (21)315

cascades continues to decrease, that for the type I and type II cascades increases slightly. Collar's data quoted in Table II, which extends only to a Reynolds number of 1.8×10^5, agree well with the present data in slope of the ζ curve, if not in absolute magnitude. Since the ζ curves for any given vane shape are similar, the optimum cascade characteristics determined at the Reynolds number of 1.5×10^5 should be applicable to all other Reynolds numbers, at least within the range of the experiments.

The change in slope of the curves beyond $Re = 1.5 \times 10^5$ is probably a function of the development of the vane boundary layers. It was shown in a previous project report [17] that at $Re = 1.5 \times 10^5$, the boundary layer for the type I vanes in cascade at $s/c = 0.48$ was probably turbulent and was just on the verge of separation at the trailing edge. There was, therefore, no room for improvement of flow with increasing Reynolds numbers as is confirmed in Fig. 108. On the other hand, for the (21)315 vanes in cascade, there appears to be a continued improvement in flow in the boundary layer up to $Re = 4.0 \times 10^5$.

Wall and vane pressure distribution also show some changes with Reynolds number. Of course, as the Reynolds number increases, the pressure gradient in the duct between measuring stations decreases and it is this change which causes the wall pressure distribution to change. The same factor contributes to a pressure variation at the trailing edges of the vanes as the Reynolds number changes.

Below a Reynolds number of 1.5×10^5 the vane pressure distribution on the convex sides of the type I vanes tends to be flattened; that is, the negative peak pressure is not so great but the low pressure region extends further back on the vanes. This is another manifestation of boundary layer behavior wherein the failure to reach a negative peak may be attributed to separation of the laminar boundary layer and return as a turbulent layer at low Reynolds numbers. The phenomenon may be seen by comparing Figs. 77 and 79 for the cascade at $s/c = 0.48$ and by comparing the Reynolds number points in Fig. 81 for the cascade at $s/c = 0.32$. If the same phenomenon were to occur at $s/c = 0.41$ (run 110), the resulting cascade would be desirable from the anticavitation viewpoint as it would have a maximum negative pressure coefficient very little greater than unity. Above $Re = 1.5 \times 10^5$, the type I vane shows no significant pressure changes. On the other hand, the vanes of the other cascades show no regular changes in pressure distribution with

Reynolds number except the decrease in pressure near the trailing edge with decreasing Reynolds number already mentioned above.

F. Other Factors in Cascade Design

Data showing effect on cascade performance of circular rather than square duct sections has already been presented in the preceding pages and also in a previous project report [17], as well as in some work by others reviewed in Part III of this report. As shown in Fig. 102, the type I vane cascade at $s/c = 0.48$ and $\theta = 100^{\circ}$ gives good results in the circular duct of a model water tunnel. The general conclusion already reached in Part II, that duct cross section is unimportant as long as the stagger angle is correct, is undoubtedly warranted.

The effect of the insertion of obstacles, such as shafts and stiffeners, between the vanes has also been considered to some extent. Figure 102 shows the distortion of the velocity profiles resulting from the insertion of an unfaired shaft through a cascade along the axis of the downstream duct; an overturning of the flow is apparent.

Stiffening struts were placed between the vanes in runs 44L and 45L for the (21)300 vane cascade at $s/c = 0.333$, and in run 28 for the type II vane cascade at $s/c = 0.45$. The arrangement and shape of these struts is shown in Figs. 51 and 52. (The stagger angle in Fig. 52 is 2° greater than the correct angle for this cascade.) A comparison of run 44L (Fig. 51) with run 46L (Fig. 46) for the same cascade without struts, shows that the single strut at the trailing edge of the vanes had very little effect on either velocity distribution or total head distribution. Figure 97 shows that it gave about the same loss as the cascade without struts. On the other hand, the use of two struts both in run 45L and in run 28 resulted in pronounced flattening of the velocity and total head profiles downstream of the cascades, in the creation of prominent secondary currents, and in an appreciable increase in head loss as may be seen in Figs. 97 and 91, respectively. Furthermore, in the case of run 45L, the flow downstream from the cascade has been disturbed sufficiently to produce an energy gradient steeper than normal. In the case of run 28, the flow was disturbed so that the energy gradient was normal where it had previously been too steep. No runs were made with continuous sheet spacers or with strut spacers near the leading edges of the vanes. The latter were considered undesirable because of the creation of negative pressure peaks

which might lead to local separation or cavitation and which in turn would greatly disturb the flow in these small cascades. The former were not usable in the experimental bend because of the resultant reduction in aspect ratio of the space between the vanes. However, some results for a continuous sheet spacer taken from the model water tunnel data are shown in Fig. 103. Unfortunately, the bend from which the data in Fig. 103 are taken follows a diffuser and the effects of a diffusing flow are superimposed on the effects of the spacer. In any event, the sheet spacer appears to give as satisfactory velocity distribution as the struts used in the present experiments. The loss for the sheet spacer could not be measured without including losses from the diffusing flow and therefore is not included.

The three-dimensional effects from sheet spacers are no more than those from two ordinary end walls, so that as long as the aspect ratio of the space between vanes is sufficiently large, such sheet spacers need not be considered undesirable. They should be particularly valuable for fairing a shaft in an installation like that shown in Fig. 102. It is probably desirable for both the leading and trailing edges of the spacer to be constructed parallel to the cascade axis rather than to use the design shown in Fig. 103. Such construction would provide a uniform increase in resistance to the flow approaching each vane and would probably increase the loss in the cascade by a small amount. For stiffening purposes, struts are probably less difficult to employ than continuous sheet spacers and the data appear to warrant their use at the trailing edges of the vanes in cascade. Whether the use of struts near the leading edge would be justified remains to be determined, but they would undoubtedly create large disturbances as did the struts near the centers of the vanes.

The effect of a distorted velocity profile on cascade performance has also been examined. In Fig. 103, as previously mentioned, the combined effect of a sheet spacer and a diffuser flow is shown. In spite of both these variations from normal conditions, the turn appears to be good. An especially distorted velocity profile was used with the cascade of type II vanes at $s/c = 0.45$ in run 27, as shown in Fig. 53. The stagger angle for run 27 is the same as that for run 26, and is about 2° too large for the normal profile, but whether it is too large for this distorted profile is not so certain. Examination of the pressure distribution on a central vane, shown in Fig. 82, shows a tendency toward the distribution accompanying smaller values of the

stagger angle. The velocity pattern behind the cascade is not good. Whether a better pattern could be obtained with another stagger angle is not known without further experimentation. It is remarkable that the secondary currents downstream from the cascade are as small as they are.

VI. CONCLUSIONS

A. Design of Guide Vane Cascades

The analysis presented in Part II, the review of the work by others in Part III, and the present experiments have produced the following points relative to design of guide vane cascades in miter bends:

1. If ideal velocity and pressure distribution are not required, there is considerable latitude in choosing cascade characteristics. For a given cascade, a variation from optimum conditions of 2° or 3° in stagger angle, or of 0.05 in spacing-chord ratio, or both, is not serious. Similarly, a variation of shape by 3 to 5 per cent in thickness or in maximum camber, or by 10 per cent in location of maximum camber, produces relatively small changes.

2. If the best possible cascade performance is desired, it is necessary to determine optimum cascade characteristics. This cannot be done as yet for an arbitrary cascade. However, optimum characteristics for the cascades examined in the present experiments are summarized in the next section of this report.

3. If resistance is not important, the following rough rules may be used for designing a cascade to produce a given turn:

   (a) For any given vane shape in cascade there exists a critical value of the spacing-chord ratio. At or below the critical value a given turn may be produced by installing the cascade so that the tangents to the trailing edges of the vanes point in the downstream direction. For 90° bends and vane shapes of adequate camber, the critical spacing-chord ratio is about 0.3 or larger, the larger values applying to the better shapes. If a spacing-chord ratio too far below the critical is chosen, the resistance will be very large and the flow may be slightly overturned. If a ratio much above the critical is chosen,

the flow will be considerably underturned when the trailing edge tangent points in the required downstream direction.

(b) To produce a turn with a guide vane cascade it is necessary to develop a certain reaction in each vane. With the trailing edge tangent of the vanes fixed in the downstream direction, the reaction is principally dependent on the maximum camber of the vanes. For 90° bends the maximum camber should be between 20 and 30 per cent of the chord length, the smaller camber applying to the thicker vanes. For 30° bends 10 per cent is probably adequate.

(c) For such rough design, the exact vane shape is not too important, but it is desirable to have a length of straight tangent near the trailing edge. Shapes made up entirely of circular arc and tangent sections are satisfactory and easy to fabricate. For a 90° bend and thin guide vane shapes made up of a 90° circular arc and two equal tangents, the critical spacing-chord ratio is 0.2 for 20 per cent camber and increases 0.1 for each 2 per cent increase in camber up to at least 30 per cent camber.

(d) The minimum resistance for a cascade designed by these rules will occur for faired vanes of some thickness whose leading edge tangent is approximately parallel to the approaching flow. This resistance will not be the least obtainable from the given vane shape, however, since the optimum value of s/c may be quite different from the one selected and may occur when the trailing edge tangent does not point in the downstream direction.

4. In installing a well designed cascade in a miter bend, there will always be some interference from the bend walls. The installation should be made so as to keep the interference effects at a minimum. This may be done by observing two precautions:

(a) The use of a large number of vanes in the cascade (perhaps 10 or more).

(b) The use of walls which follow homologous streamlines of the flow. (This requirement would probably be satisfied with sufficient approximation by making the walls the same shape as the vane mean line and, in a rectangular duct, placing them about one-half vane space each side of the outside vanes of the cascade.)

5. Even with optimum cascade characteristics the resistance of a cascade will be altered by changing the chord length, the size of the installation, or the Reynolds number of the flow. In general, larger chord length and larger installations give smaller resistance. There is an optimum Reynolds number below which the resistance increases rapidly and above which the resistance increases slowly. This optimum is probably 1.5×10^5 or more, based on chord length as a length parameter; it depends on the vane shape.

6. The cross-sectional shape of a duct does not affect guide vane cascade performance. The form of the velocity profile approaching the cascade may have some effect on performance, but with a profile typical of a diffuser flow, no bad effects were observed.

7. When it is necessary to pass an obstruction such as a drive shaft through a cascade, a faired splitter similar to that shown in Fig. 103 but with leading edge parallel to the cascade axis, should be used to house the obstruction. When it is necessary to brace the vanes against buckling or excessive vibration, a faired splitter like that just mentioned or a strut across the trailing edges of the vanes would be satisfactory. The effect of a strut across the leading edges was not determined.

For model testing of a confined guide vane cascade, dynamic similarity is obtainable only by exact duplication of the prototype installation. However, if the exact resistance is not required in the tests, similarity is obtained when the two cascades have the same characteristics (profile shape, stagger angle, and spacing-chord ratio) and are operated at the same vane Reynolds number; the chord length and size of the installation are then immaterial.

In checking the performance of model cascades, or of prototype cascades also, it is not always possible to determine whether the cascade is

giving its best performance by making a velocity traverse at some point downstream. The following criteria have been developed for judging cascade performance in a uniform velocity field. They are given in order of ease of application and sensitivity.

1. The pressure gradient measured along the duct walls in a plane near mid-depth of the vanes should be very similar to the normal gradient in a straight duct, particularly upstream from the cascade. Excessive pressure drop on the outside wall generally indicates overturning and pressure rise indicates underturning.

2. The above pressures, when integrated over the duct walls and imaginary walls across the duct upstream and downstream from the cascade, should give a wall reaction per unit depth between zero and the load of one vane (given in subparagraph 4, below). The exact wall load depends on the shape of the walls and the space between the end vanes and the walls. Excessive wall load indicates underturning and deficient wall load indicates overturning.

3. The pressures at corresponding points on several vanes of the cascade should be equal. Lower pressures on the inside vanes indicate underturning and lower pressures on the outside vanes indicate overturning.

4. For cascades with many vanes, the integrated pressure around one vane should be $2s\,\rho\,\frac{W_1^2}{2}\,\sin\Delta$ per unit span. Excessive loading indicates overturning and deficient loading indicates underturning. This criterion should not be applied to a cascade with only a few guide vanes unless the walls have been very carefully designed.

5. The total head or energy loss gradient within about 10 chord lengths behind the cascade should be close to the gradient for a straight duct.

6. Except for a small fraction of a chord length either side of the cascade, the directions of the flow streamlines, particularly before the cascade, must be parallel to the duct walls. Overturning is indicated by streamlines bent toward the outside wall and underturning by those bent toward the inside wall.

B. Recommended Cascades for 90° Miter Bends

Optimum cascade characteristics for the vane shapes examined in this investigation are given in Table VIII, page 57, of this paper. Combining these results with those of other investigators which have been reviewed in Part III, the following cascades are especially recommended for use in 90° miter bends of constant cross section:

1. Thick sections

(a) (21)315 vane shape, s/c = 0.50, θ = 105°

At a vane Reynolds number of about 1.5 x 10^5 in a large cascade, the head loss should be 10 per cent or less of the entrance velocity head, and it should decrease with further increase in Reynolds number. This vane shape is particularly valuable for flows with variable Reynolds numbers since it shows the greatest stability in velocity distribution with change in Reynolds number. It also gives a low negative pressure peak, about 1.3 stagnation pressures below the local static pressure as compared to 1.5 and more for some of the other cascades tested. (With further experimentation it should be possible to extend the useful range of this shape to higher values of s/c.)

(b) Collar's section "C" [21], s/c = 0.56, θ = 100°

At a vane Reynolds number of about 1.8 x 10^5 in a large cascade, the head loss is about 5 per cent of the entrance velocity head when the cascade is unconfined by walls.

2. Thin sections

(a) Krober no. 1 shape [10], s/c = 0.47, θ = 101.5°

A head loss of about 13 per cent of the entrance velocity head is to be expected with this cascade at a vane Reynolds number of about 1 x 10^5.

(b) Klein, Tupper, and Green no. 3 shape [19], s/c = 0.5, θ = 90°

In a large cascade using long chord length vanes at a Reynolds number of about 2 x 10^5, a head loss of 20 per cent or less of the entrance velocity head may be expected.

C. Additional Research Required

It is probable that the cascades discussed in the preceding section of this report are as effective for general use in 90° miter bends of constant cross section as any that will be developed in the future. This paper has left some old questions unanswered and has raised some new ones with regard to the employment of cascades, that must be answered by additional research. Fields for future research fall into several groups:

1. Experiments of the type conducted in this investigation should be continued in order to establish more definitely the relation between guide vane shape parameters and optimum cascade characteristics. In particular, an effort should be made to find the vane shape that permits the use of a maximum spacing-chord ratio with a reasonably small resistance. A cascade made up of such shapes would be relatively inexpensive to make and it would also permit the passage of water carrying detritus.

2. The effect of chord length and number of vanes in a cascade on resistance must be more definitely established and explained.

3. The effect of vane roughness and duct wall roughness is yet to be investigated.

4. Experiments on the effects of struts and splitters, as well as distorted entrance velocity profiles should be carried a little further.

5. Sufficient research on bends of other than 90° deflection should be conducted to establish the effect of deflection angle on the required cascade characteristics.

6. An investigation of the use of cascades in combination with expanding or contracting flow should be conducted. Such cascades would be useful in water and wind tunnel design.

7. An attempt should be made to correlate such theoretical design methods as those of Garrick [5] and Mutterperl [6] with the results obtained in the present experiments. If reasonable correlation can be obtained it will be possible to design cascades for various deflection angles without resorting to further experiment. It will also be possible to compute the negative pressure peaks when the cavitation index must be determined.

In conducting research in the future it should be possible to improve upon the apparatus used in these experiments and, thereby, to increase both the reliability and speed of the work. The following improvements are suggested:

1. Some comparative experiments should be made between results obtained in the present apparatus and those obtainable with the same cascades in a free discharge of air. If the results are comparable, the test stand should be redesigned to use air only at vane Reynolds numbers varying from about 0.5 to 4.0 x 10^5. The discharge of air should be free to the atmosphere beyond the cascade, and the bend walls at the cascade should be flexible to permit adjustment for vane shape. The miter line of the bend should be long enough to permit the use of a minimum of 10 vanes in cascade. The same criteria as outlined in Part VI, Section A3, would govern the experiments, but determination of the pressure gradient and energy-loss gradient downstream from the cascade would be unnecessary.

2. Thin vane shapes used in future research should be confined to combinations of circular arcs and straight tangents. The length of both tangents could be varied, separately or together, to obtain changes in maximum camber and location of maximum camber. Thick vane shapes may be based on the above thin vanes as mean lines or on the NACA four-digit series as in these experiments.

LIST OF ILLUSTRATIONS

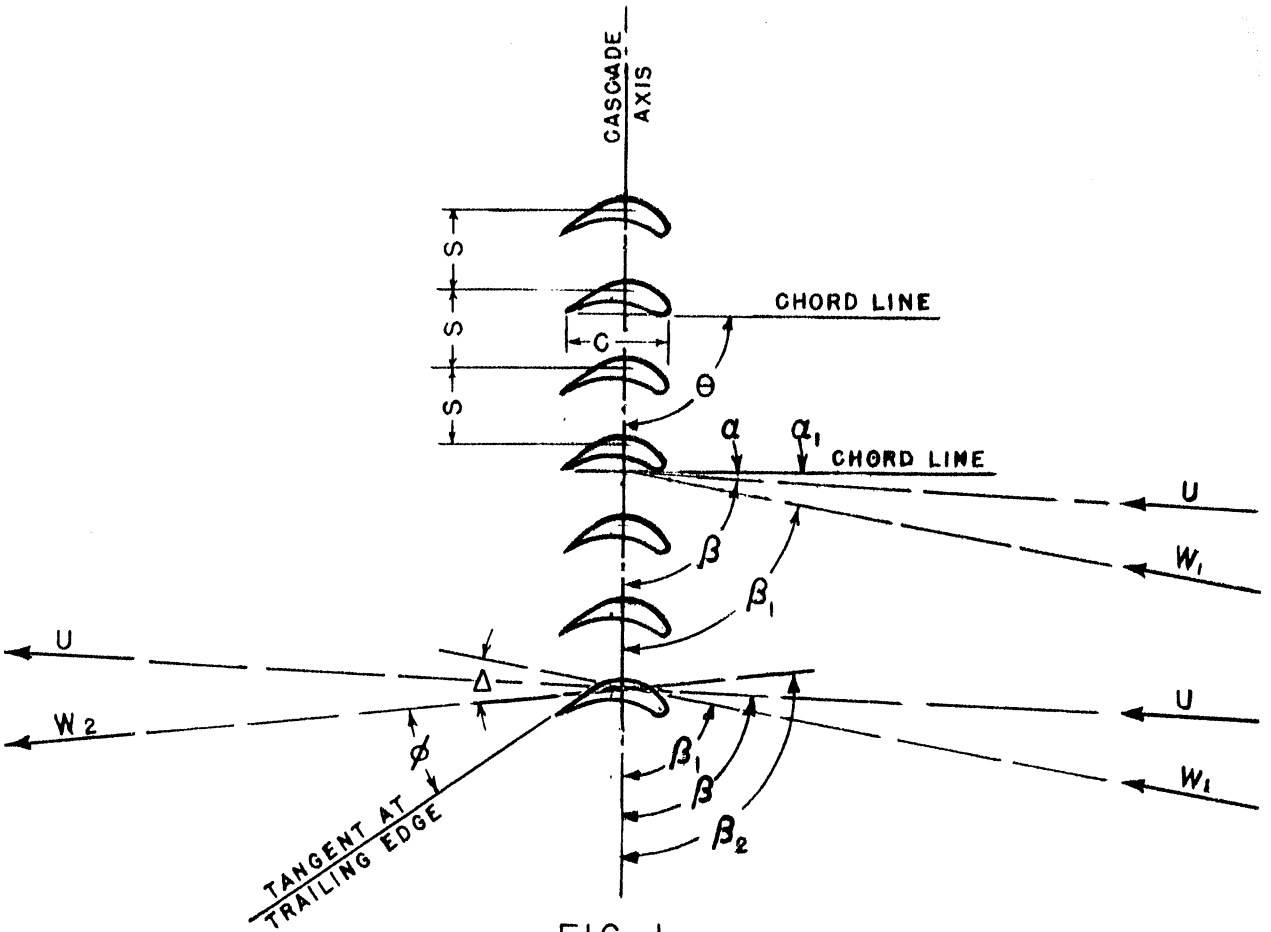

FIG. 1
A CASCADE OF VANES

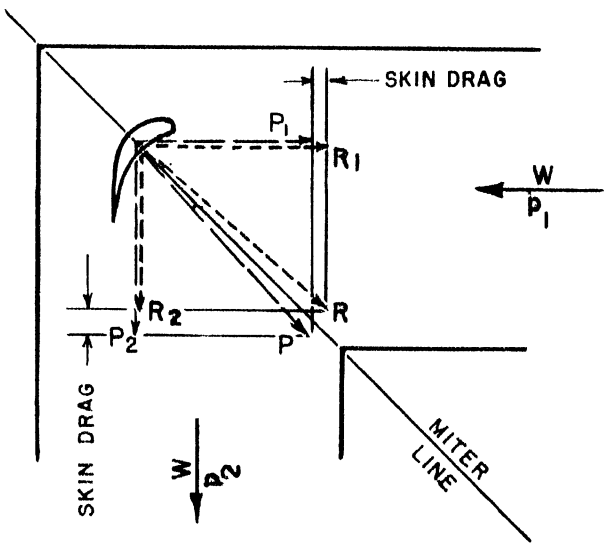

FIG. 2
FORCES ON A GUIDE VANE

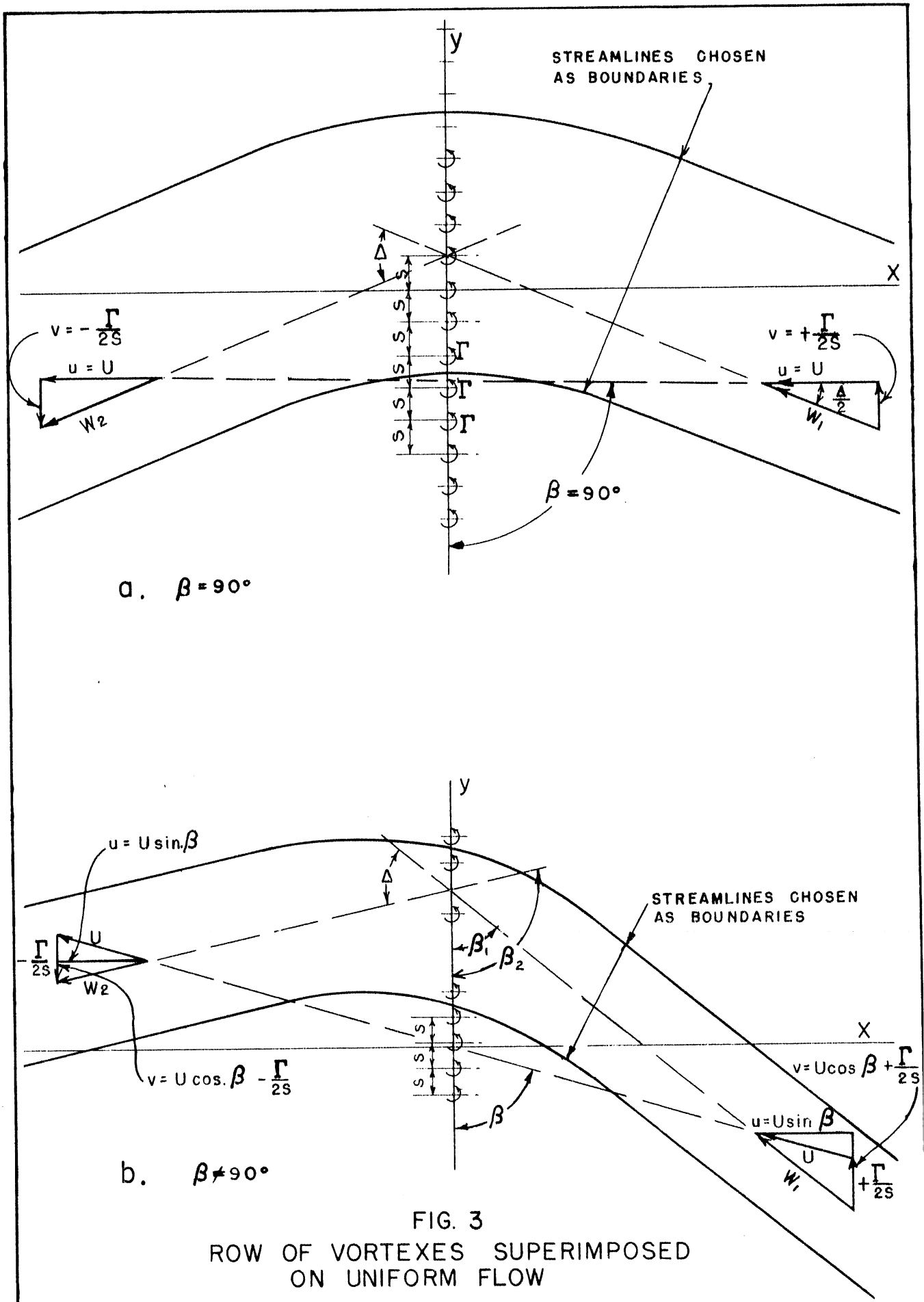

FIG. 3
ROW OF VORTEXES SUPERIMPOSED
ON UNIFORM FLOW

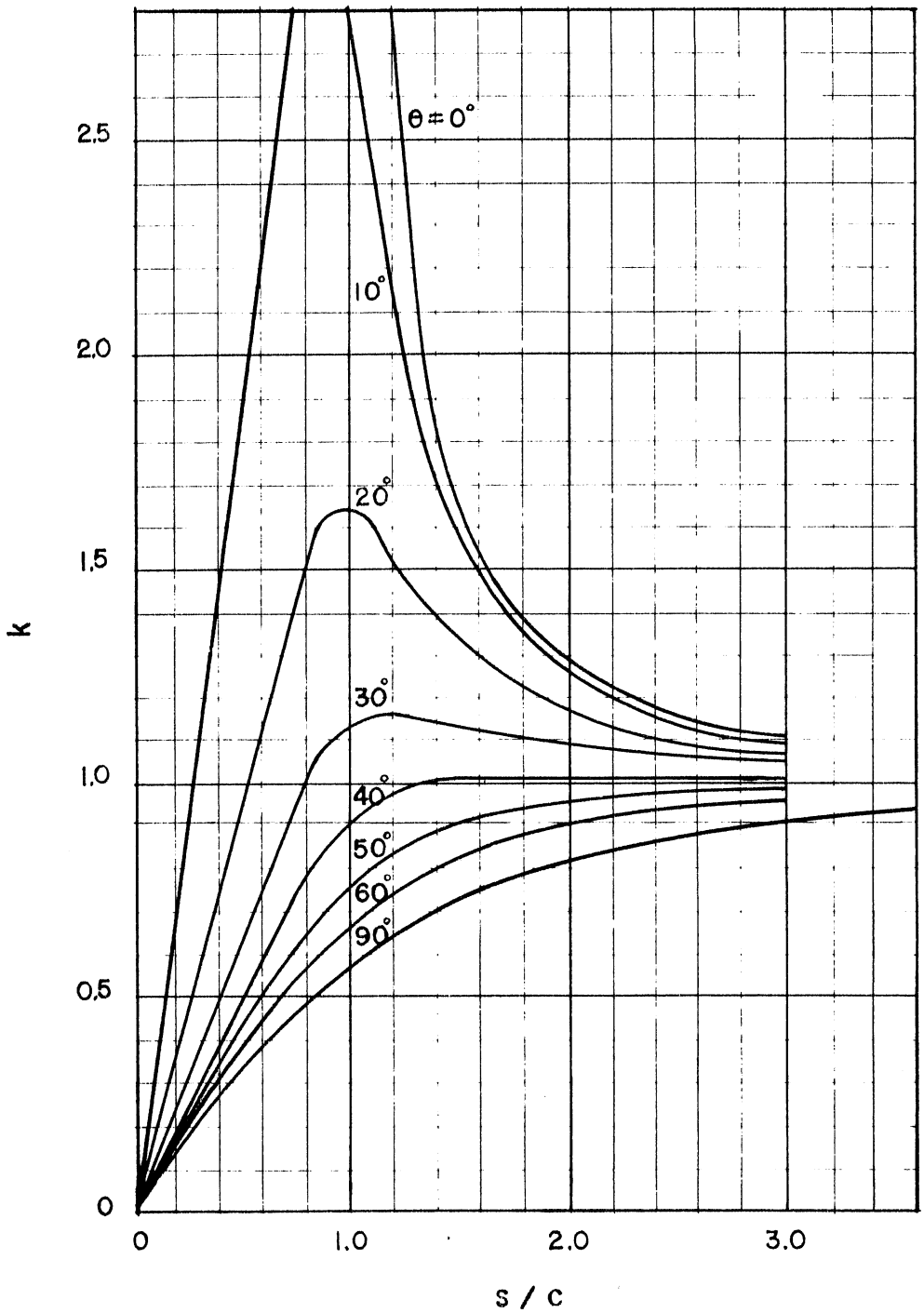

FIG.–4

k AS A FUNCTION OF S/C AND θ FOR A FLAT PLATE VANE (TAKEN FROM WEINIG (8))

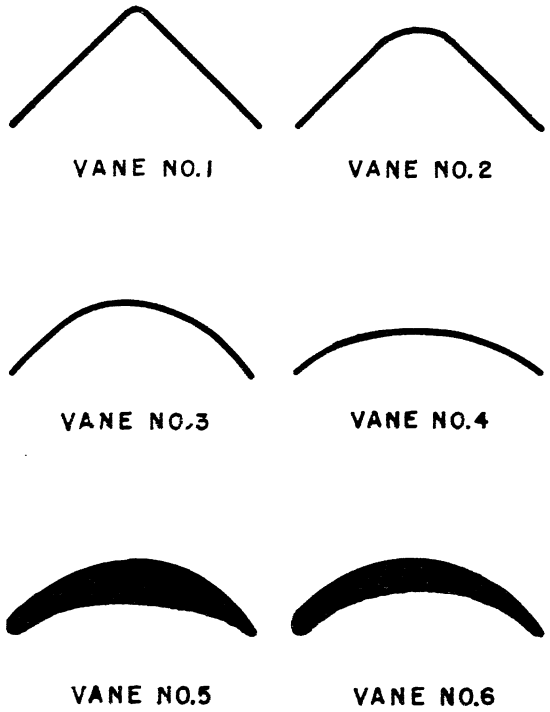

FIG. 5
VANE SHAPES USED BY KLEIN, TUPPER & GREEN

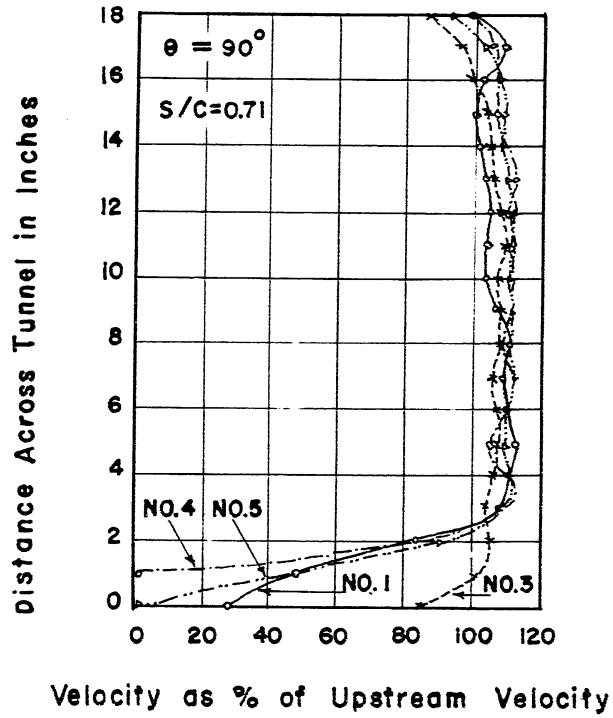

FIG. 6
INFLUENCE OF VANE SHAPES ON THE VELOCITY DISTRIBUTION DOWNSTREAM OF KLEIN TUPPER & GREEN VANES

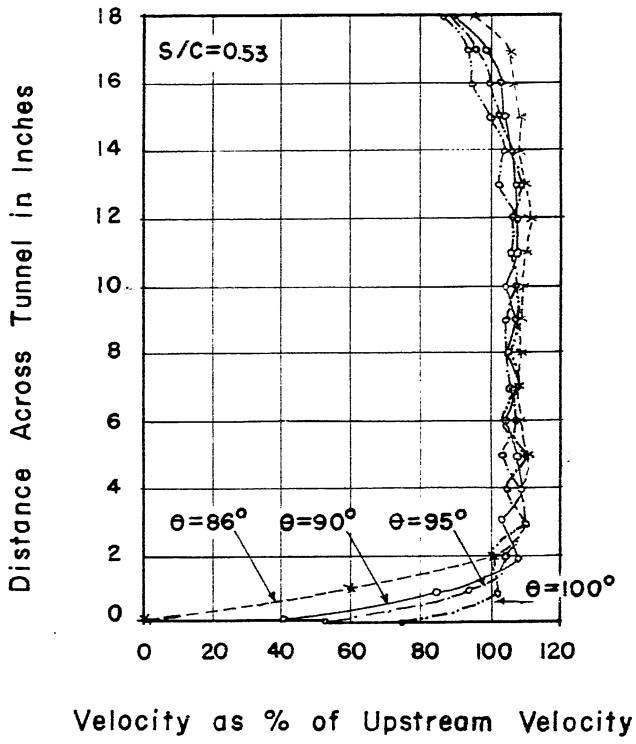

FIG. 7
INFLUENCE OF θ ON THE VELOCITY DISTRIBUTION DOWNSTREAM OF KLEIN, TUPPER & GREEN NO.5 VANES

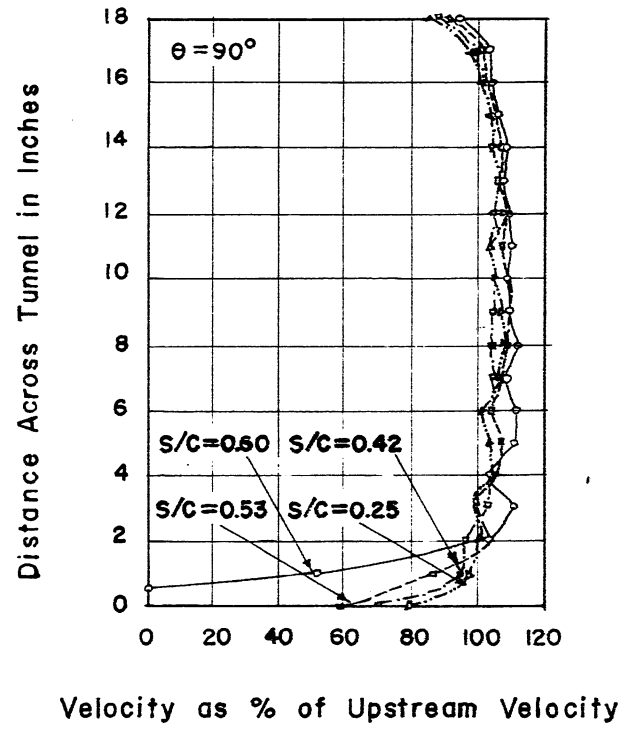

FIG. 8
INFLUENCE OF S/C ON THE VELOCITY DISTRIBUTION DOWNSTREAM OF KLEIN, TUPPER & GREEN NO.4 VANES

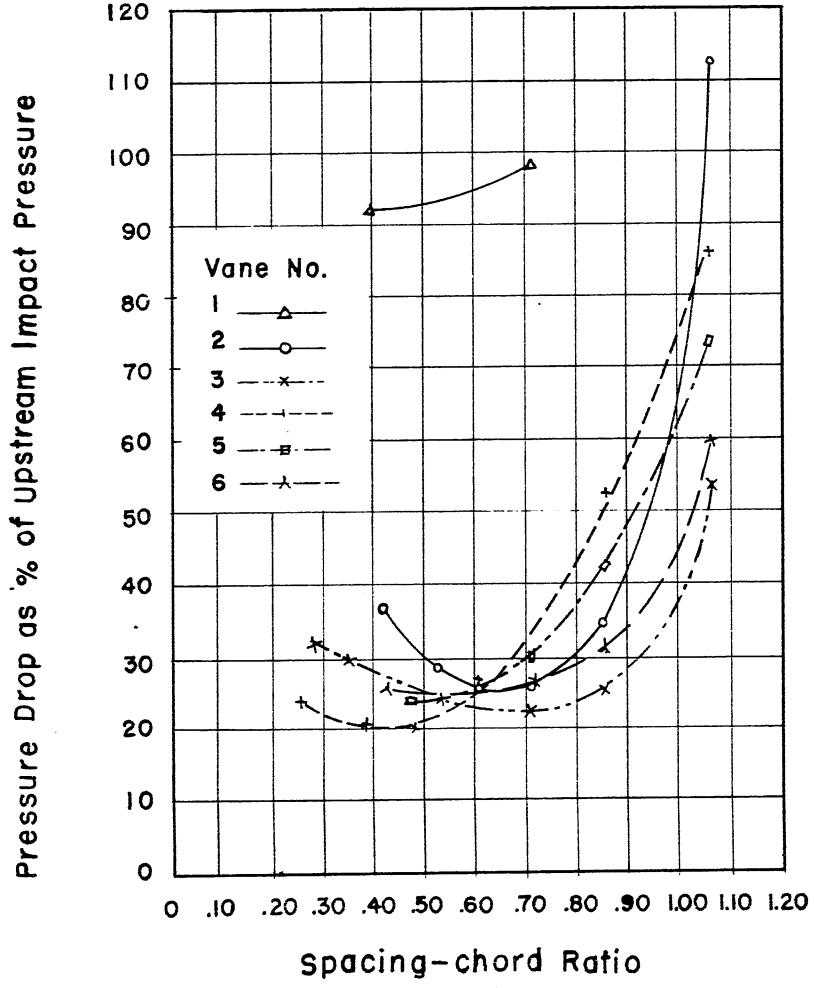

FIG. 9
TOTAL CORNER RESISTANCE OF CASCADES OF KLEIN TUPPER & GREEN VANES ($\theta=90°$)

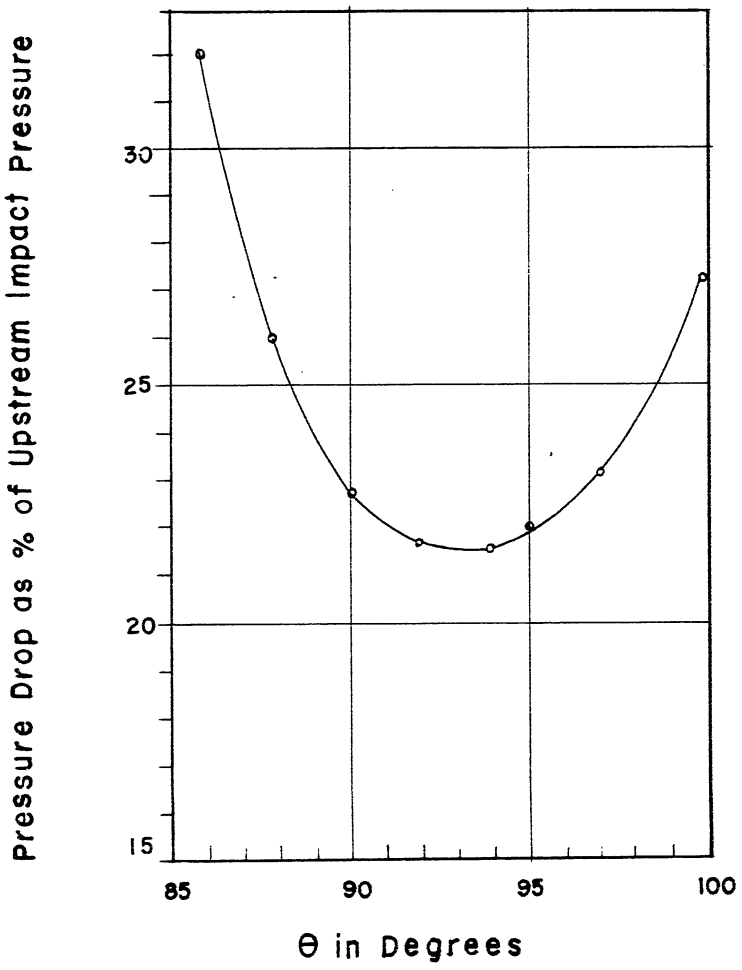

FIG. 10
INFLUENCE OF θ ON TOTAL CORNER RESISTANCE OF CASCADES OF K.T.G. NO.5 VANES ($S/C=0.53$)

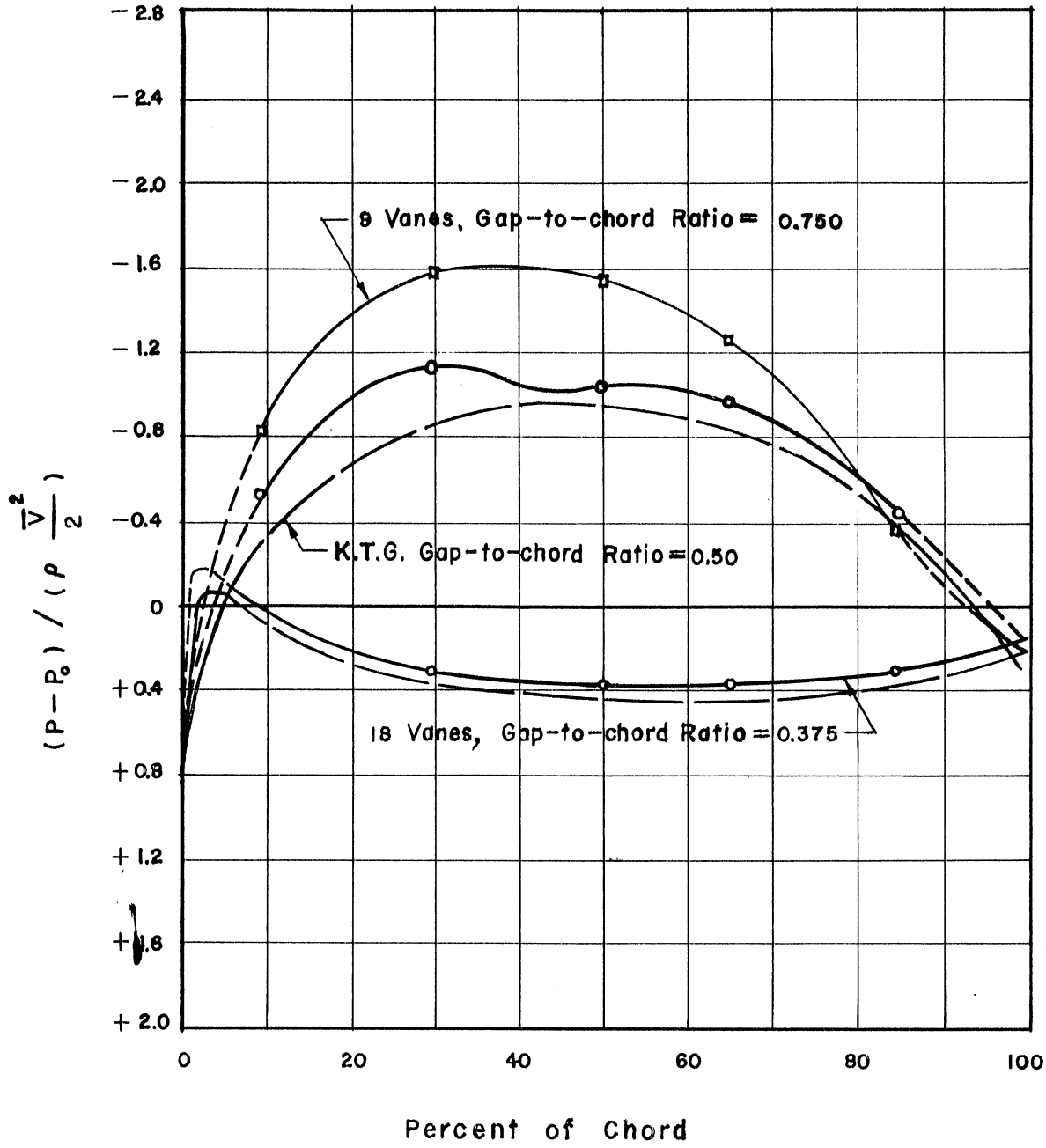

FIG. 11

PRESSURE DISTRIBUTION ON A VANE IN CASCADE FOR KLEIN TUPPER & GREEN NO.5 VANE AND PENNSYLVANIA STATE VANE

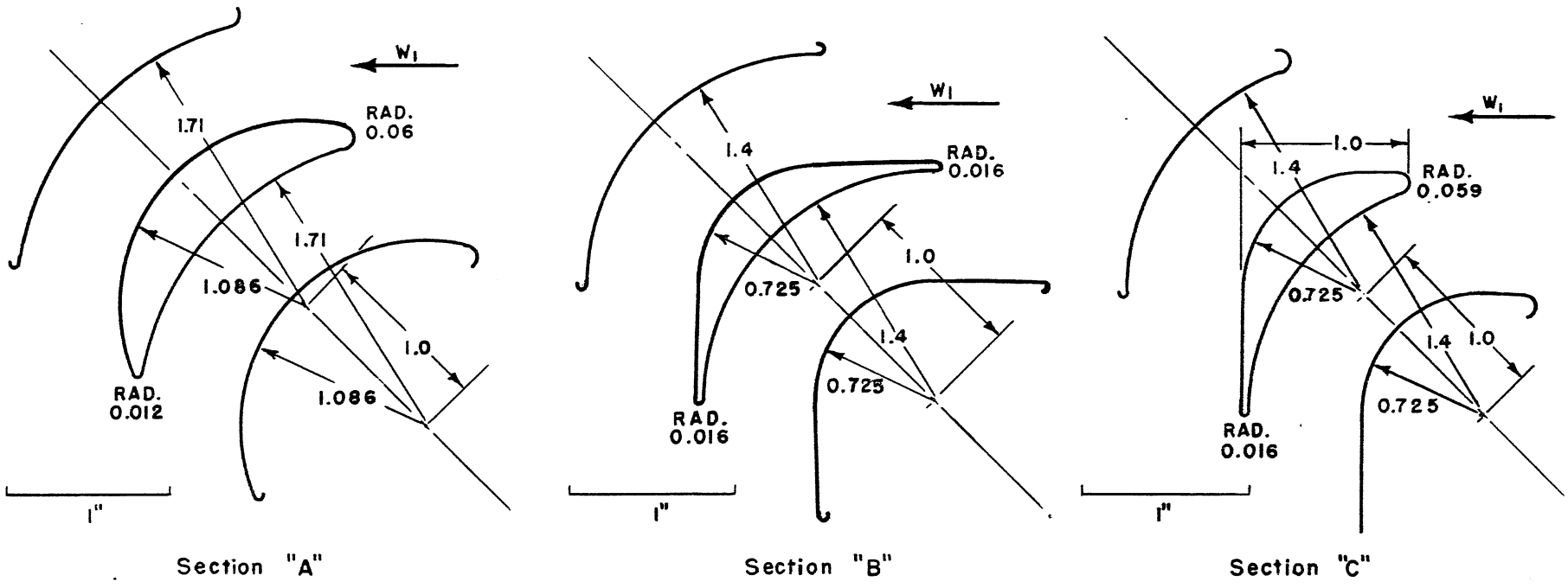

FIG. 12

CASCADES OF COLLAR VANES

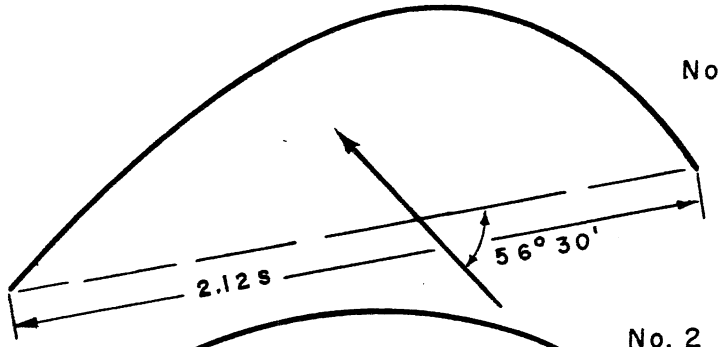

No. 1 90° turn

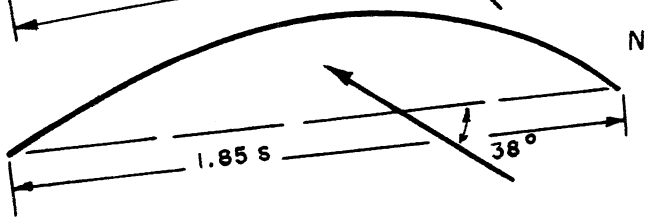

No. 2 60° turn

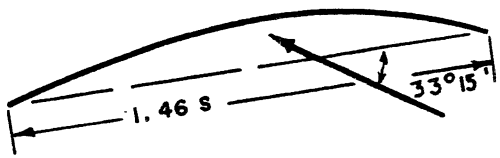

No. 3 45° turn

No. 4 30° turn

s = spacing between vanes

FIG. 13

KROBER VANES

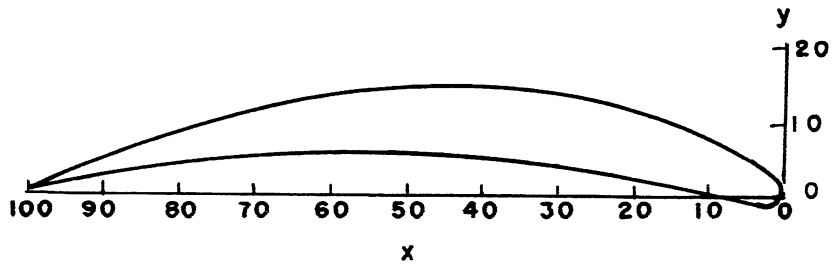

x, % chord	y, % chord	
	Upper	Lower
0.	0.	0.
0.7	+ 1.7 6	- 0.5 6
2.9	+ 3.6 7	- 0.8 0
6.4	5.8 5	- 0.5 1
1 1.3	8.2 1	+ 0.3 0
1 7.2	10.4 2	1.3 3
2 4.1	12.2 7	2.5 6
3 1.8	13.6 8	3.7 8
4 0.2	14.4 1	4.8 3
4 9.1	14.4 4	5.5 6
5 7.7	13.6 7	5.8 5
6 6.6	12.2 3	5.7 1
7 4.9	10.2 1	5.0 6
8 2.8	7.7 0	3.9 8
8 9.6	5.0 7	2.6 4
9 5.4	2.5 1	1.1 7
1 0 0.0	0.	0.

FIG. 14

HARRIS AND FAIRTHORNE VANE

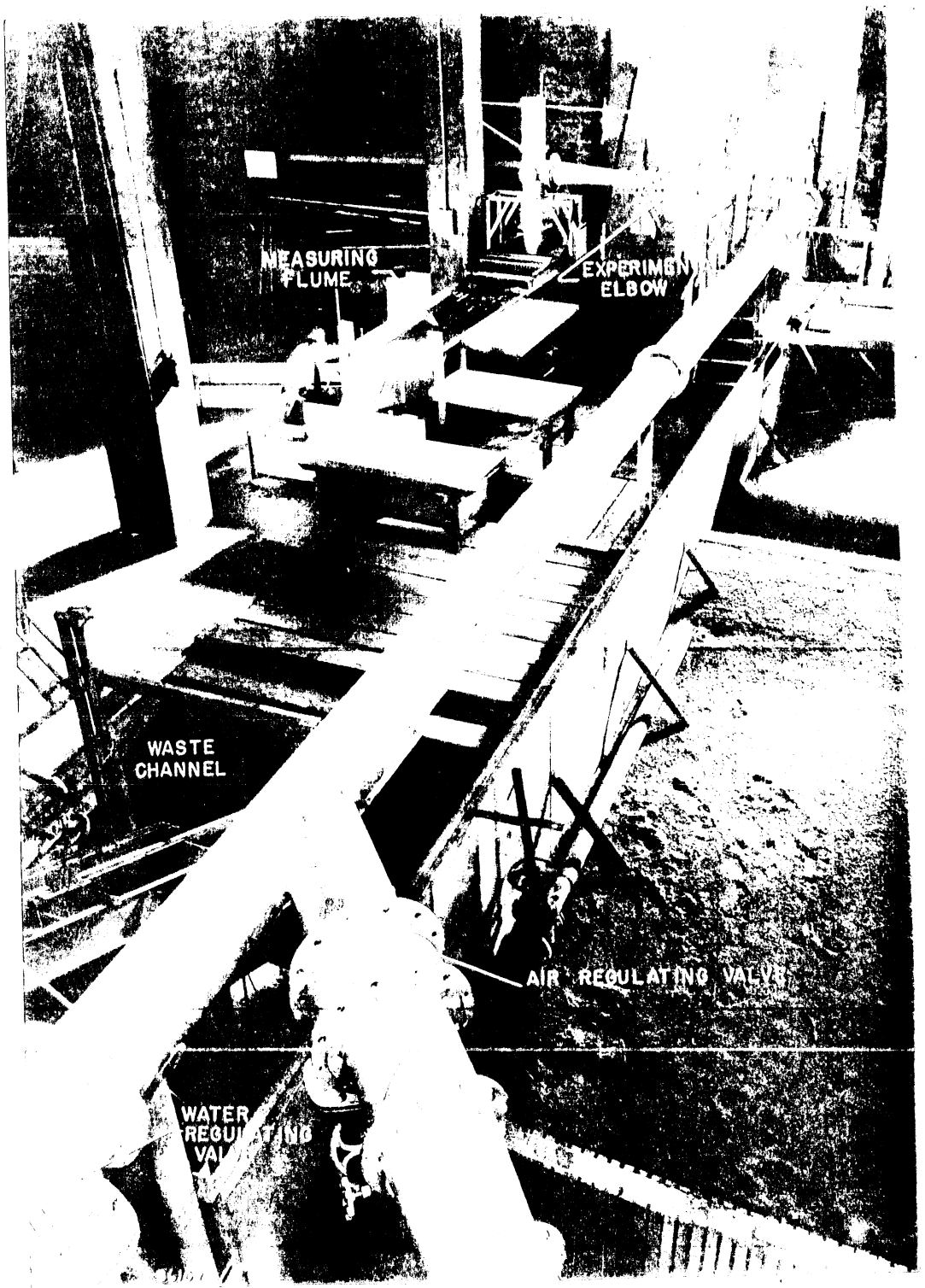

FIG. 15

THE FLOW DIVERSION TEST INSTALLATION

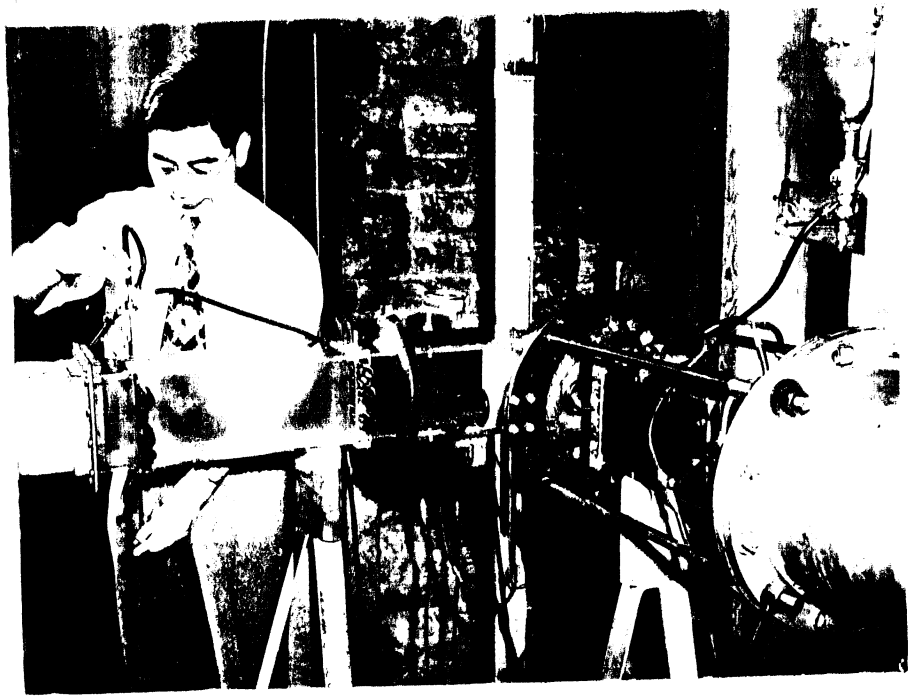

(B) THE BEND IN USE

(A) BEND WITH TYPE I VANES IN PLACE

FIG. 16
THE TEST BEND

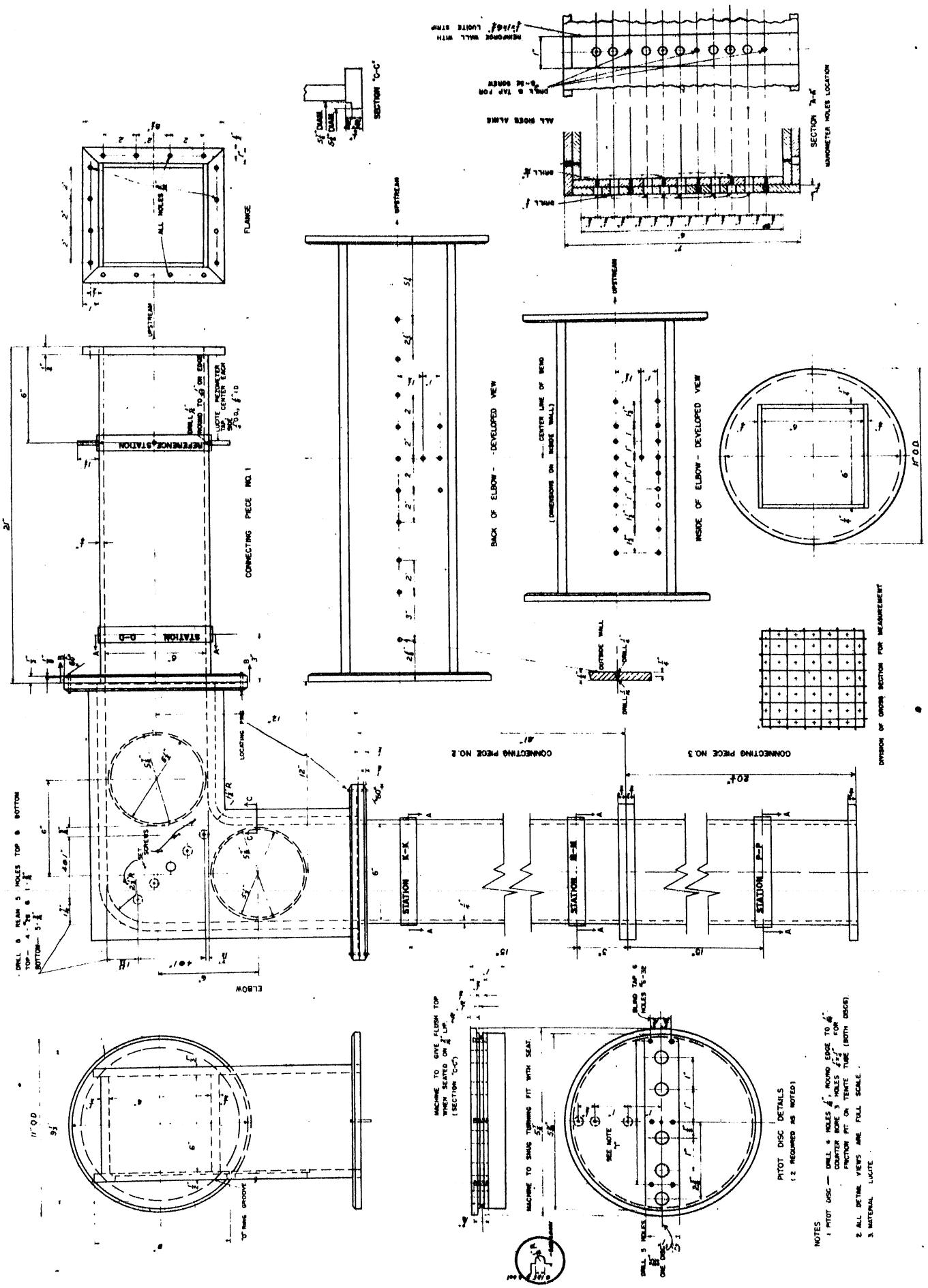

FIG. 17

BEND AND DUCT DETAILS

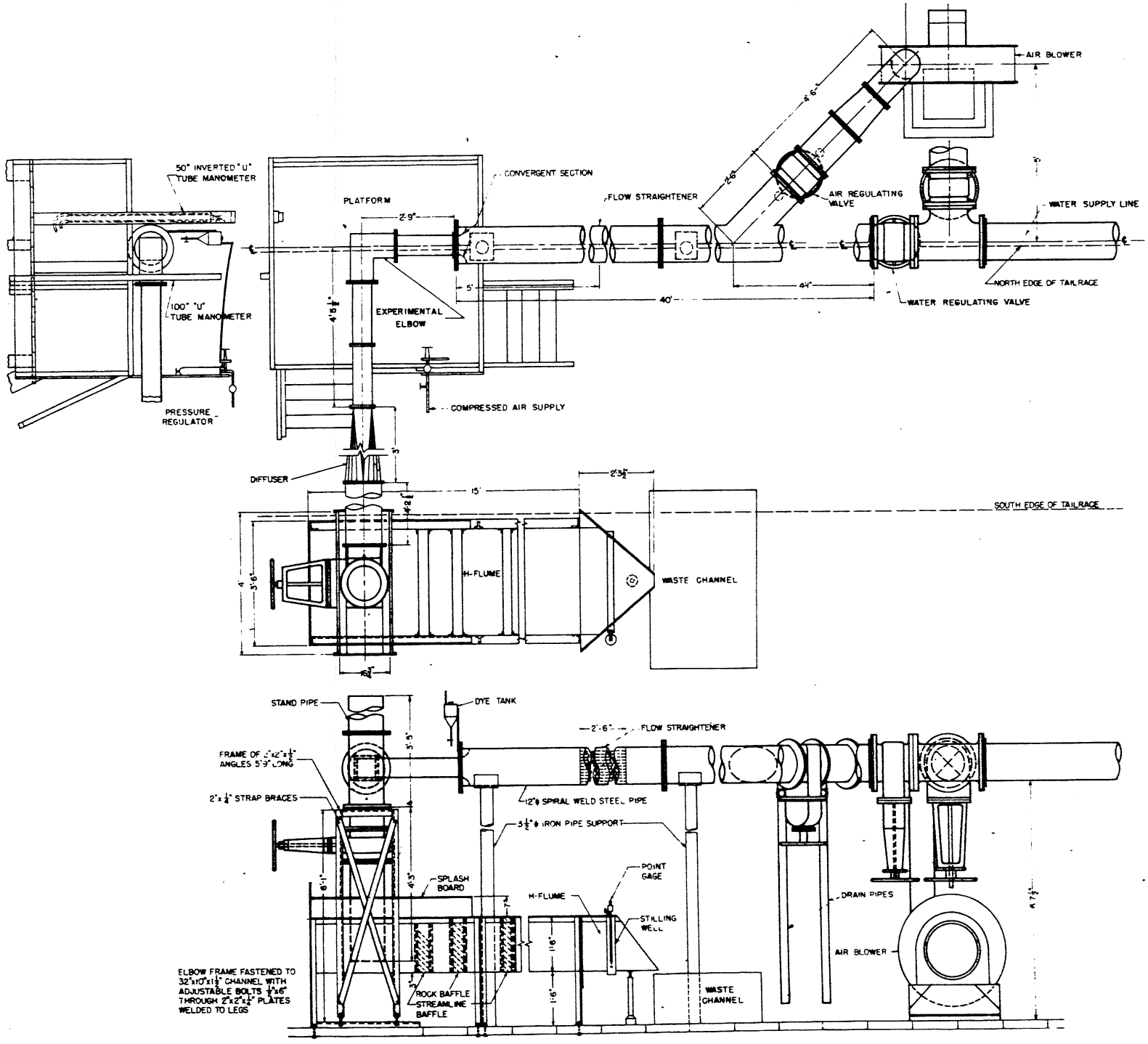

FIG. 18 TEST INSTALLATION

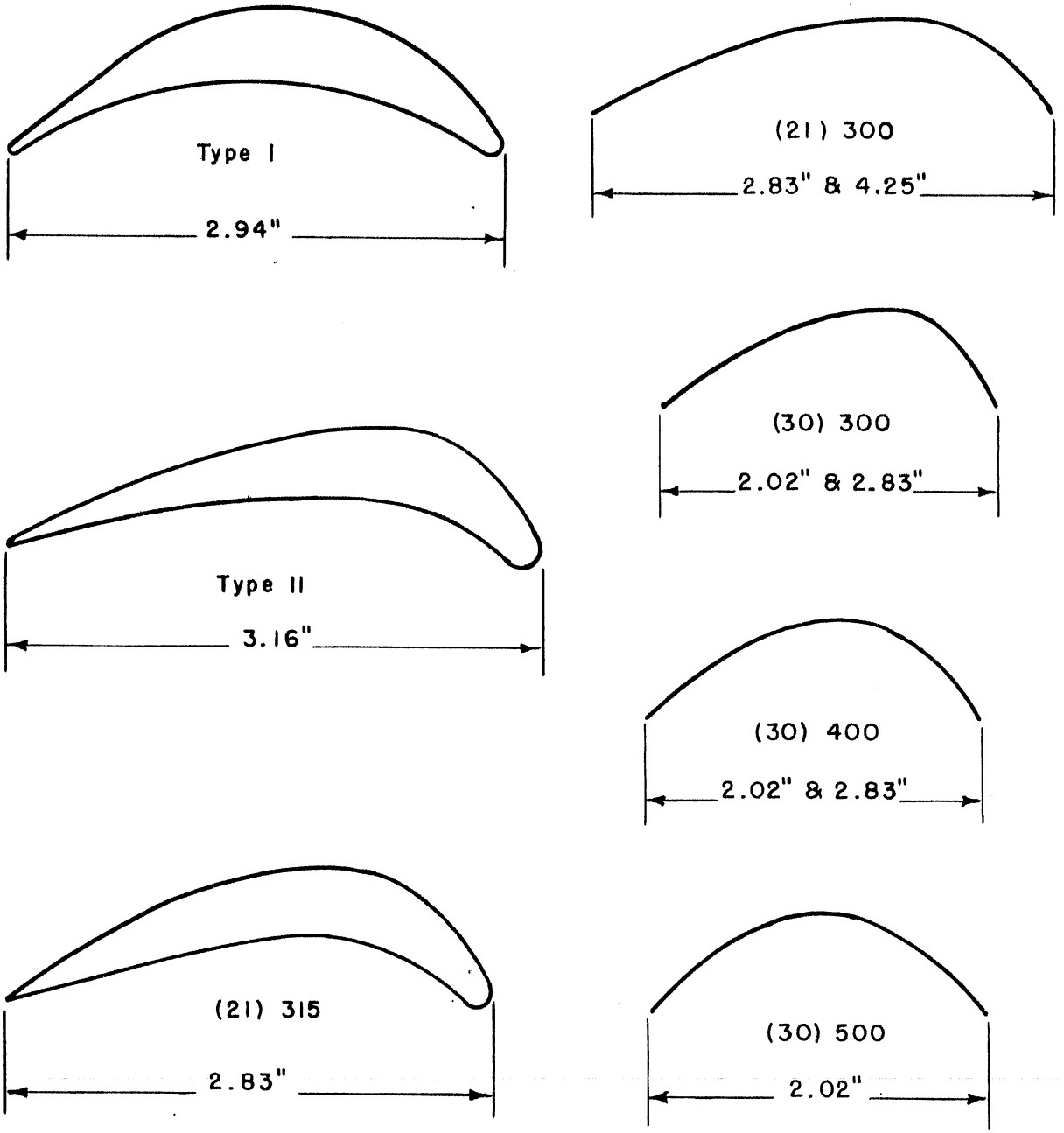

FIG. 19
GUIDE VANE PROFILES

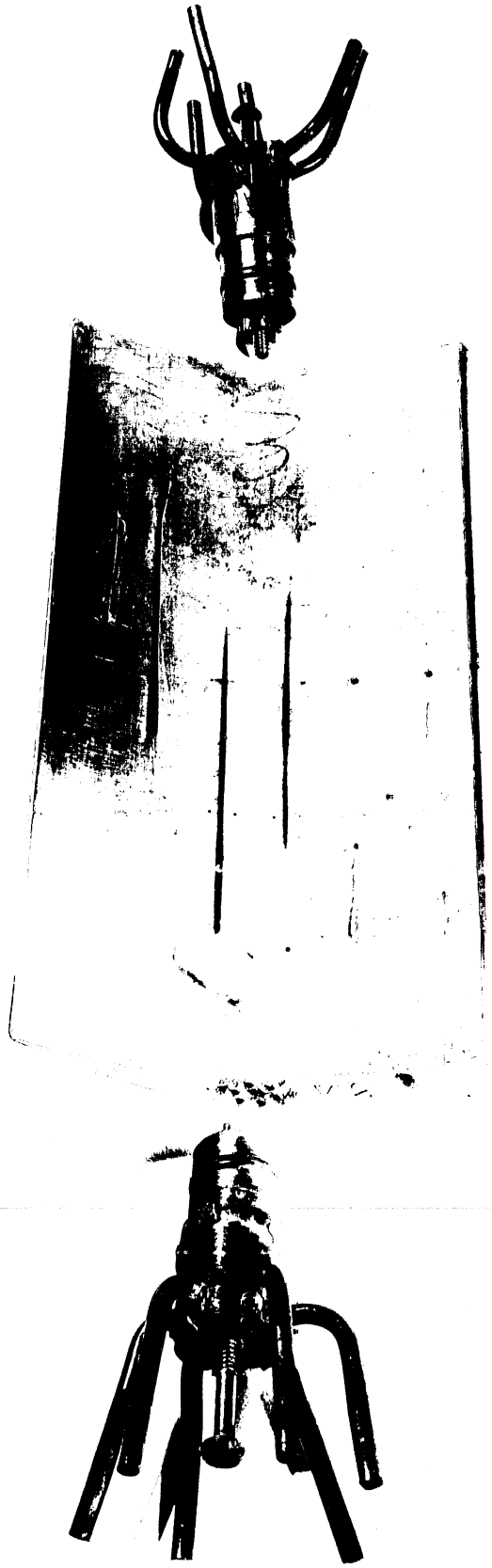

FIG. 20
TYPE I VANE AND TRUNNIONS SHOWING
PRESSURE TAPS AND CONNECTIONS
(VANE SURFACE IS POLISHED SMOOTH BUT IS SLIGHTLY DISCOLORED)

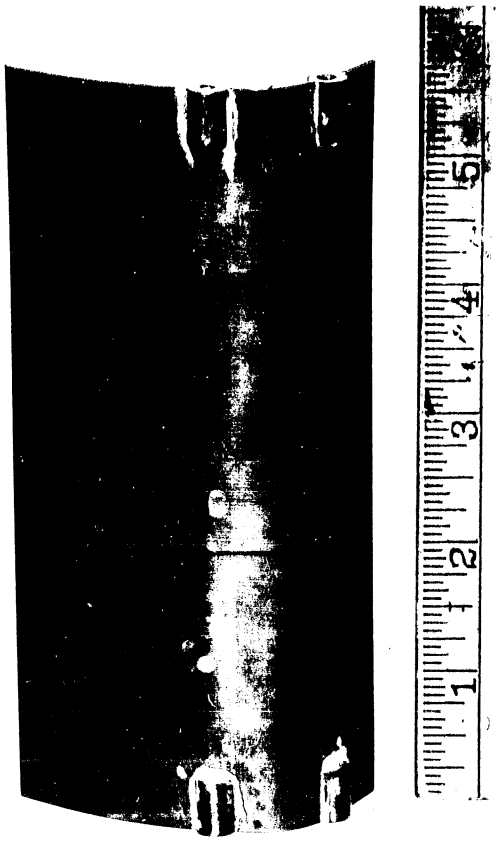

FIG. 21

(30) 300 VANE

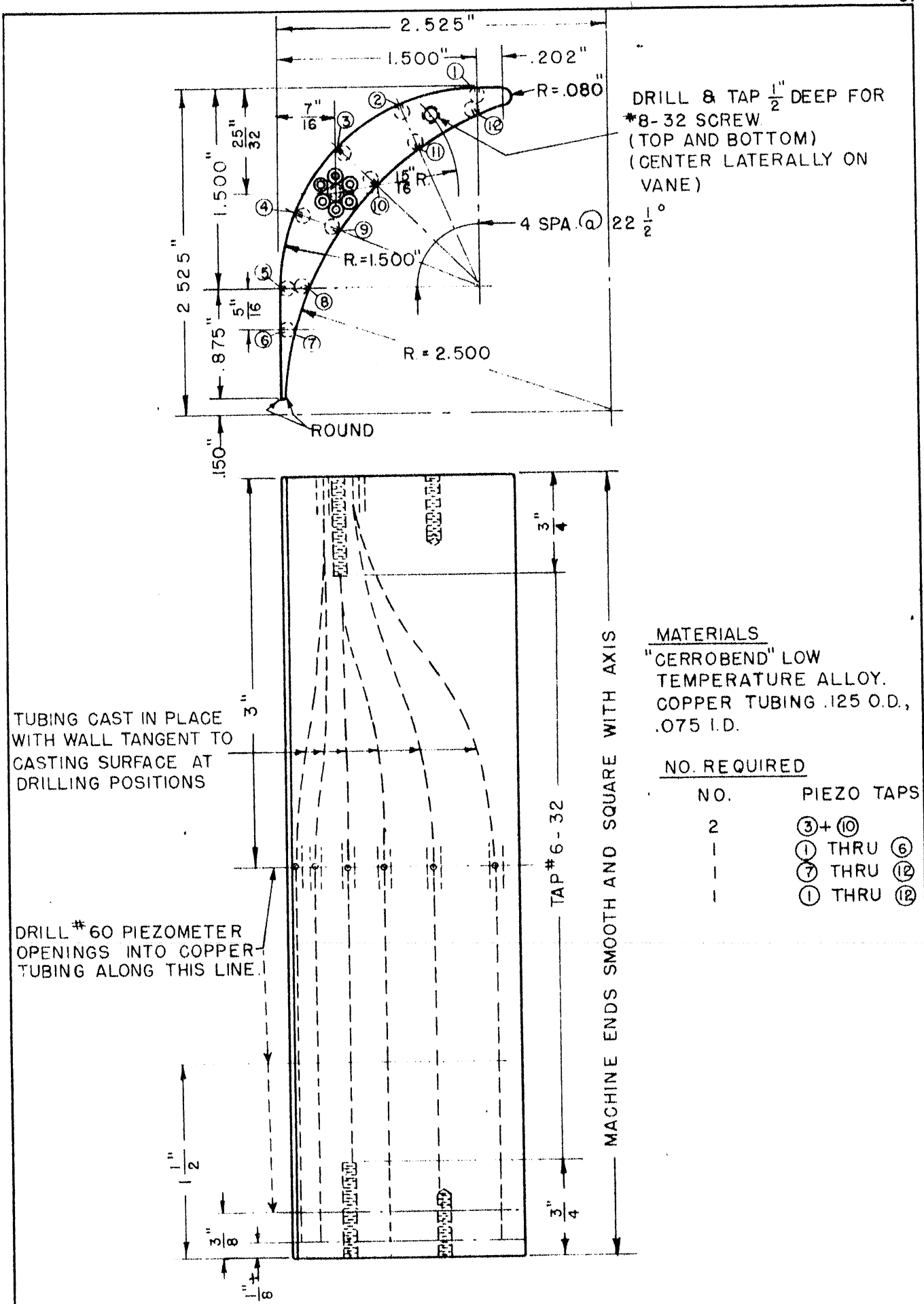

MATERIALS

"CERROBEND" LOW TEMPERATURE ALLOY. COPPER TUBING .125 O.D., .075 I.D.

NO. REQUIRED

NO.	PIEZO TAPS
2	③+⑩
1	① THRU ⑥
1	⑦ THRU ⑫
1	① THRU ⑫

FIG. 22

DETAILS OF TYPE I VANE

a. AIR BUBBLES IN WATER
RUN 62 (30) 300 VANE
(Vel. about 8 ft./sec.)

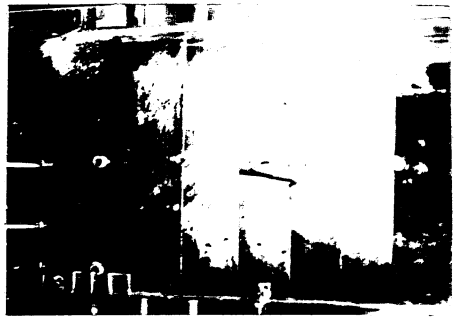

c. ON CONVEX VANE SURFACE
NEAR MIDSPAN

e. ON CONVEX VANE SURFACES AND
INSIDE WALL A FEW MINUTES
AFTER STARTING

b. THREADS IN AIR
RUN 23 TYPE II VANE
(Vel. about 100 ft./sec.)

d. ON CONVEX VANE SURFACE
NEAR END

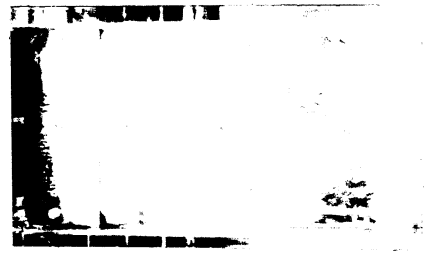

f. THE SAME VIEW LATER

FLOW DIRECTION ⟶

c. and d. COLORED WATER FILAMENTS
AIR RUN 23 TYPE II VANE
(Vel. about 100 ft./sec.)

e. and f. ALUMINUM POWDER AND OIL
WATER RUN 10 TYPE I VANE
(Vel. about 11.5 ft./sec.)

FIG. 23

TECHNIQUES OF OBSERVING FLOW

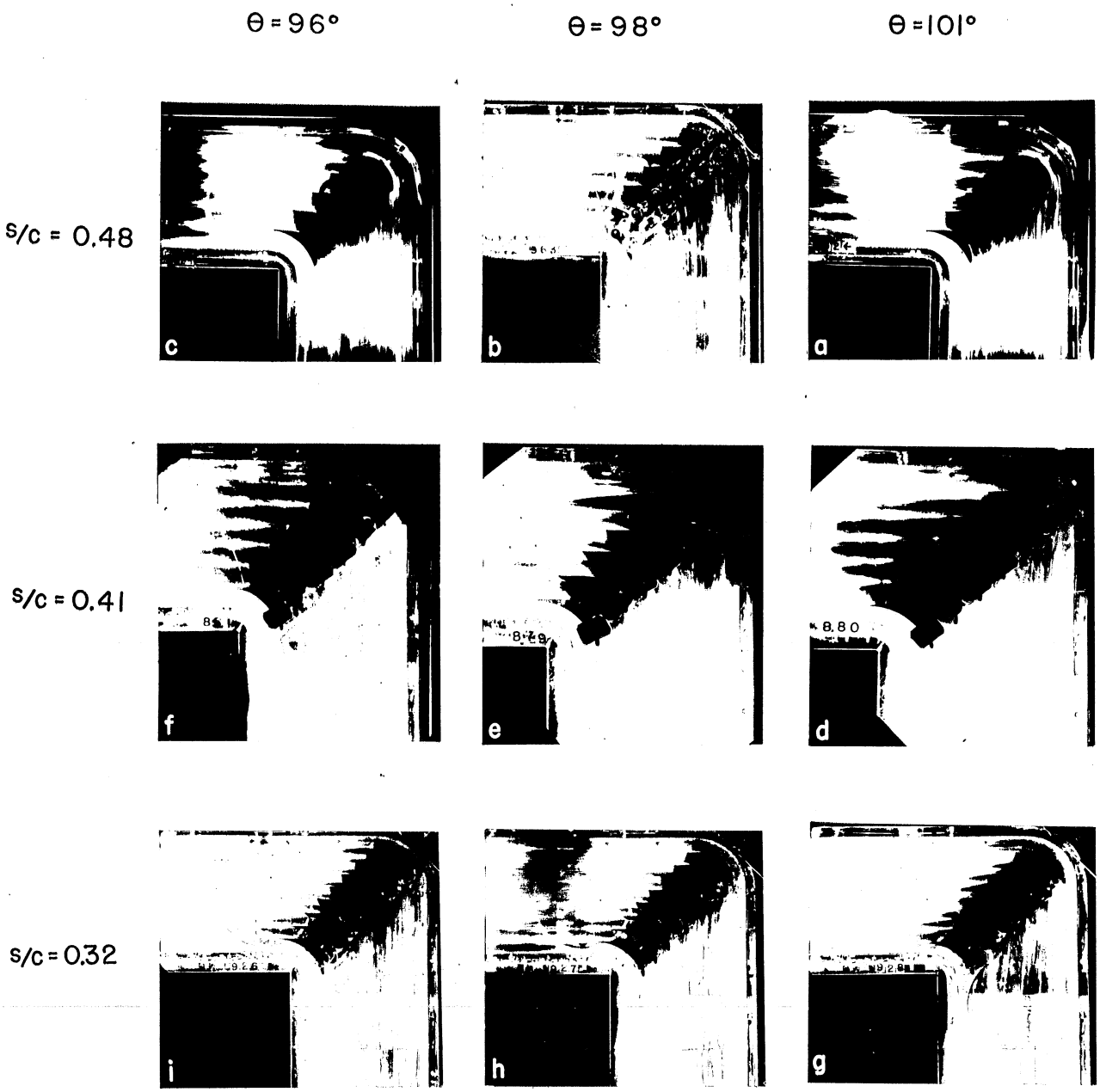

FIG. 24
FLOW STREAMLINES
TYPE I VANES

(A) AIR BUBBLES IN WATER ALONG TOP BOUNDARY
TYPE I VANES, RUN 10

NOTE THAT THE BUBBLES ARE DRAWN TO THE CONVEX SURFACE OF THE VANES. MANY OF THE BUBBLES EMERGING FROM THE CASCADE ARE IN THE INTERIOR OF THE FLUID.

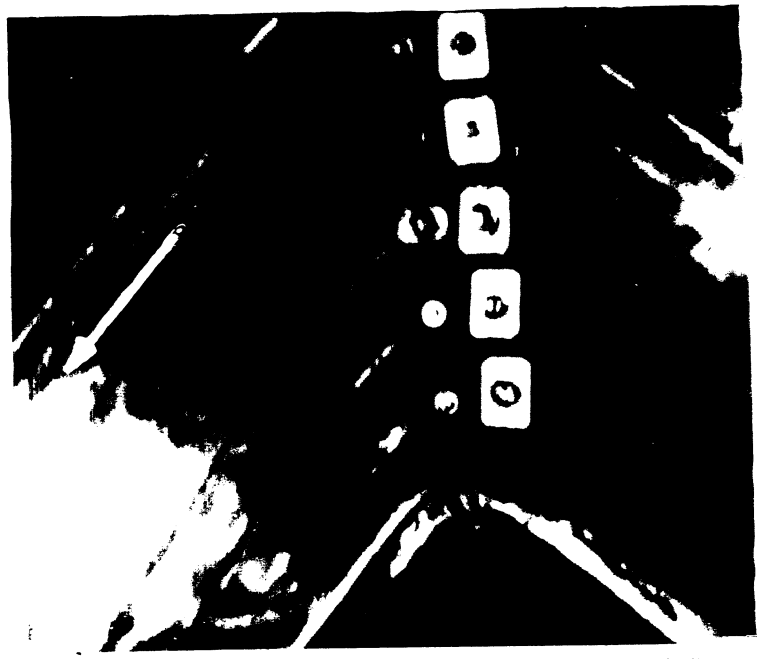

(B) COLORED WATER FILAMENTS IN AIR
(21) 300 VANES, RUN 40

ALONG BOTTOM BOUNDARY

NOTE THAT THE WIDE STREAM APPROACHING THE CASCADE EMERGES AS TWO NARROWER STREAMS FROM THE CONVEX SURFACES OF THE VANES.

FIG. 25

INFLUENCE OF THE BOUNDARY ON THE FLOW PATTERN

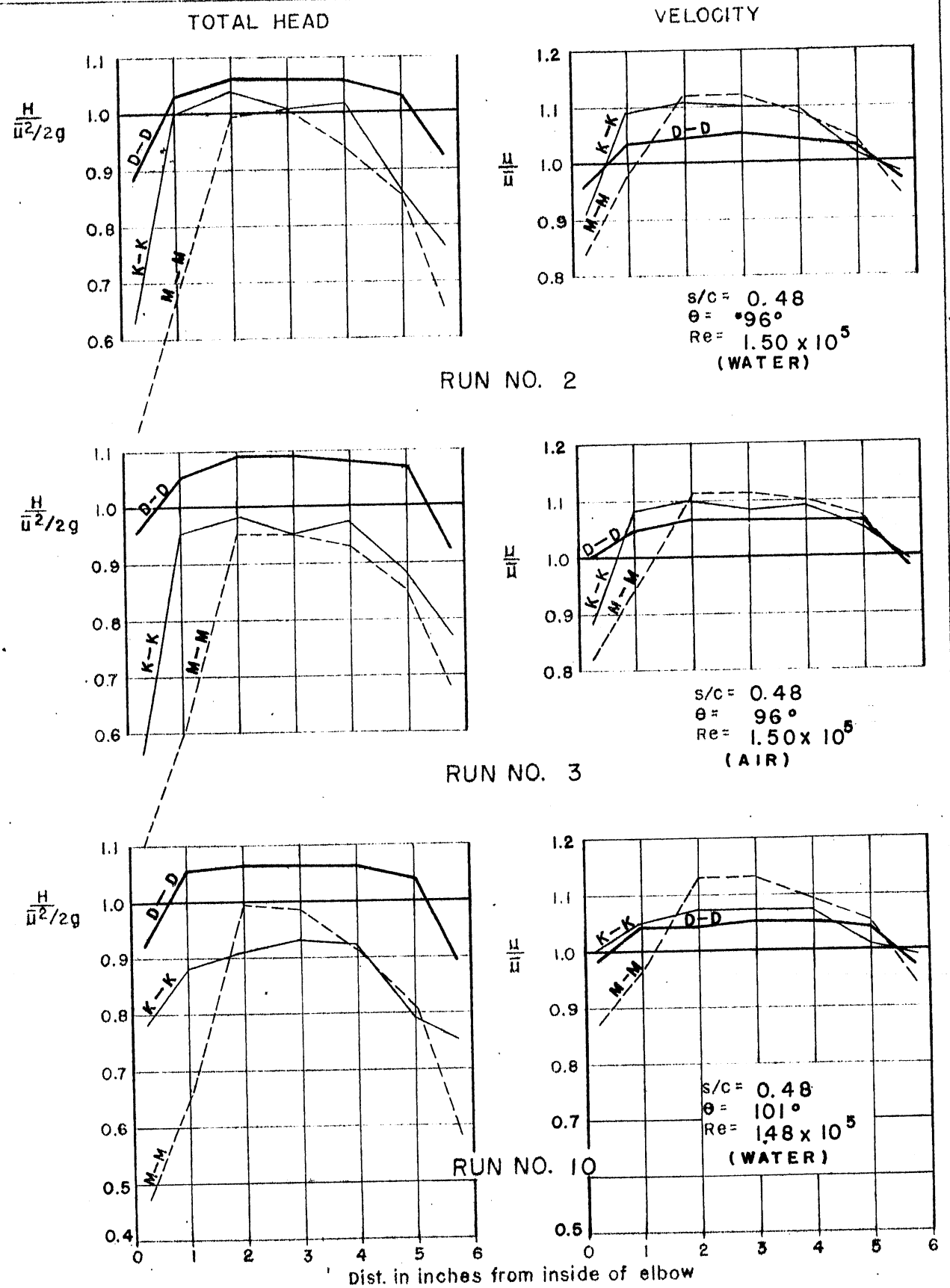

FIG. 26
TOTAL HEAD AND VELOCITY DISTRIBUTION
AT MID-DEPTH AT SEVERAL MEASURING STATIONS
RUN NOS. 2, 3, 10
(TYPE I VANE)

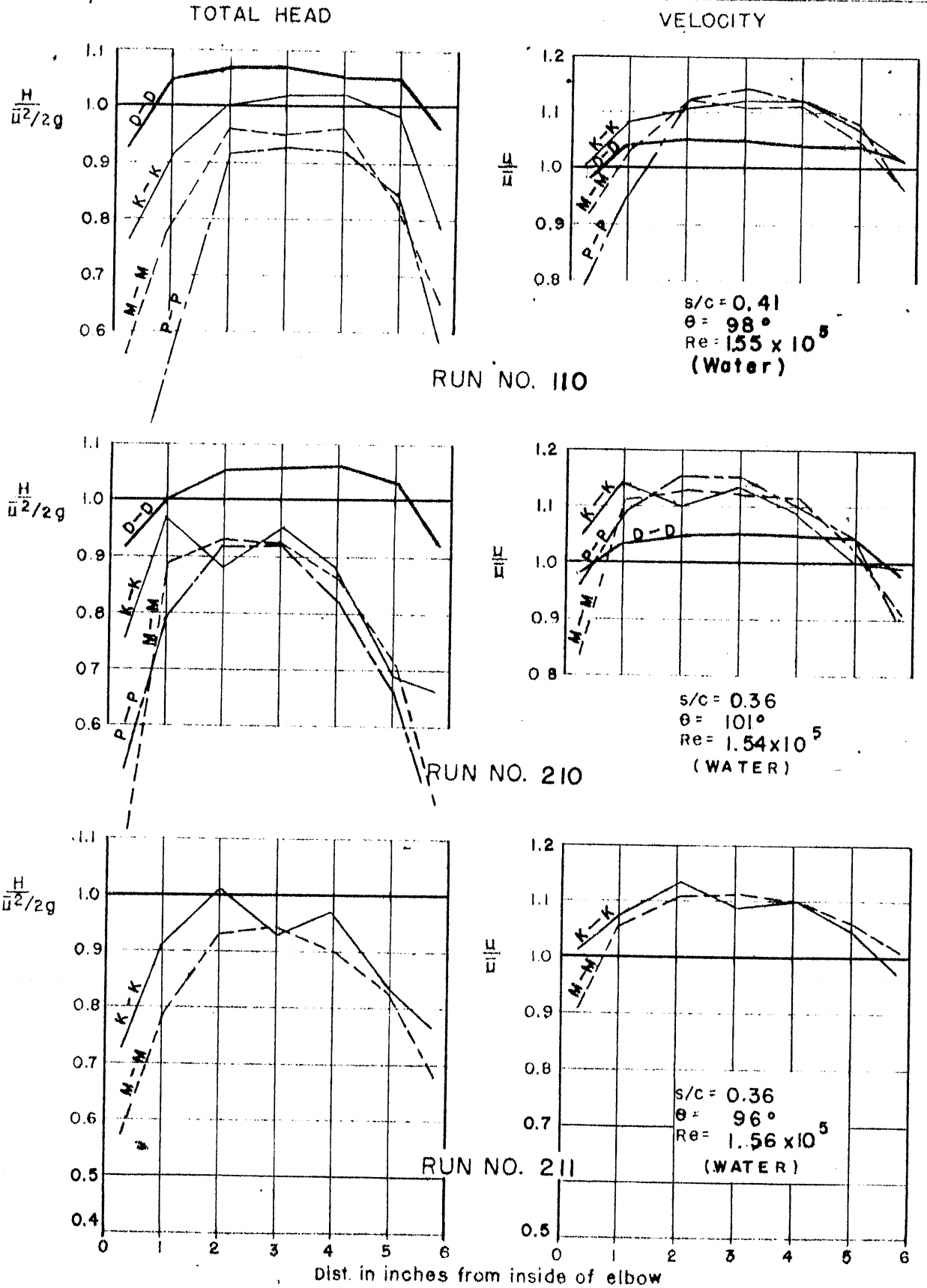

FIG. 27
TOTAL HEAD AND VELOCITY DISTRIBUTION
AT MID-DEPTH AT SEVERAL MEASURING STATIONS
RUN NOS. 110, 210, 211
(TYPE I VANE)

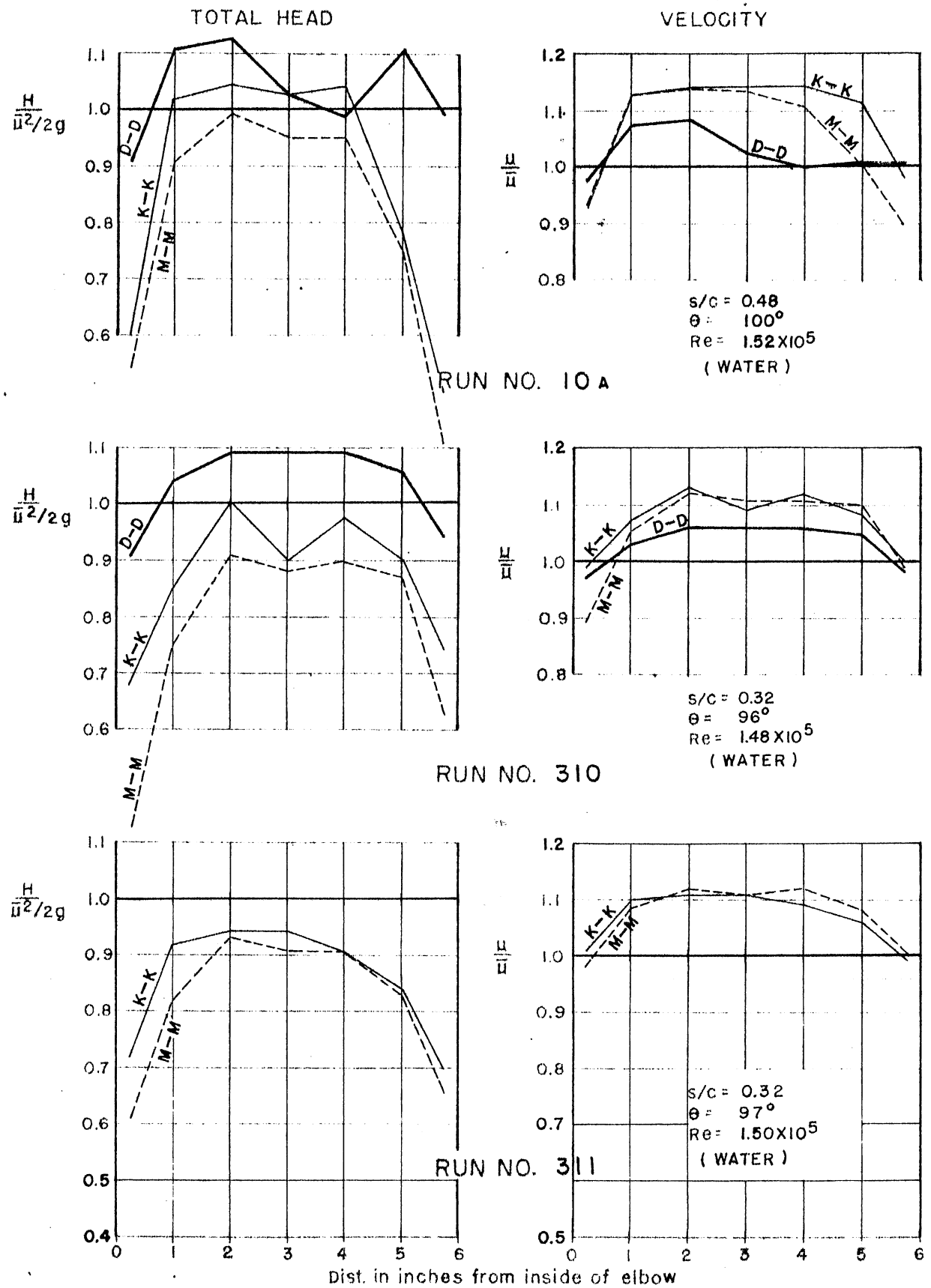

FIG. 28
TOTAL HEAD AND VELOCITY DISTRIBUTION
AT MID-DEPTH AT SEVERAL MEASURING STATIONS
RUN NOS. 10A, 310, 311
(TYPE I VANE)

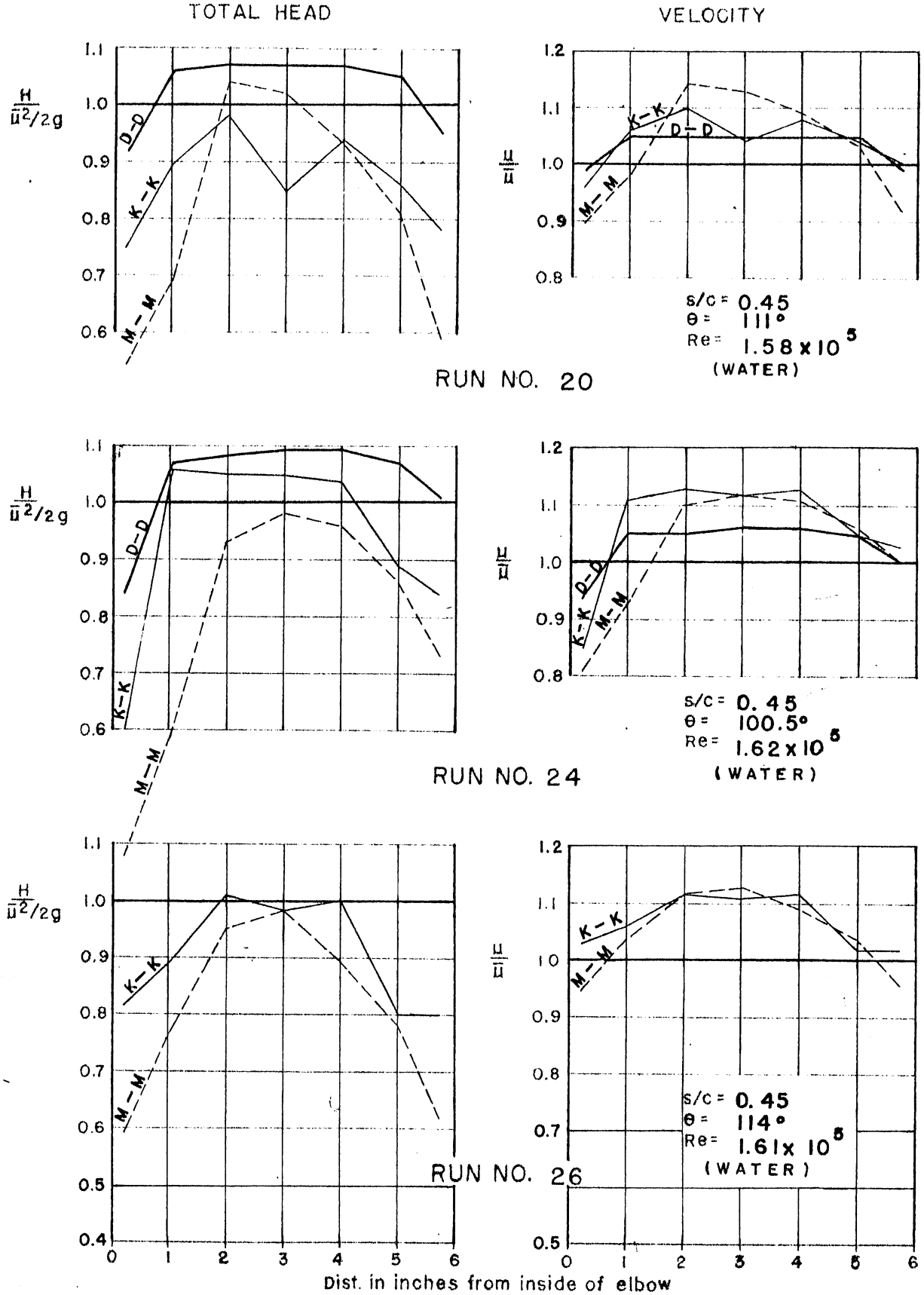

FIG. 29
TOTAL HEAD AND VELOCITY DISTRIBUTION
AT MID-DEPTH AT SEVERAL MEASURING STATIONS
RUN NOS. 20, 24, 26
(TYPE II VANE)

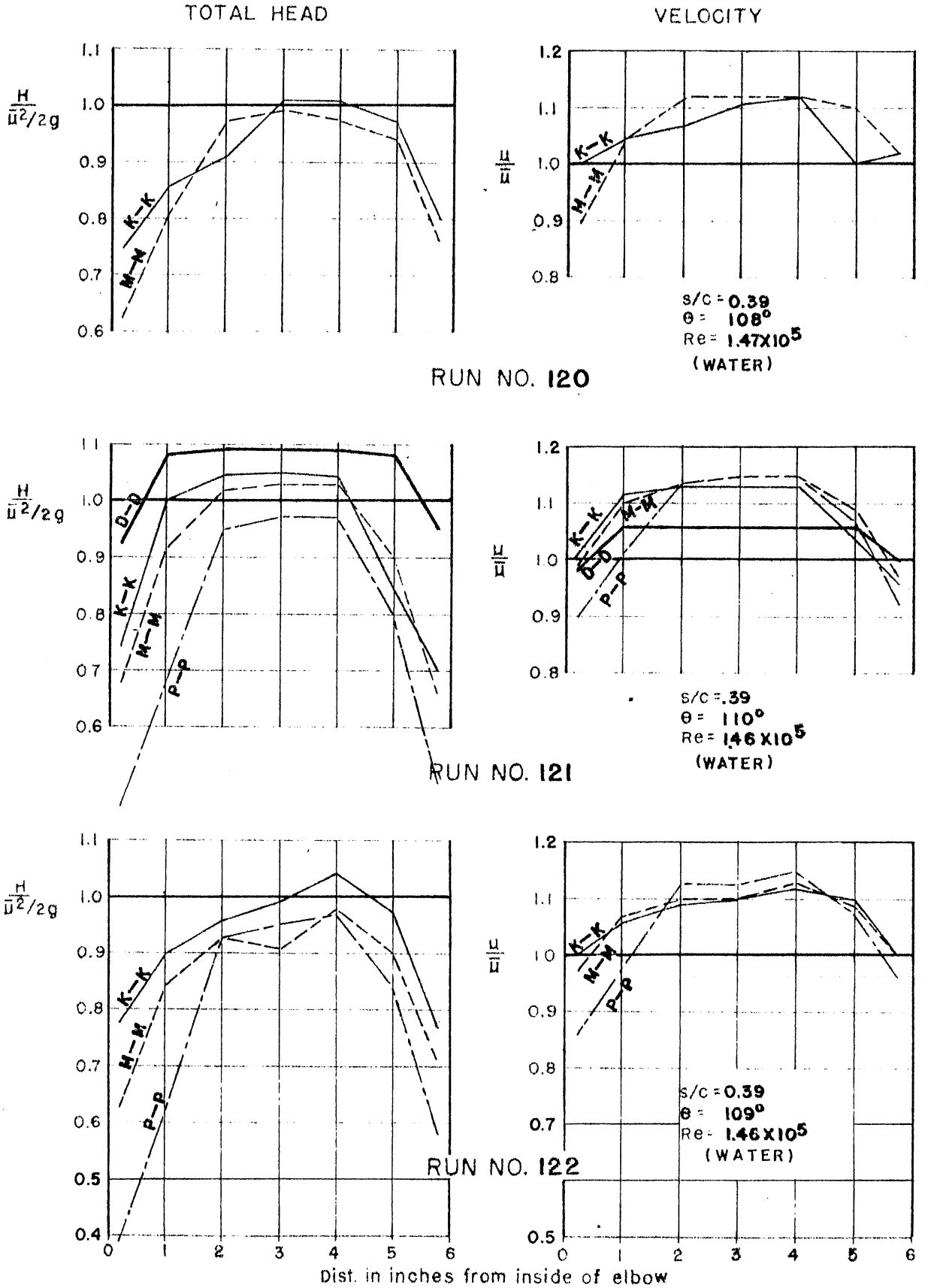

FIG. 30
TOTAL HEAD AND VELOCITY DISTRIBUTION
AT MID-DEPTH AT SEVERAL MEASURING STATIONS
RUN NOS. 120, 121, 122
(TYPE II VANE)

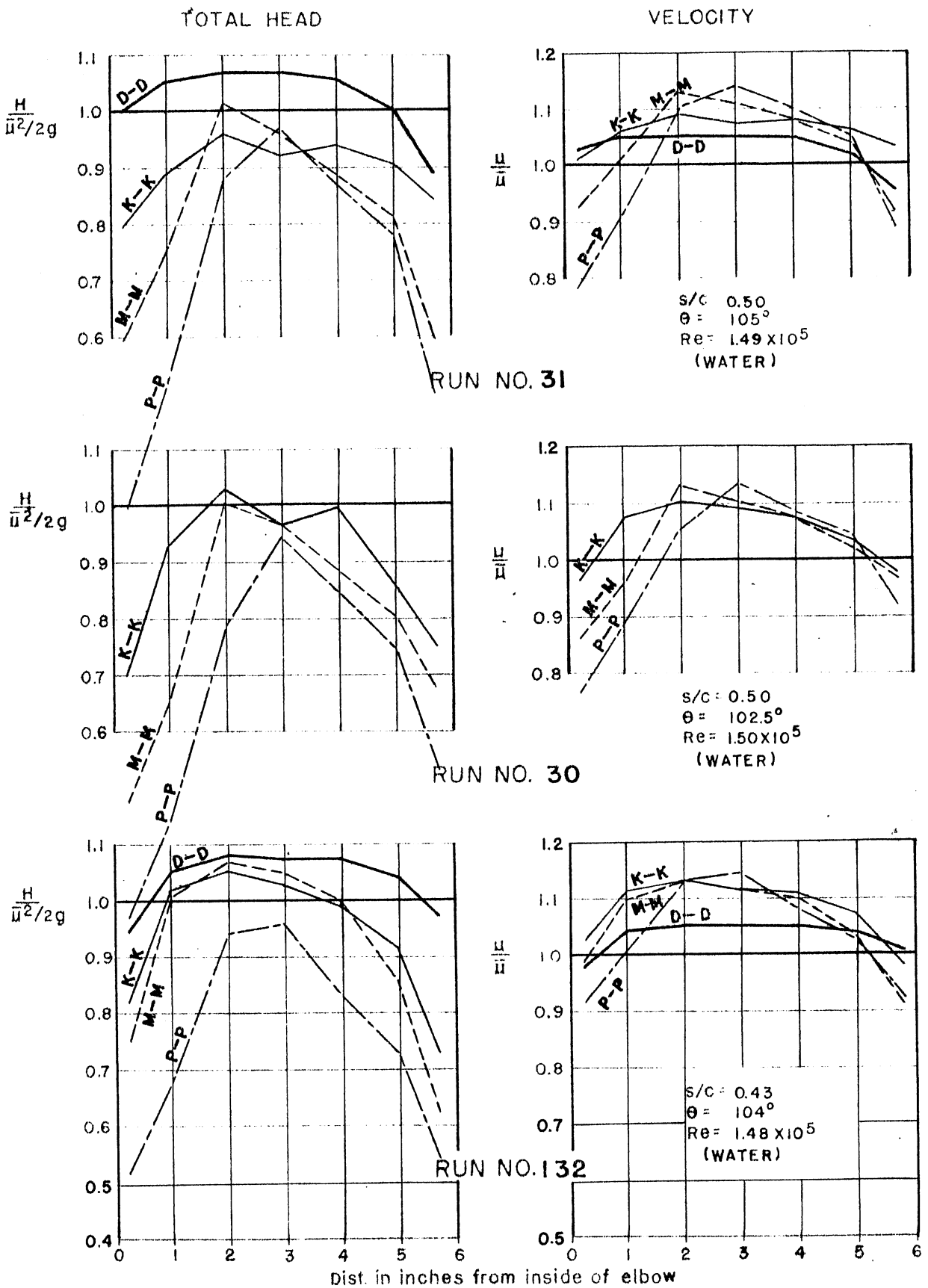

FIG. 31
TOTAL HEAD AND VELOCITY DISTRIBUTION
AT MID-DEPTH AT SEVERAL MEASURING STATIONS
RUN NOS. 31, 30, 132
((21) 315 VANE)

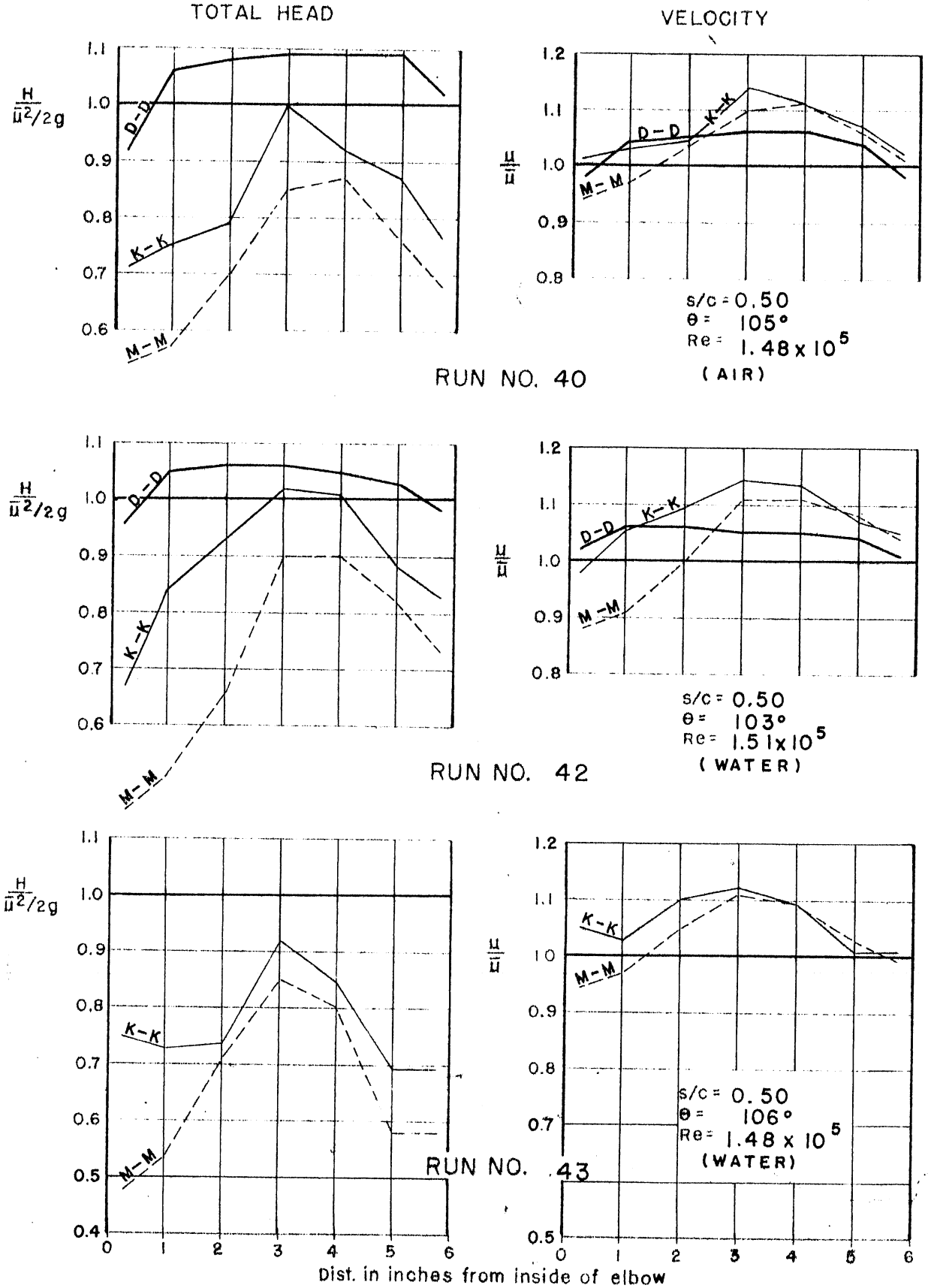

FIG. 32
TOTAL HEAD AND VELOCITY DISTRIBUTION
AT MID-DEPTH AT SEVERAL MEASURING STATIONS
RUN NOS. 40, 42, 43
((21) 300 VANE)

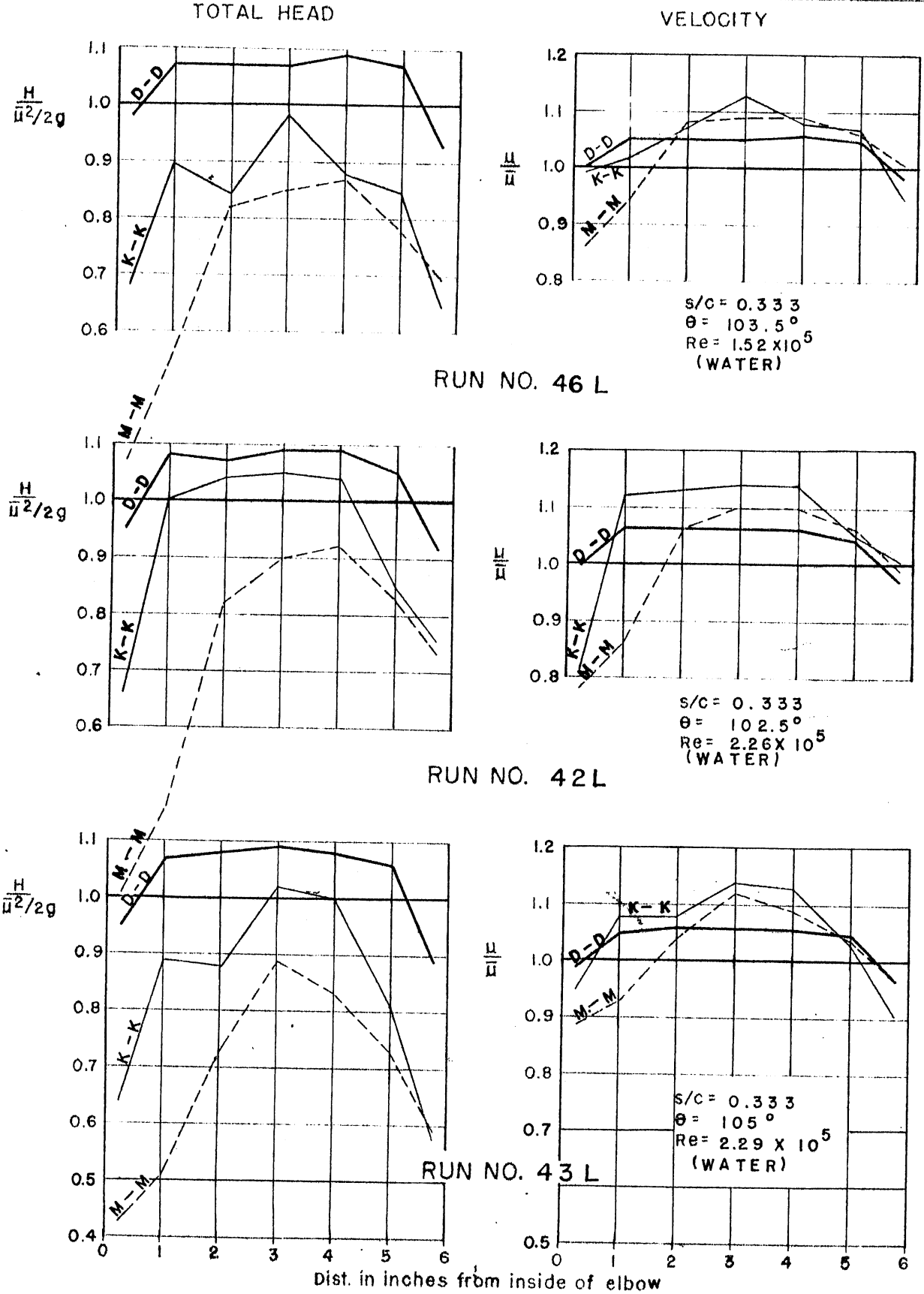

FIG. 33
TOTAL HEAD AND VELOCITY DISTRIBUTION
AT MID-DEPTH AT SEVERAL MEASURING STATIONS
RUN NOS. 46 L, 42 L, 43 L
((21) 300 VANE)

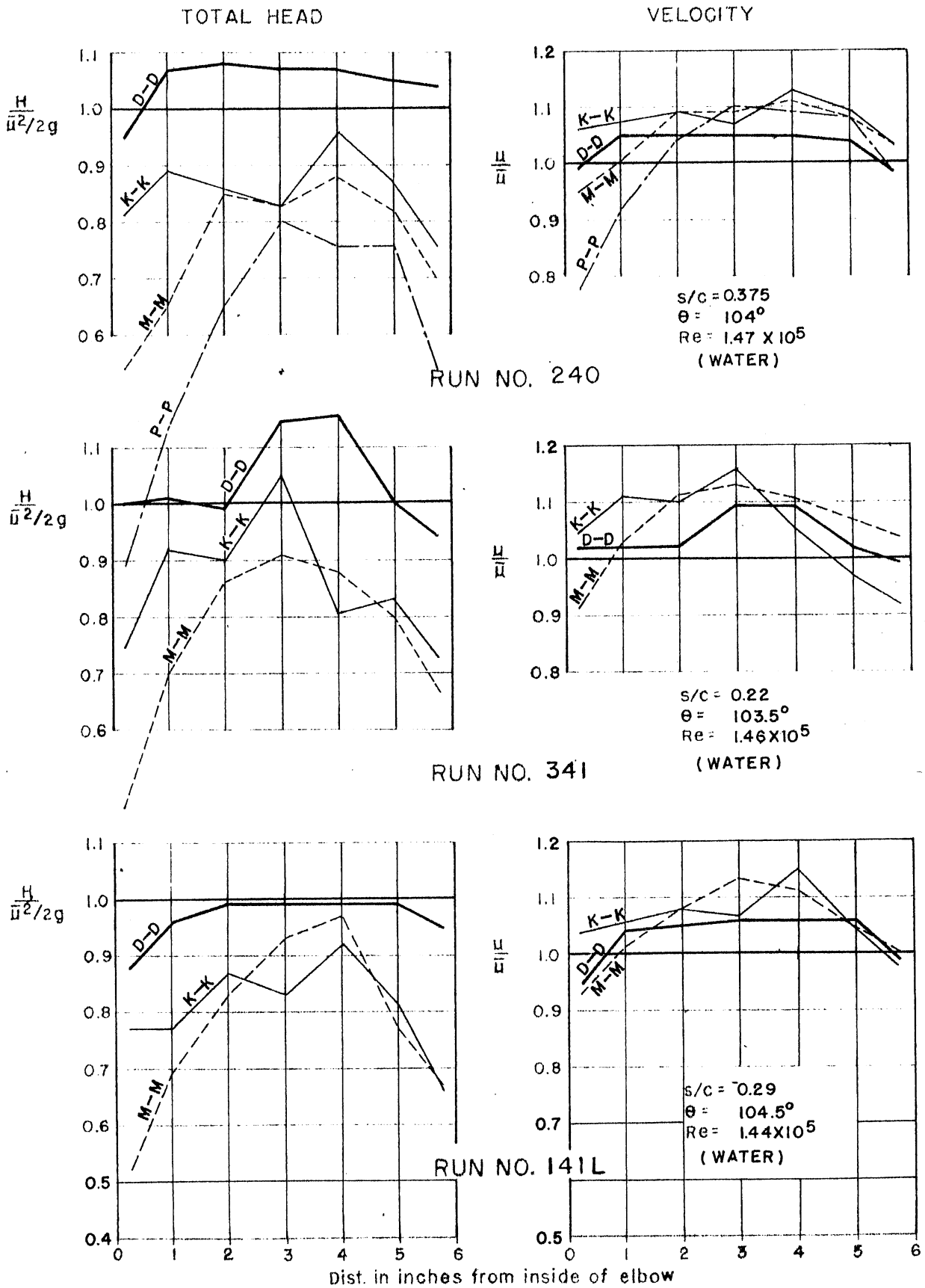

FIG. 34
TOTAL HEAD AND VELOCITY DISTRIBUTION
AT MID-DEPTH AT SEVERAL MEASURING STATIONS
RUN NOS. 240, 341, 141L
((21) 300 VANE)

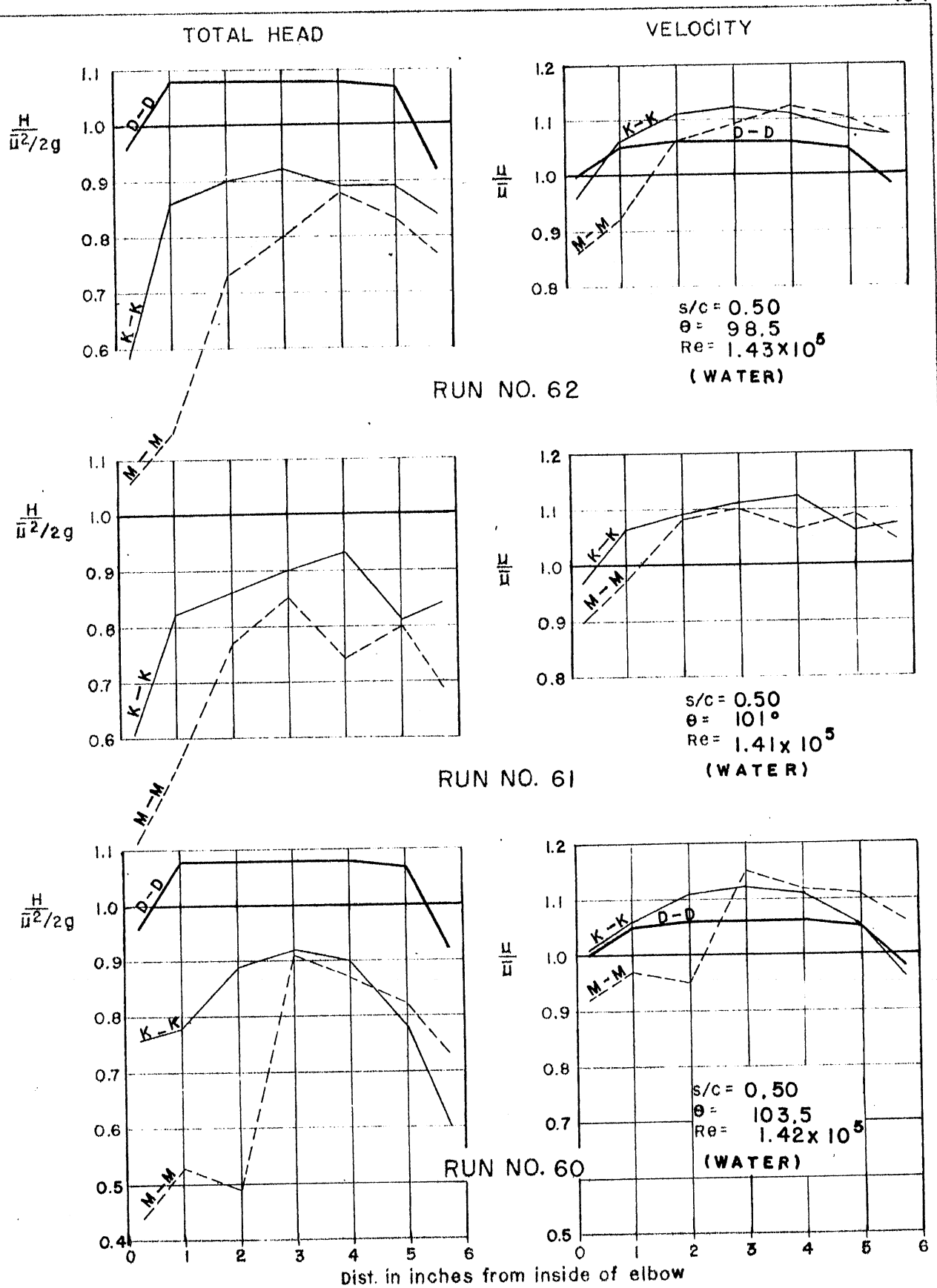

FIG. 35
TOTAL HEAD AND VELOCITY DISTRIBUTION
AT MID-DEPTH AT SEVERAL MEASURING STATIONS
RUN NOS. 60, 61, 62
((30) 30° VANE)

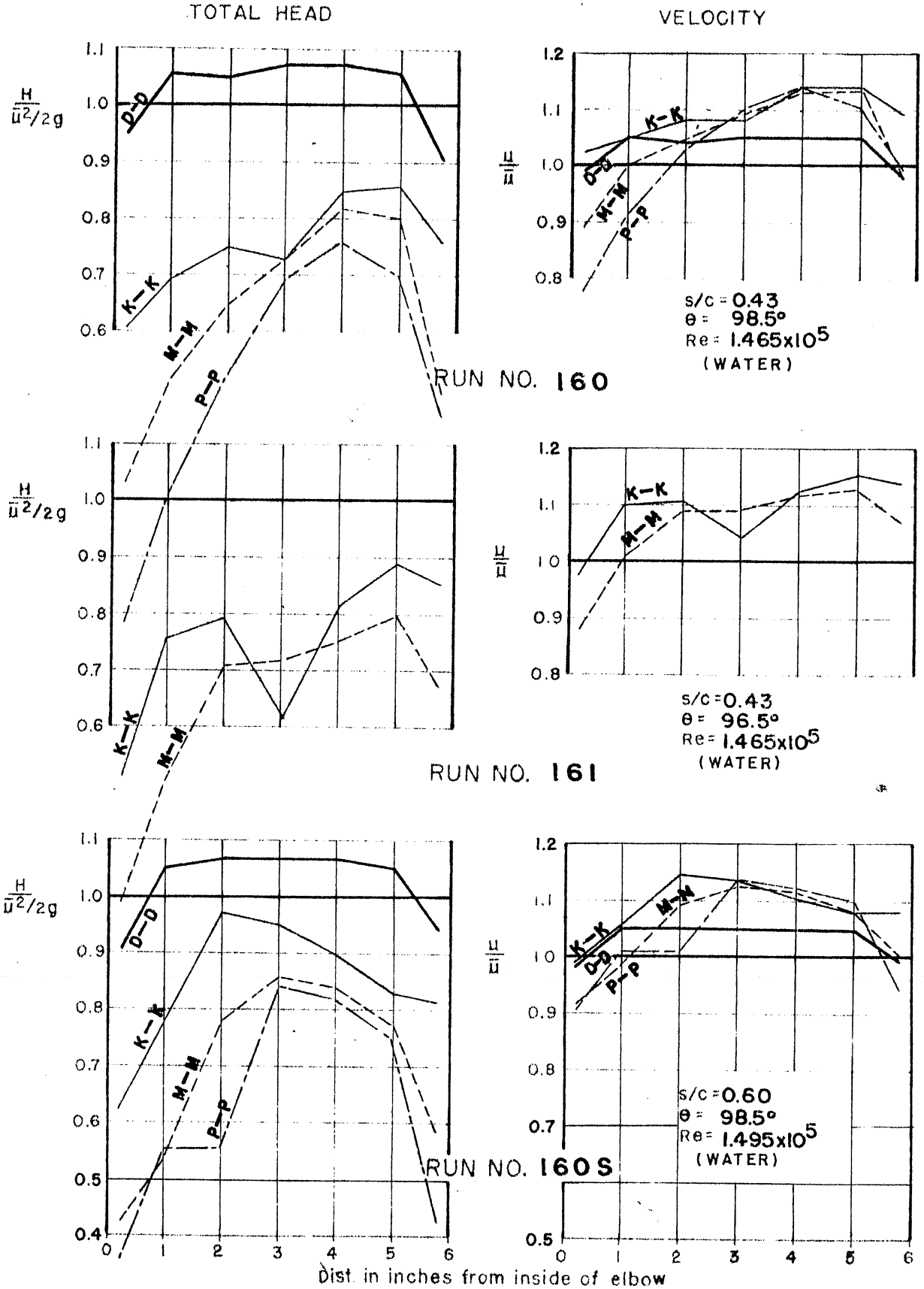

FIG. 36
TOTAL HEAD AND VELOCITY DISTRIBUTION
AT MID-DEPTH AT SEVERAL MEASURING STATIONS
RUN NOS. 160, 161, 160 S
((30) 300 VANE)

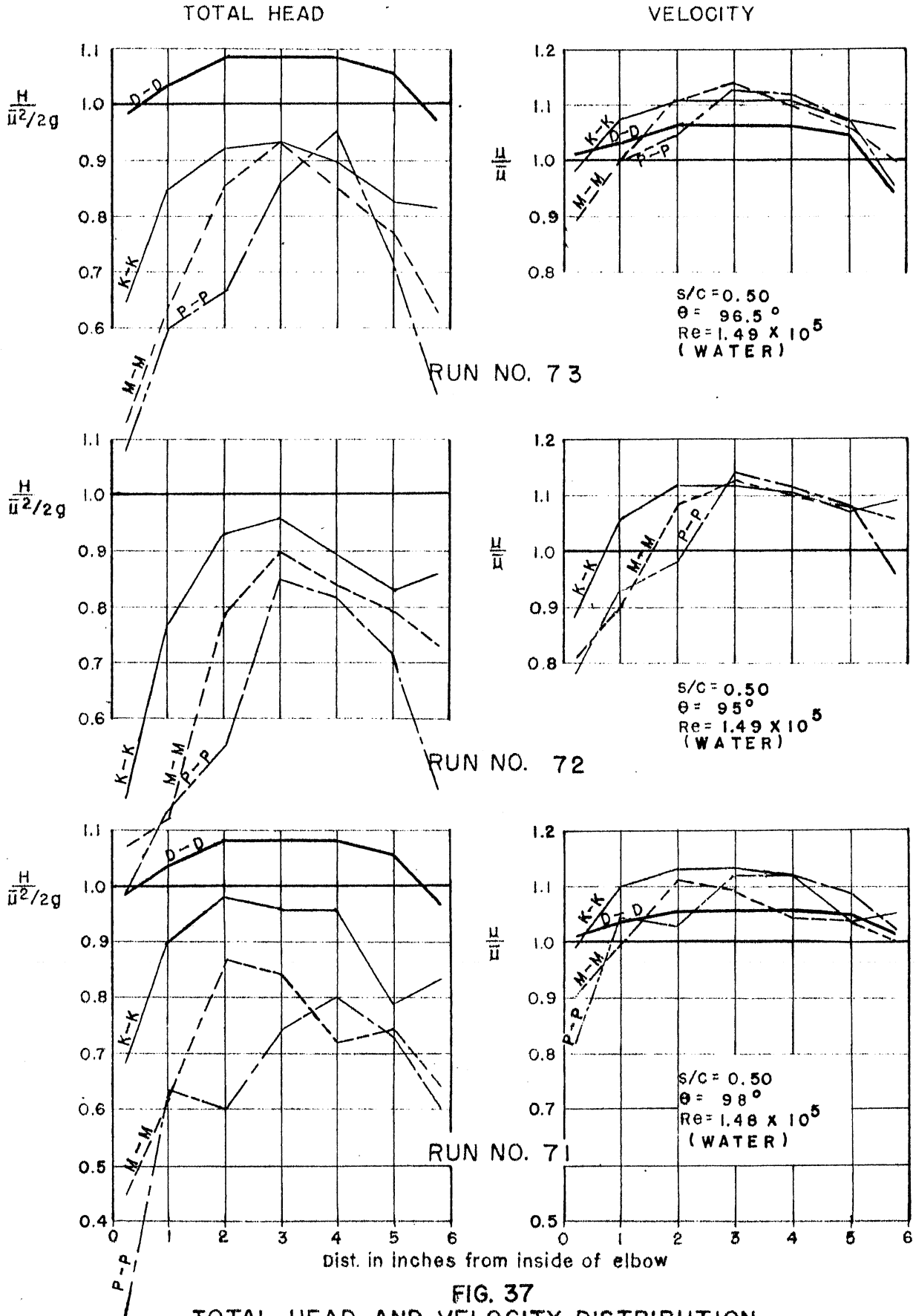

FIG. 37
TOTAL HEAD AND VELOCITY DISTRIBUTION
AT MID-DEPTH AT SEVERAL MEASURING STATIONS
RUN NOS. 71, 72, 73
((30) 400 VANE)

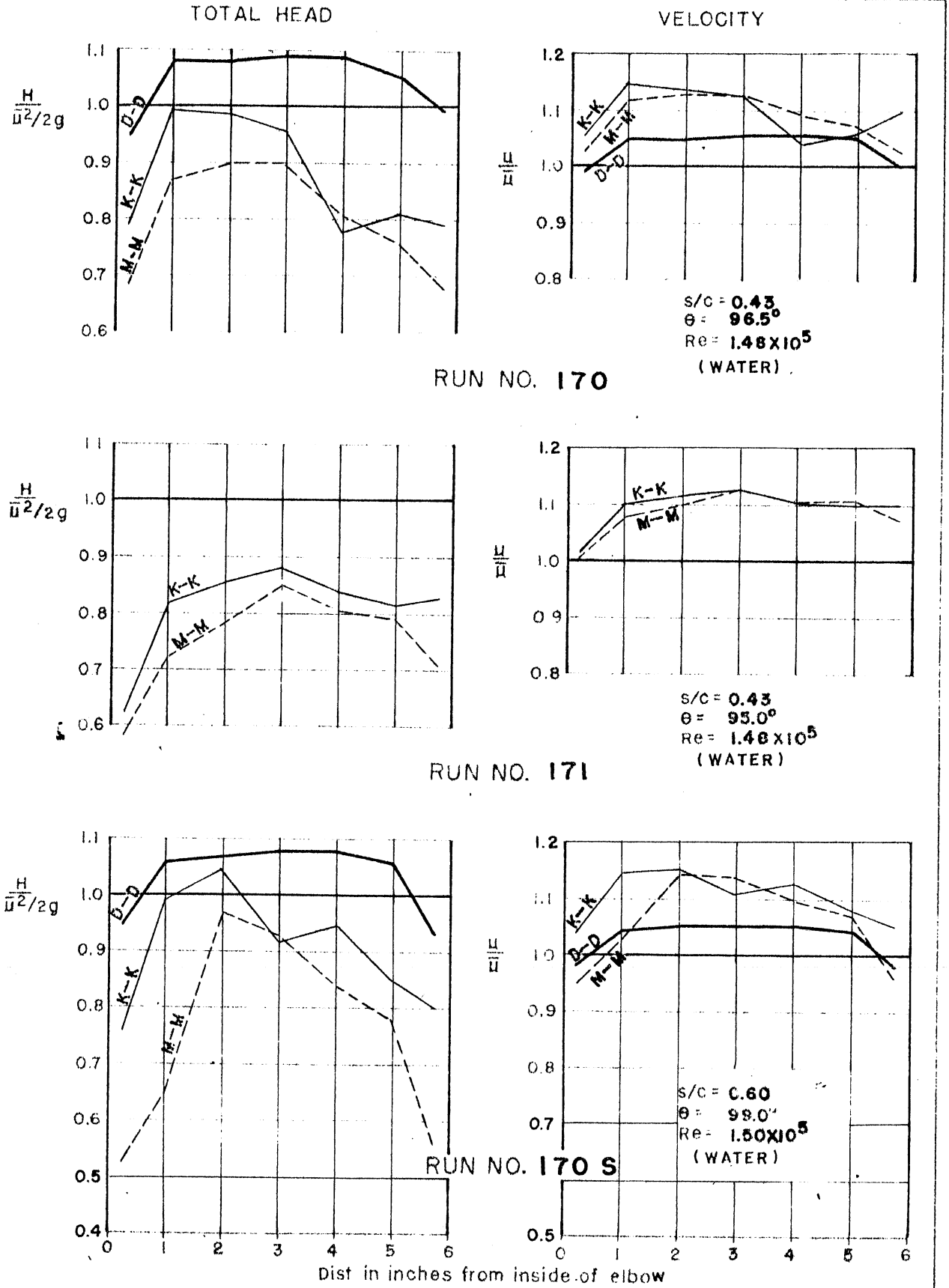

FIG. 38
TOTAL HEAD AND VELOCITY DISTRIBUTION
AT MID-DEPTH AT SEVERAL MEASURING STATIONS
RUN NOS. 170, 171, 170 S
((30) 400 VANE)

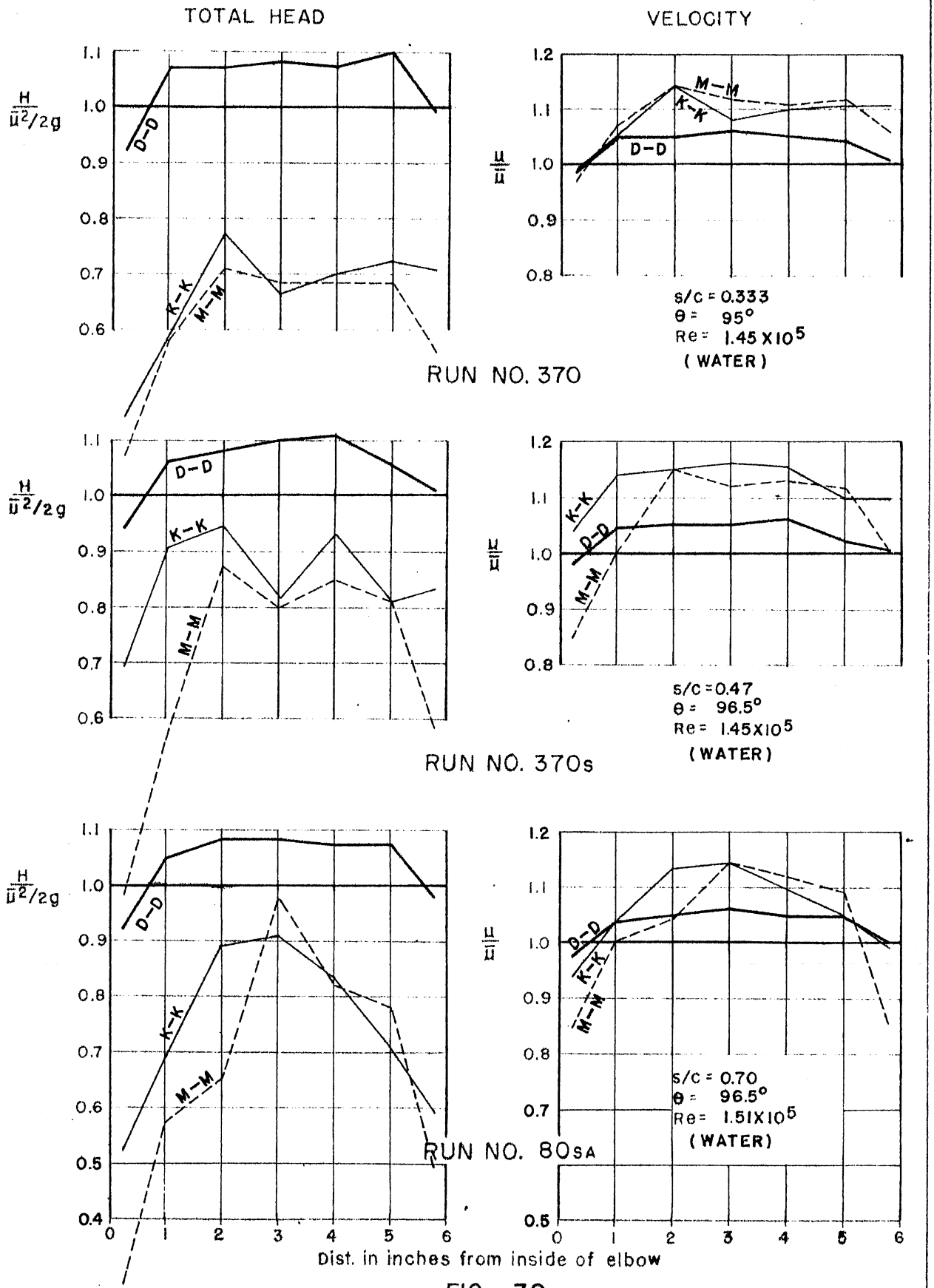

FIG. 39
TOTAL HEAD AND VELOCITY DISTRIBUTION
AT MID-DEPTH AT SEVERAL MEASURING STATIONS
RUN NOS. 370, 370s, 80sA
((30)400 VANE)

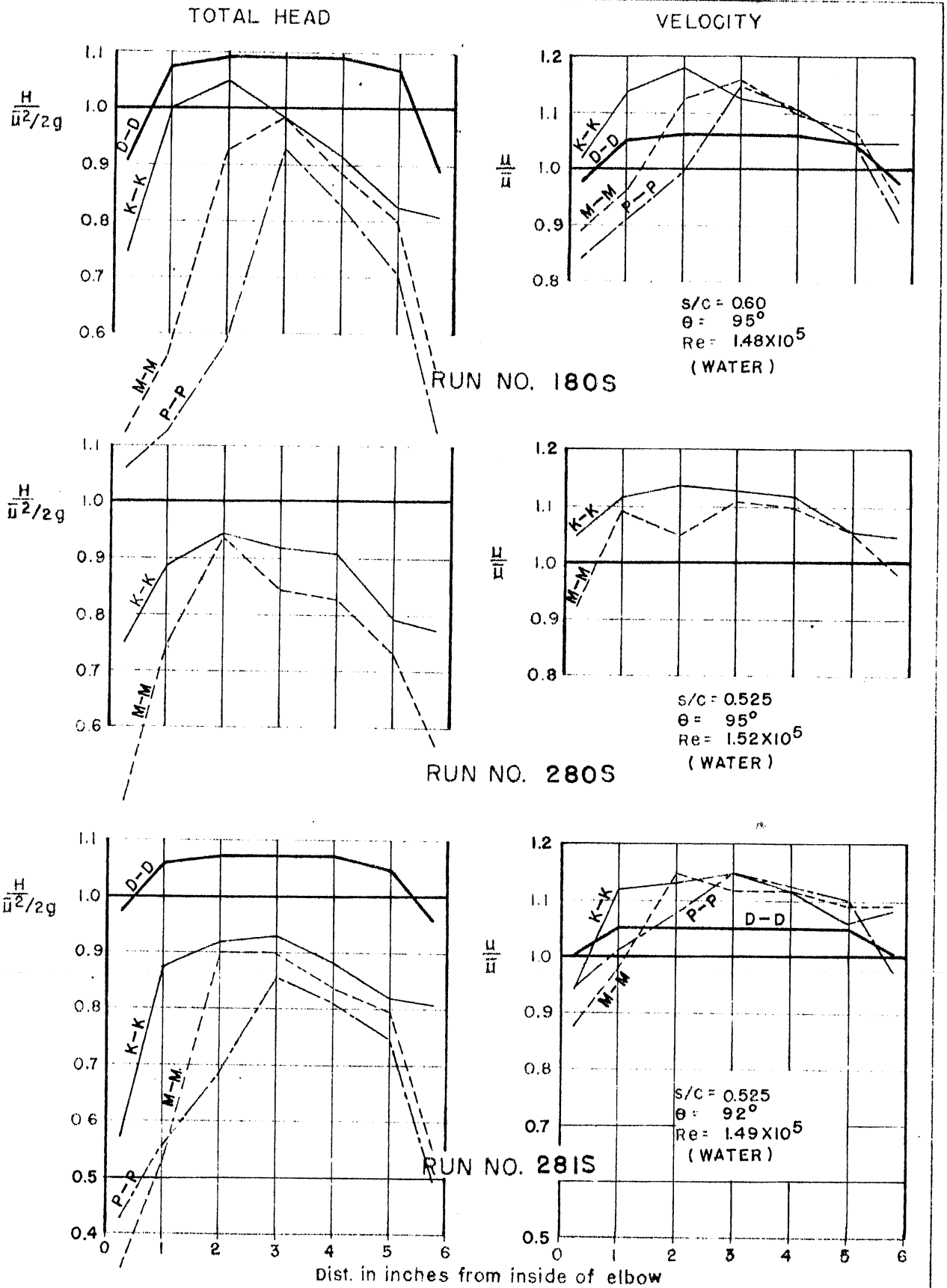

FIG. 40
TOTAL HEAD AND VELOCITY DISTRIBUTION
AT MID-DEPTH AT SEVERAL MEASURING STATIONS
RUN NOS. 180S, 280S, 281S
((30)500 VANE)

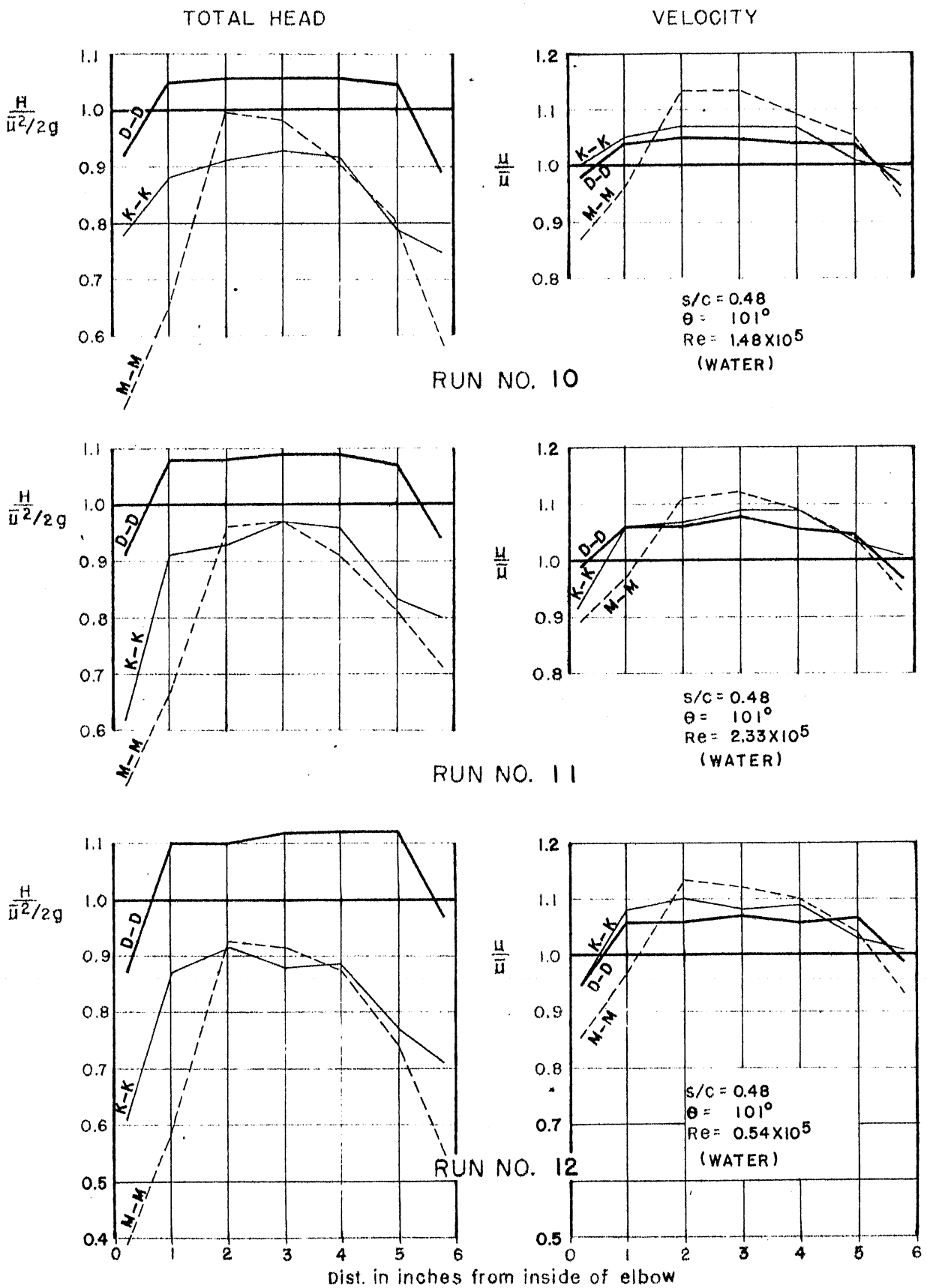

FIG. 41
TOTAL HEAD AND VELOCITY DISTRIBUTION
AT MID-DEPTH AT SEVERAL MEASURING STATIONS
RUN NOS. 10, 11, 12
(TYPE I VANE)

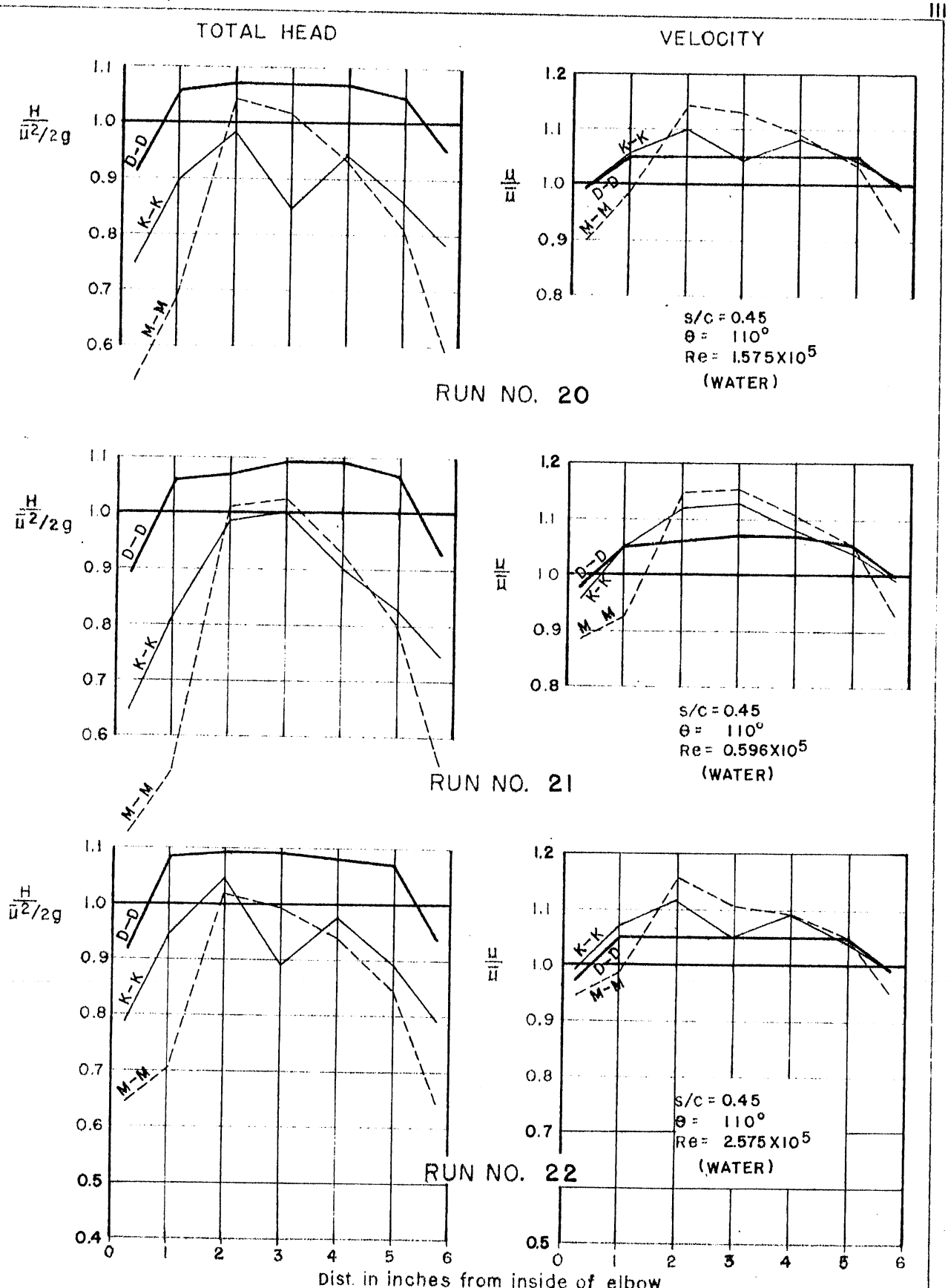

FIG. 42
TOTAL HEAD AND VELOCITY DISTRIBUTION
AT MID-DEPTH AT SEVERAL MEASURING STATIONS
RUN NOS. 20, 21, 22
(TYPE II VANE)

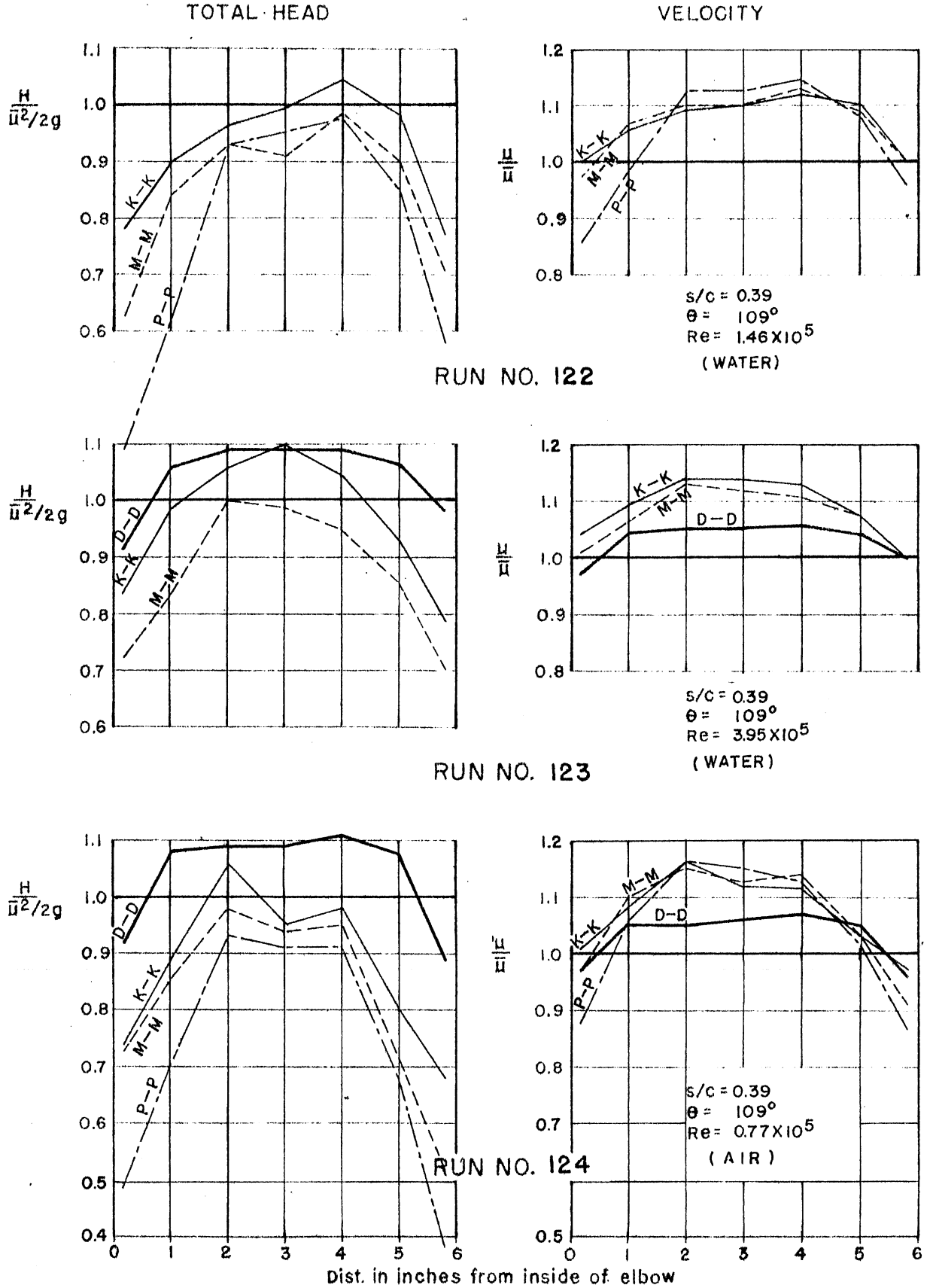

FIG. 43
TOTAL HEAD AND VELOCITY DISTRIBUTION
AT MID-DEPTH AT SEVERAL MEASURING STATIONS
RUN NOS. 122, 123, 124
(TYPE II VANE)

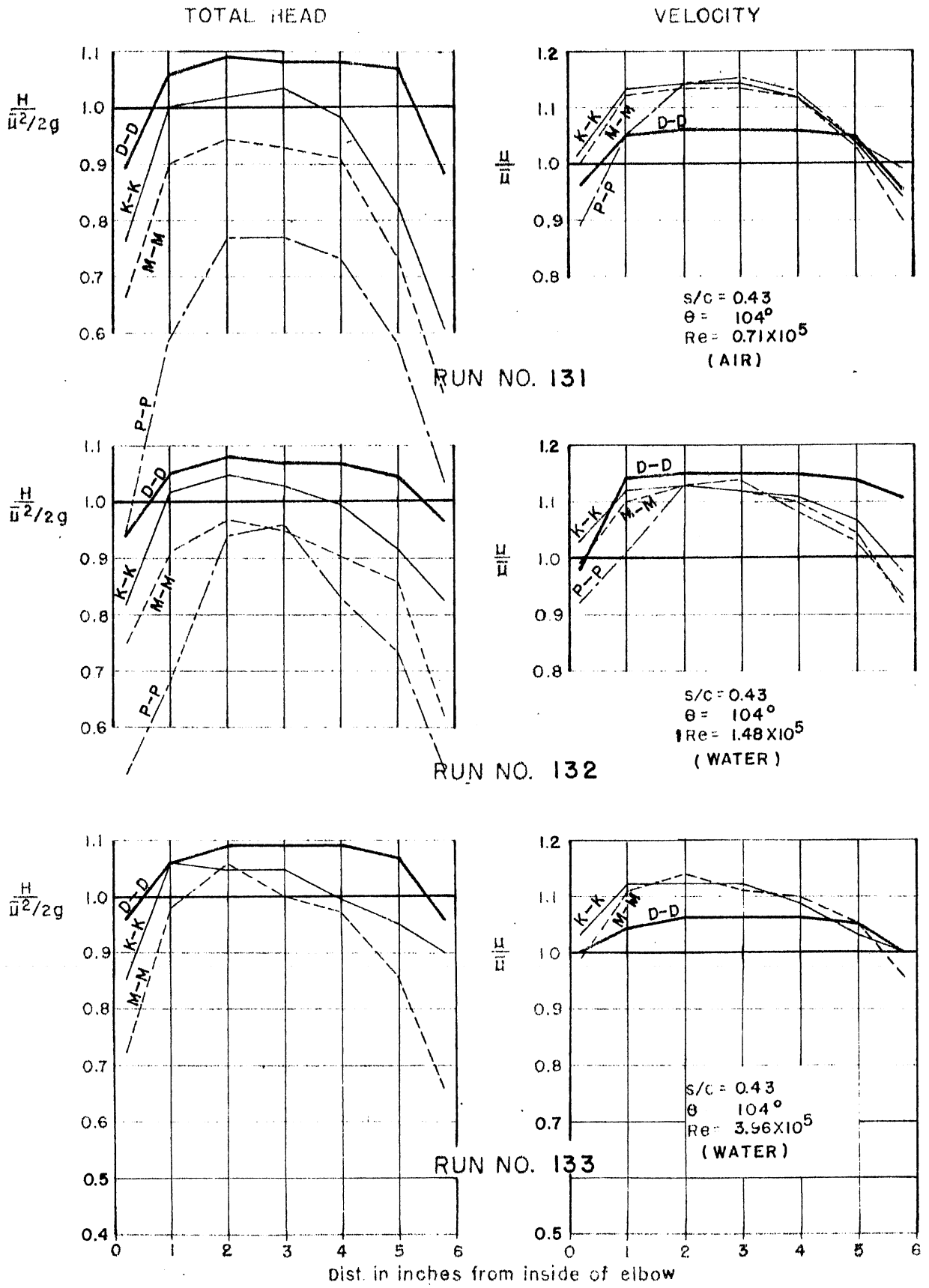

FIG. 44
TOTAL HEAD AND VELOCITY DISTRIBUTION
AT MID-DEPTH AT SEVERAL MEASURING STATIONS
RUN NOS. 131, 132, 133
((21) 315 VANE)

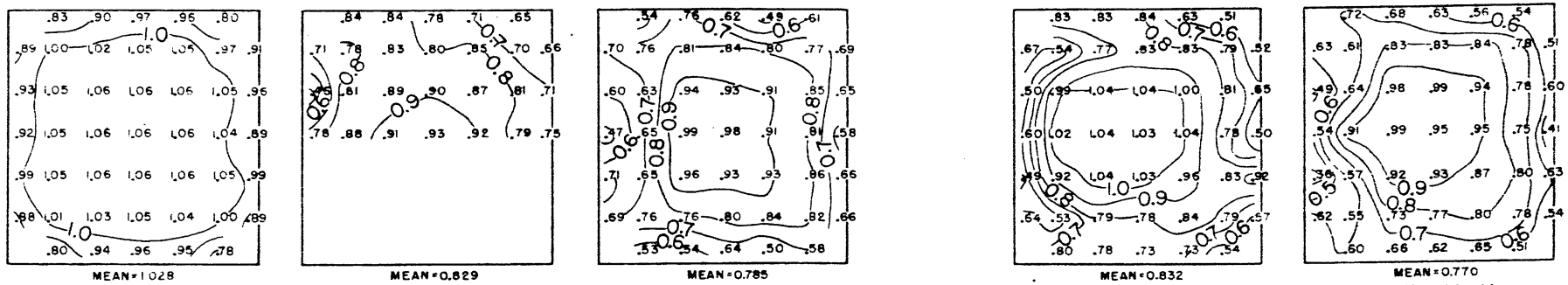

INSIDE OF BEND

OUTSIDE OF BEND

TOTAL HEAD CONTOURS
(Total Head in Ft. Divided by Mean Vel. Head in Ft.)

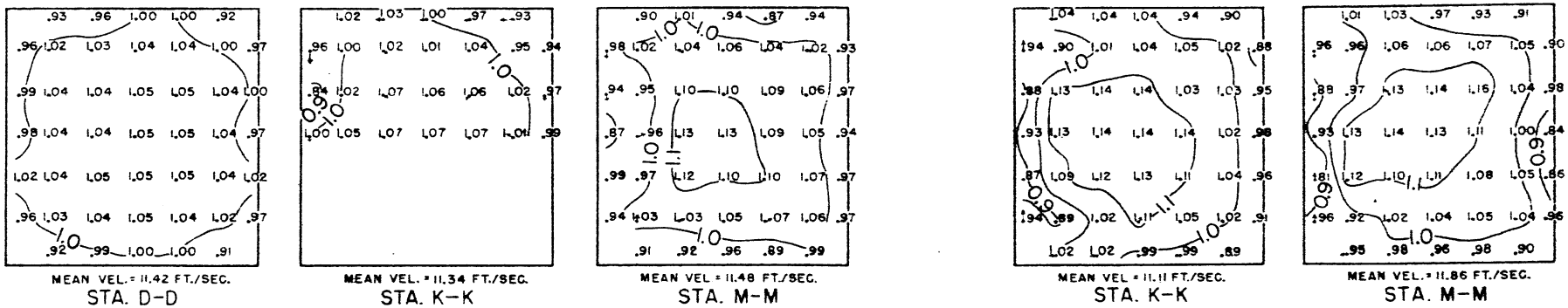

VELOCITY CONTOURS
(Velocity in Ft./Sec. Divided by Mean Velocity in Ft./Sec.)

S/c = 0.48
θ = 100°–101°
Re = 1.48–1.52 X 10^5

0.0 .1 .2 .3 .4 0.5
Scale of Velocity Vectors
Units of Mean Vel.

RUN NO. 10
(Large Space Between Vanes and Walls)

TYPE I VANE

RUN NO. 10A
(Small Space Between Vanes and Walls)

FIG. 45
TOTAL HEAD AND VELOCITY DATA SHOWING EFFECT OF LATERAL WALLS

INSIDE OF BEND

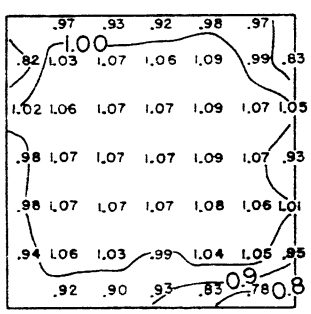

STA. D–D

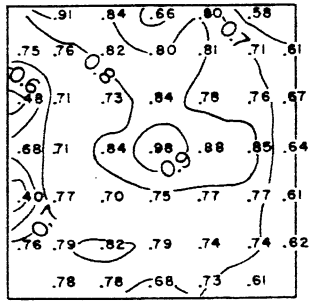

STA. K–K

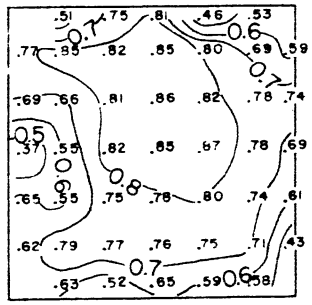

STA. M–M

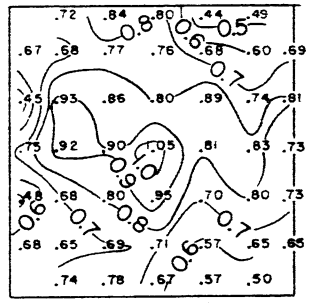

STA. K–K

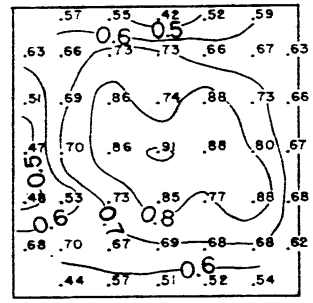

STA. M–M

OUTSIDE OF BEND

TOTAL HEAD CONTOURS
(Total Head in Ft. Divided by Mean Vel. Head in Ft.)

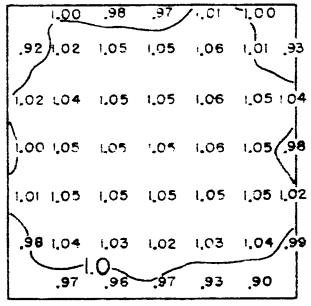

STA. D–D

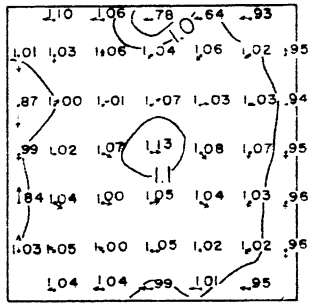

STA. K–K

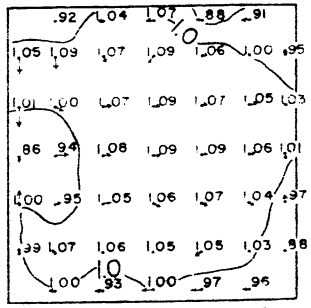

STA. M–M

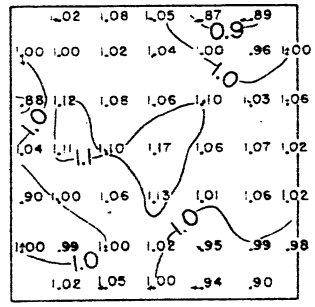

STA. K–K

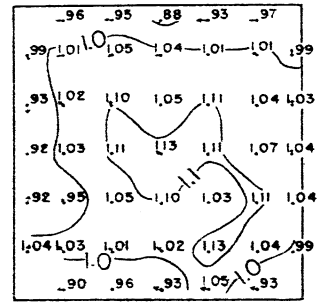

STA. M–M

VELOCITY CONTOURS
(Velocity in Ft./Sec. Divided by Mean Velocity in Ft./Sec.)

S/c = 0.333
θ = 103.5°
Re = 1.50 X 10^5

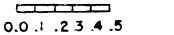

RUN NO. 46L
(4.25" CHORD)

(21)300 VANE

RUN NO. 341
(2.83" CHORD)

FIG. 46
TOTAL HEAD AND VELOCITY DATA
SHOWING EFFECT OF CHORD LENGTH

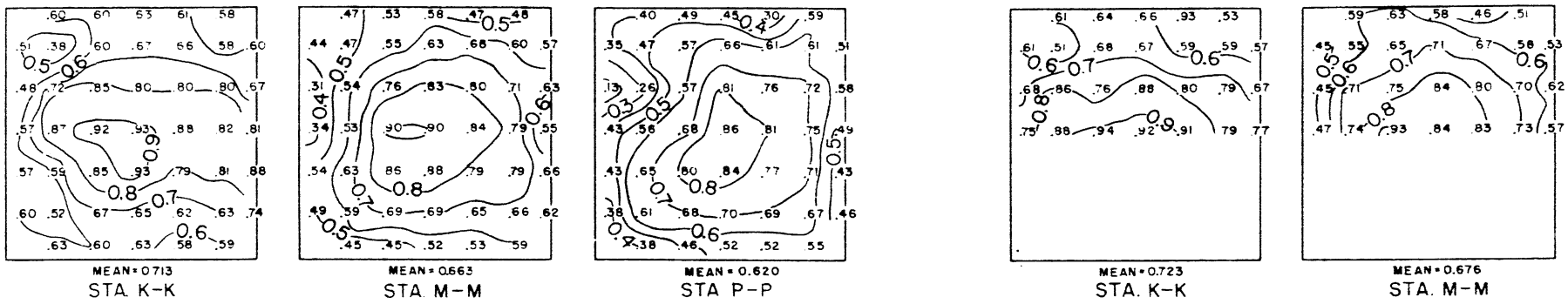

INSIDE OF BEND

OUTSIDE OF BEND

TOTAL HEAD CONTOURS
(Total Head in Ft. Divided by Mean Vel. Head in Ft.)

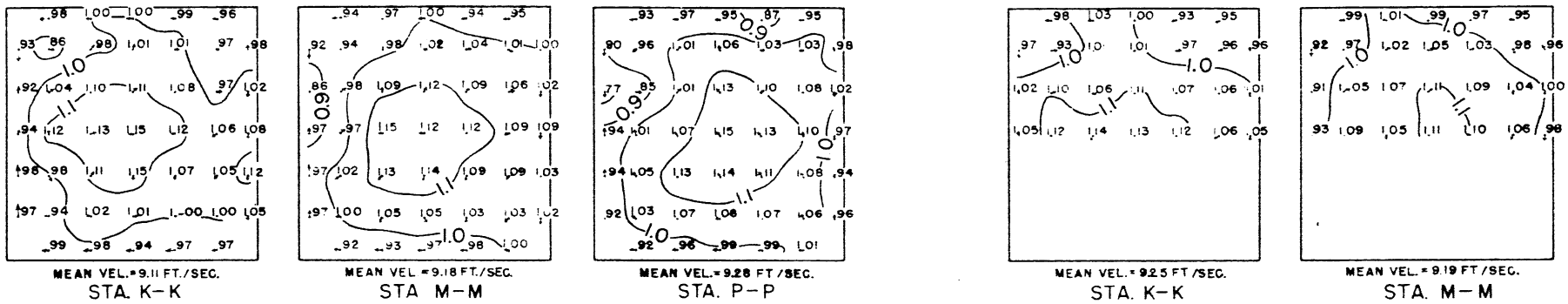

VELOCITY CONTOURS
(Velocity in Ft./Sec. Divided by Mean Velocity in Ft./Sec.)

S/c = 0.525
Re = 1.49 X 10^5

0.0 1 2 3 4 0.5
Scale of Velocity Vectors
Units of Mean Vel.

RUN NO. 281S
(θ = 92°)

(30) 500 VANE

RUN NO. 280S
(θ = 95°)

FIG. 47
TOTAL HEAD AND VELOCITY DATA SHOWING EFFECT OF OVERTURNING AND UNDERTURNING

INSIDE OF BEND

OUTSIDE OF BEND

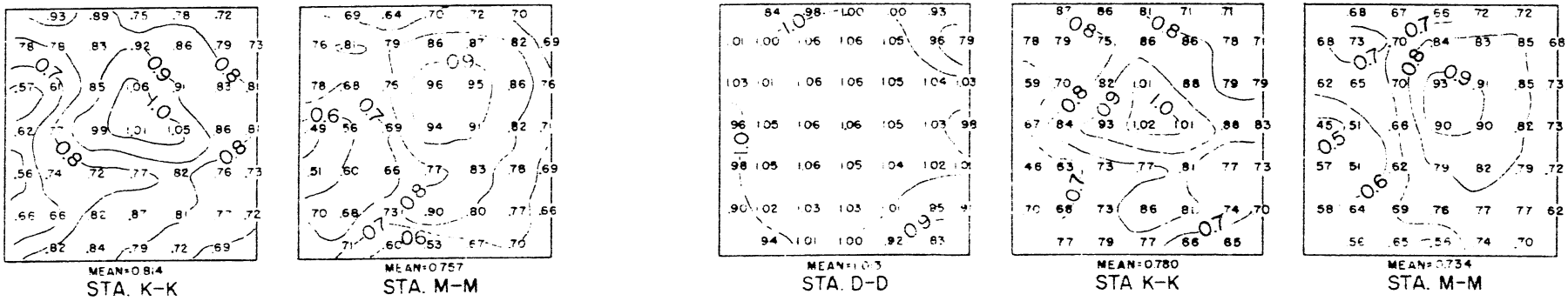

TOTAL HEAD CONTOURS
(Total Head in Ft. Divided by Mean Vel. Head in Ft.)

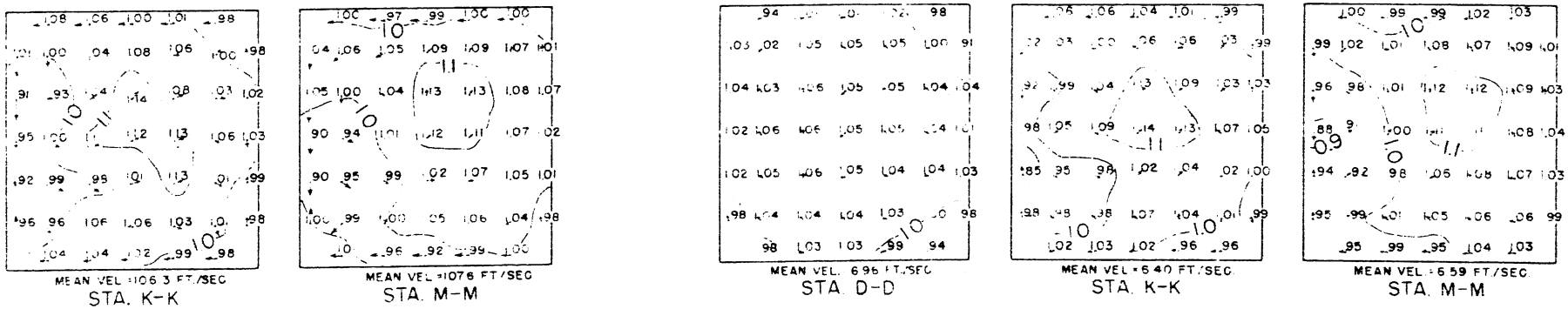

S/c = 0.50
θ = 103°
Re = 1.48 x 10^5

VELOCITY CONTOURS
(Velocity in Ft./Sec. Divided by Mean Velocity in Ft./Sec.)

RUN NO. 41
(AIR)

(21)300 VANE

RUN NO. 42
(WATER)

FIG. 48
TOTAL HEAD AND VELOCITY DATA
SHOWING EFFECT OF FLUID

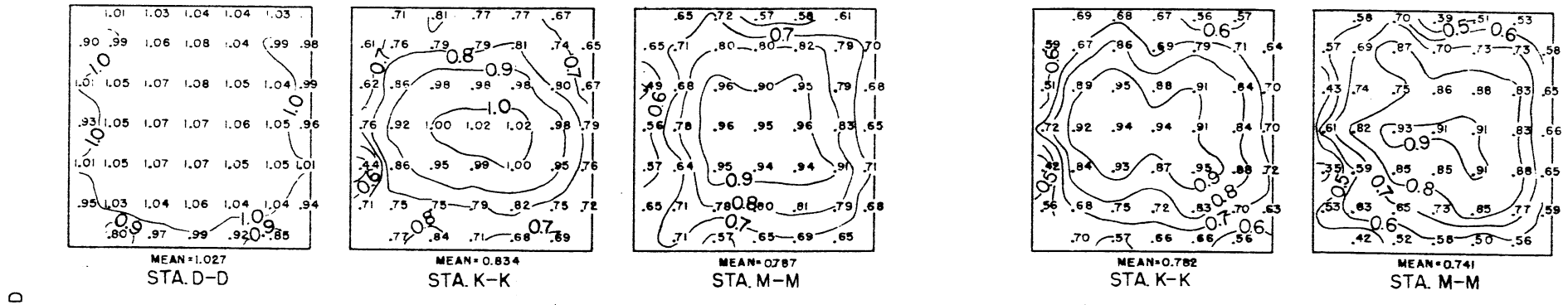

TOTAL HEAD CONTOURS
(Total Head in Ft. Divided by Mean Vel. Head in Ft.)

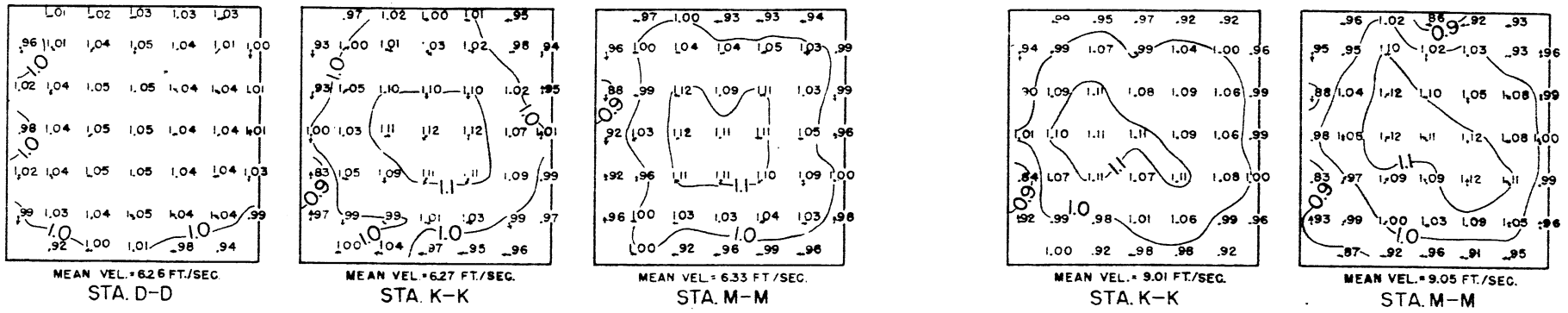

VELOCITY CONTOURS
(Velocity in Ft./Sec. Divided by Mean Velocity in Ft./Sec.)

$Re = 1.50 \times 10^5$

0.0 .1 .2 .3 .4 0.5
Scale of Velocity Vectors
Units of Mean Vel.

RUN NO. 110
(S/c = 0.41)
(θ=98°)

TYPE I VANE

RUN NO. 311
(S/c = 0.32)
(θ=97°)

FIG. 49
TOTAL HEAD AND VELOCITY DATA SHOWING EFFECT OF SPACING ON VELOCITY DISTRIBUTION

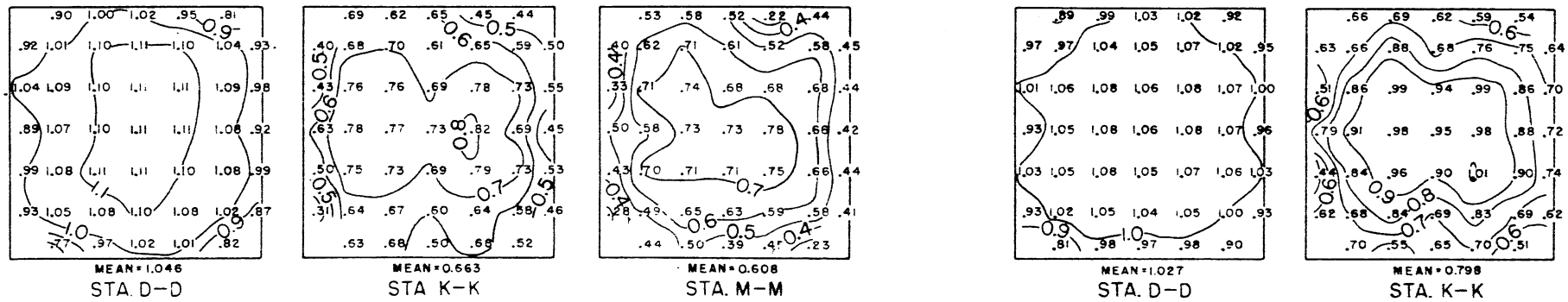

INSIDE OF BEND

OUTSIDE OF BEND

TOTAL HEAD CONTOURS
(Total Head in Ft. Divided by Mean Vel. Head in Ft.)

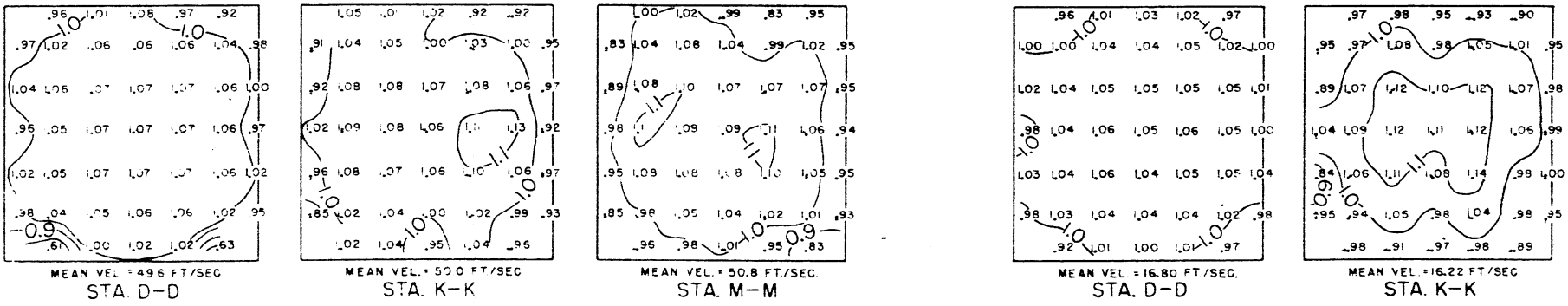

VELOCITY CONTOURS
(Velocity in Ft./Sec. Divided by Mean Velocity in Ft./Sec.)

S/δ = 0.32

θ = 97°

Scale of velocity vectors
Units of Mean ve

RUN NO. 312
(Re = 0.7 X 10^5)
(AIR)

TYPE I VANE

RUN NO. 314
(Re = 3.0 X 10^5)
(WATER)

FIG. 50
TOTAL HEAD AND VELOCITY DATA SHOWING EFFECT OF REYNOLDS NUMBER

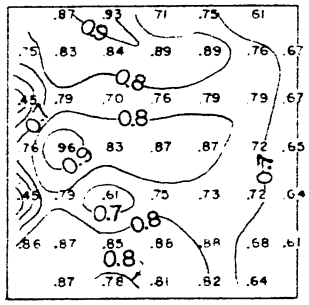

STA. K-K

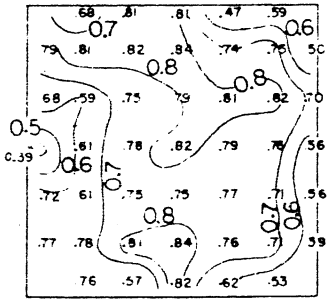

STA. M-M

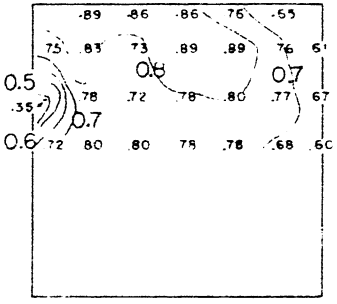

STA. K-K

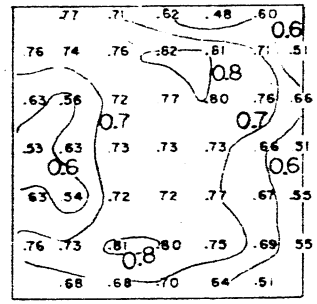

STA. M-M

INSIDE OF BEND

OUTSIDE OF BEND

TOTAL HEAD CONTOURS
(Total Head in Ft. Divided by Mean Vel. Head in Ft.)

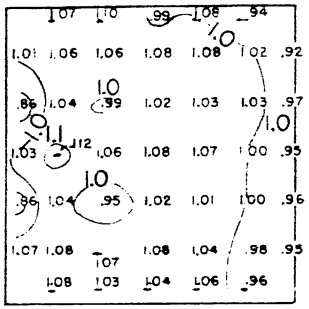

STA. K-K

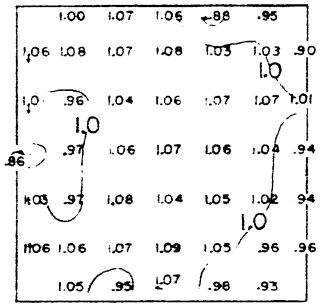

STA. M-M

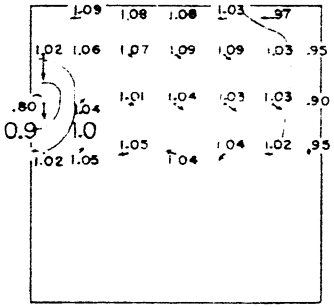

STA. K-K

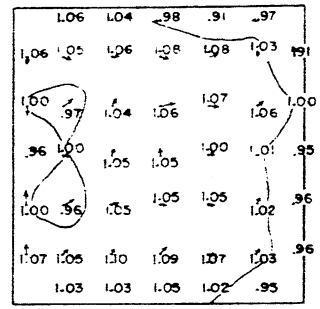

STA. M-M

VELOCITY CONTOURS
(Velocity in Ft./Sec. Divided by Mean Velocity in Ft./Sec.)

S/c = 0.333
θ = 103.5°
Re = 2.22 X 10^5

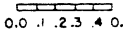

Scale of Velocity Vectors
Units of Mean Vel

RUN NO. 44L
(STRUT "A" ONLY)

(21)300 VANE

RUN NO. 45L
(STRUTS "A" AND "B")

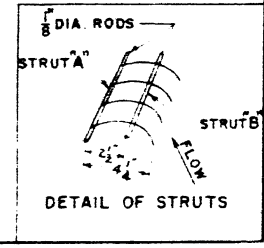

DETAIL OF STRUTS

FIG. 51
TOTAL HEAD AND VELOCITY DATA SHOWING EFFECT OF STRUTS

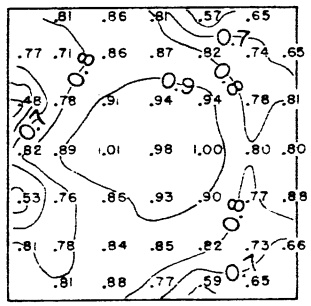

STA. K-K

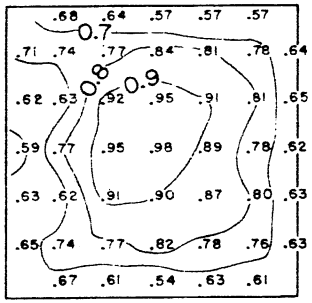

STA. M-M

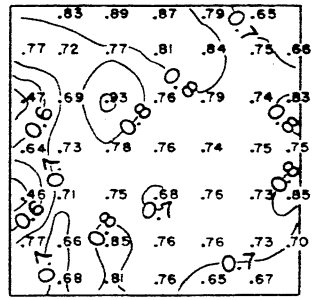

STA. K-K

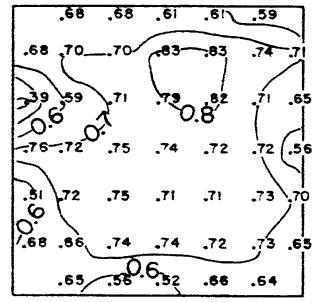

STA. M-M

INSIDE OF BEND

OUTSIDE OF BEND

TOTAL HEAD CONTOURS
(Total Head in Ft. Divided by Mean Vel. Head in Ft.)

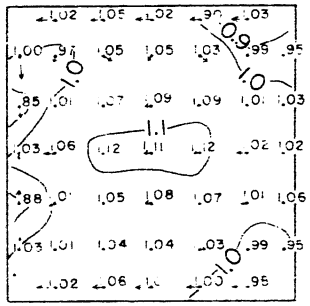

STA. K-K

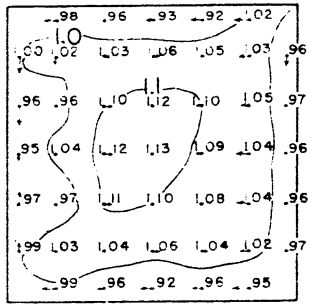

STA. M-M

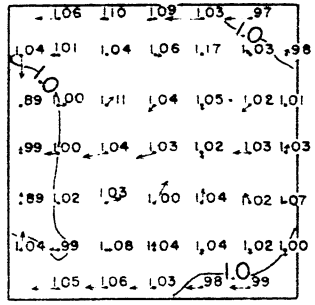

STA. K-K

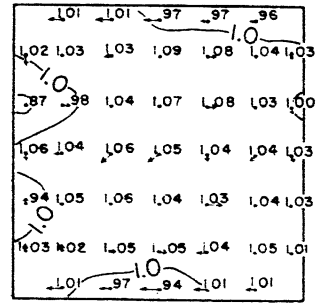

STA. M-M

VELOCITY CONTOURS
(Velocity in Ft./Sec. Divided by Mean Velocity in Ft./Sec.)

S/c = 0.45

θ = 114°

Re = 1.94 X 10^5

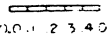

Scale of Velocity Vectors
Units of Mean Vel

RUN NO. 26
(Without Struts)

TYPE II VANE

RUN NO. 28
(With Struts)

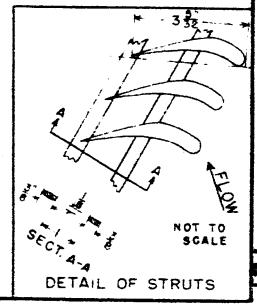

DETAIL OF STRUTS

FIG. 52
TOTAL HEAD AND VELOCITY DATA
SHOWING EFFECT OF STRUTS

INSIDE OF BEND

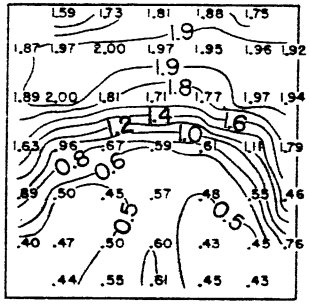

STA. D-D

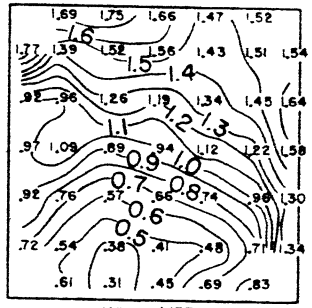

STA. K-K

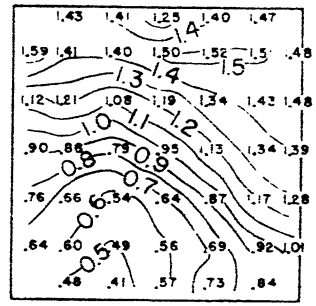

STA. M-M

OUTSIDE OF BEND

TOTAL HEAD CONTOURS
(Total Head in Ft. Divided by Mean Vel. Head in Ft.)

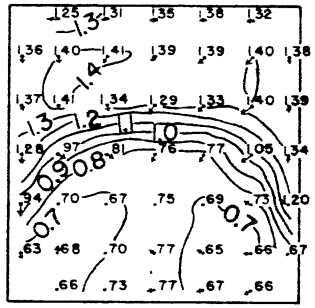

STA. D-D

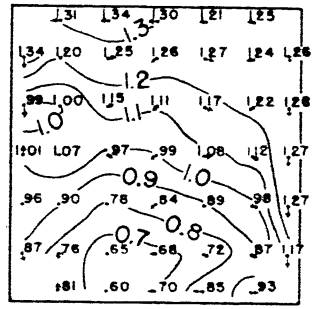

STA. K-K

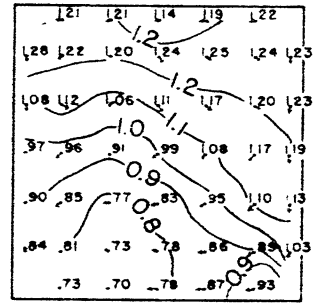

STA. M-M

VELOCITY CONTOURS
(Velocity in Ft./Sec. Divided by Mean Velocity in Ft./Sec.)

RUN NO. 27
(This should be compared with Run No. 26)

S/c = 0.45
θ = 114°
Re = 1.62 X 10^5

Scale of Velocity Vectors
Units of Mean Vel.

TYPE II VANE

FIG. 53
TOTAL HEAD AND VELOCITY DATA
SHOWING EFFECT OF VELOCITY DISTRIBUTION

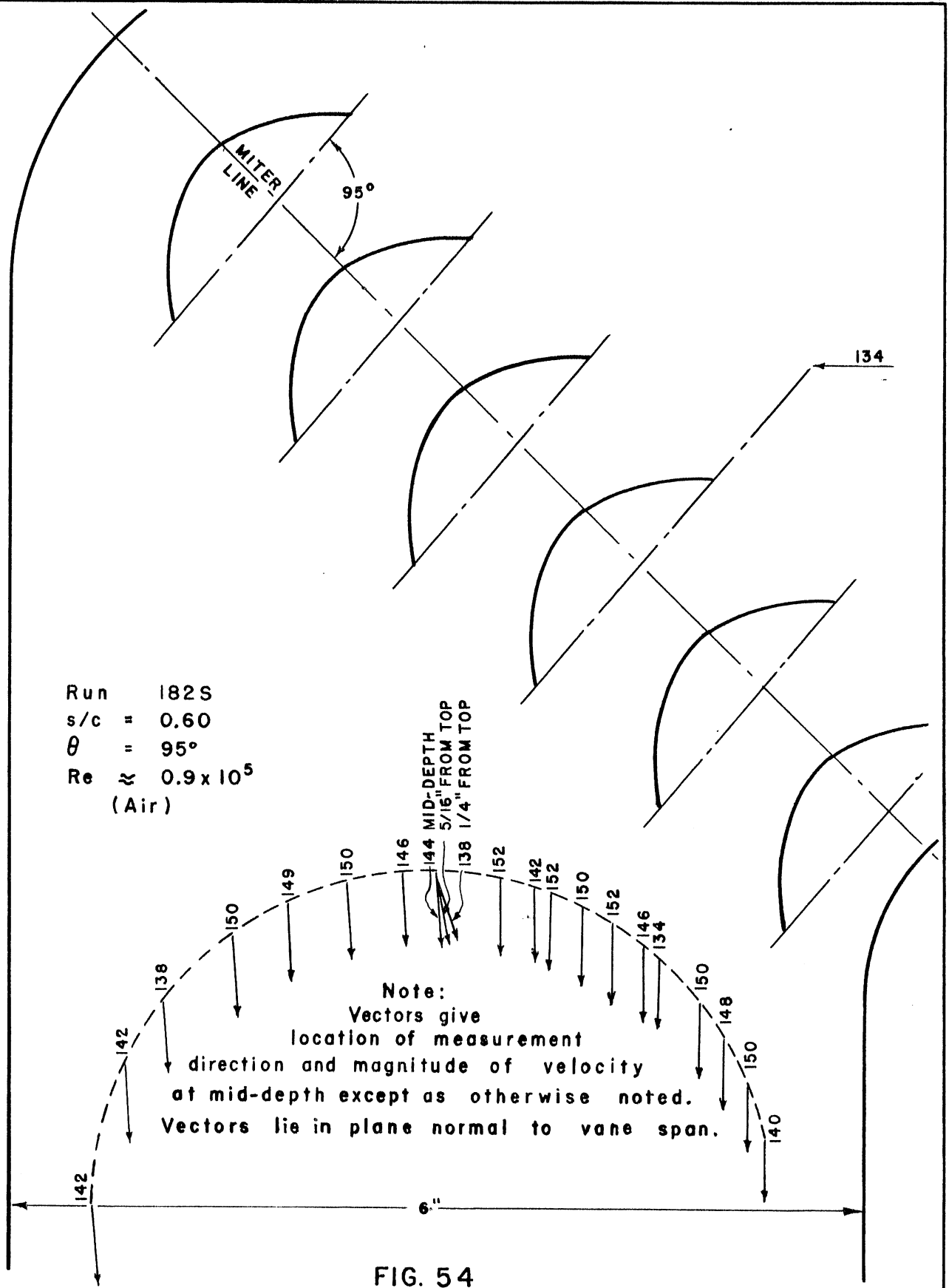

FIG. 54

MEASUREMENTS BY HOT WIRE

BEHIND A CASCADE OF (30) 500 VANES

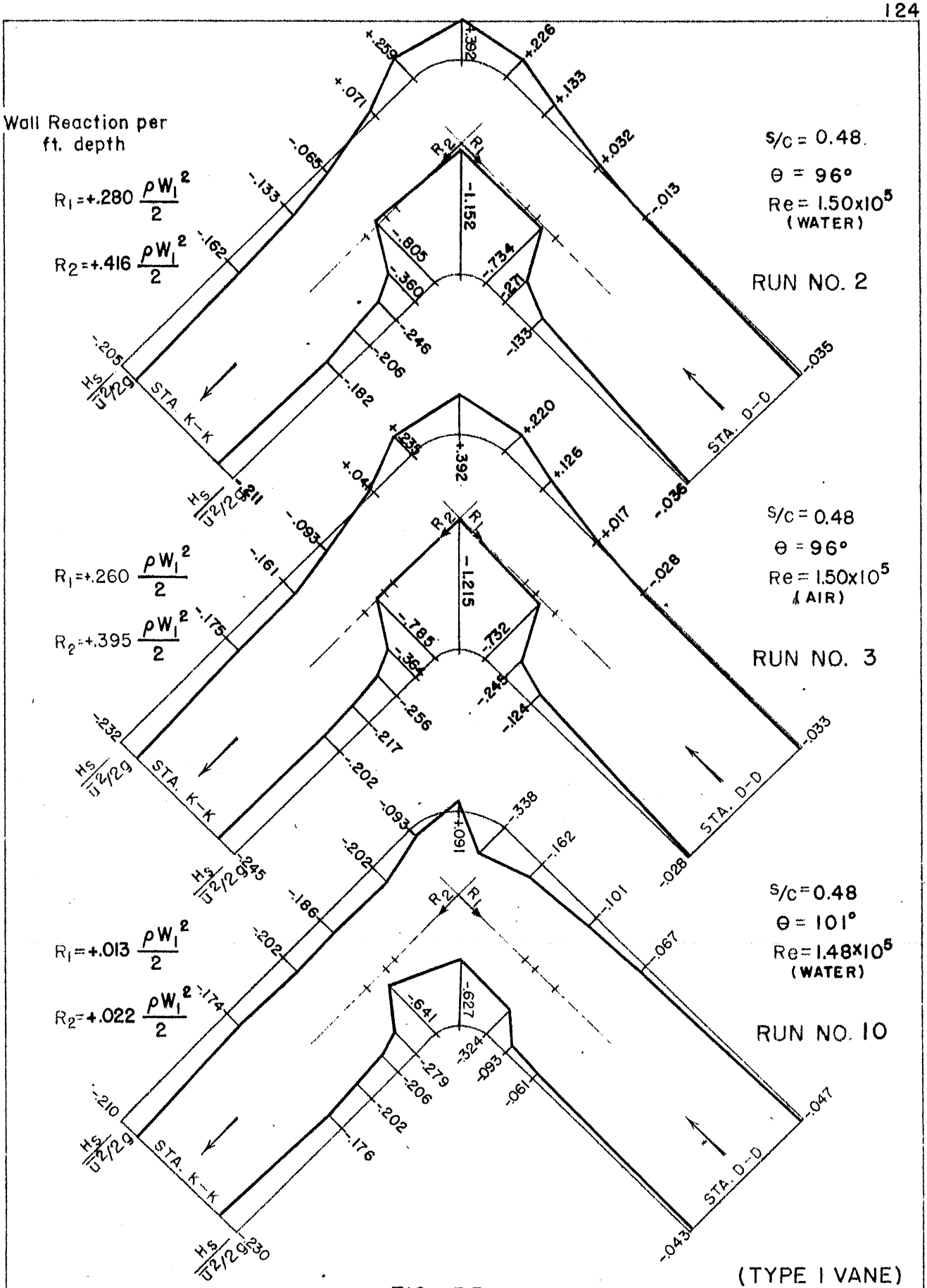

FIG. 55
STATIC HEAD AND REACTION ON WALLS
RUN NO. 2,3,10

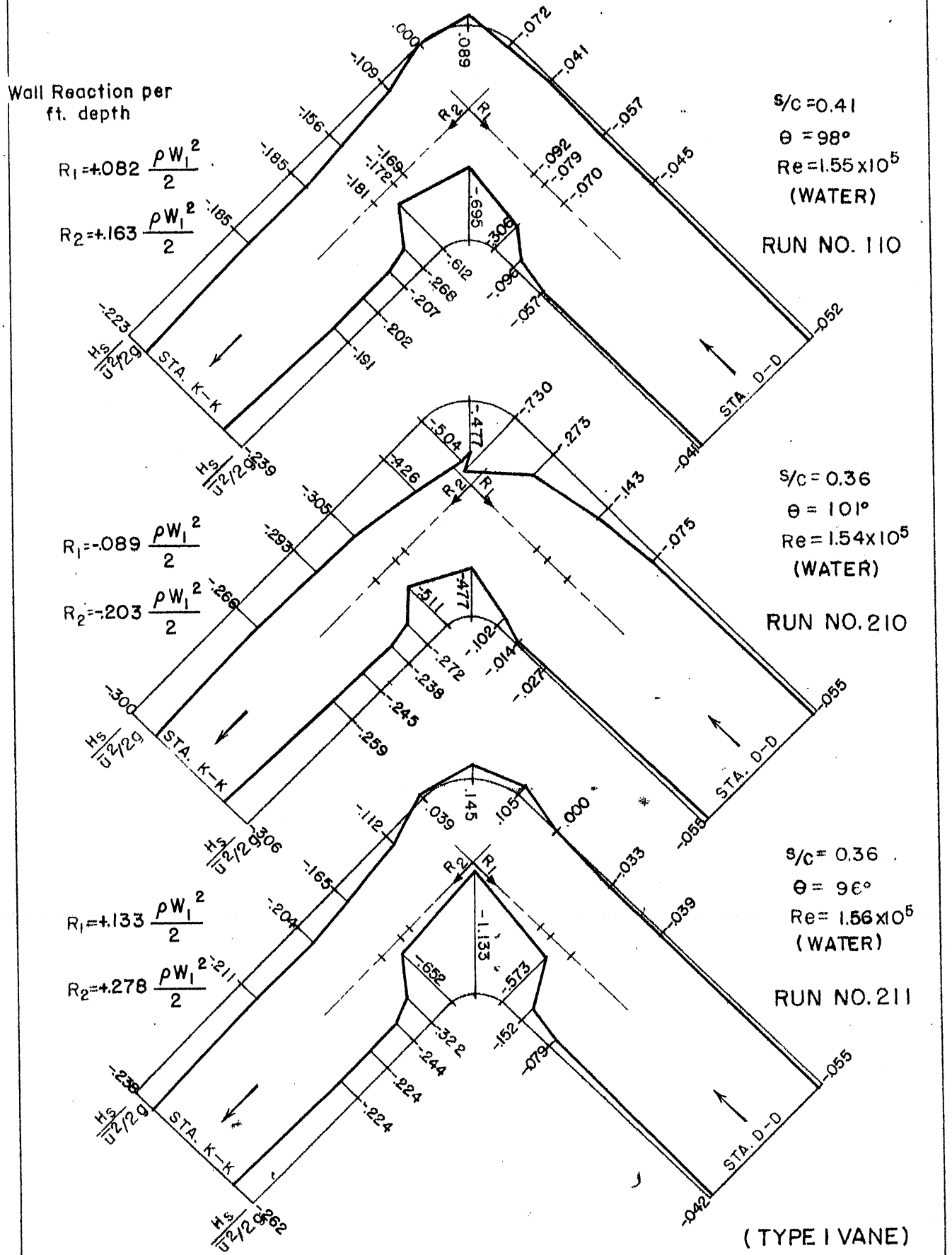

FIG. 56
STATIC HEAD AND REACTION ON WALLS
RUN NO. 110, 210, 211

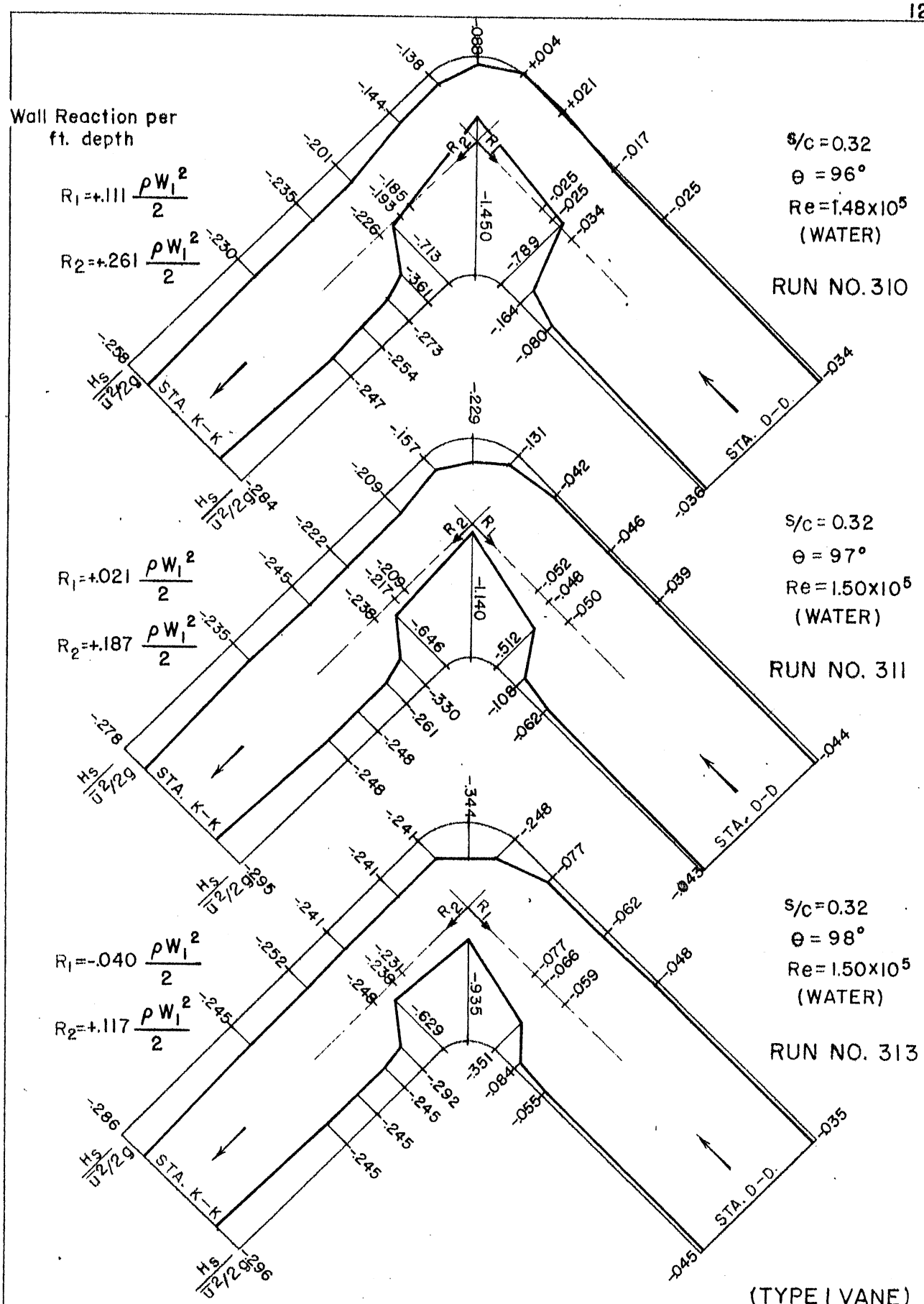

FIG. 57
STATIC HEAD AND REACTION ON WALLS
RUN NO. 310,311,313

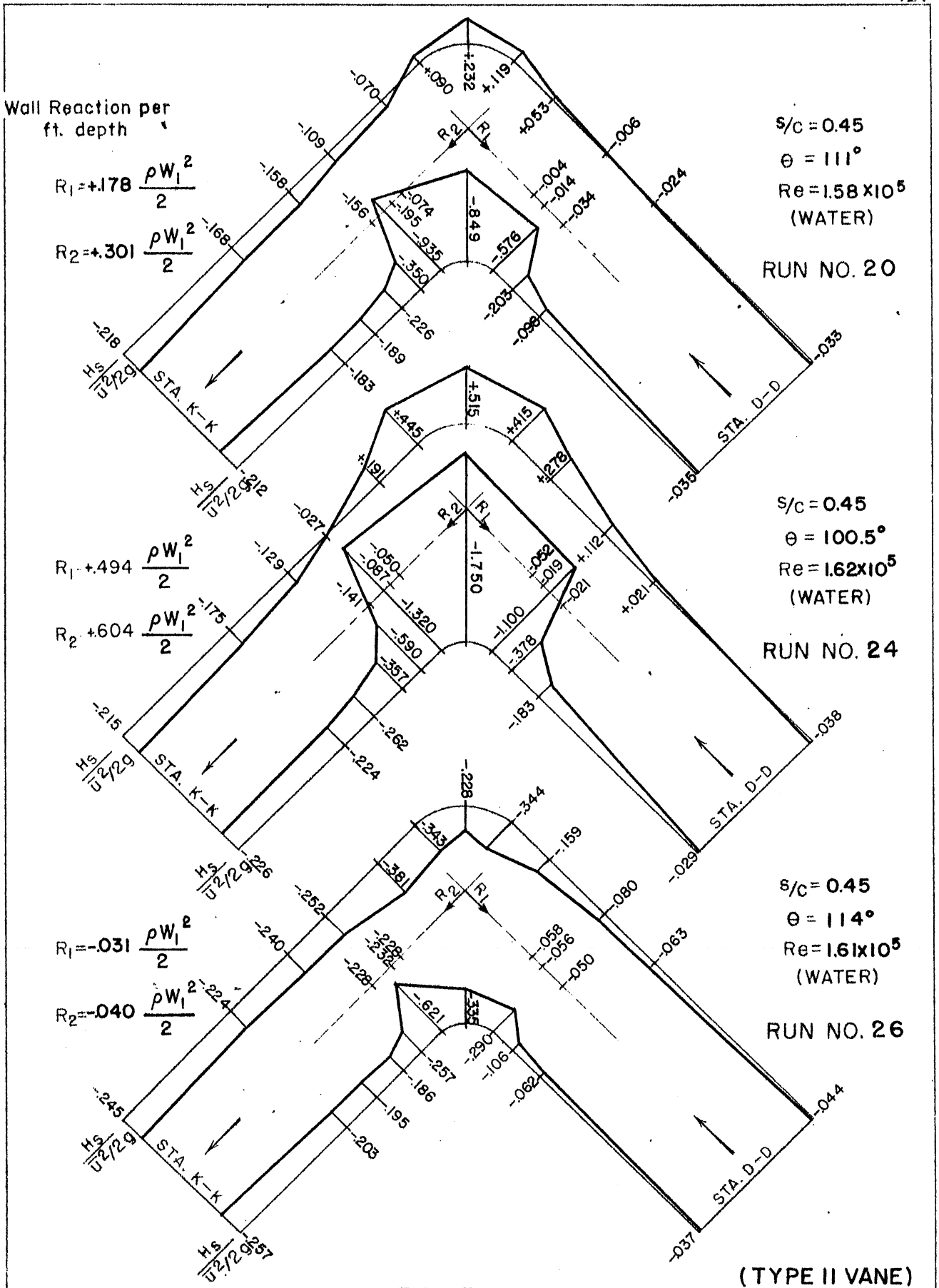

FIG. 58
STATIC HEAD AND REACTION ON WALLS
RUN NO. 20, 24, 26

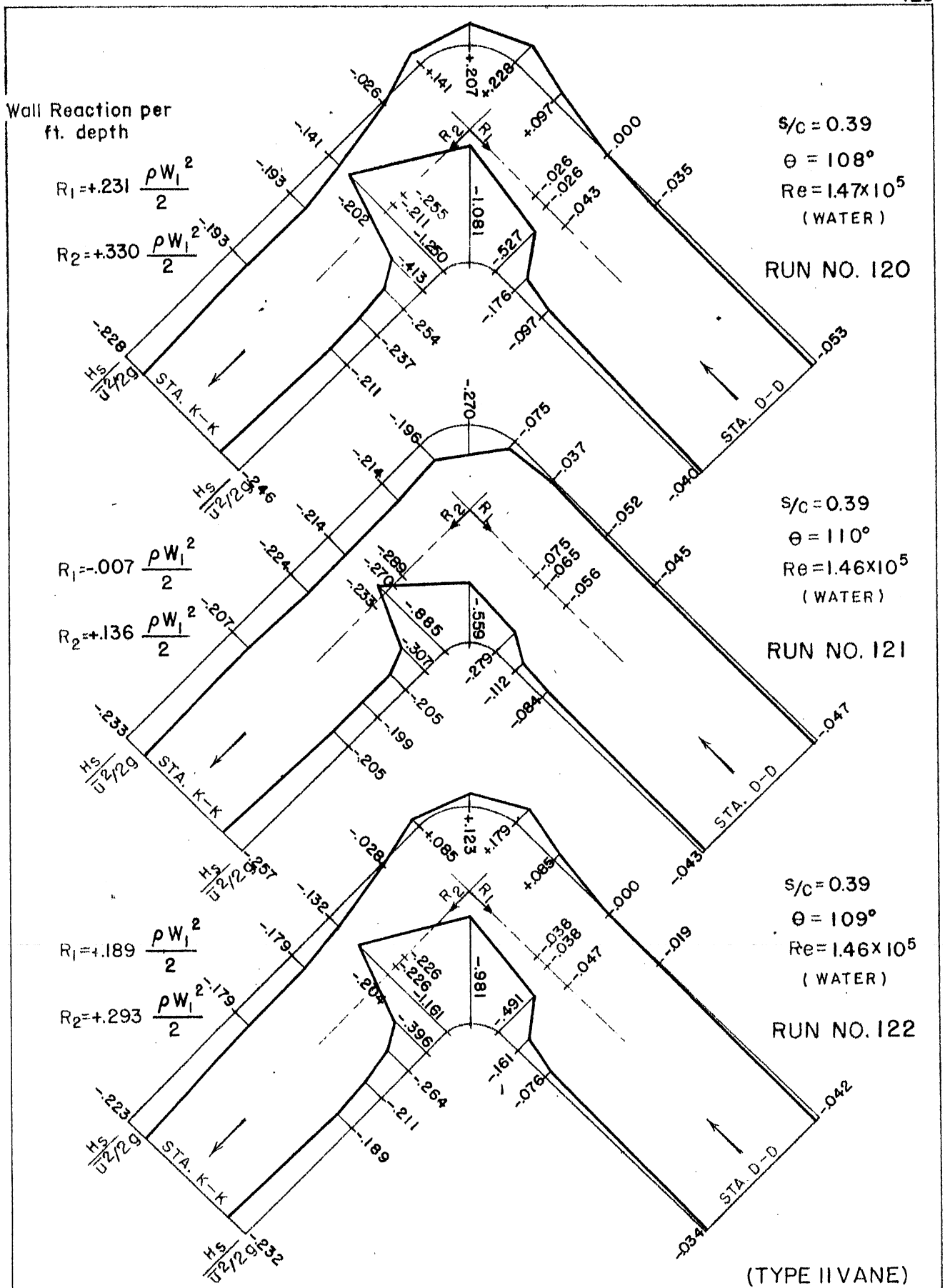

FIG. 59
STATIC HEAD AND REACTION ON WALLS
RUN NO. 120, 121, 122

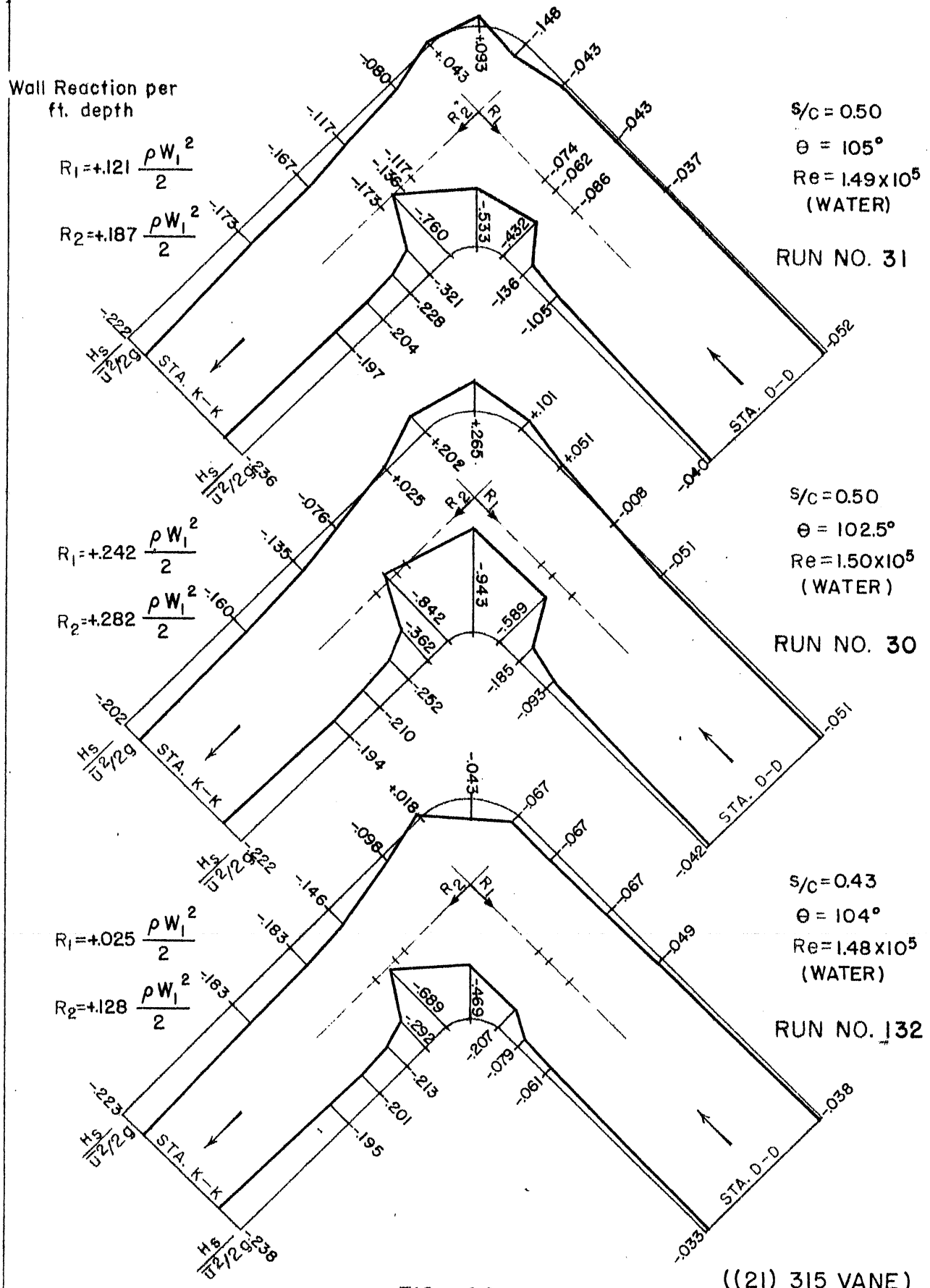

FIG. 60
STATIC HEAD AND REACTION ON WALLS
RUN NO. 31, 30, 132

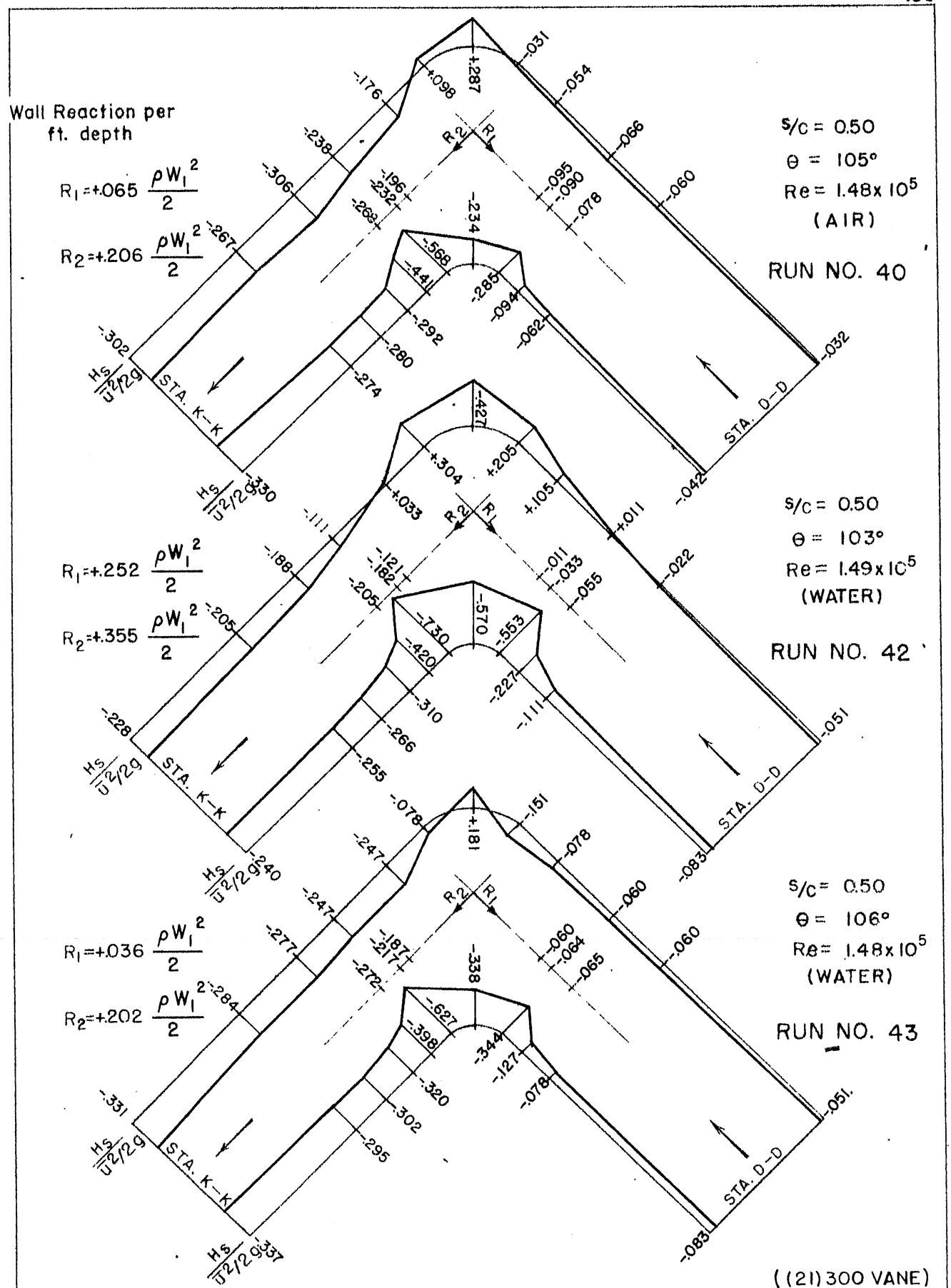

FIG. 61
STATIC HEAD AND REACTION ON WALLS
RUN NO. 40, 42, 43

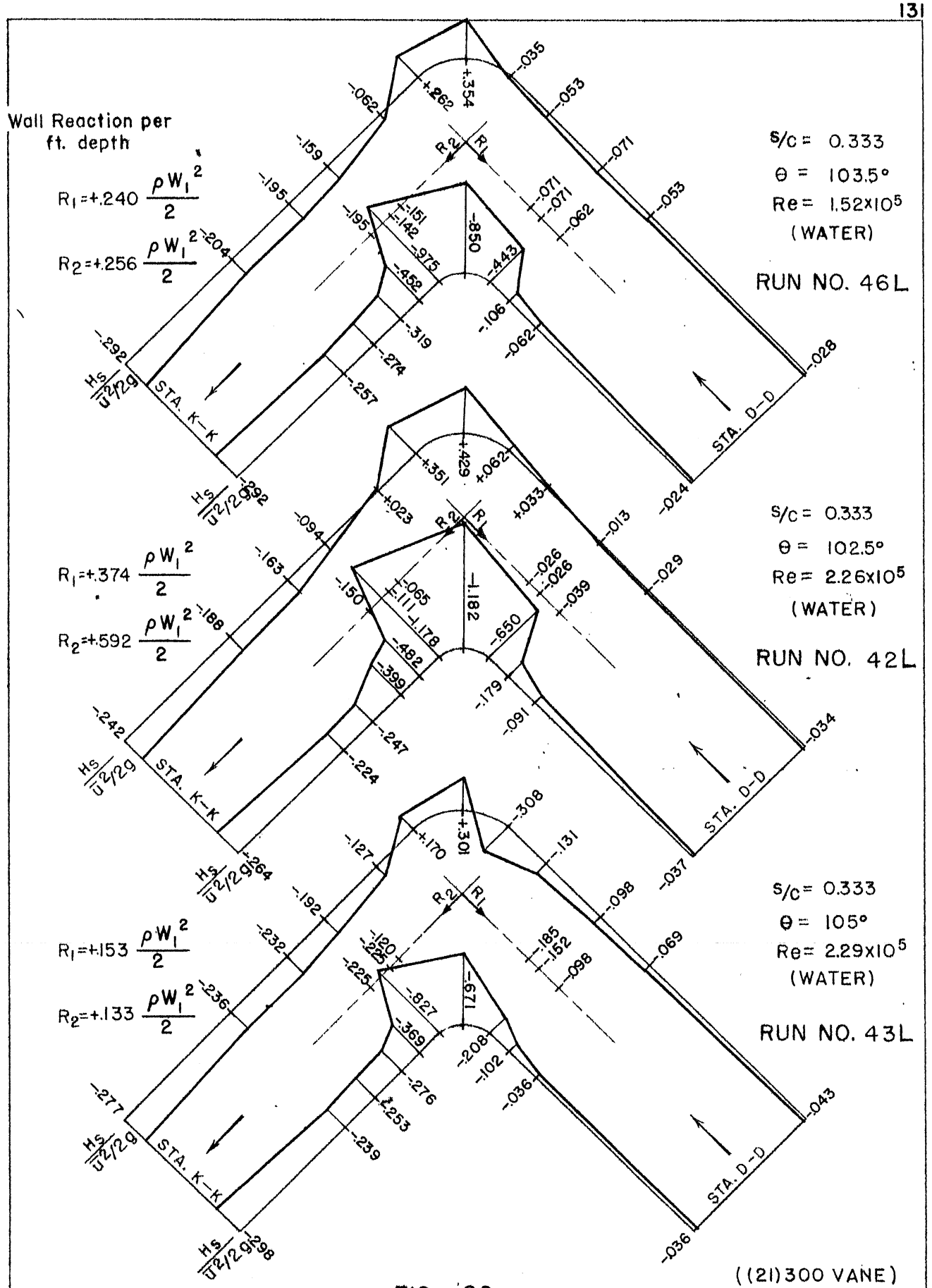

FIG. 62
STATIC HEAD AND REACTION ON WALLS
RUN NO. 46L, 42L, 43L

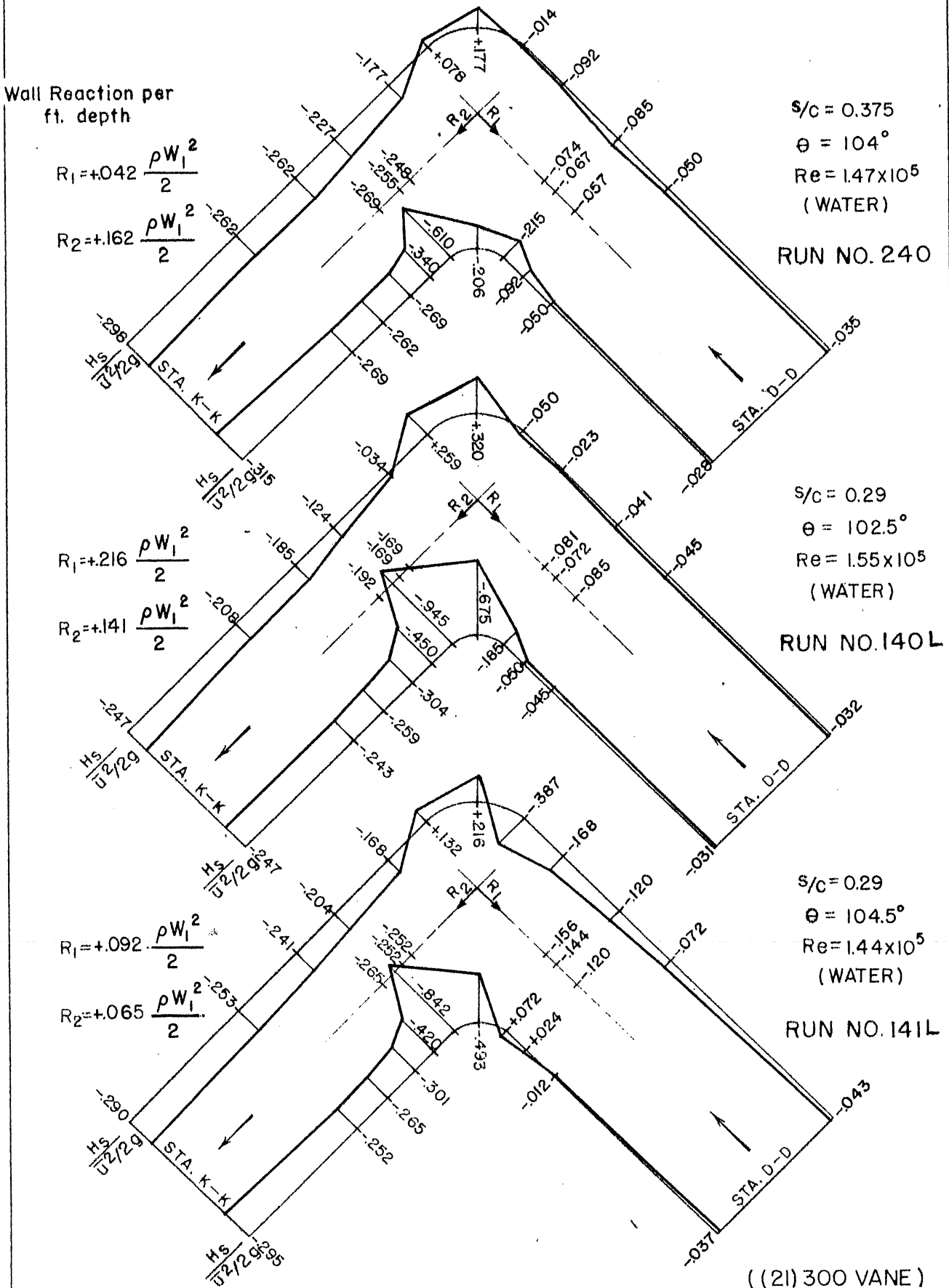

FIG. 63
STATIC HEAD AND REACTION ON WALLS
RUN NO. 240, 140L, 141L

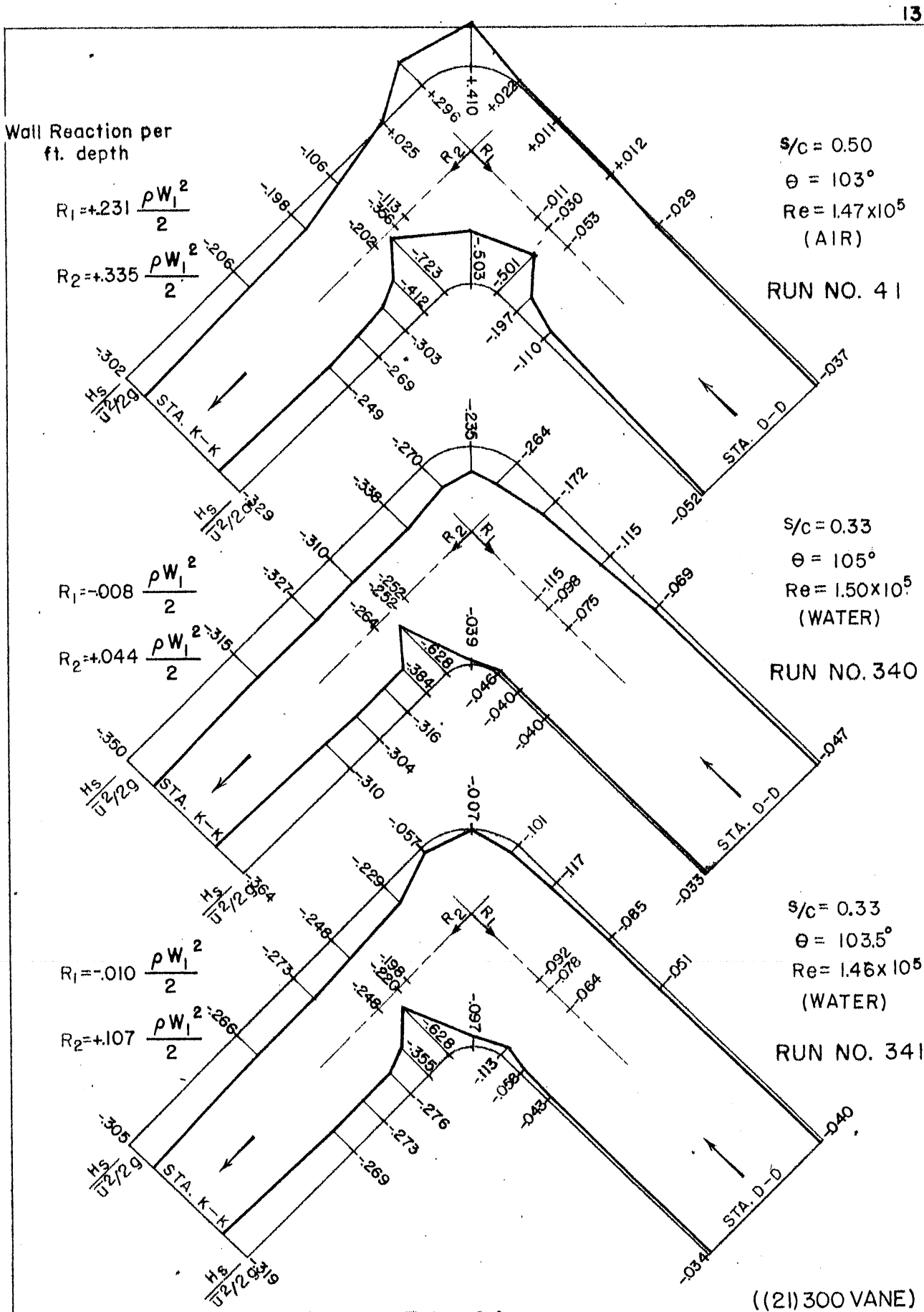

FIG. 64
STATIC HEAD AND REACTION ON WALLS
RUN NO. 41, 340, 341

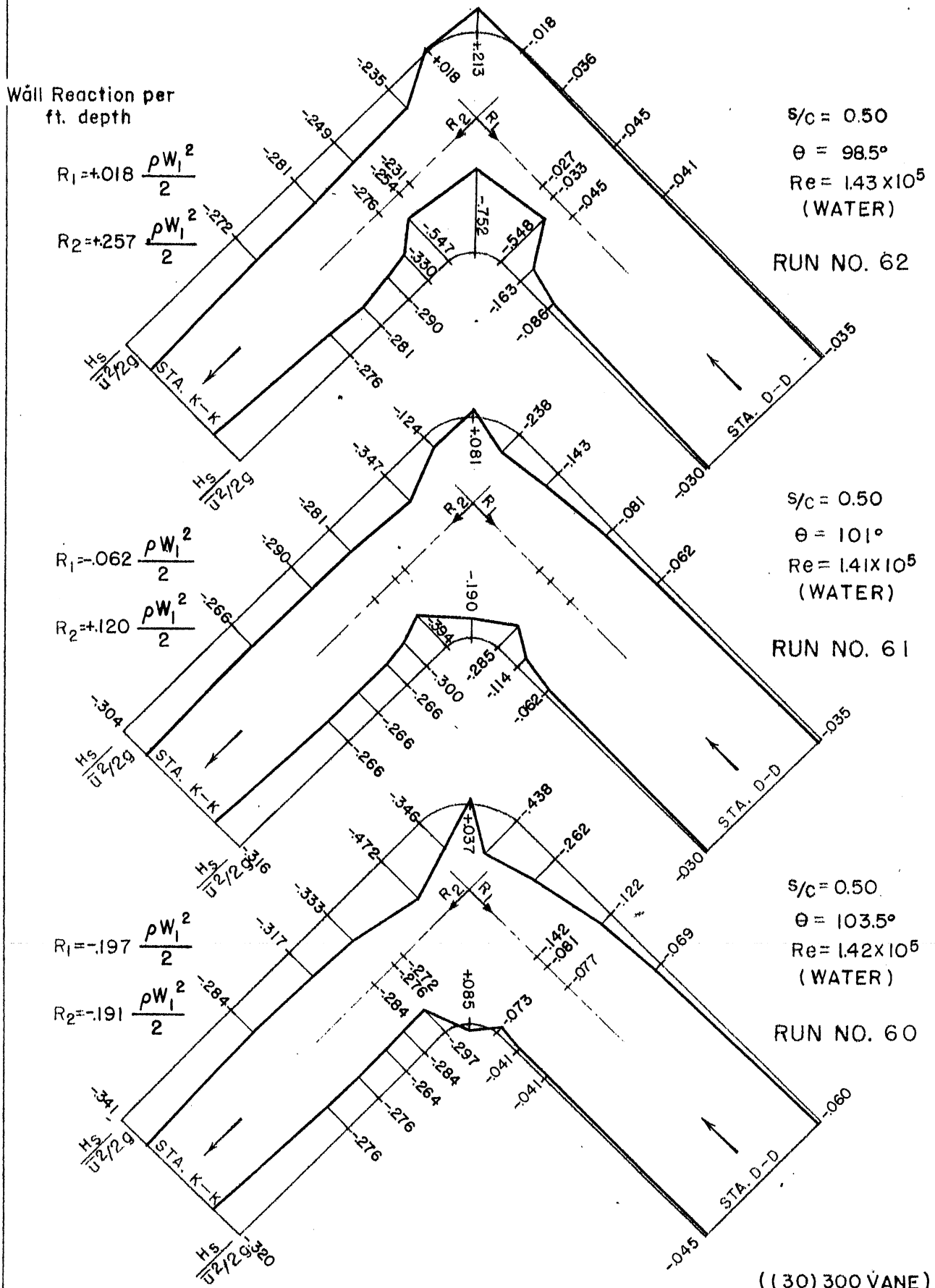

FIG. 65
STATIC HEAD AND REACTION ON WALLS
RUN NO. 62, 61, 60

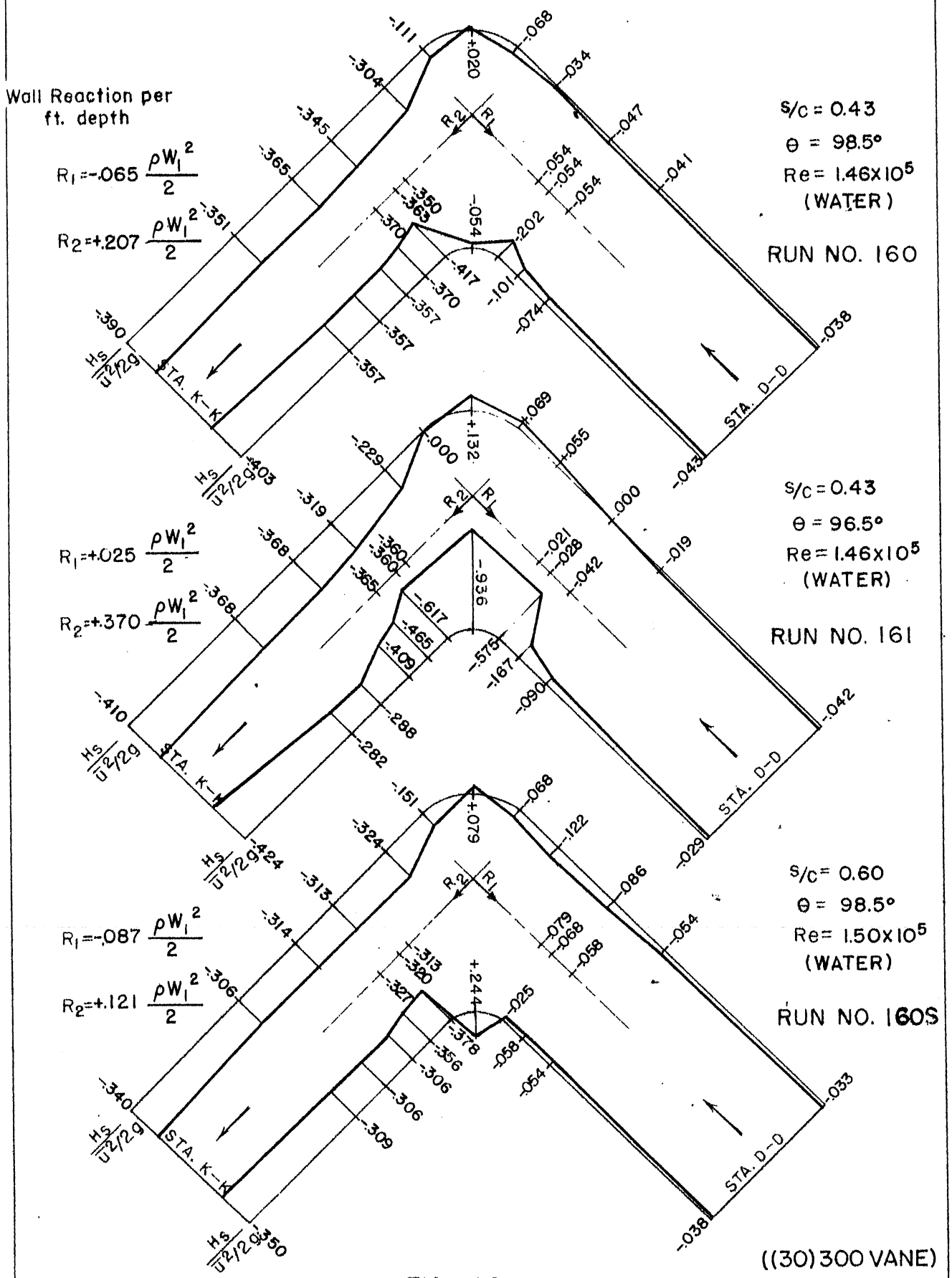

FIG. 66
STATIC HEAD AND REACTION ON WALLS
RUN NO. 160, 161, 160S

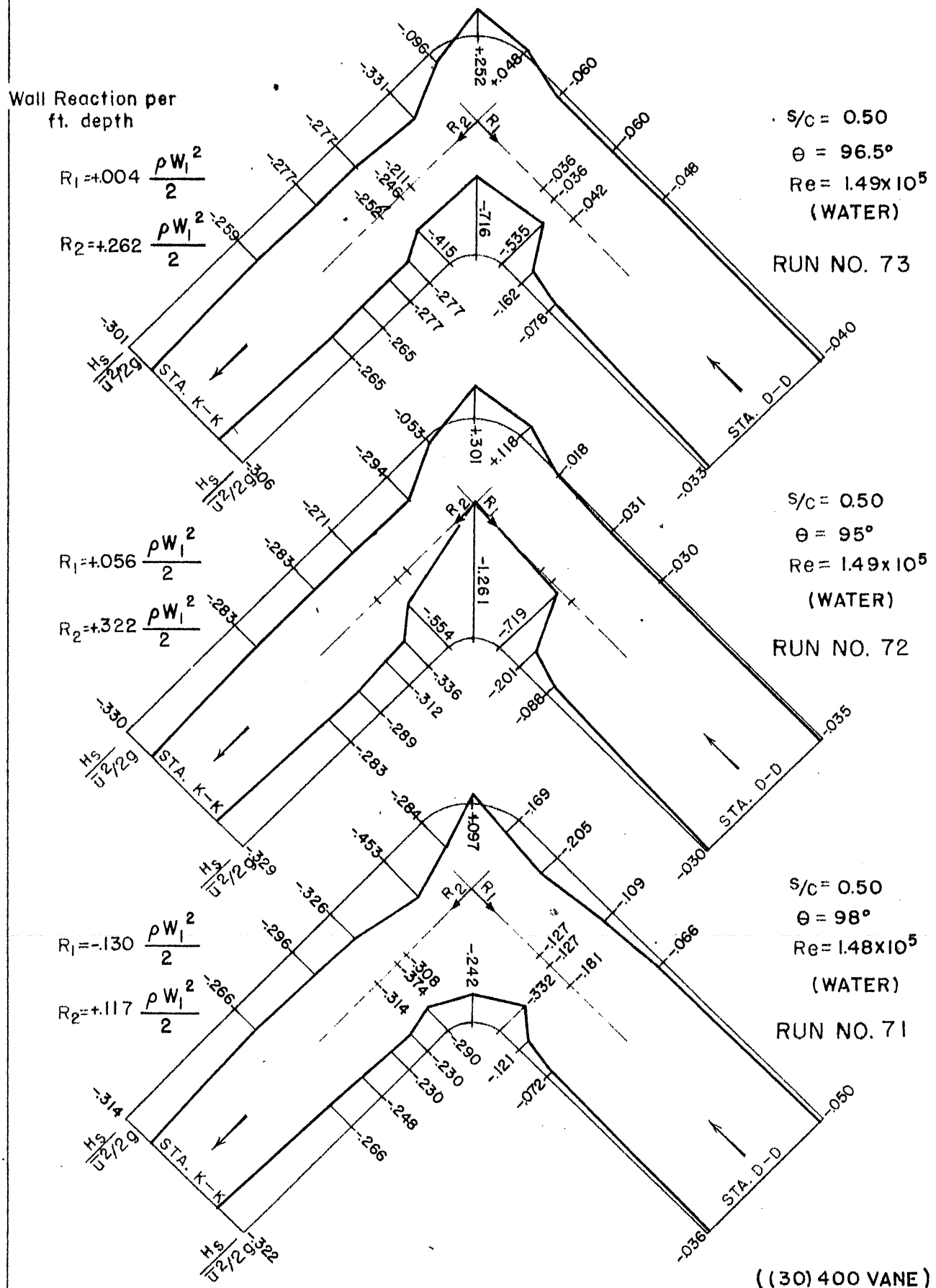

FIG. 67
STATIC HEAD AND REACTION ON WALLS
RUN NO. 73,72,71

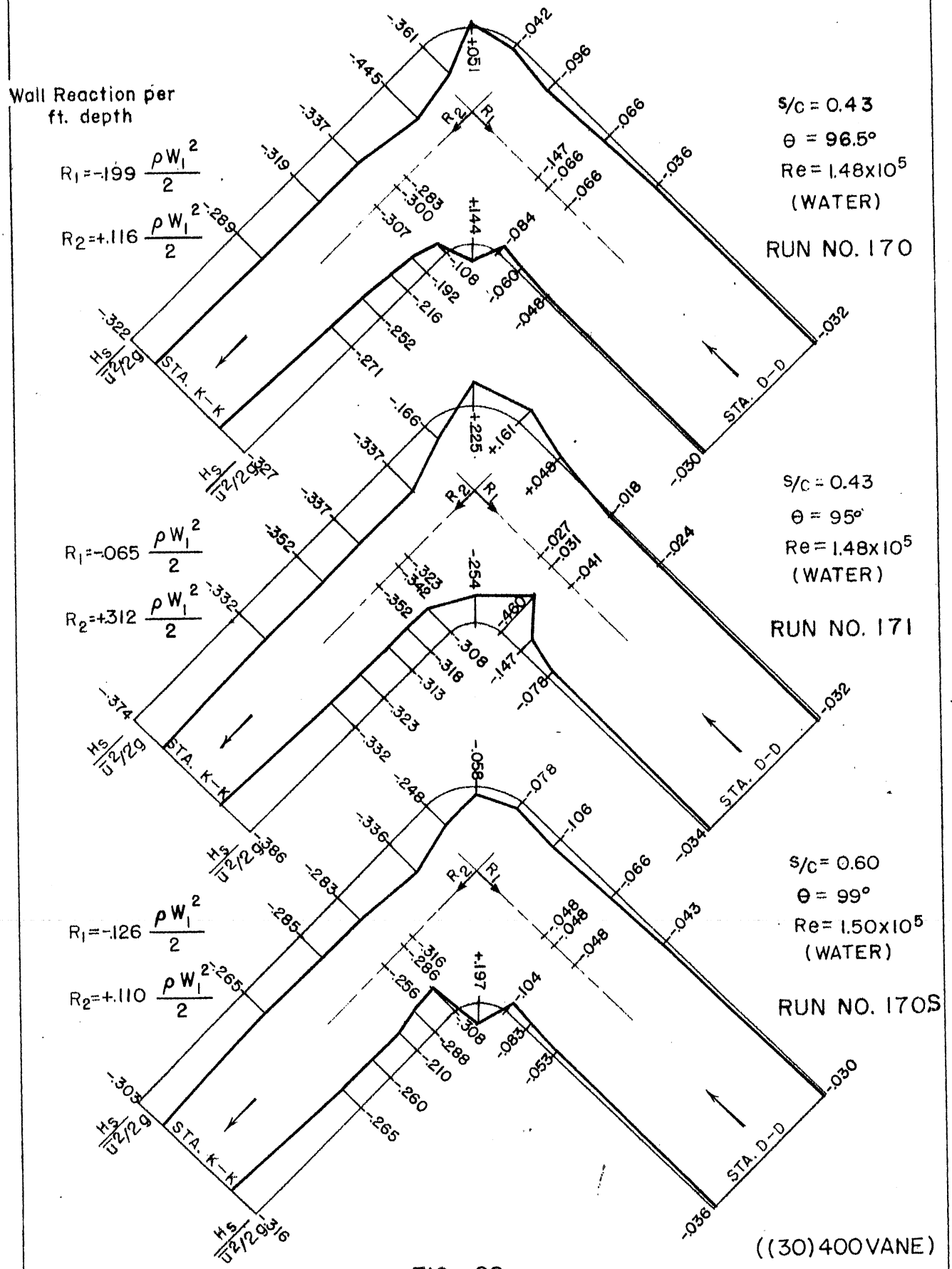

FIG. 68
STATIC HEAD AND REACTION ON WALLS
RUN NO. 170,171,170S

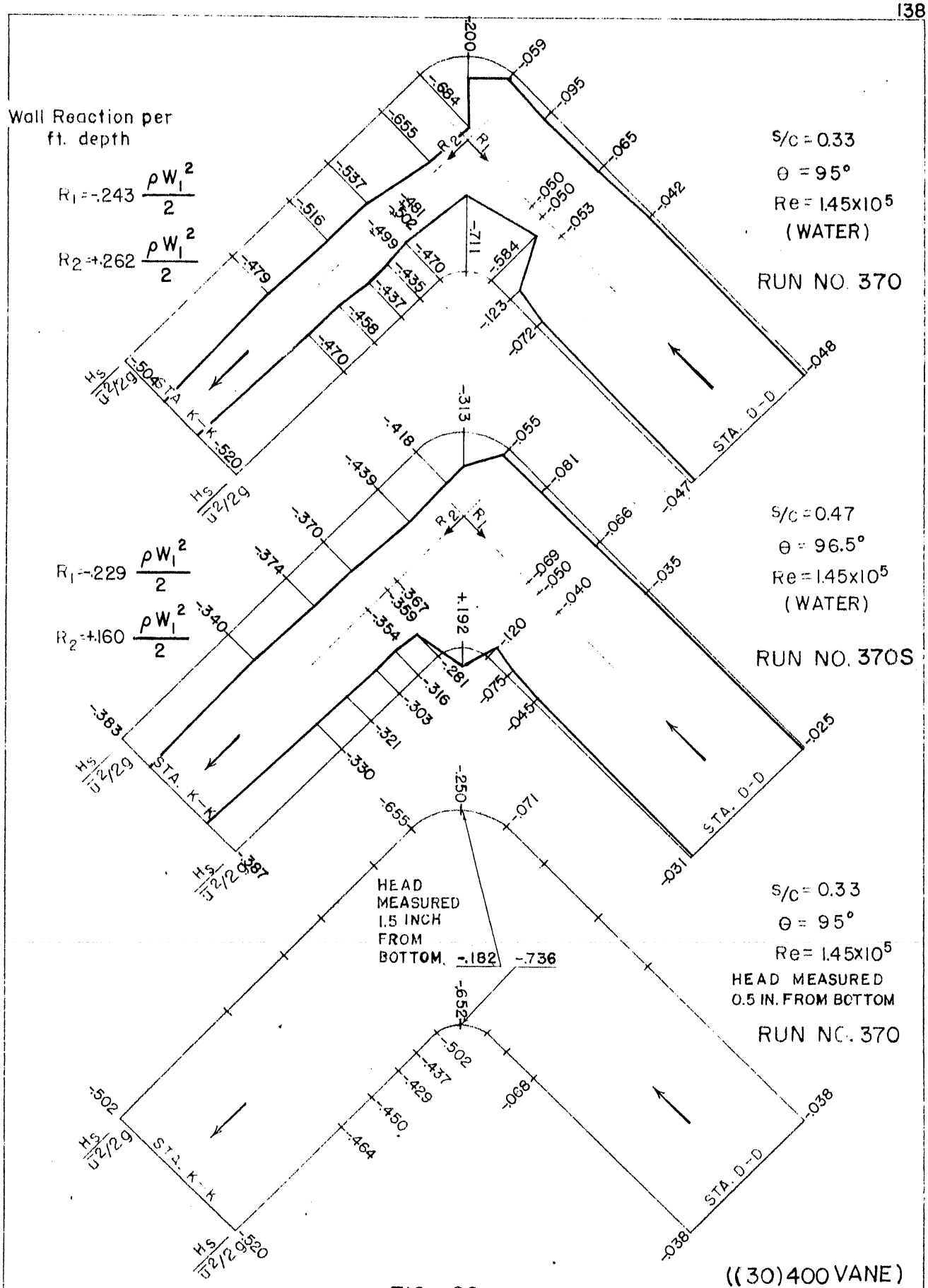

FIG. 69
STATIC HEAD AND REACTION ON WALLS
RUN NO. 370, 370S

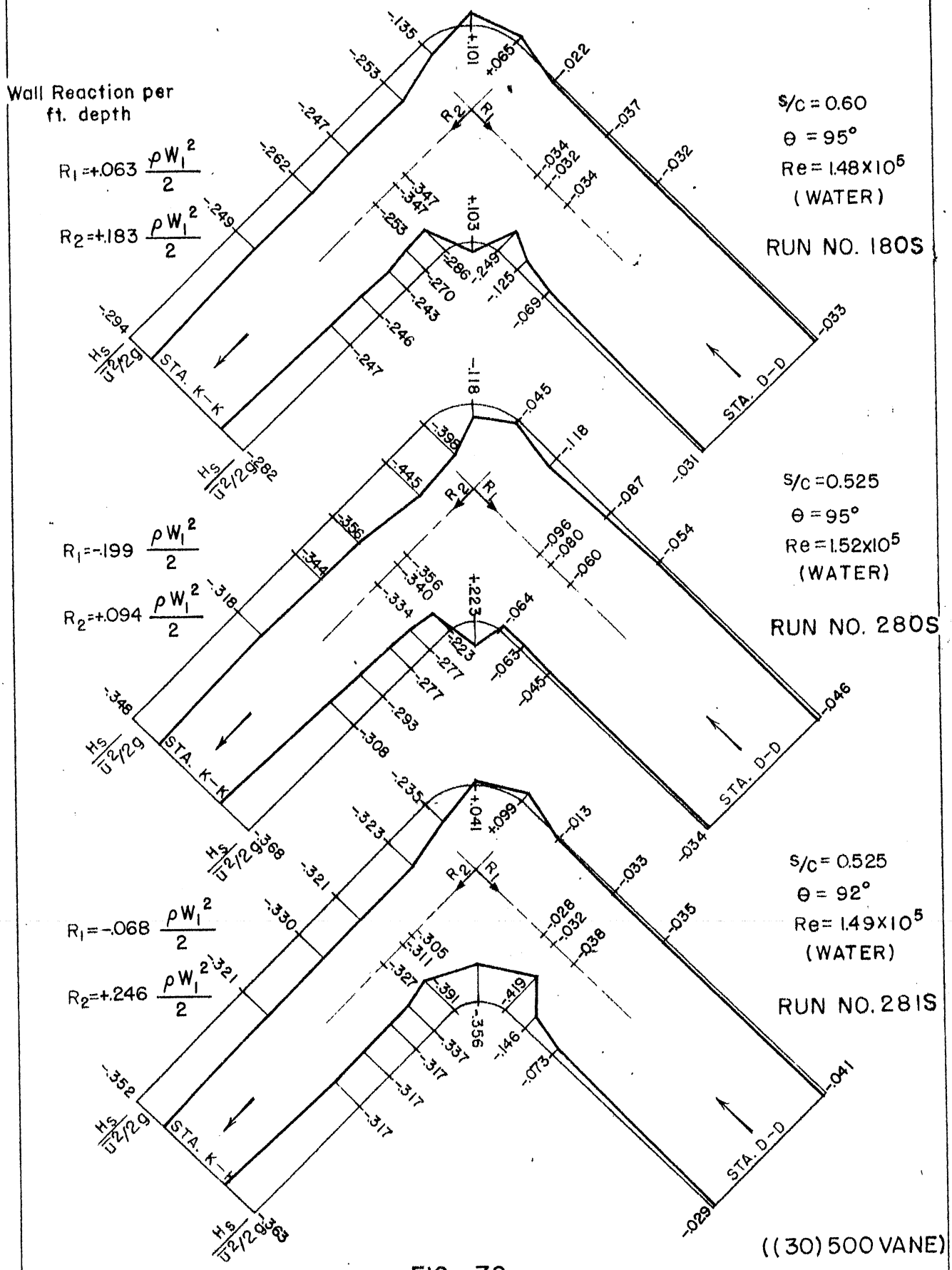

FIG. 70
STATIC HEAD AND REACTION ON WALLS
RUN NO. 180S, 280S, 281S

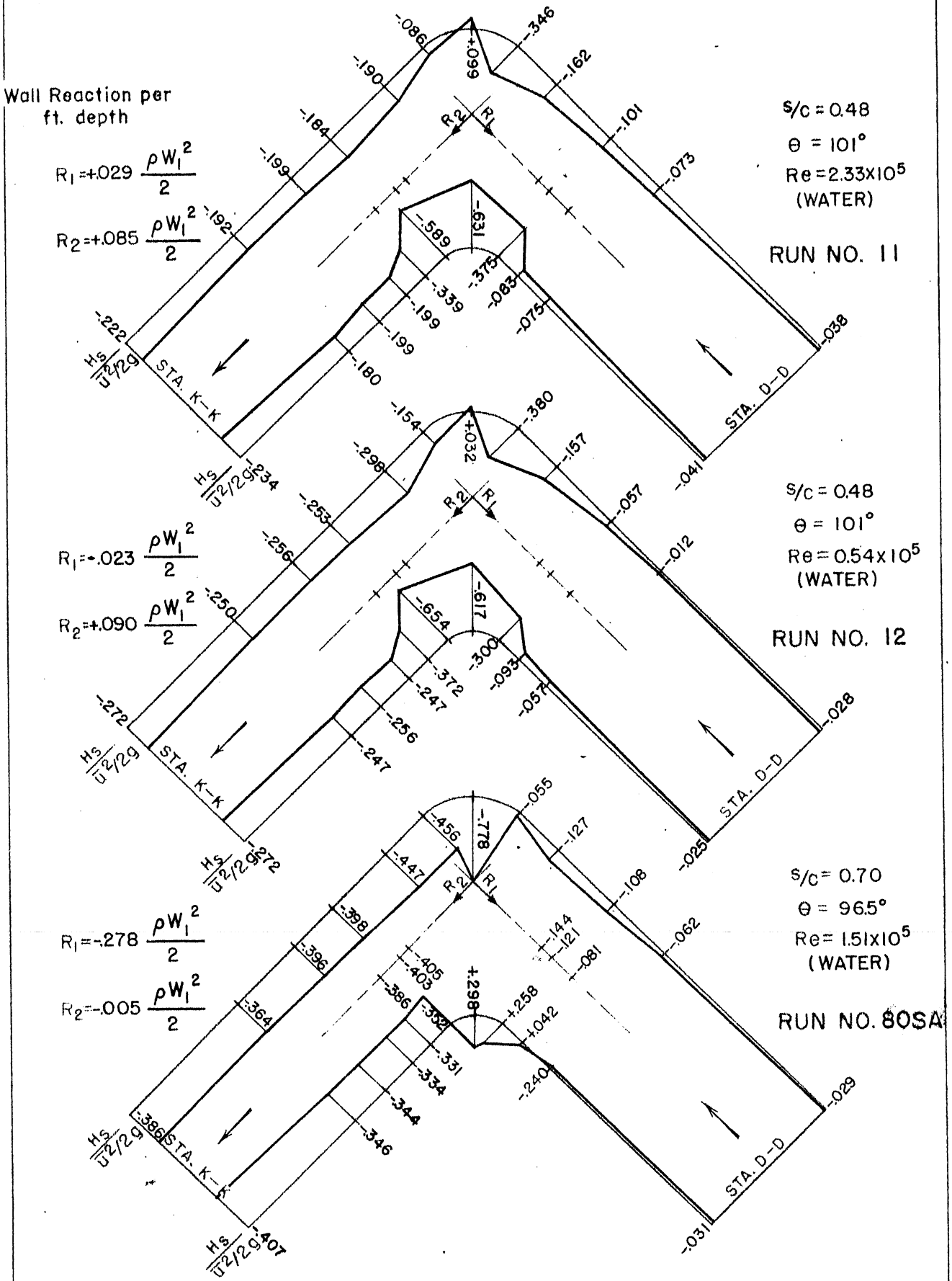

FIG. 71
STATIC HEAD AND REACTION ON WALLS
RUN NO. 11, 12, 80SA

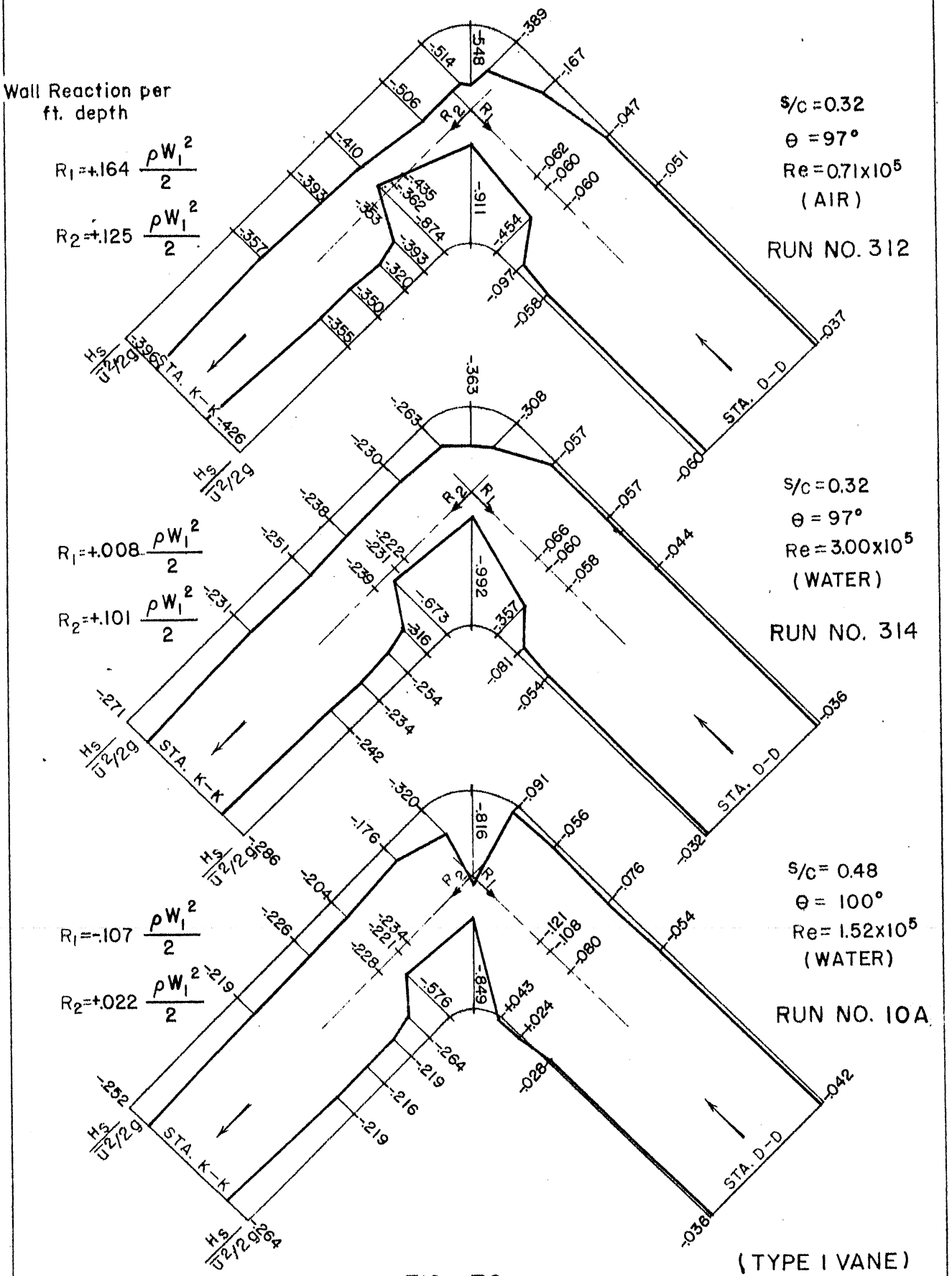

FIG. 72
STATIC HEAD AND REACTION ON WALLS
RUN NO. 312, 314, 10A

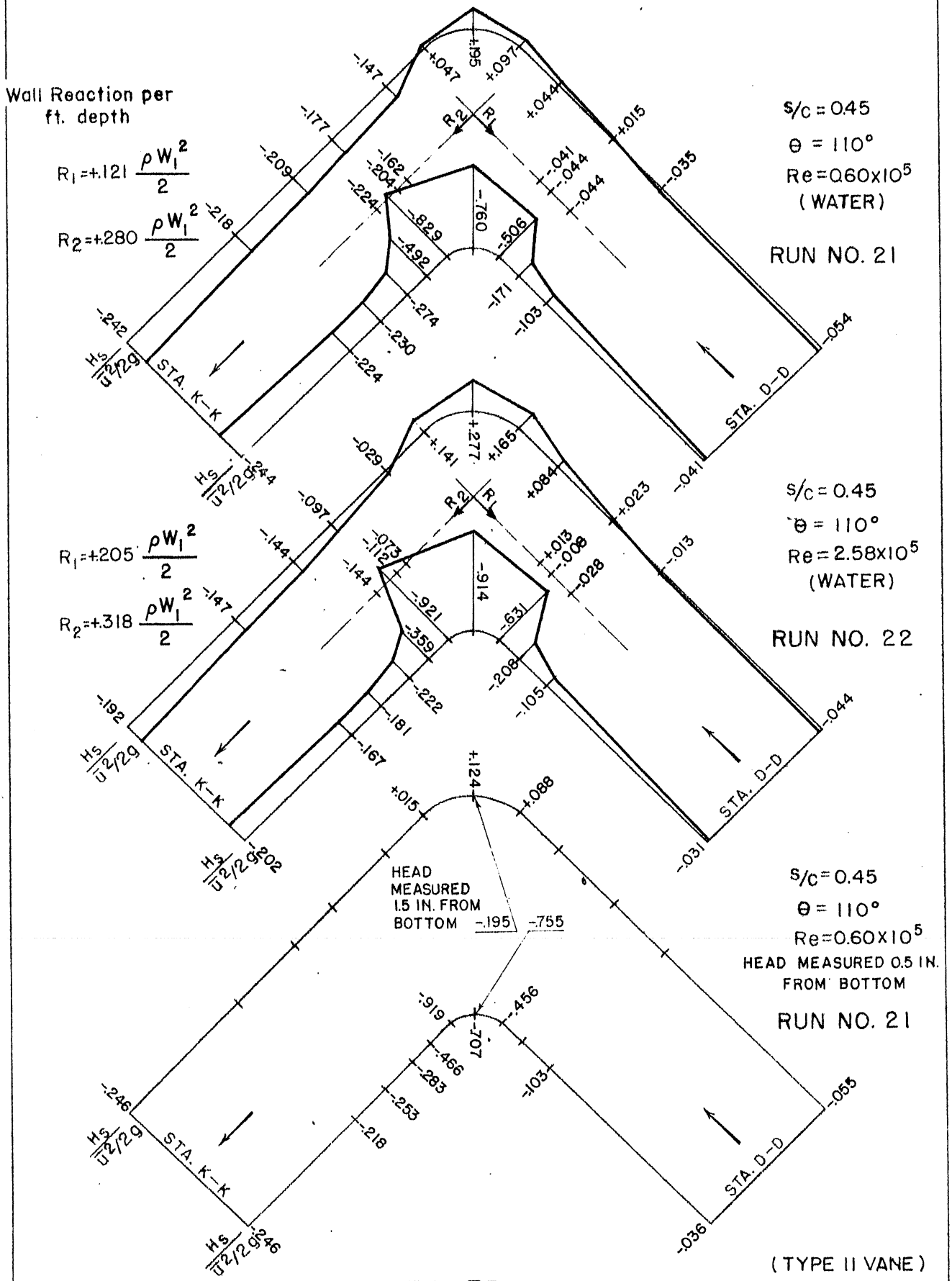

FIG. 73
STATIC HEAD AND REACTION ON WALLS
RUN NO. 21, 22

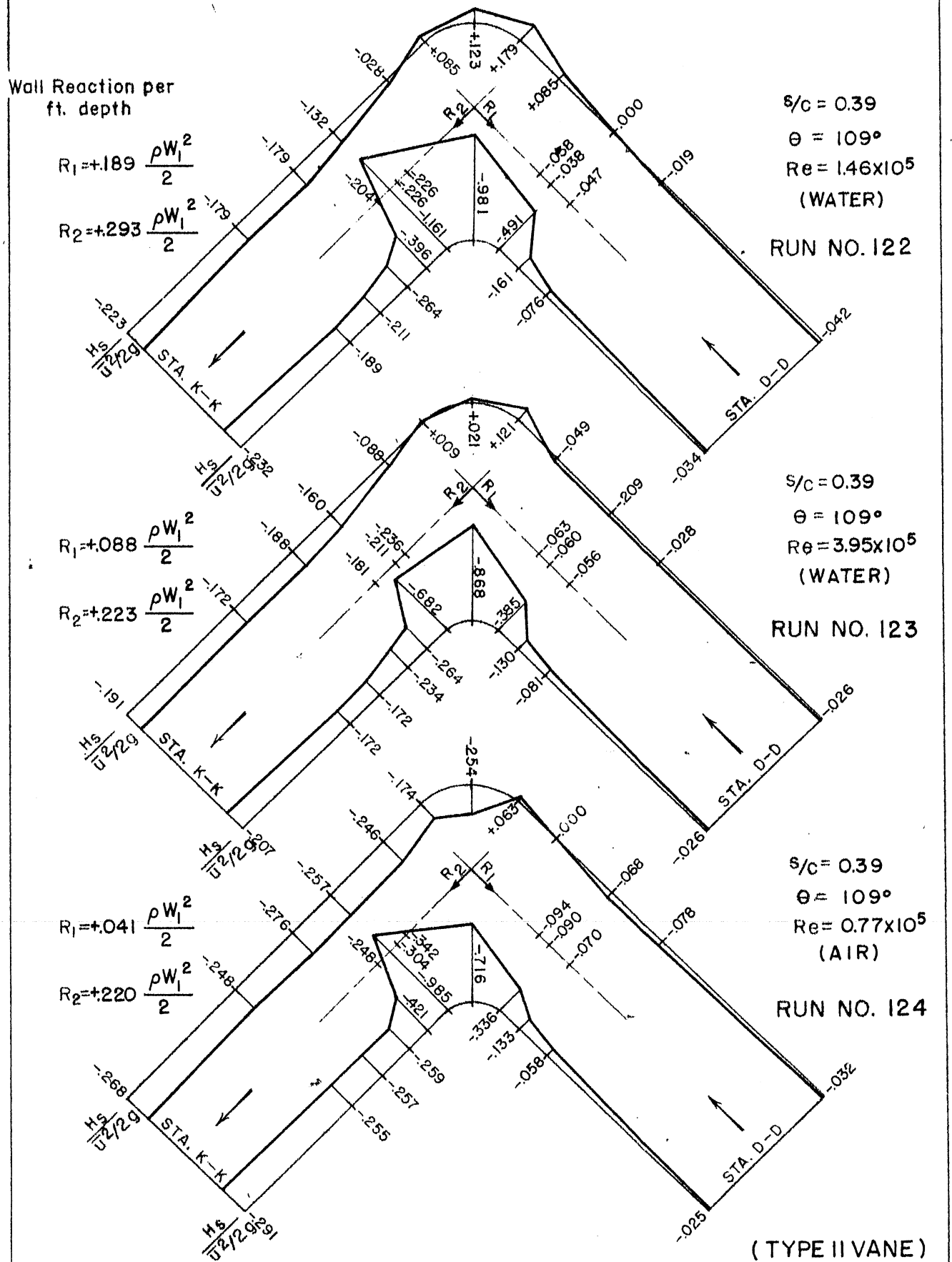

FIG. 74
STATIC HEAD AND REACTION ON WALLS
RUN NO. 122,123,124

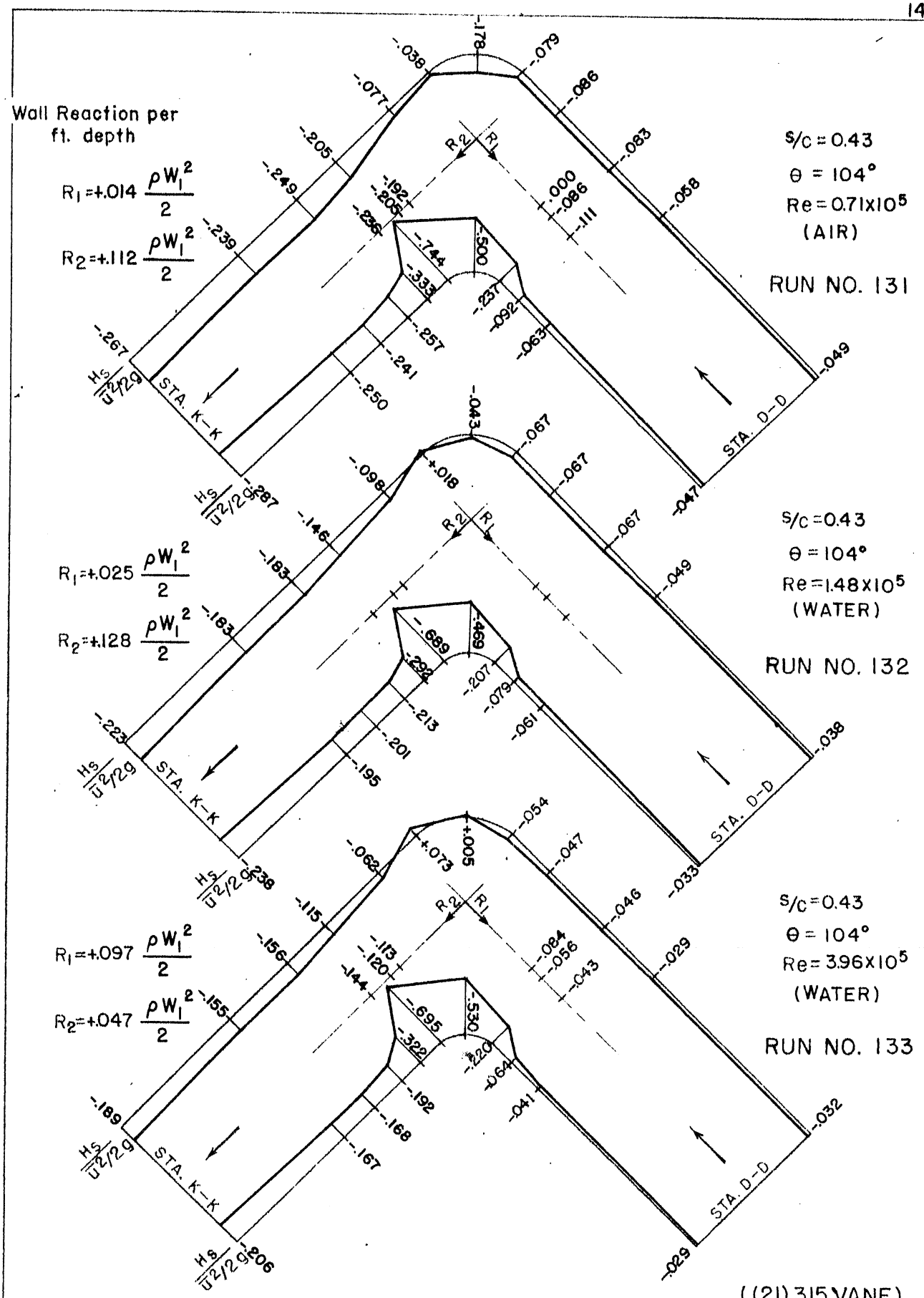

FIG. 75
STATIC HEAD AND REACTION ON WALLS
RUN NO. 131, 132, 133

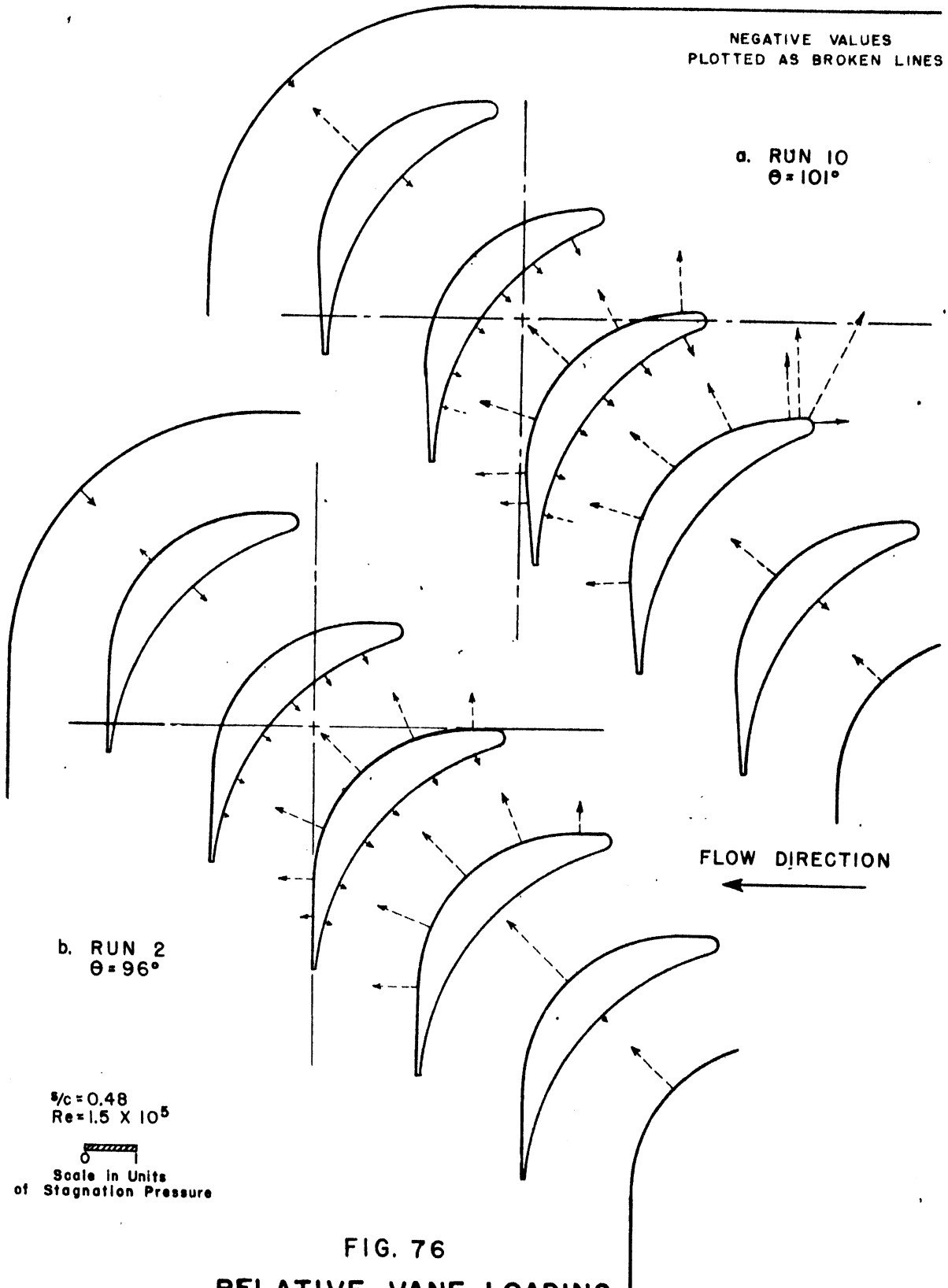

FIG. 76

RELATIVE VANE LOADING

AS INFLUENCED BY CHANGES IN θ

TYPE I VANE

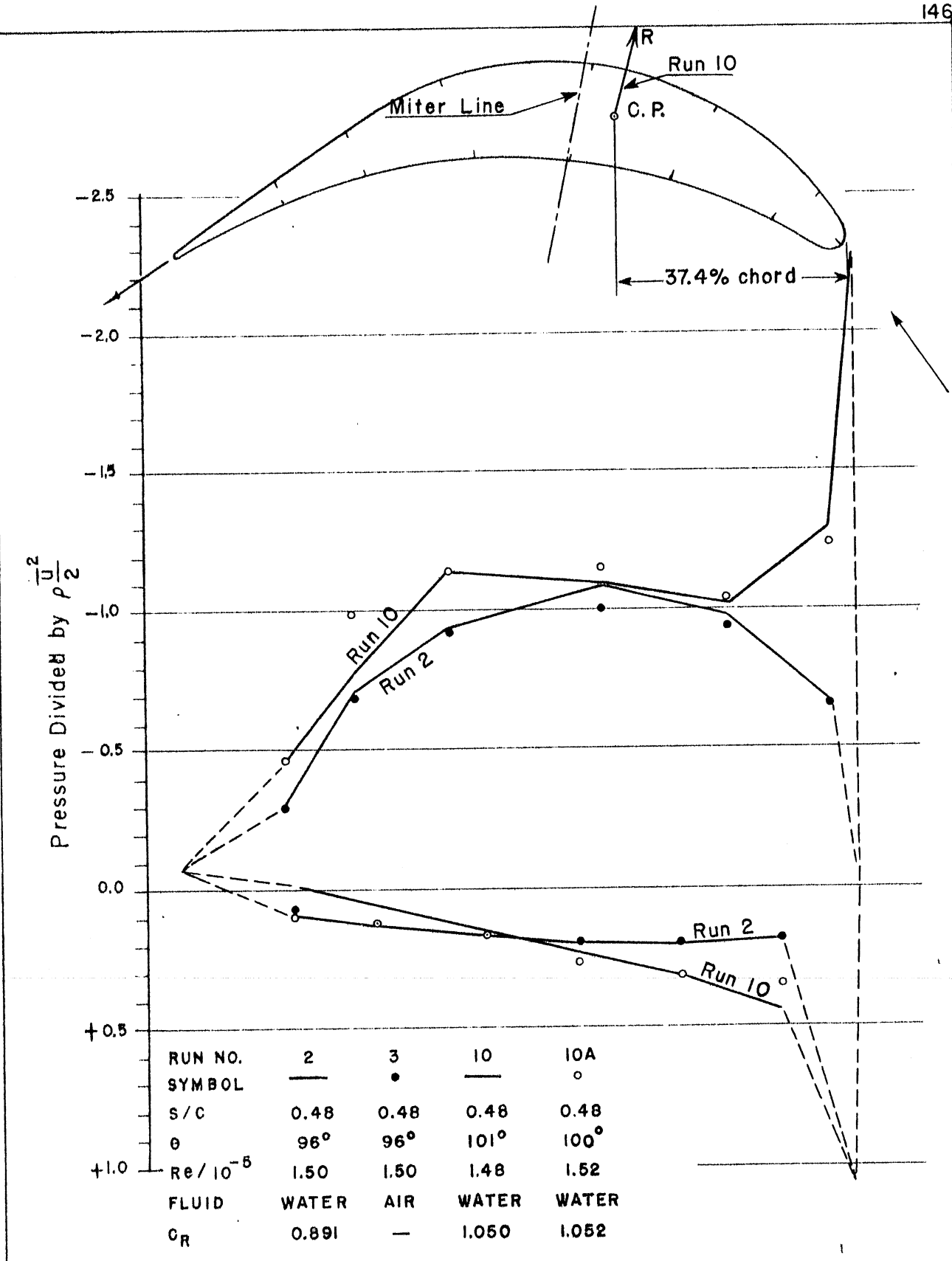

FIG. 77
PRESSURE DISTRIBUTION ON A CENTRAL VANE (TYPE I)
RUN NO. 2, 3, 10, 10A

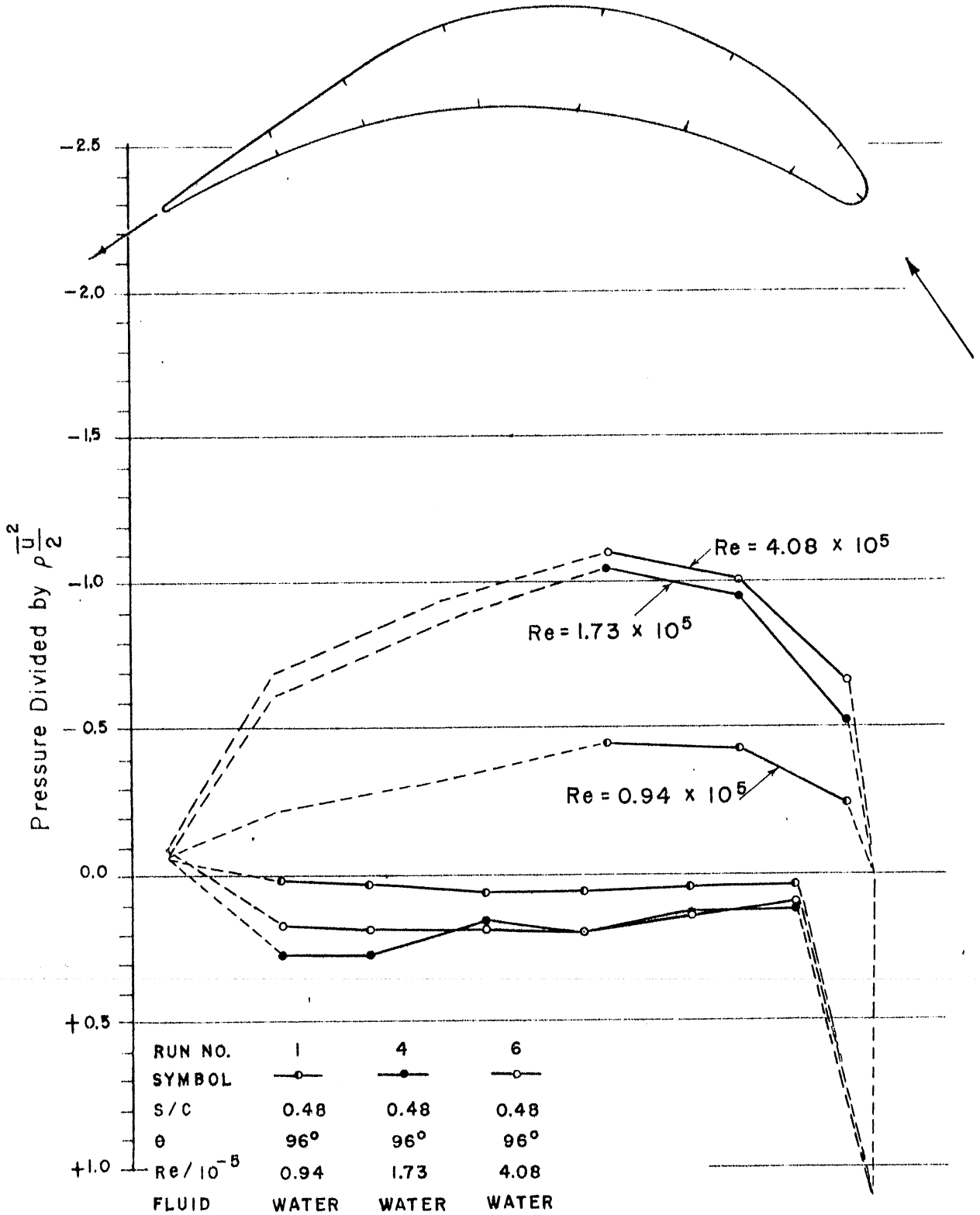

PRESSURES MEASURED NEAR ENDS OF VANES

FIG. 78
PRESSURE DISTRIBUTION ON A CENTRAL VANE (TYPE I)
RUN NO. 1, 4, 6

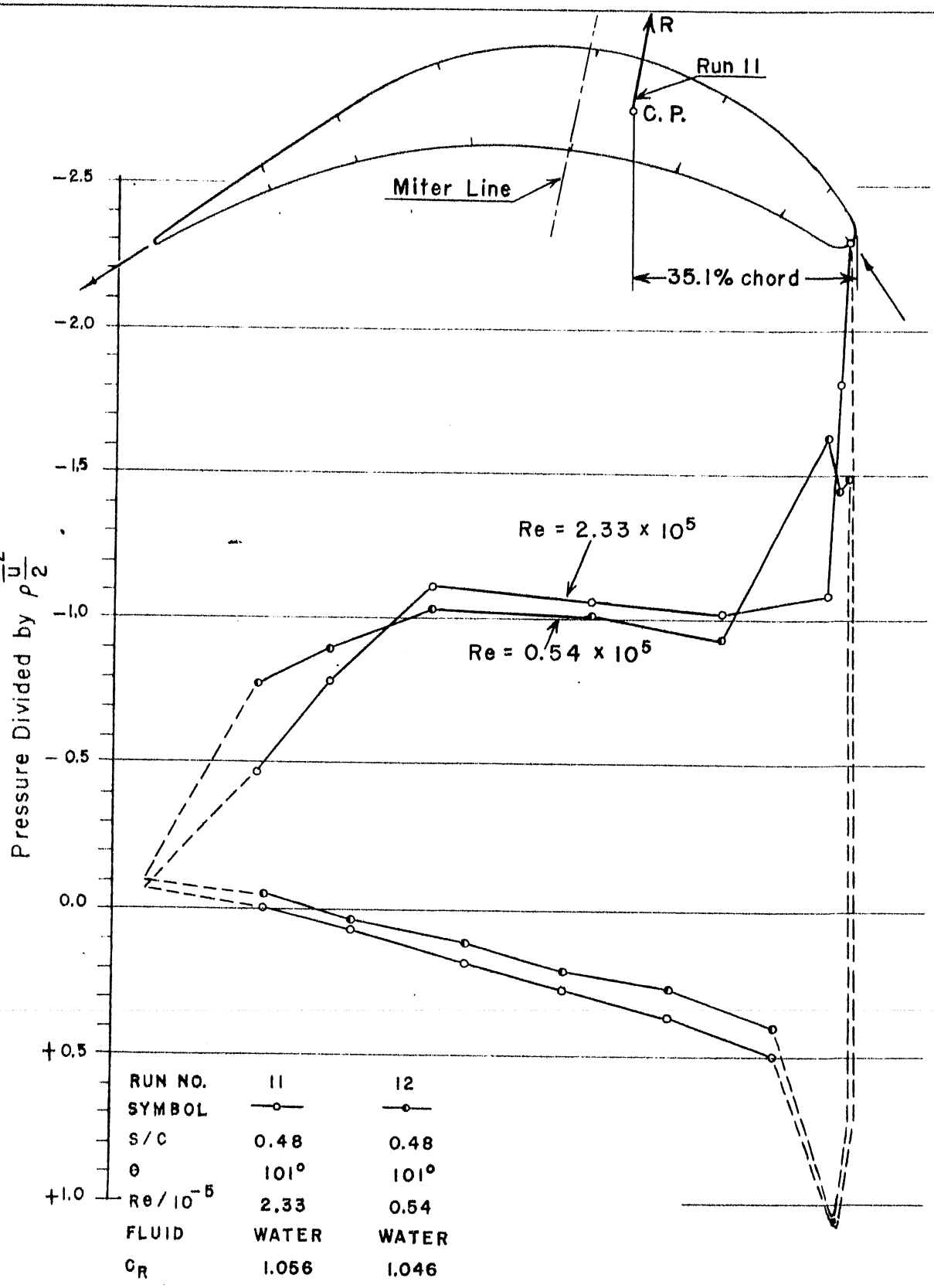

FIG. 79
PRESSURE DISTRIBUTION ON A CENTRAL VANE (TYPE I)
RUN NO. 11, 12

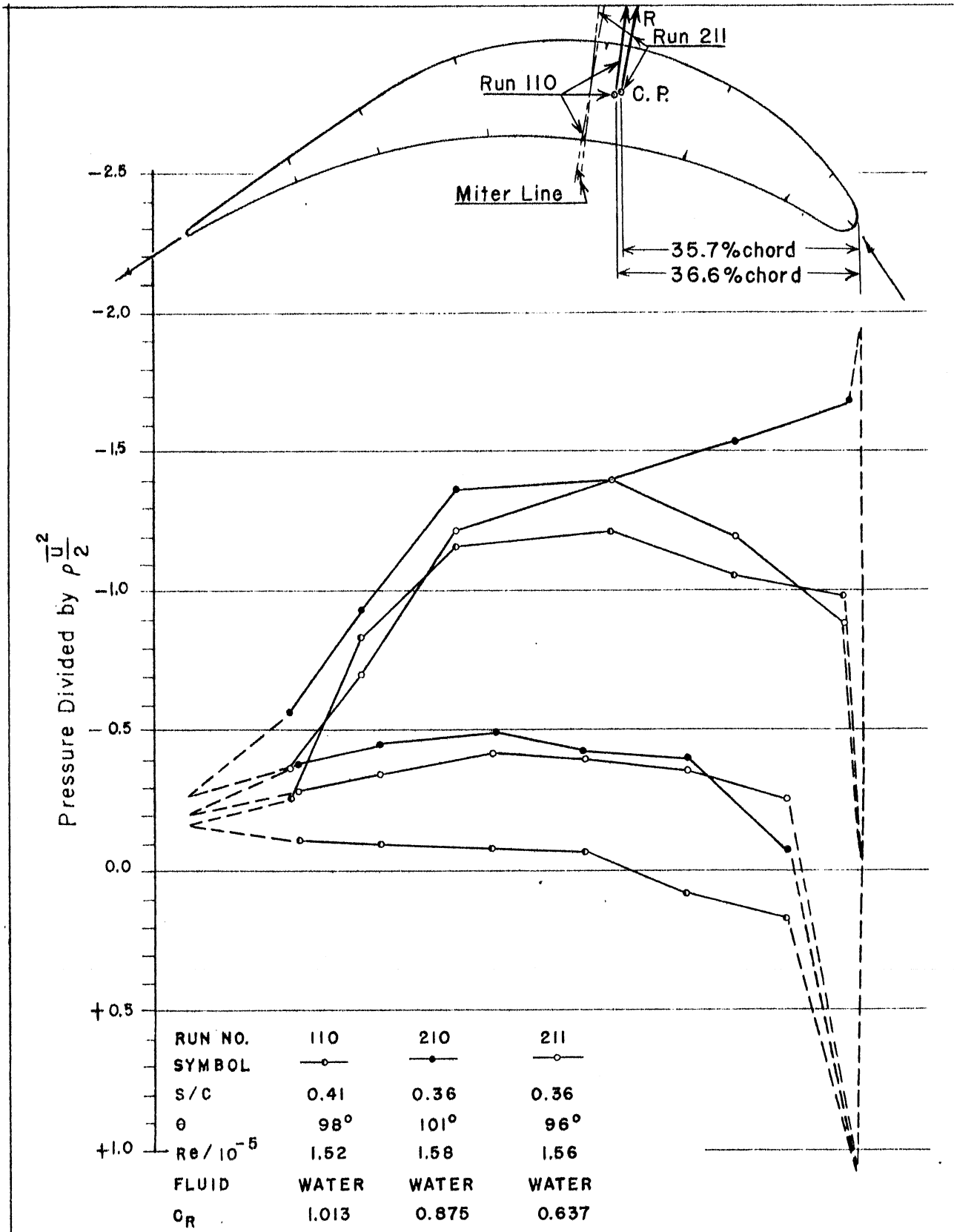

FIG. 80
PRESSURE DISTRIBUTION ON A CENTRAL VANE (TYPE I)
RUN NO. 110, 210, 211

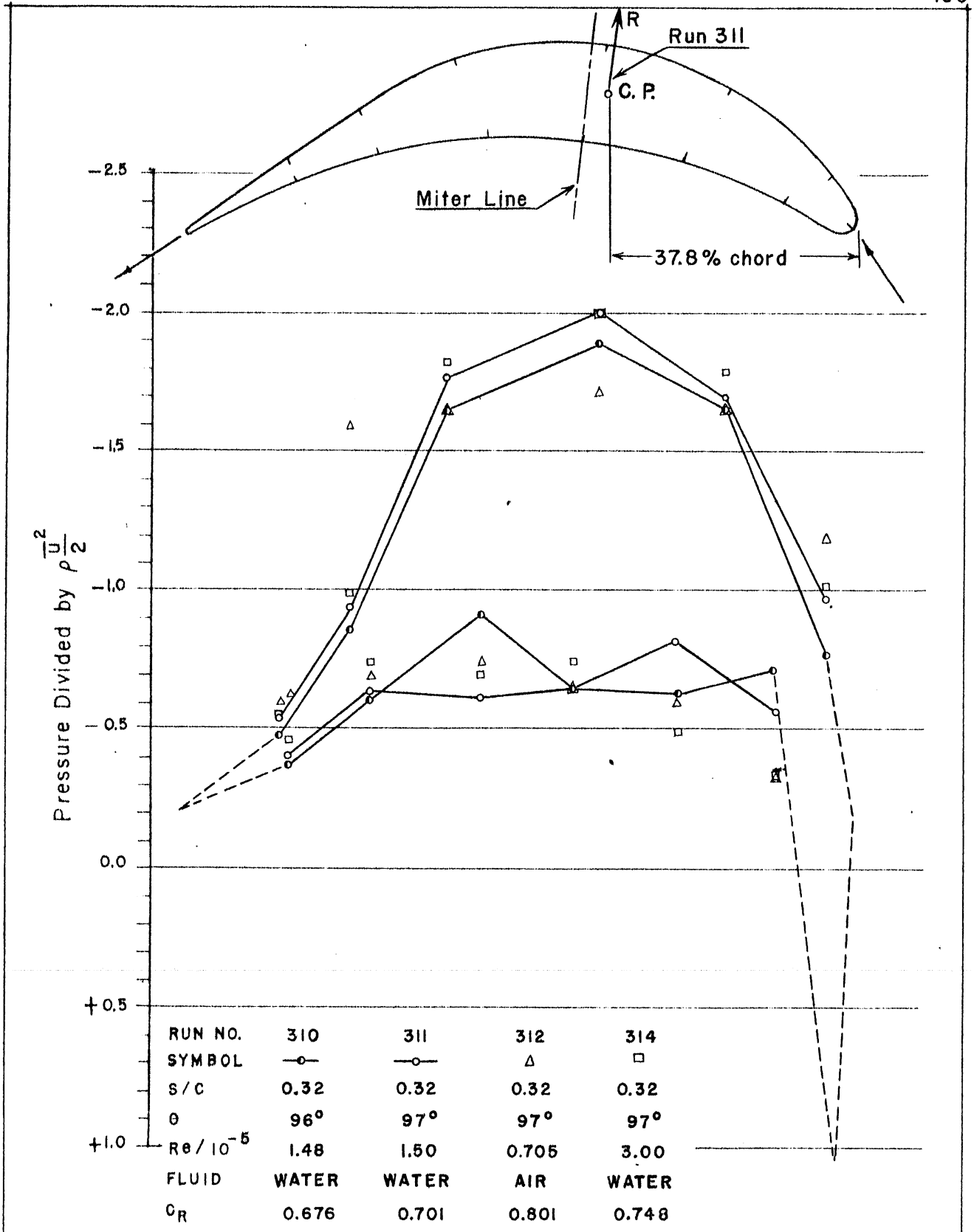

FIG. 81
PRESSURE DISTRIBUTION ON A CENTRAL VANE (TYPE I)
RUN NO. 310, 311, 312, 314

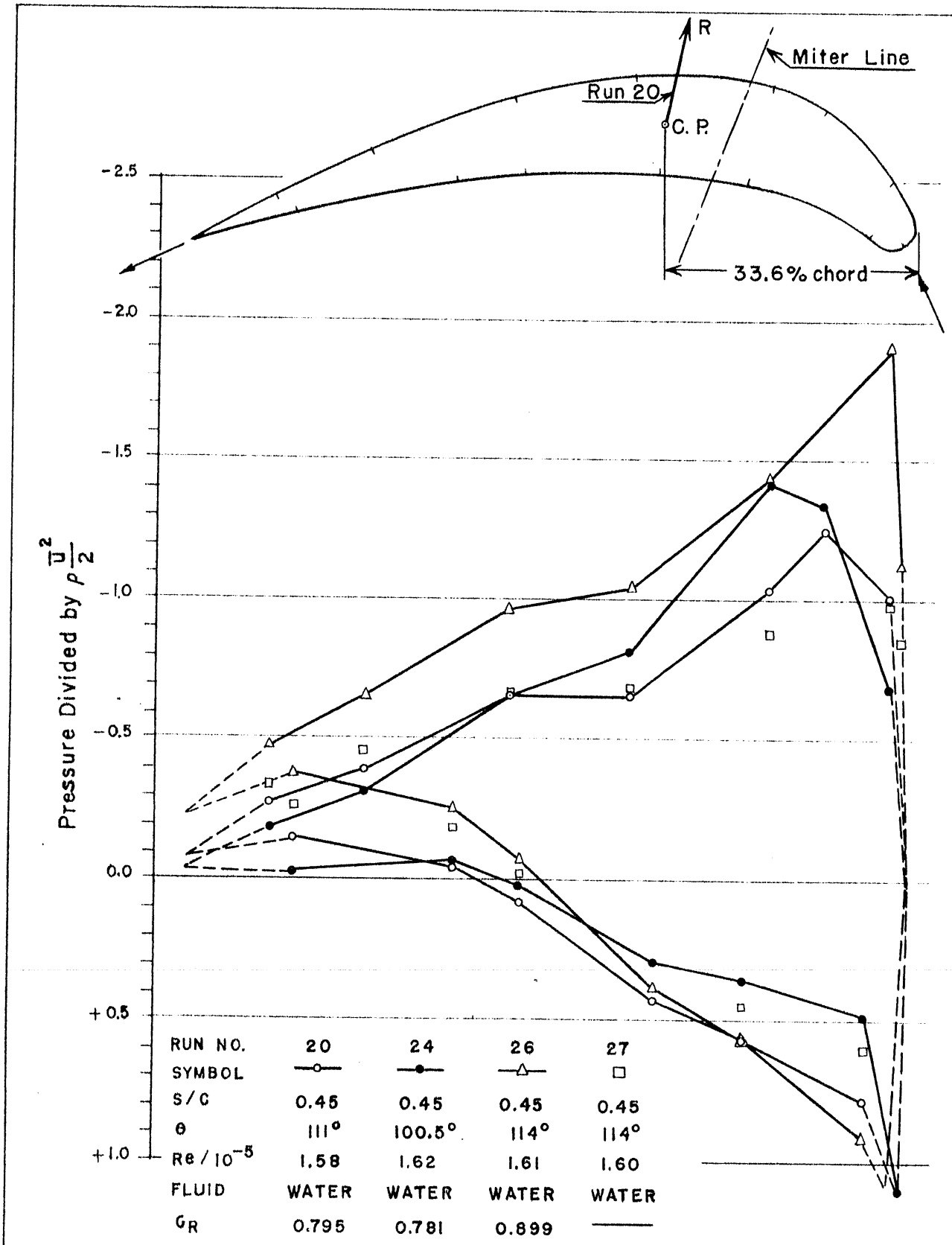

FIG. 82
PRESSURE DISTRIBUTION ON A CENTRAL VANE (TYPE II)
RUN NO. 20, 24, 26, 27

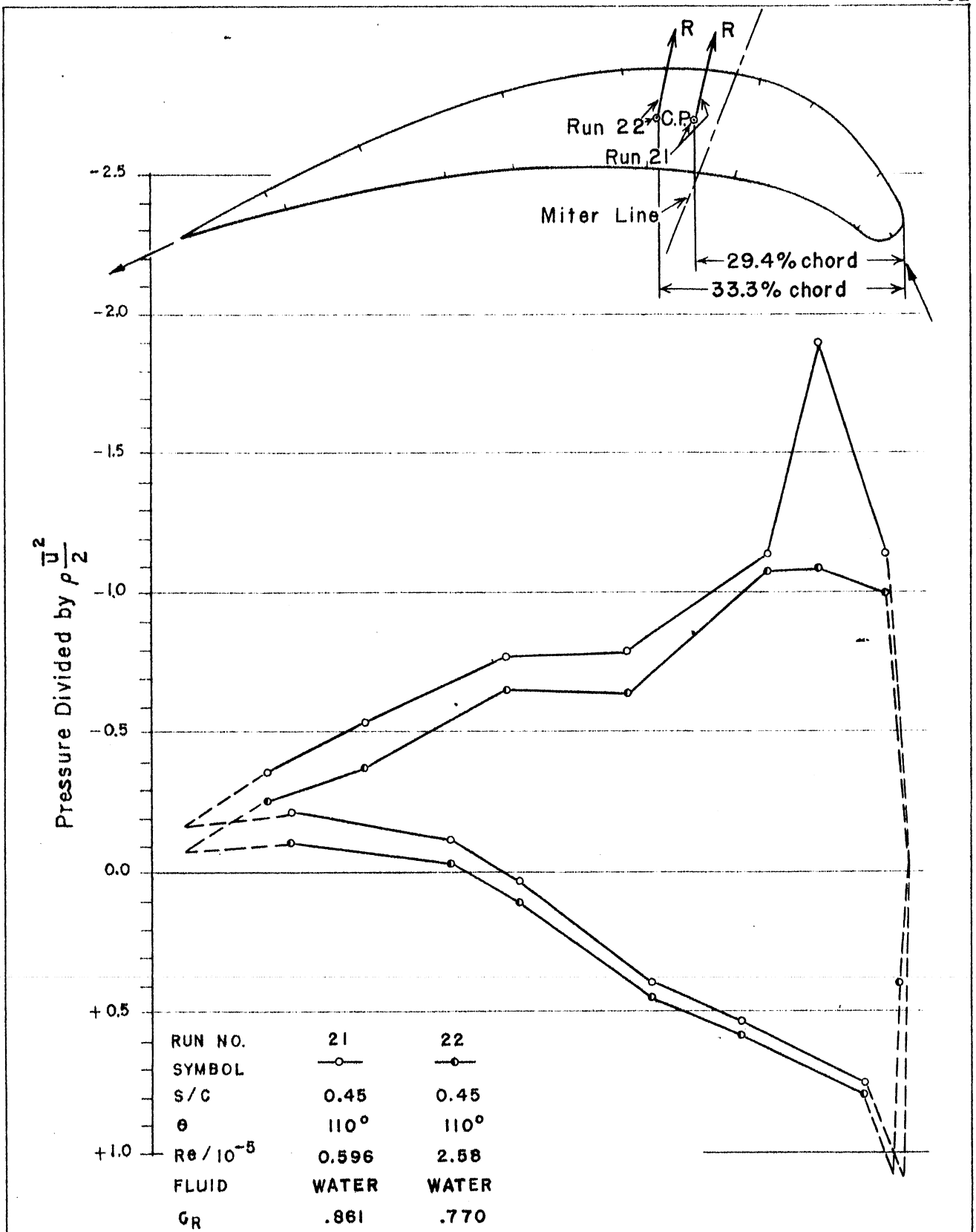

FIG. 83
PRESSURE DISTRIBUTION ON A CENTRAL VANE (TYPE II)
RUN NO. 21, 22

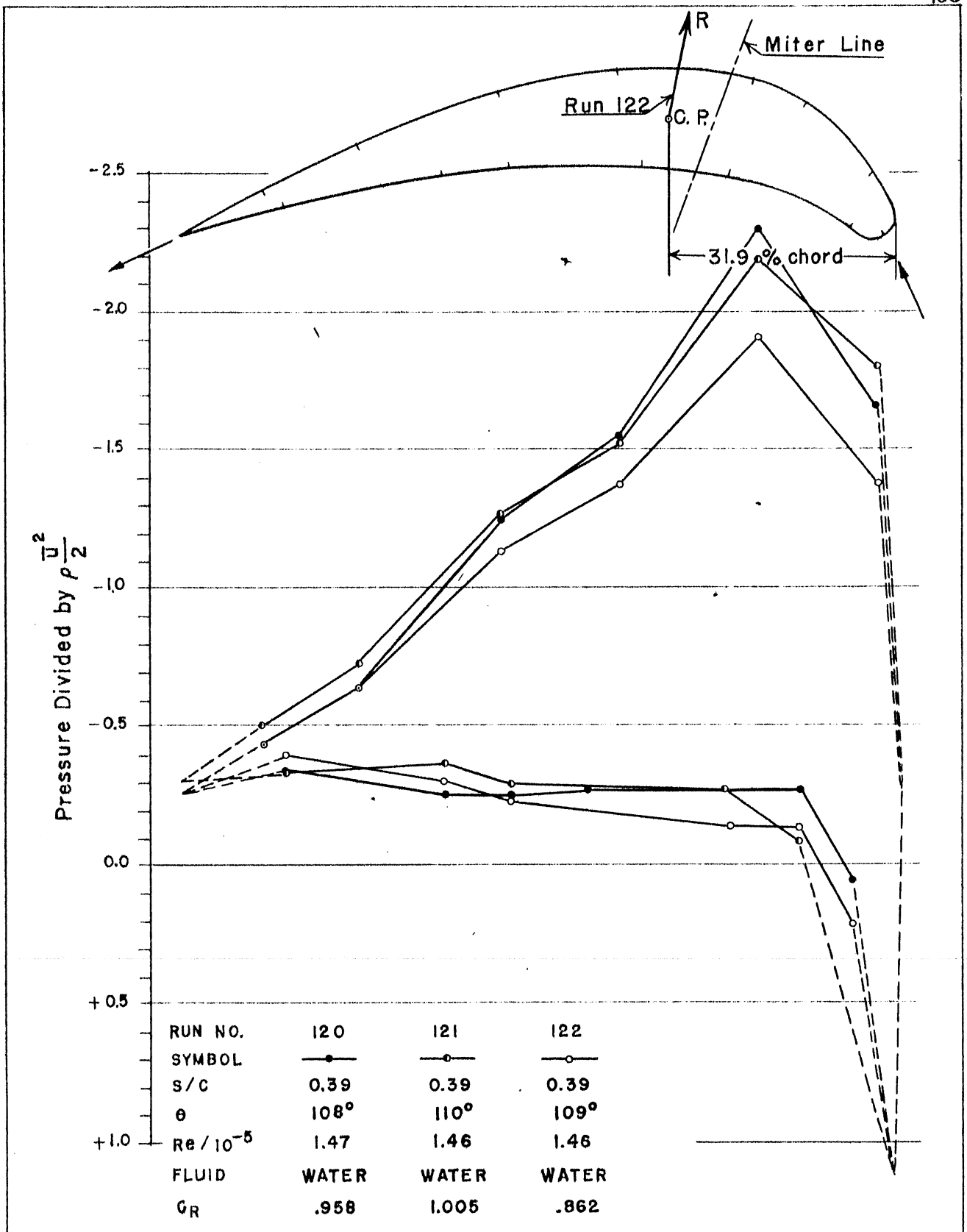

FIG. 84
PRESSURE DISTRIBUTION ON A CENTRAL VANE (TYPE II)
RUN NO. 120, 121, 122

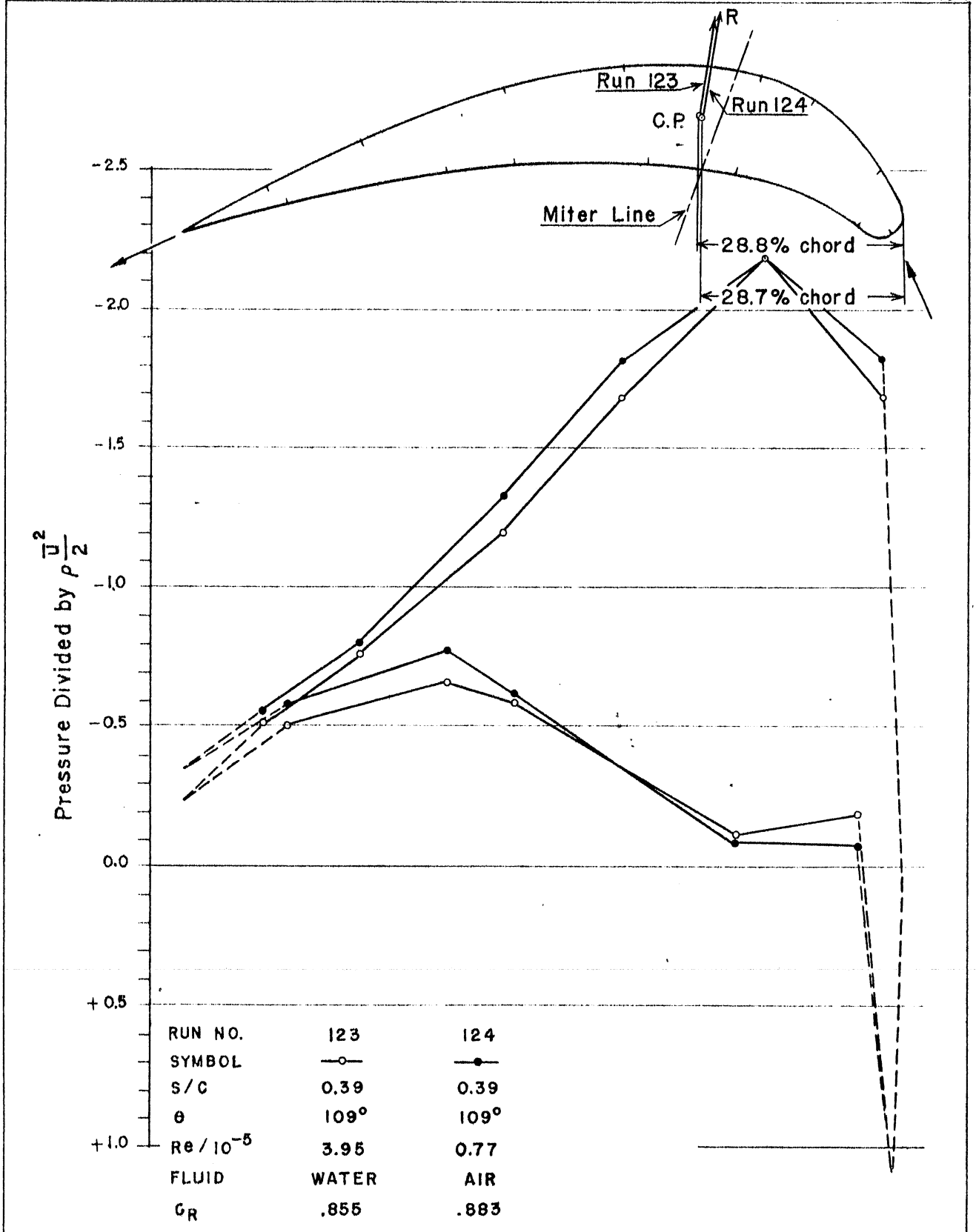

FIG. 85
PRESSURE DISTRIBUTION ON A CENTRAL VANE (TYPE II)
RUN NO. 123, 124

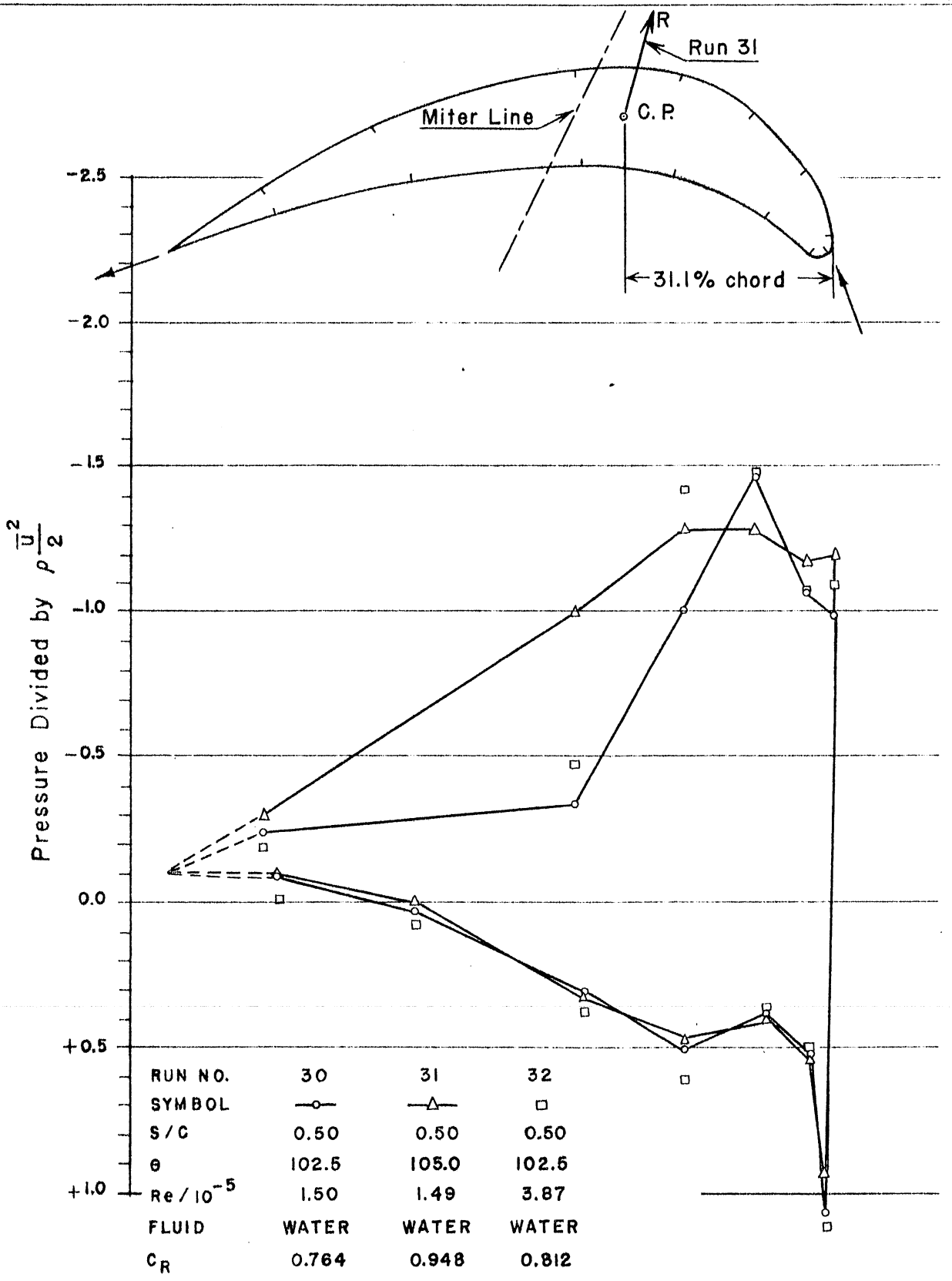

FIG. 86
PRESSURE DISTRIBUTION ON A CENTRAL VANE (21)315
RUN NO. 30, 31, 32

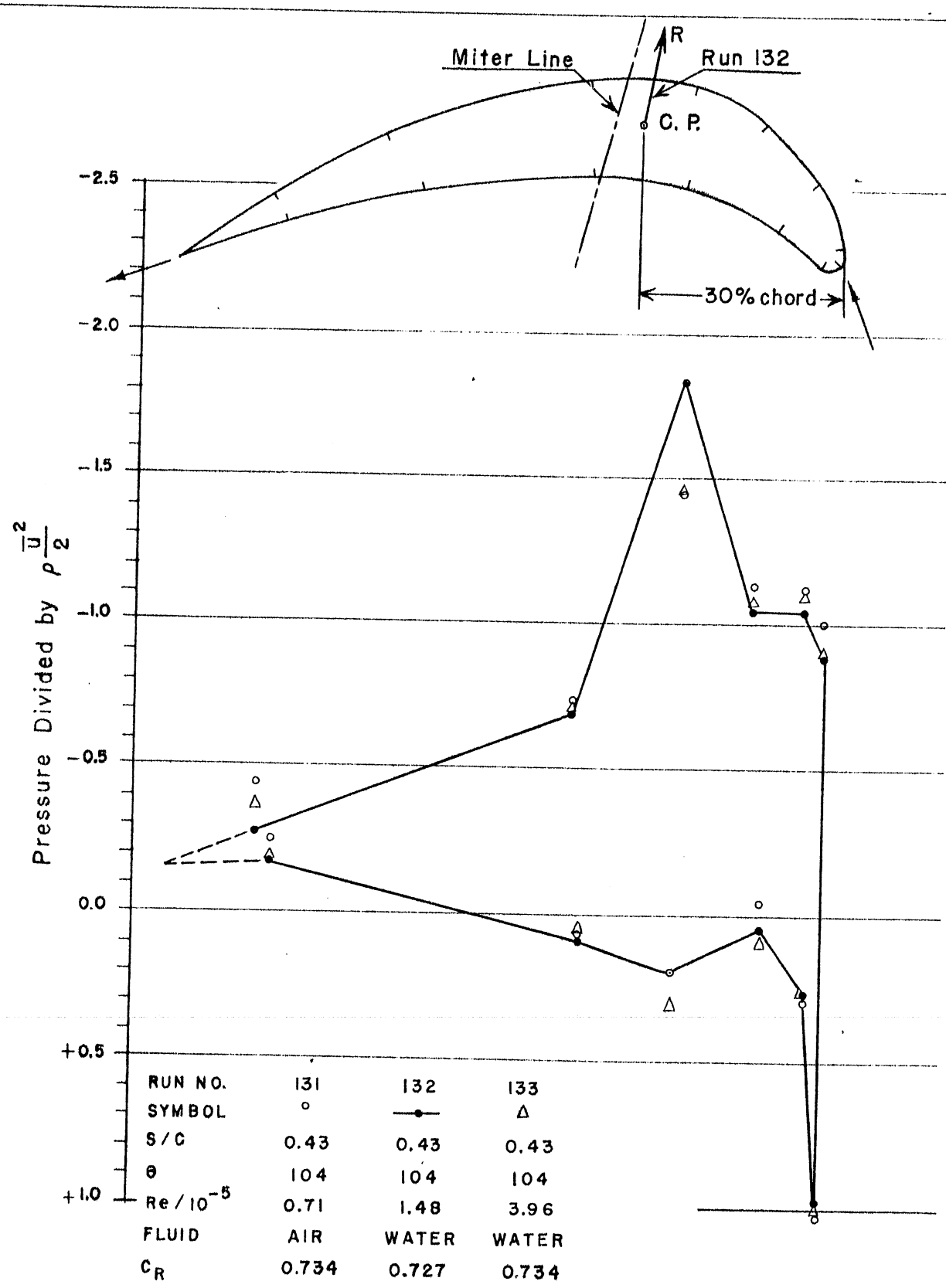

FIG. 87
PRESSURE DISTRIBUTION ON A CENTRAL VANE (21)315
RUN NO. 131, 132, 133

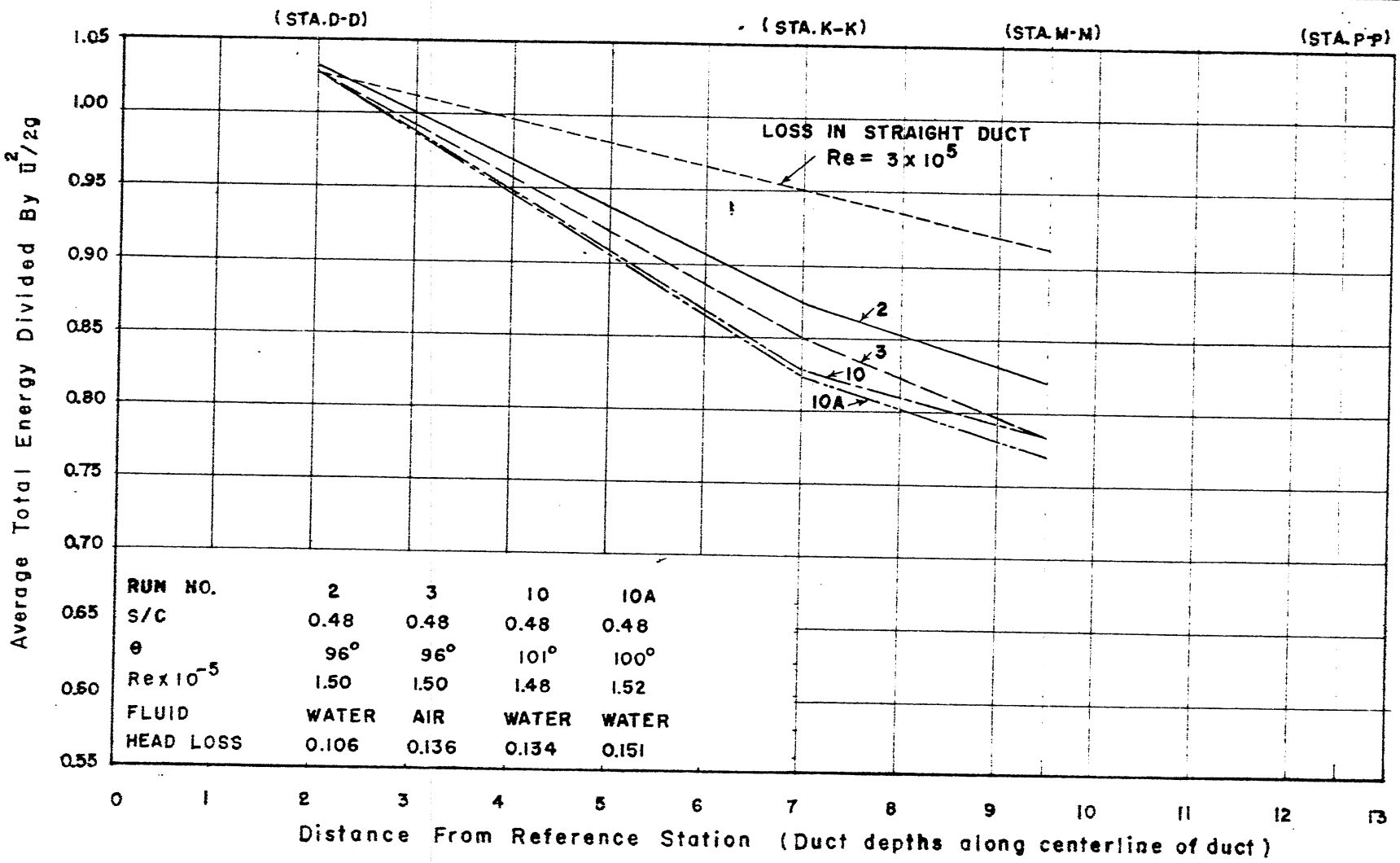

FIG. 88
AVERAGE TOTAL ENERGY BY STATIONS
RUN NO. 2, 3, 10, 10A

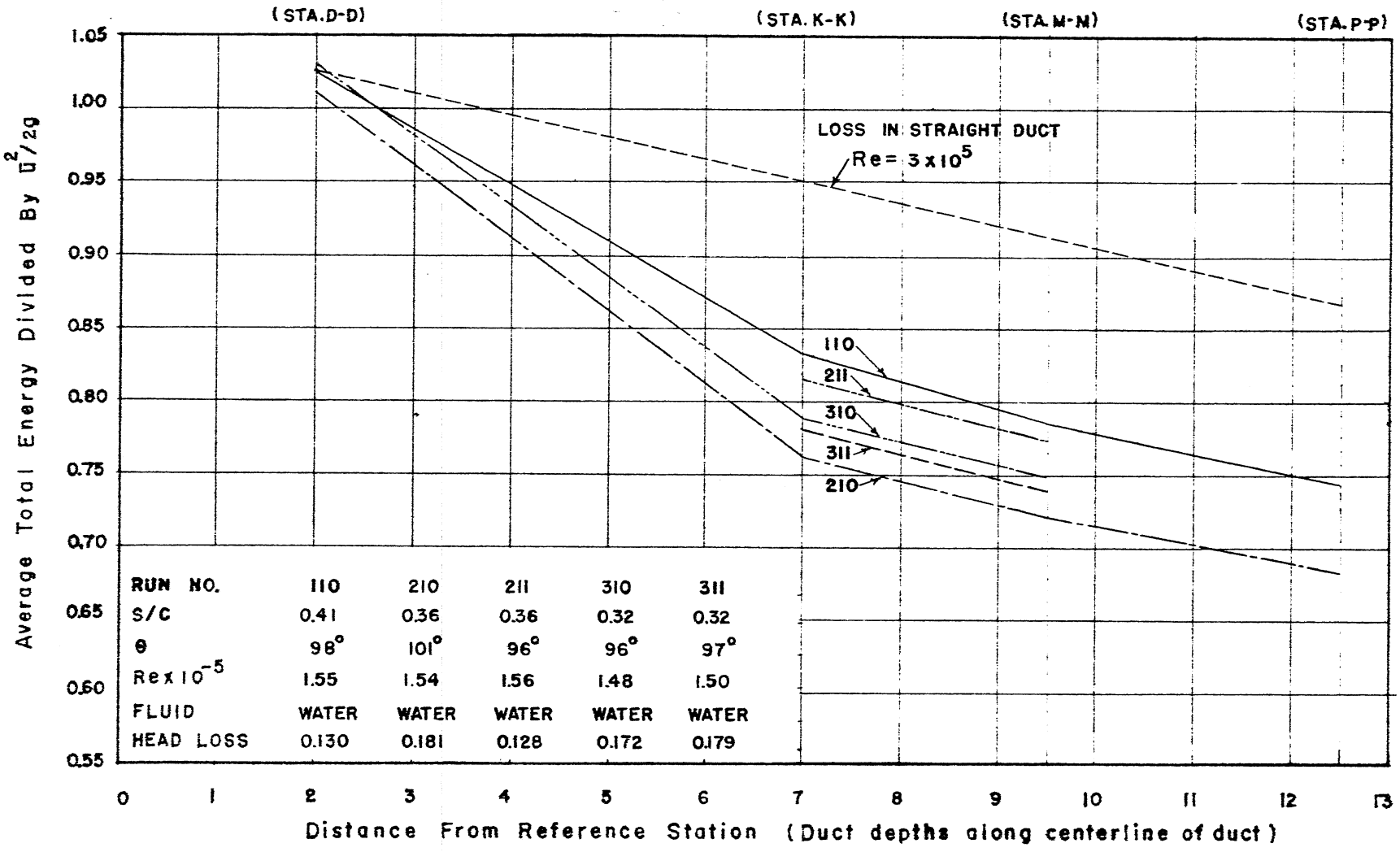

FIG. 89

AVERAGE TOTAL ENERGY BY STATIONS

RUN NO. 110,210,211,310,311

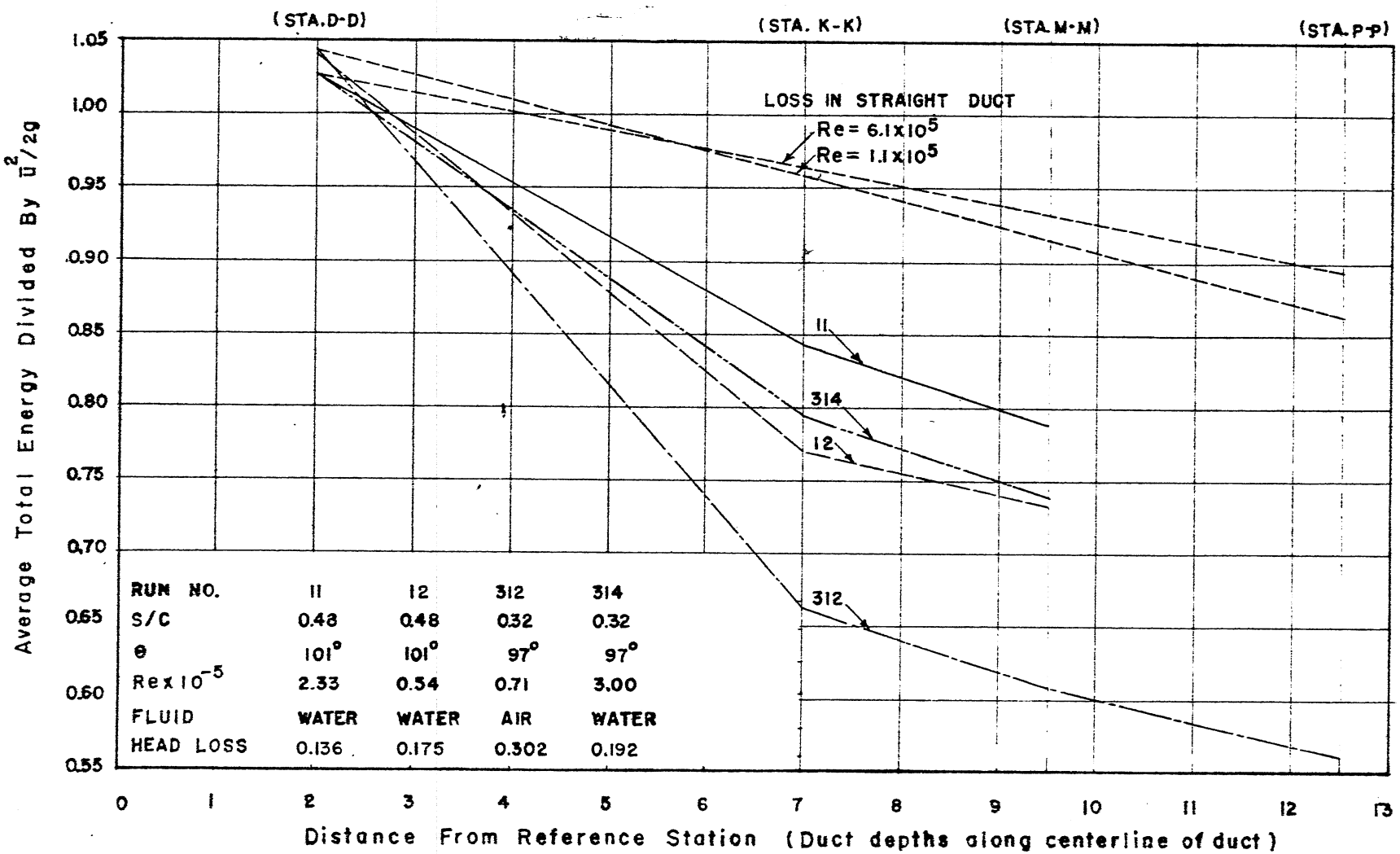

FIG. 90
AVERAGE TOTAL ENERGY BY STATIONS
RUN NO. 11, 12, 312, 314

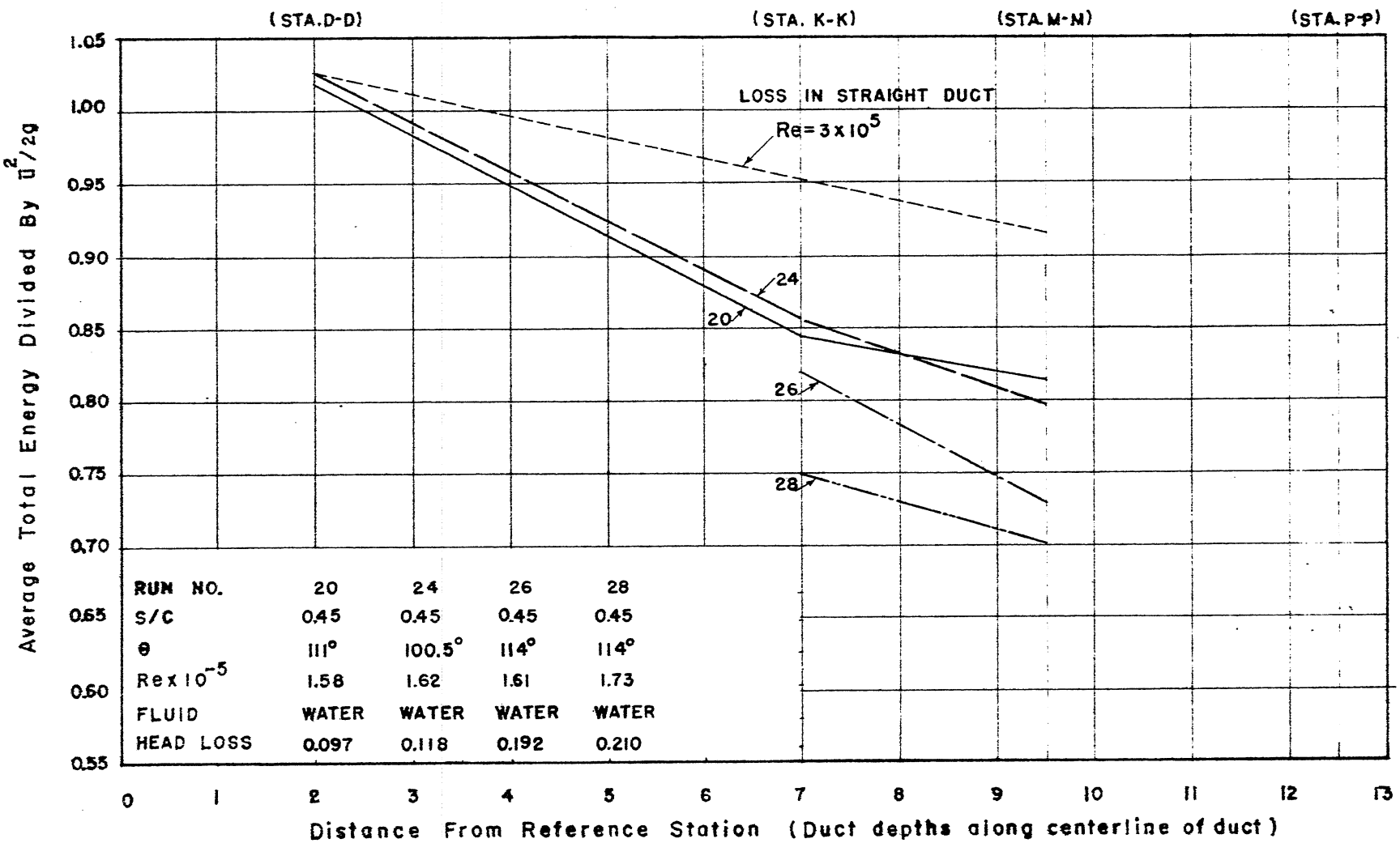

FIG. 91

AVERAGE TOTAL ENERGY BY STATIONS

RUN NO. 20, 24, 26, 28

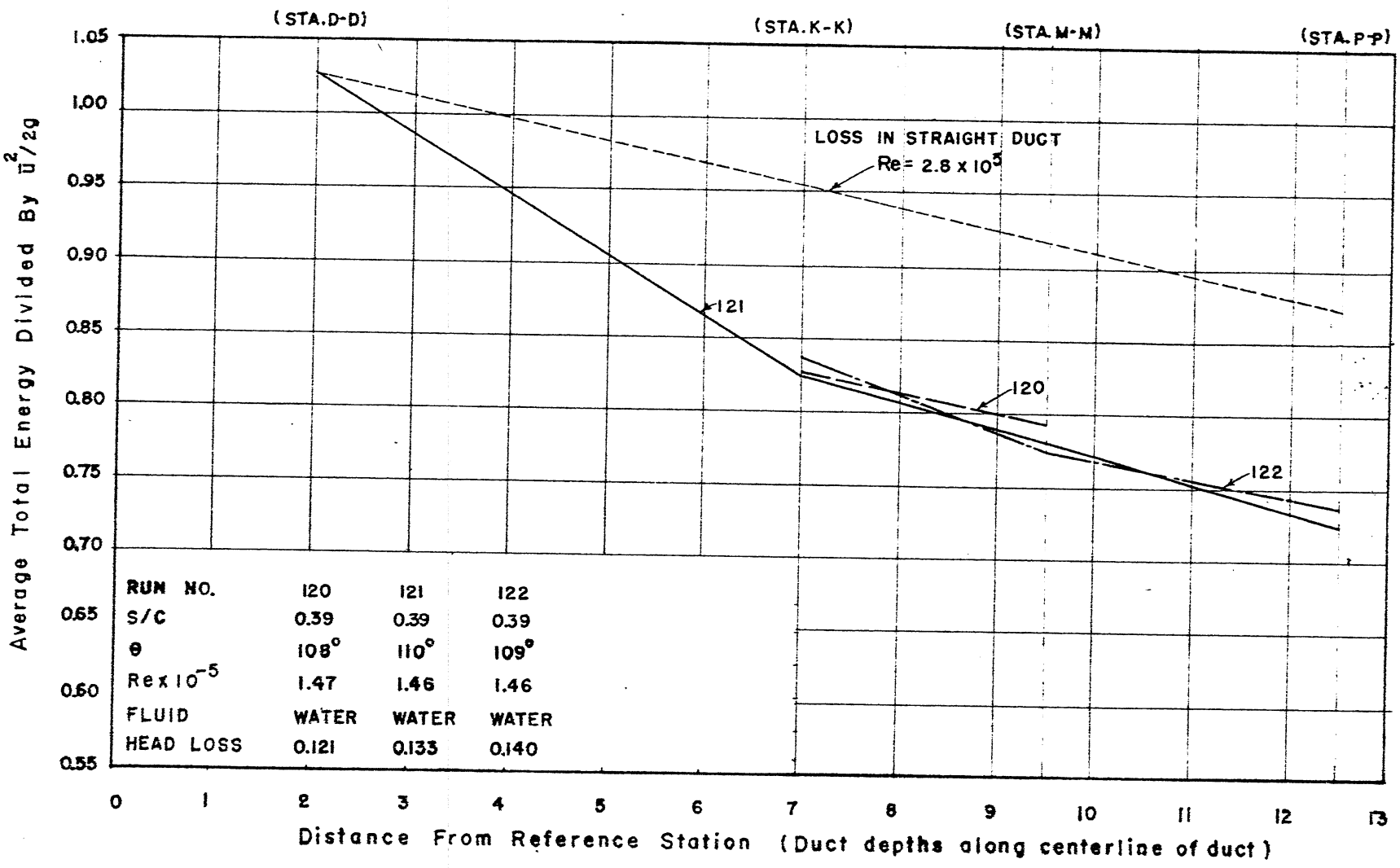

FIG. 92

AVERAGE TOTAL ENERGY BY STATIONS

RUN NO. 120, 121, 122

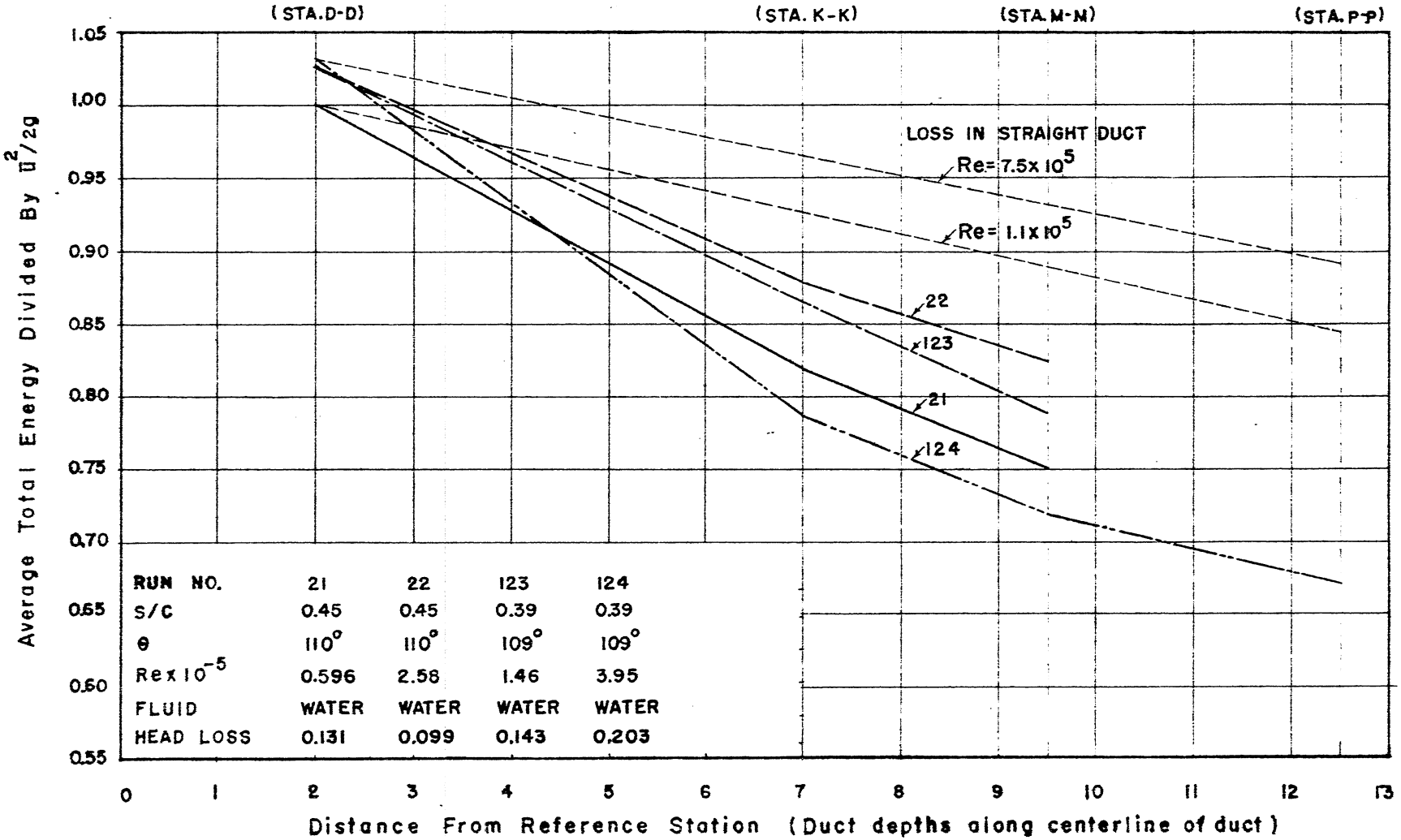

FIG. 93

AVERAGE TOTAL ENERGY BY STATIONS

RUN NO. 21, 22, 123, 124

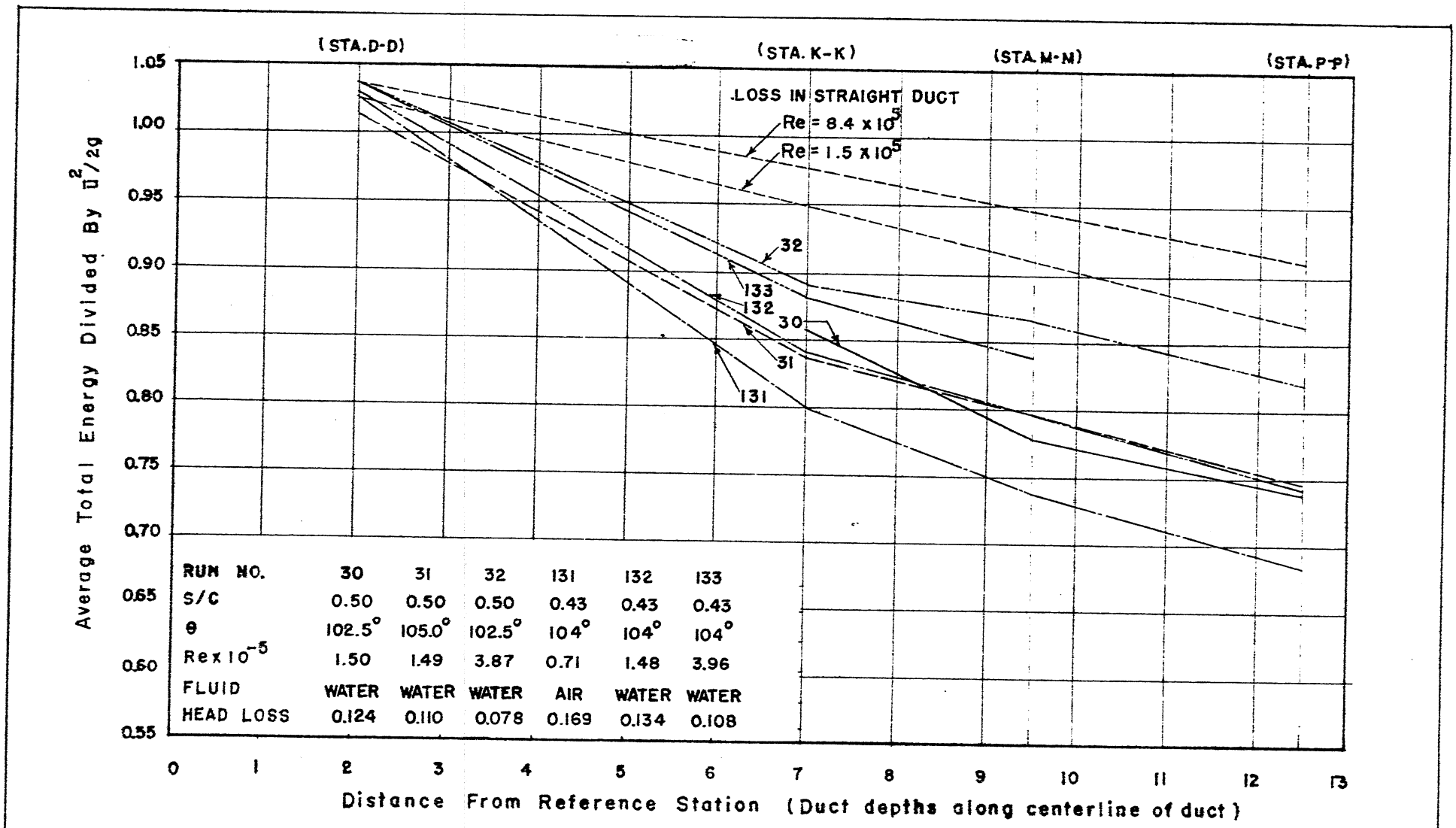

RUN NO.	30	31	32	131	132	133
S/C	0.50	0.50	0.50	0.43	0.43	0.43
θ	102.5°	105.0°	102.5°	104°	104°	104°
Re x 10^{-5}	1.50	1.49	3.87	0.71	1.48	3.96
FLUID	WATER	WATER	WATER	AIR	WATER	WATER
HEAD LOSS	0.124	0.110	0.078	0.169	0.134	0.108

FIG. 94

AVERAGE TOTAL ENERGY BY STATIONS

RUN NO. 30, 31, 32, 131, 132, 133

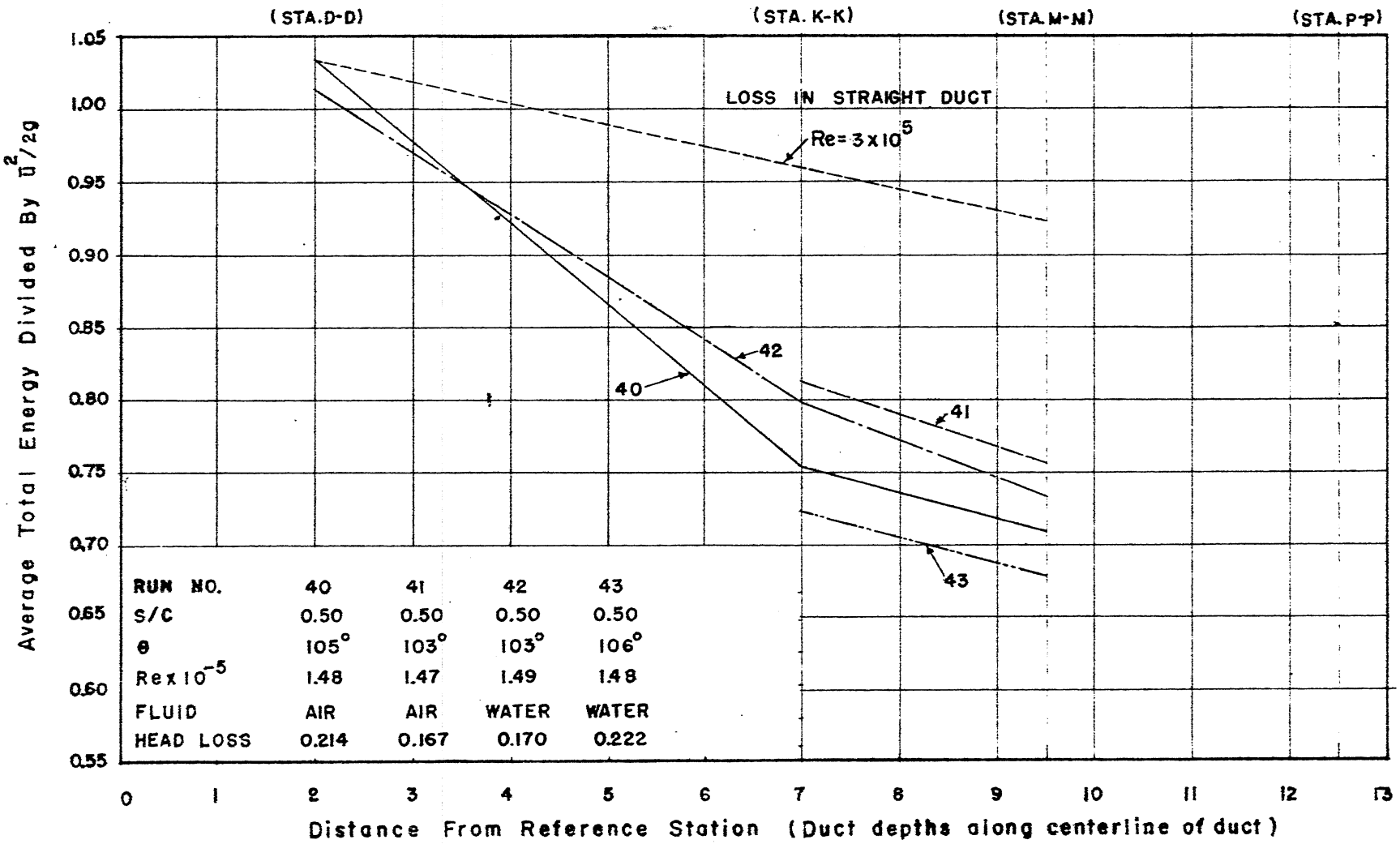

FIG. 95
AVERAGE TOTAL ENERGY BY STATIONS
RUN NO. 40, 41, 42, 43

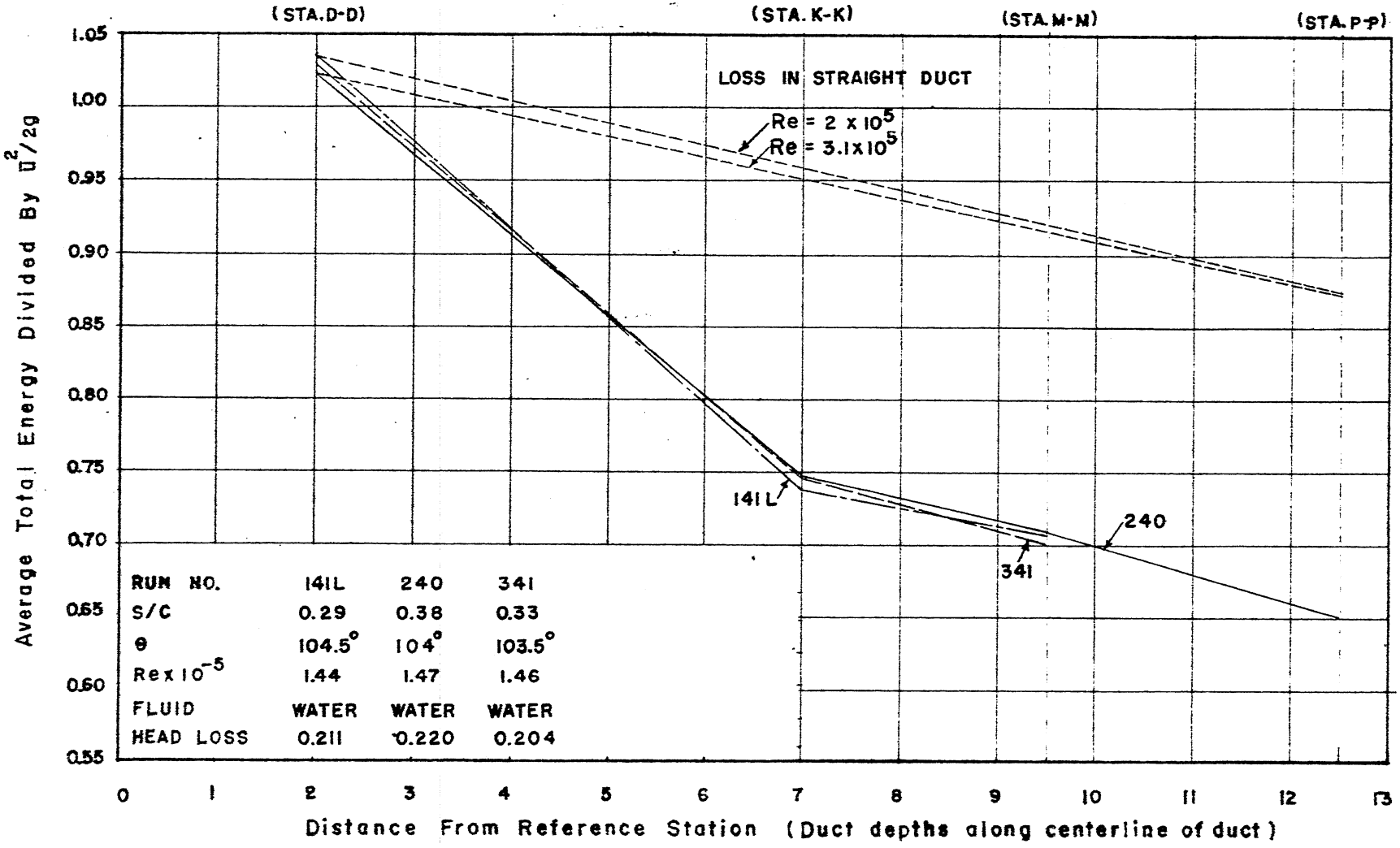

FIG. 96

AVERAGE TOTAL ENERGY BY STATIONS

RUN NO. 141L, 240, 341

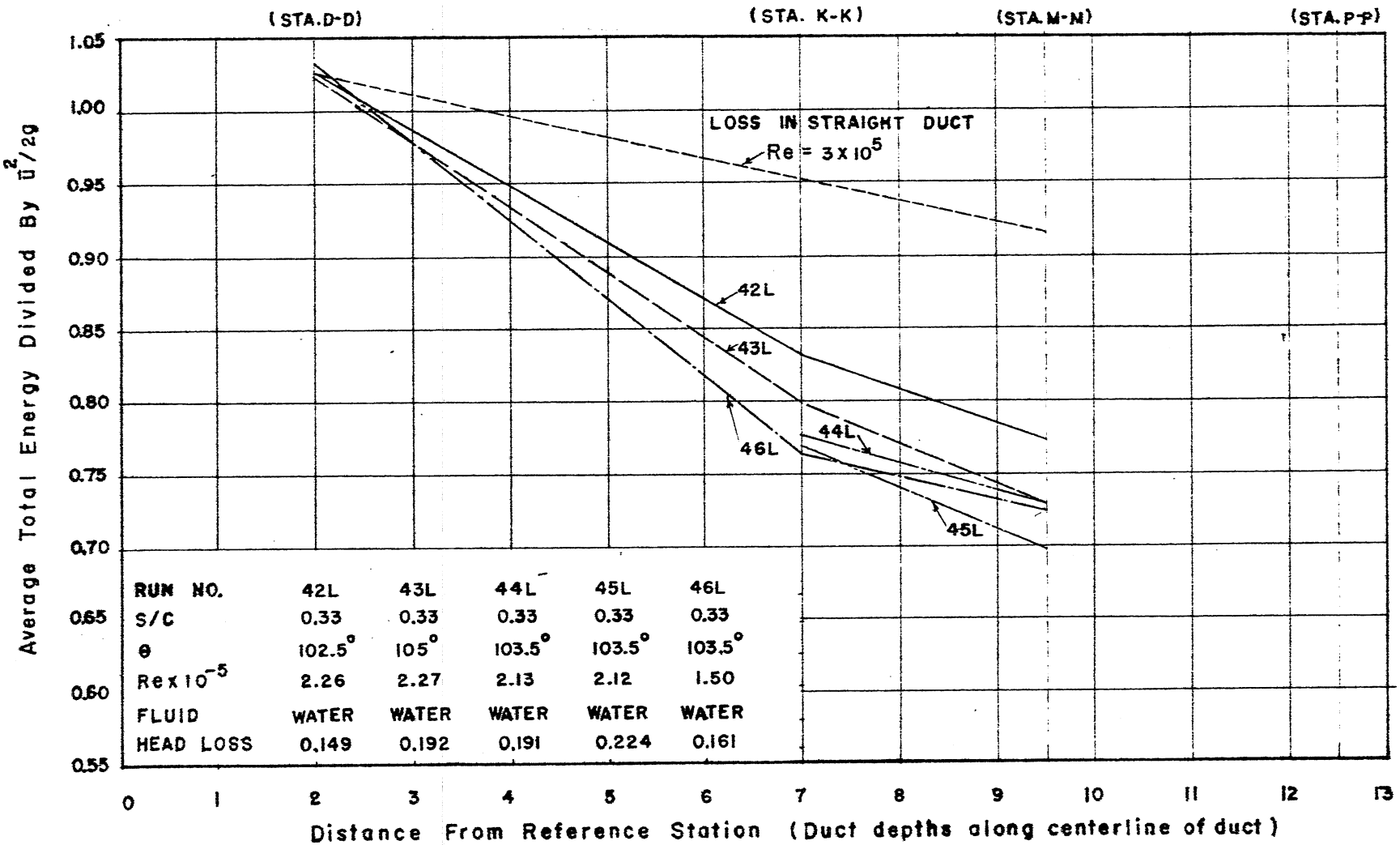

FIG. 97

AVERAGE TOTAL ENERGY BY STATIONS

RUN NO. 42L, 43L, 44L, 45L, 46L

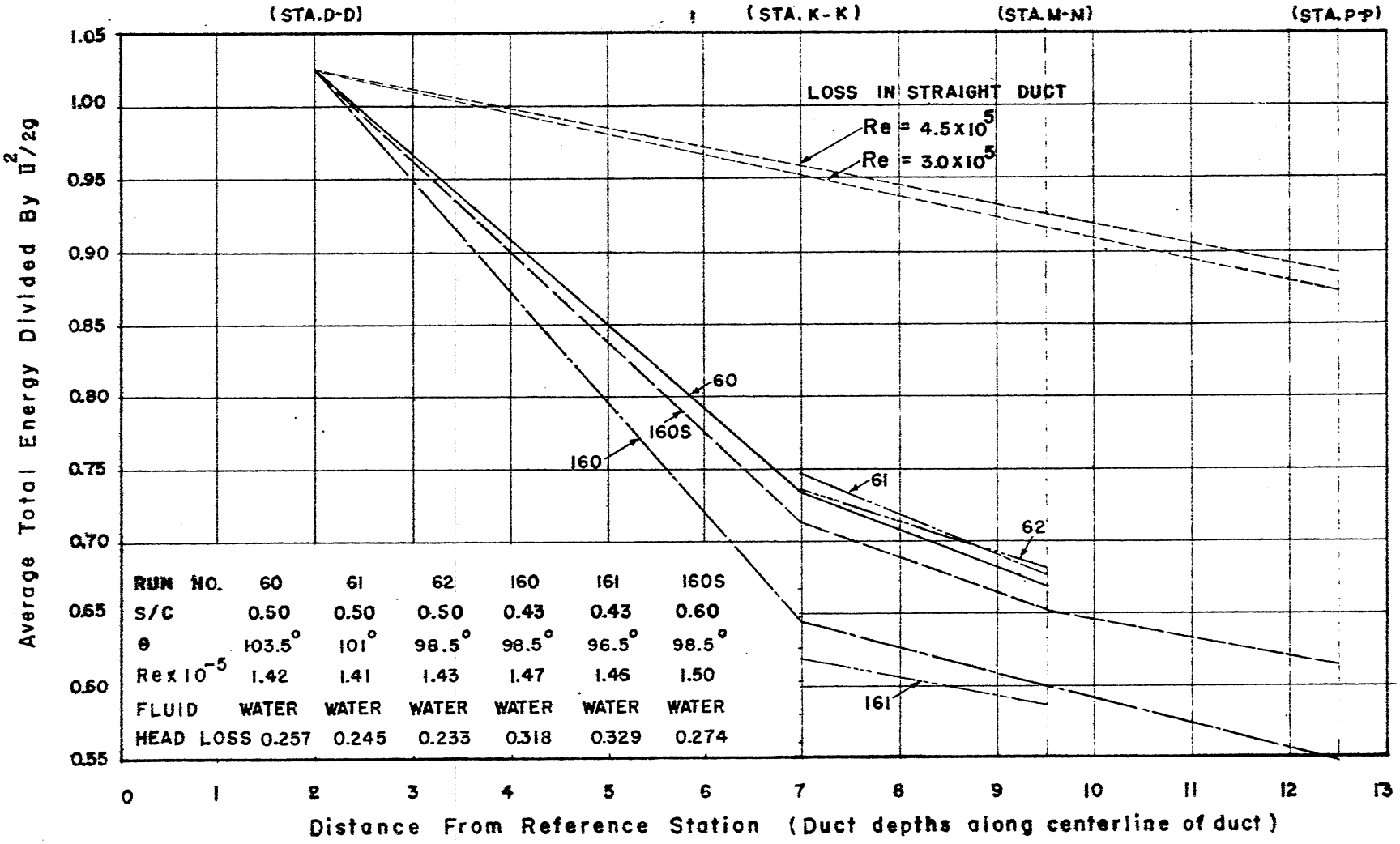

FIG. 98

AVERAGE TOTAL ENERGY BY STATIONS

RUN NO. 60, 61, 62, 160, 161, 160S

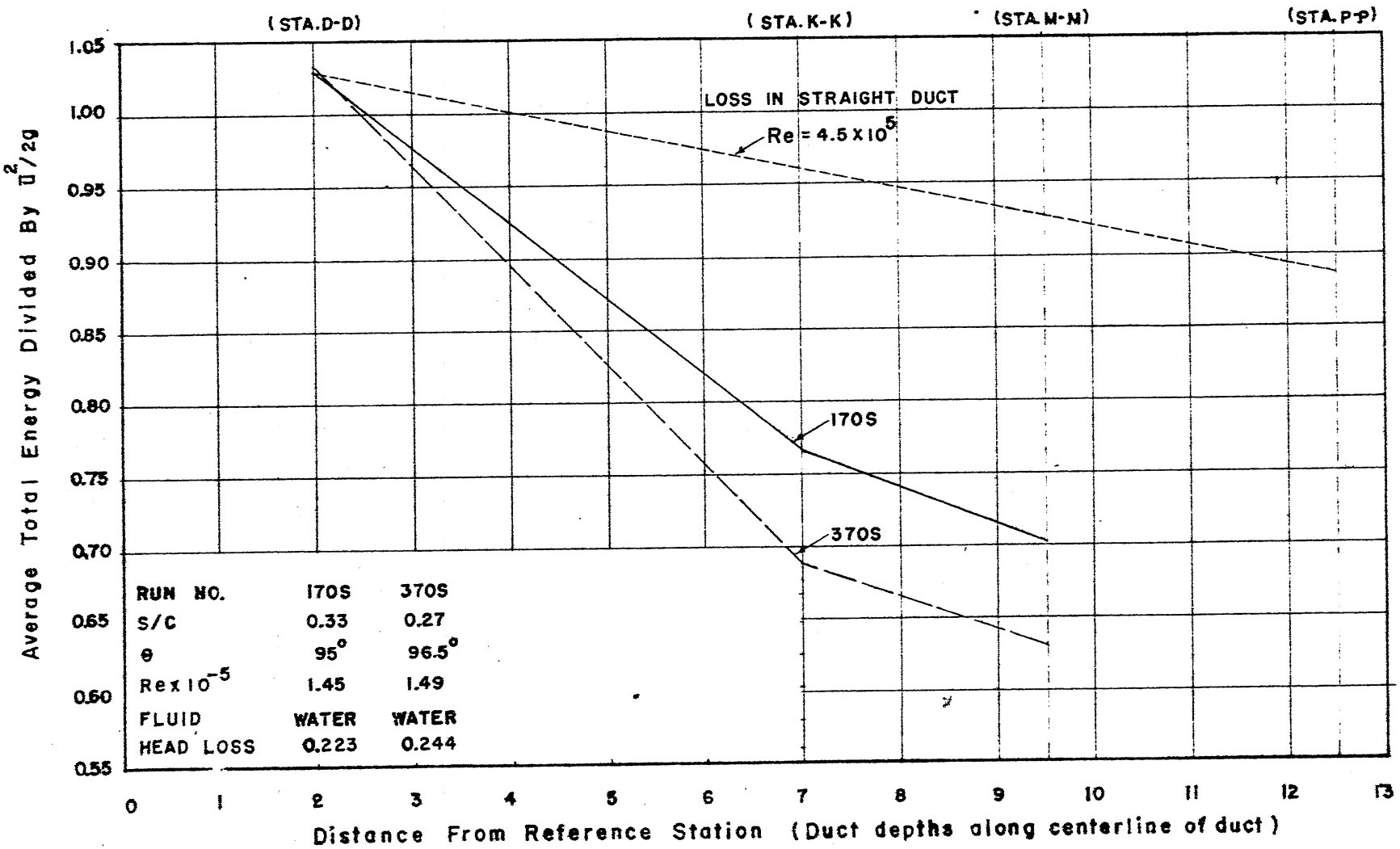

FIG. 99

AVERAGE TOTAL ENERGY BY STATIONS

RUN NO. 170S, 370S

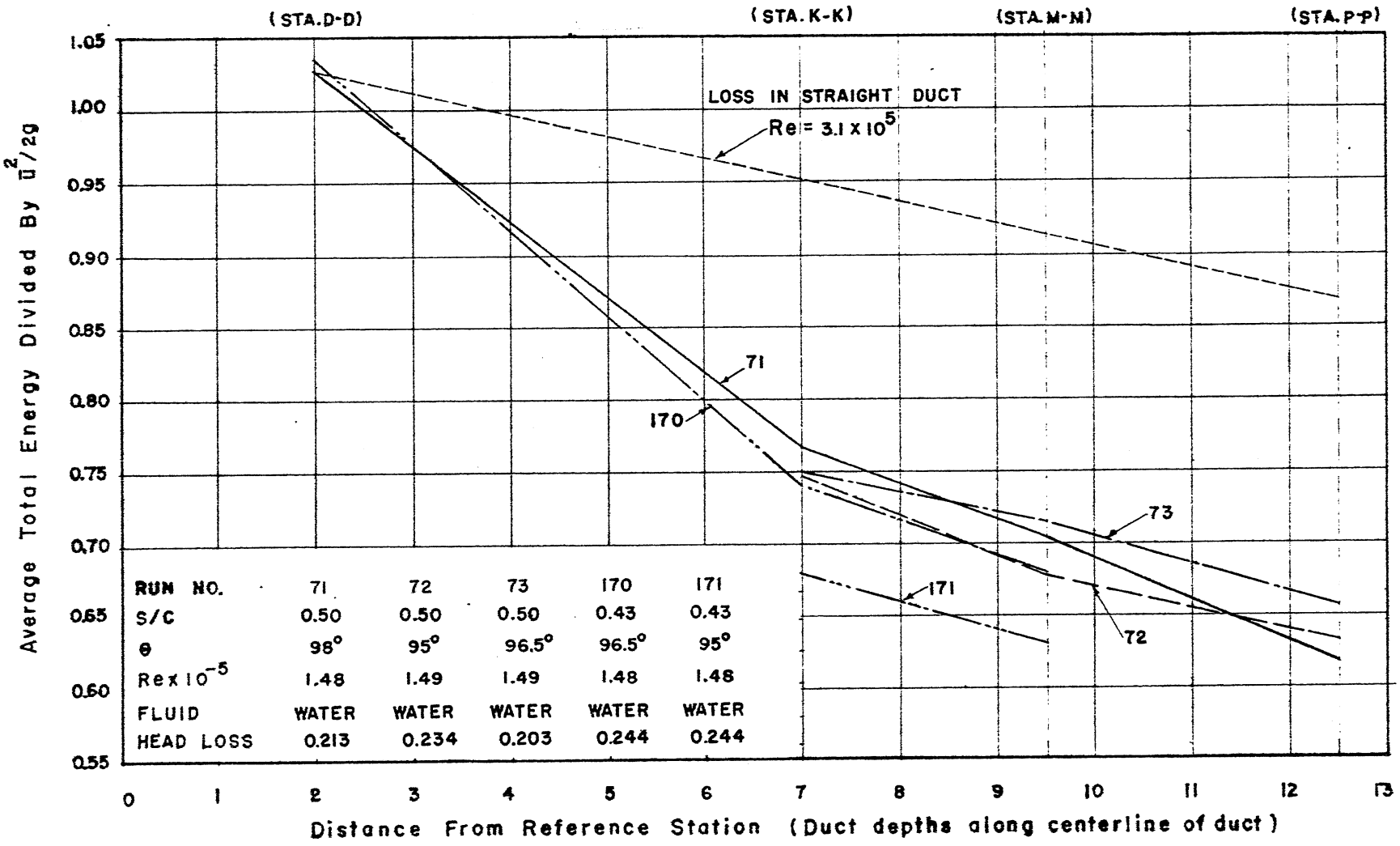

FIG. 100

AVERAGE TOTAL ENERGY BY STATIONS

RUN NO. 71, 72, 73, 170, 171

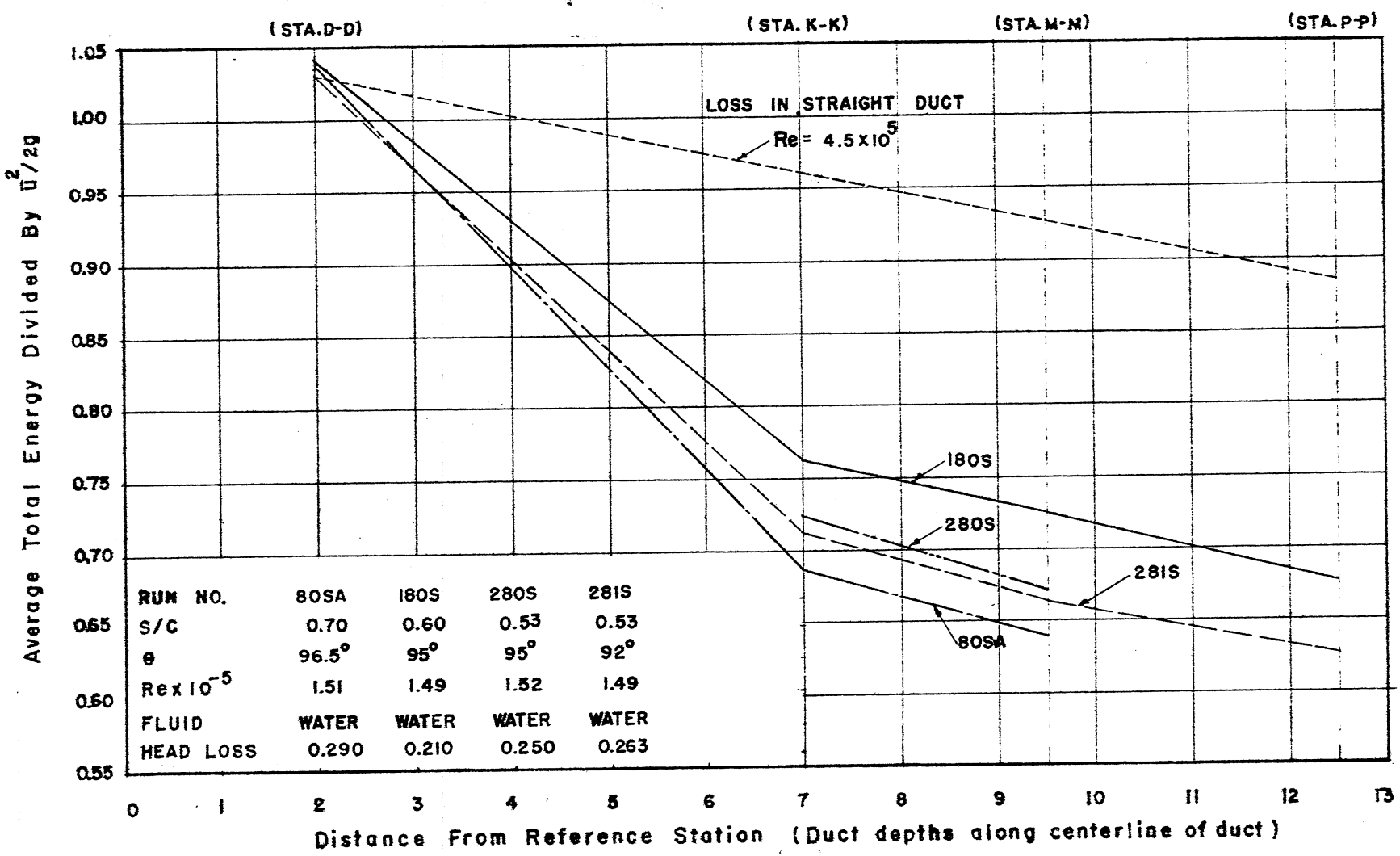

FIG. 101

AVERAGE TOTAL ENERGY BY STATIONS

RUN NO. 80SA, 180S, 280S, 281S

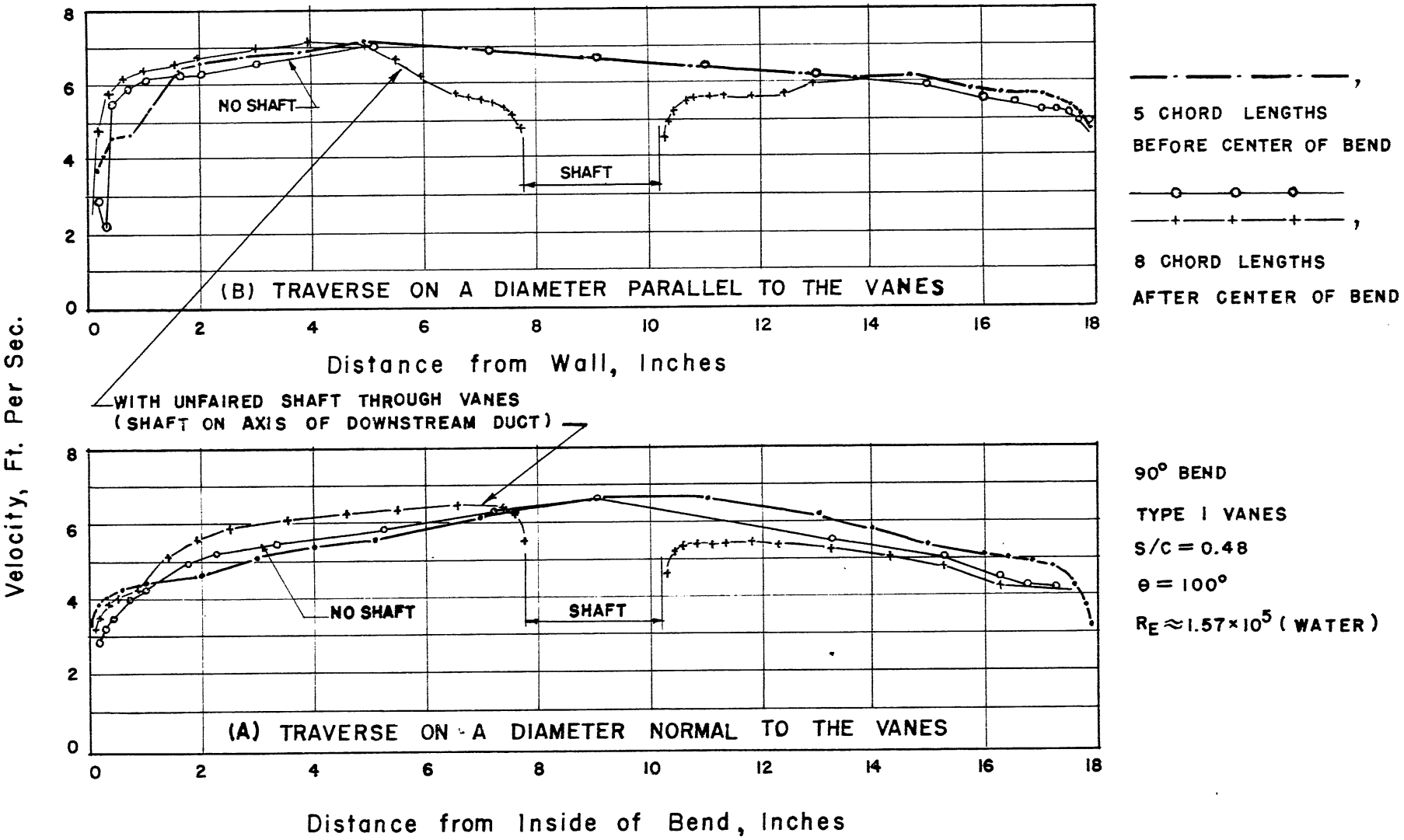

FIG. 102

VELOCITY DISTRIBUTION BEFORE AND AFTER A GUIDE VANE BEND IN A CIRCULAR DUCT

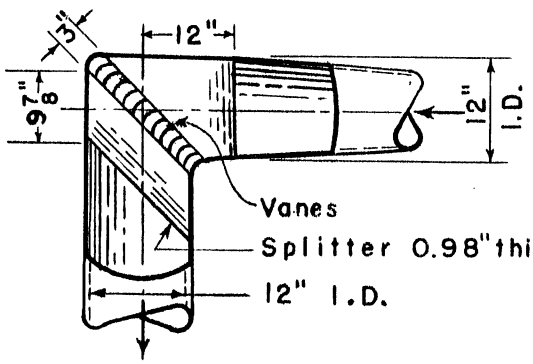

Type I Vanes
s/c = 0.48
θ = 100°
(water)
Max Re ≈ 7×10^5 ——
Max Re ≈ 4.5×10^5 - - - -

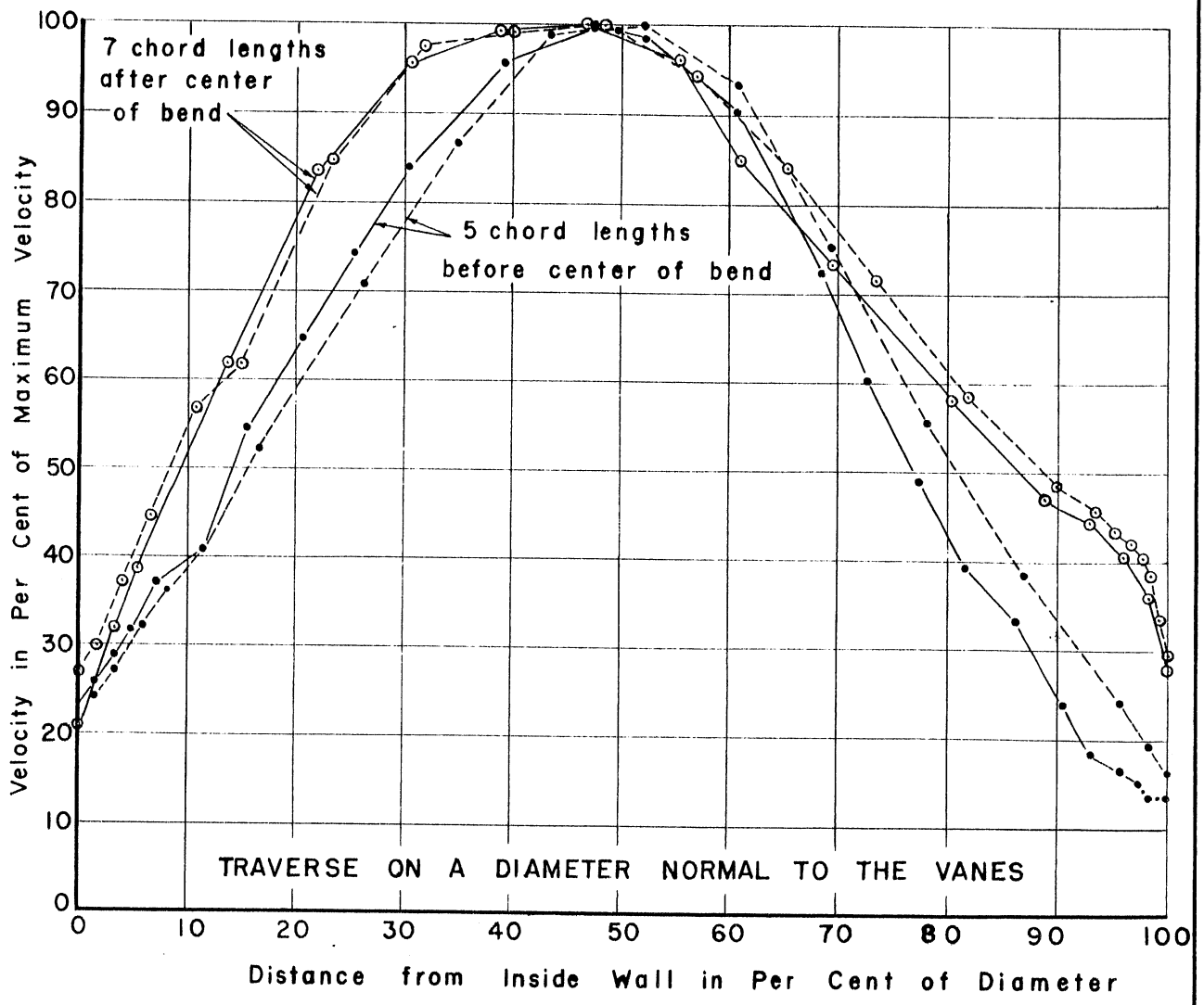

FIG. 103
VELOCITY DISTRIBUTION FOR A GUIDE VANE BEND CONTAINING A SPLITTER AND FOLLOWING A DIFFUSER IN A CIRCULAR DUCT

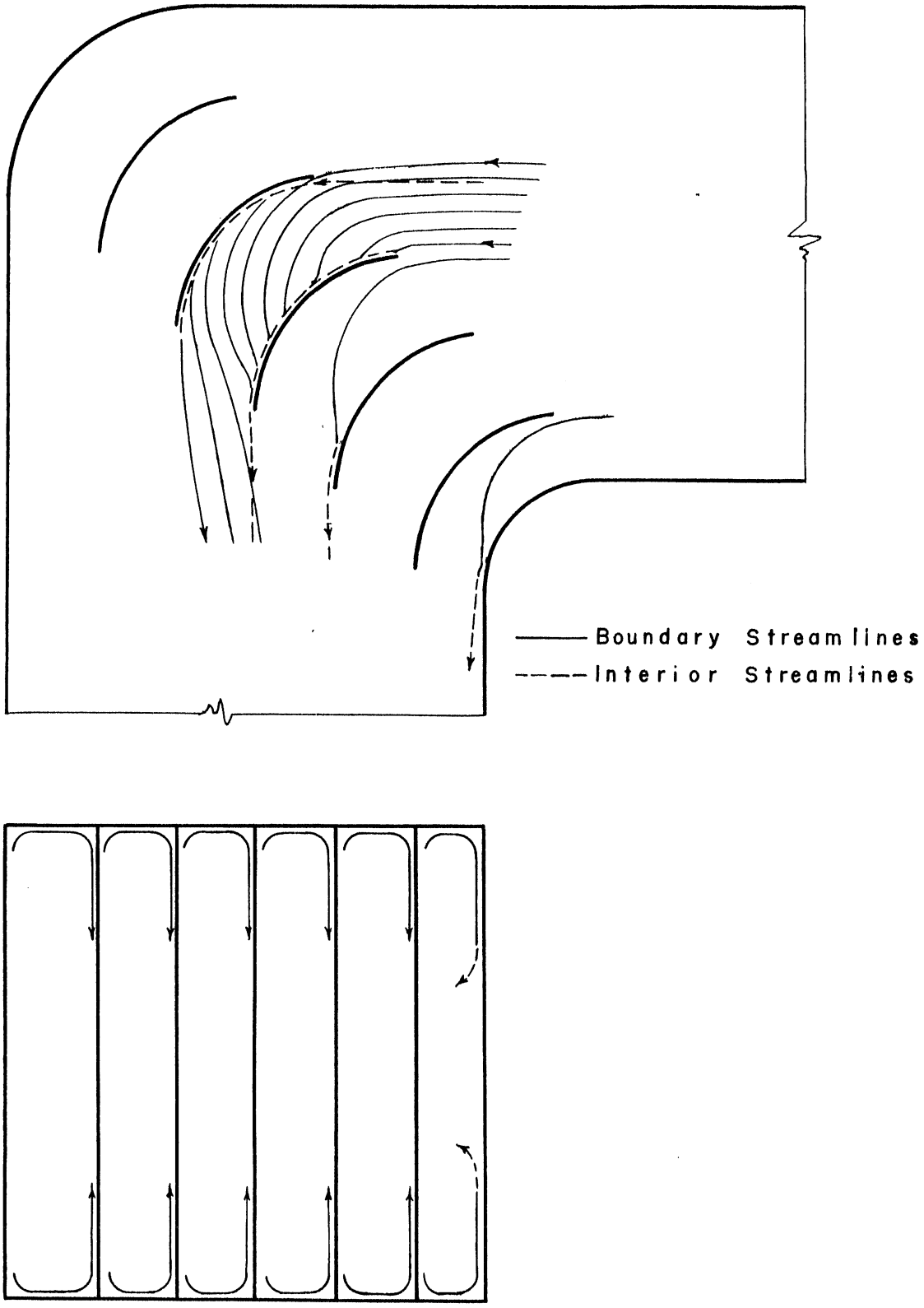

FIG. 104

SCHEMATIC BOUNDARY STREAMLINES

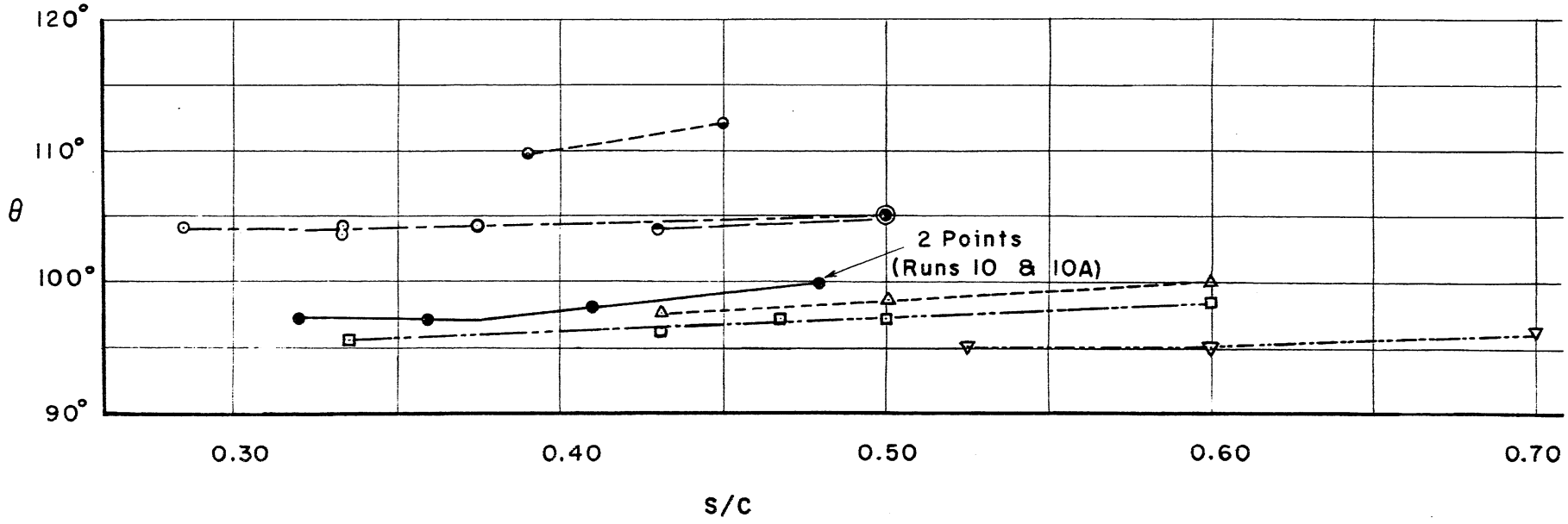

Type I Vane
Type II Vane
(21) 315 Vane
} Thick Vanes

(21) 300 Vane
(30) 300 Vane
(30) 400 Vane
(30) 500 Vane
} Thin Vanes

$Re \approx 1.5 \times 10^5$

$\Delta = 90°$

FIG. 105

VARIATION OF CORRECT STAGGER ANGLE
WITH SPACING-CHORD RATIO
FOR SEVERAL VANE SHAPES

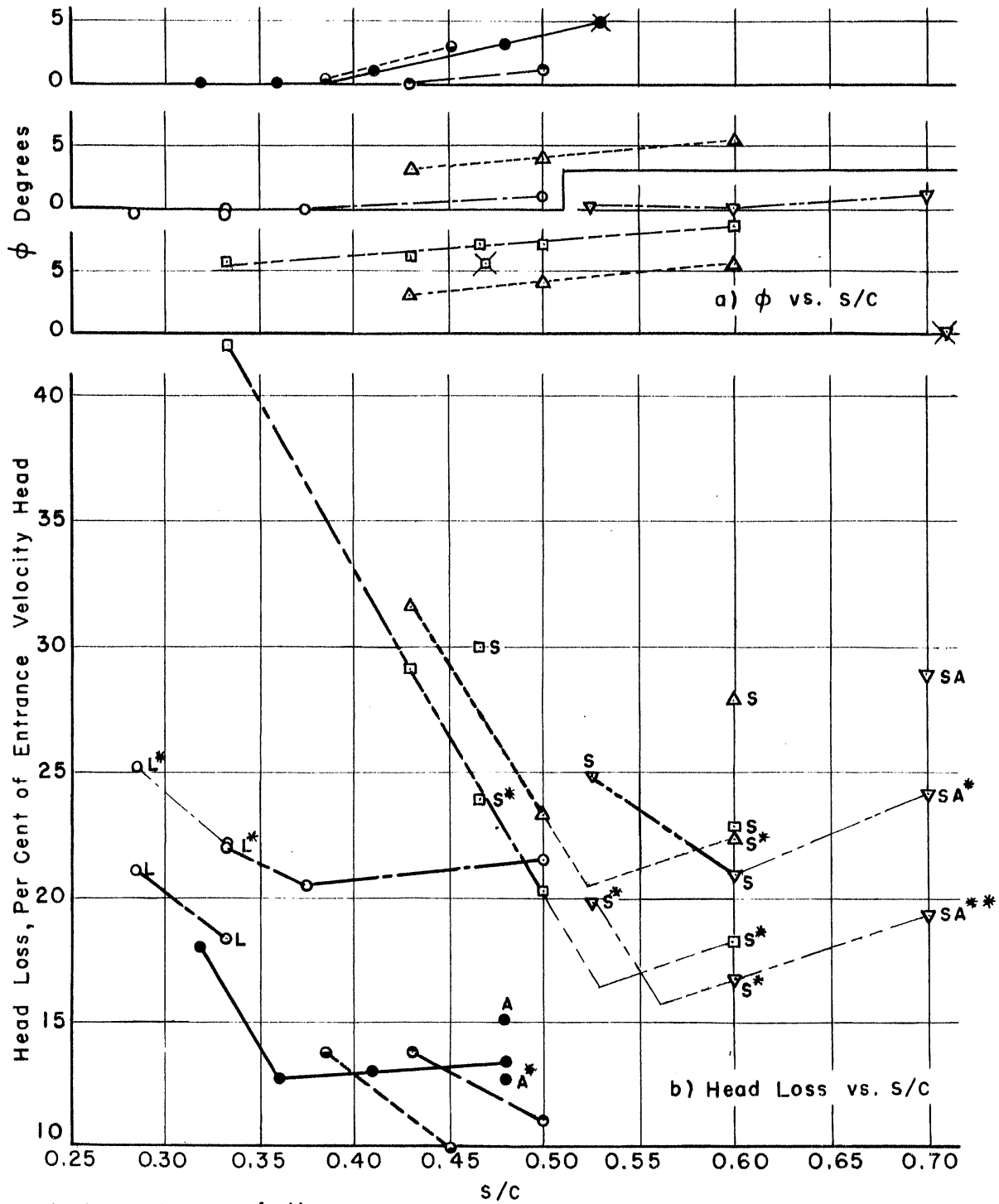

Symbol	Type of Vanes	
●—●—●	I	Thick Vanes
—●—	II	
—○—	(21) 315	
—○—	(21) 300	Thin Vanes
—△—	(30) 300	
—□—	(30) 400	
—▽—	(30) 500	
✱	Klein, Tupper & Green No.5 Vane	
⊠	Krober No. I Vane	
⋈	Klein, Tupper & Green No.3 Vane	

Notes

S Vane with 2.02" Chord
L Vane with 4.25" Chord
A Small Space Between Vanes and Wall
* Corrected Value
* * Twice Corrected Value

$Re \approx 1.5 \times 10^5$
$\Delta = 90°$

FIG. 106
PERFORMANCE OF GUIDE VANE CASCADES

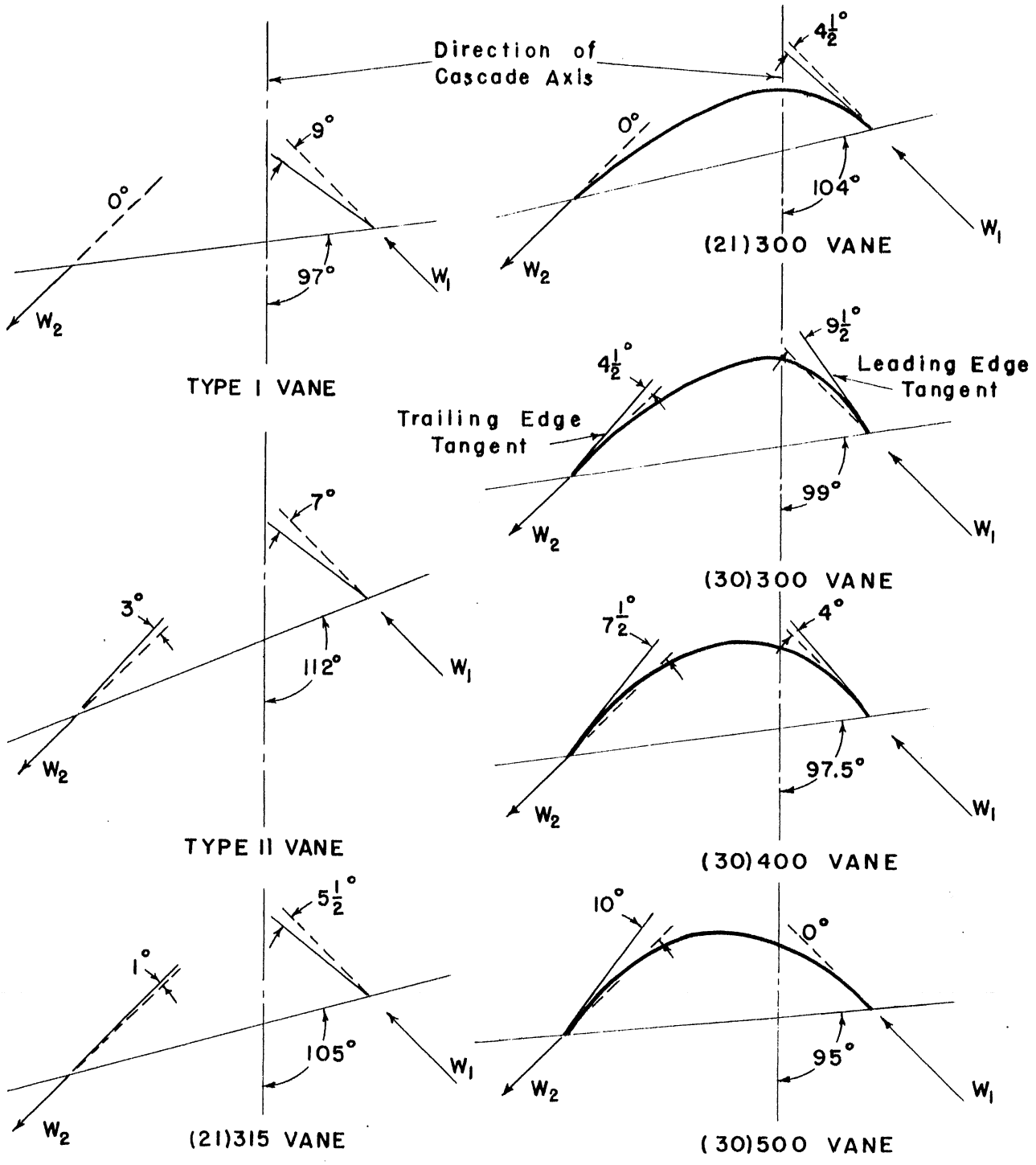

FIG. 107
GEOMETRY OF FLOW
AT OPTIMUM s/c

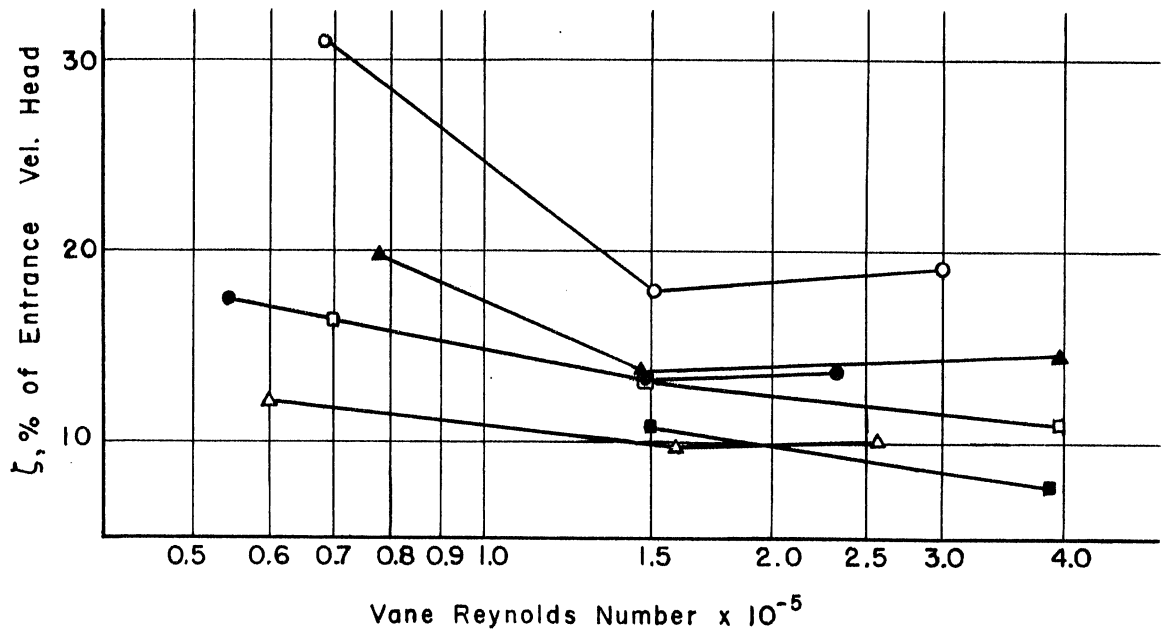

s/c = 0.32 —○— } Type I Vanes
s/c = 0.48 —●— }
s/c = 0.45 —△— } Type II Vanes
s/c = 0.38 —▲— }
s/c = 0.43 —□— } (30)315 Vanes
s/c = 0.50 —■— }

FIG. 108

VARIATION OF ζ WITH REYNOLDS NUMBER

BIBLIOGRAPHY

(1) Anderson, A. G. FLUID FLOW DIVERSION: A SUMMARY AND BIBLIOGRAPHY OF LITERATURE. St. Anthony Falls Hydraulic Laboratory, University of Minnesota, Project Report No. 1, August 1947.

(2) Silberman, E. THE NATURE OF FLOW IN AN ELBOW. St. Anthony Falls Hydraulic Laboratory, University of Minnesota, Project Report No. 5, December 1947.

(3) Spannhake, W. ANALYSIS OF MODERN PROPELLER-PUMP DESIGN. David Taylor Model Basin, Report 621, June 1948.

(4) Marcinowski, H. THE SIGNIFICANCE OF THE MEASURED LATTICE CHARACTERISTICS FOR CALCULATION AND DESIGN OF AXIAL FLOW TURBINES AND COMPRESSORS. Translated from the German and published by Research and Standards Branch, Bureau of Ships, Navy Department, May 1946.

(5) Garrick, I. E. ON THE PLANE POTENTIAL FLOW PAST A LATTICE OF ARBITRARY AIRFOILS. U. S. National Advisory Committee for Aeronautics, Report No. 788, 1944.

(6) Mutterperl, W. A SOLUTION OF THE DIRECT AND INVERSE POTENTIAL PROBLEMS FOR ARBITRARY CASCADES OF AIRFOILS. U. S. National Advisory Committee for Aeronautics, Wartime Report L-81, December 1944.

(7) Merchant, W. "Flow of an Ideal Fluid Past a Cascade of Blades." Part I, TECHNICAL REPORT OF THE AERONAUTICAL RESEARCH COMMITTEE, R & M. 1890, 1940.

(8) Weinig, F. DIE STRÖMUNG UM DIE SCHAUFELN VON TURBOMASCHINEN (The Flow Around Turbine and Compressor Blades). Translated from the German by Research and Standards Branch, Bureau of Ships, Navy Department, May 1946.

(9) Ackeret, J. "Zum Enturt ditchstehender Schaufelgitter," (The Design of Closely Spaced Blade Lattices). SCHWEIZESISCHE BAUZEITUNG, Vol. 120, No. 9, August 29, 1942, pp. 103-08.

(10) Krober, G. "Schaufelgitter zur Umlenkung von Flüssigkeitströmungen mit geringem Emergieverlust" (Guide Vanes for Deflecting Fluid Currents with Small Loss of Energy). INGENIEUR ARCHIV, Vol. III, 1932. Translated and published as Technical Memorandum No. 722, National Advisory Committee for Aeronautics, 1933.

(11) Lamb, H. HYDRODYNAMICS, 6th ed., 1932.

(12) Shimoyama, Yoshinori. "Experiments on Rows of Aerofoils for Retarded Flow." MEMOIRS OF THE FACULTY OF ENGINEERING, KYUSHU IMPERIAL UNIVERSITY, Fukuoka, Japan. Vol. 8, 1936-40, pp. 281-329.

(13) Lieblein, V. ZUR BERECHNUNG DER AUFTRIEBSCHARACTERISTIK EINES PROFILES IM GITTERVERBAND (The Calculation of the Lift Characteristics of an Aerofoil Section in a Cascade). Translated from the German by

W. Bente, Aeronautical Research Committee, Reports and Translations No. 442, February 1947.

(14) Weske, S. R. "Drag og Airfoils in Grids of High Solidity." JOURNAL OF AERONAUTICAL SCIENCES, October 1944.

(15) Kirschmer, O. "Untersuchungen über den Geffällsverlust an Rechen" (Investigations of Loss of Head in Gratings). TRANSACTIONS, Munich Hydraulic Institute, Vol. 1, 1926, pp. 21-41.

(16) Abbott, I. H., von Doenhoff, A. E., and Stivers, L. S., Jr., SUMMARY OF AIRFOIL DATA. U.S. National Advisory Committee for Aeronautics, Wartime Report L-560, March 1945.

(17) Holdhusen, J. S. and Lamb, O. P. MODEL EXPERIMENTS FOR THE DESIGN OF A SIXTY-INCH WATER TUNNEL, PART V, VANED ELBOW STUDIES. St. Anthony Falls Hydraulic Laboratory, Project Report No. 14, September 1948.

(18) Jacobs, E. N., Ward, K. E., and Pinkerton, R. M. THE CHARACTERISTICS OF 78 RELATED AIRFOIL SECTIONS FROM TESTS IN THE VARIABLE-DENSITY WIND TUNNEL. U. S. National Advisory Committee for Aeronautics, Report No. 460, 1933.

(19) Klein, G. J., Tupper, K.F., and Green, J. J. "The Design of Corners in Fluid Channels." CANADIAN JOURNAL OF RESEARCH, Vol. 3, 1930, pp. 272-85.

(20) WATER TUNNEL VANED-TURN STUDIES. Ordnance Research Laboratory, Pennsylvania State College, September 10, 1947.

(21) Collar, A. R. "Some Experiments with Cascades of Aerofoils." TECHNICAL REPORT OF THE AERONAUTICAL RESEARCH COMMITTEE, R. & M. 1768, Vol. II, 1937, pp. 1281-87.

(22) Harris, R. G. and Fairthorne, R. A. "Wind Tunnel Experiments with Infinite Cascades of Aerofoils." TECHNICAL REPORT OF THE AERONAUTICAL RESEARCH COMMITTEE, R. & M. 1206, Vol. I, 1928-29, pp. 286-304.

(23) Silberman, E. THE PITOT CYLINDER. St. Anthony Falls Hydraulic Laboratory, Circular No. 2, October 1947.

APPENDIX I

FLOW FIELD FOR A UNIFORM FLOW AND ROW OF VORTEXES NOT AT RIGHT ANGLES TO EACH OTHER

Referring to Fig. 3b, consider the row of vortexes to be placed on the y-axis and the uniform flow of velocity $\vec{U}$ to make an angle β ($\neq 90^\circ$) with the y-axis. The flow will be turned through an angle Δ where $\Delta = \beta_2 - \beta_1$, and β_1 and β_2 are the angles between the vortex axis and the directions of the approaching and departing flow, respectively. Again, $\vec{W} = \vec{U} \pm \frac{\Gamma}{2s}$ added vectorially; the velocities $\vec{W}_1$ and $\vec{W}_2$ are now unequal in magnitude, however. The magnitudes of the various velocities are related by the expressions,

$$U \sin\beta = W_1 \sin \beta_1 = W_2 \sin \beta_2$$

or

$$\frac{W_2}{W_1} = \frac{\sin \beta_1}{\sin \beta_2} = \frac{\sin \beta_1}{\sin (\beta_1 + \Delta)} \qquad \text{(A-1)}$$

and*

$$\frac{U}{W_1} = \frac{\sin \beta_1}{\sin \beta} = \sqrt{1 - K \cos \beta_1 + \frac{K^2}{4}} \qquad \text{(A-2)}$$

where

$$K = \frac{\sin \Delta}{\sin (\beta_1 + \Delta)}$$

---

* β may be obtained in terms of β_1 as follows:

$$W_1 \cos \beta_1 - U \cos \beta = \frac{\Gamma}{2s}$$

$$W_2 \cos \beta_2 - U \cos \beta = -\frac{\Gamma}{2s}$$

The result of adding these two equations is $W_1 \cos \beta_1 + W_2 \cos \beta_2 = 2U \cos \beta$

or

$$W_1 (\cos \beta_1 + \sin \beta_1 \cot \beta_2) = 2W_1 \sin \beta_1 \cot \beta$$

hence,

$$\cot \beta = 1/2(\cot \beta_1 + \cot \beta_2) = 1/2 [\cot \beta_1 + \cot (\beta_1 + \Delta)]$$

also

$$\sin \beta = \frac{\sin \beta_1}{\sqrt{1 - K \cos \beta_1 + \frac{K^2}{4}}}$$

where

$$K = \frac{\sin \Delta}{\sin (\beta_1 + \Delta)}$$

In connection with the preceding Eqs. (A-1) and (A-2) and Fig. 3b, it is interesting to observe the following points:

(a) If $\beta = 90^\circ$, then $\beta_1 = 90^\circ - \frac{\Delta}{2}$ and $\frac{W_2}{W_1} = 1$. This system produces a deflection Δ in a uniform stream without changing the velocity of flow. It is applicable to flow in an ordinary miter bend in a duct of constant cross section. This is the case considered in this paper.

(b) If $\beta < 90^\circ$, then $\frac{W_2}{W_1} < 1$. This system produces a deflection Δ in a uniform stream and retards the velocity. It is applicable to flow in a miter bend in a duct with an expansion at the corner. It is also applicable to pump rotors or propellers where the velocity U may be considered as the resultant of the axial flow and tangential velocity at a cylindrical section of the rotor. (Figure 3b is readily reducible to the deflection triangles of axial pump theory.)

(c) If $\beta > 90^\circ$, then $\frac{W_2}{W_1} > 1$. This system produces a deflection Δ in a uniform stream and accelerates the velocity. It is applicable to flow in a miter bend in a duct with a contraction. It is also applicable to turbine runners.

If it is desired to provide for a turn with a given deflection and given ratio $\frac{W_1}{W_2}$, then

$$\tan \beta_1 = \frac{\sin \Delta}{W_1/W_2 - \cos \Delta} \qquad \text{(A-3)}$$

Equation (A-3) locates the vortex axis (and cascade axis) with respect to the approaching flow direction. The circulation required of uniformly spaced vortexes in order to produce this turn becomes

$$\Gamma = sW_1 \frac{\sin \Delta}{\sin (\beta_1 + \Delta)} = KsW_1 \qquad \text{(A-4)}$$

When $\frac{W_1}{W_2} = 1$ ($\beta = 90^\circ$), Eq. (A-4) reduces to Eq. (3). If s is reduced, Γ is reduced and the turn is made in a shorter distance with less disturbance. If two neutral corresponding streamlines are chosen for frictionless lateral boundaries, the flow may be confined (Fig. 3b). Using guide vanes to produce

the circulation, the reaction on each vane is found by the Kutta-Joukowski theorem:

$$R = \rho \Gamma U = 2\, sK\sqrt{1 - K \cos \beta_1 + \frac{K^2}{4}}\,\left(\frac{\rho W_1^2}{2}\right) \qquad \text{(A-5)}$$

The reaction must act normally to the direction of U or make an angle of $90^\circ - \beta$ with the vortex axis. (Considering the resistance, however, the reaction must make still another angle with the axis.) Writing C_R in terms of the approach velocity W_1, as before

$$C_R = 2\,\frac{s}{c}\,K\sqrt{1 - K \cos \beta_1 + \frac{K^2}{4}} \qquad \text{(A-6)}$$

Eq. (A-6) reduces to Eq. (2a) when $\beta = 90^\circ$ and $\Delta = 90^\circ$.

APPENDIX II

STRUCTURAL PROPERTIES OF A THIN VANE

If the thin vane profiles are assumed to be composed of circular arcs or of two parabolic arcs as in the NACA four-digit series and to be of uniform thickness throughout, such properties as the location of the centroid and the moment of inertia may be determined from geometry. Considering profiles of parabolic arcs and referring to figure A-1, if the equation for each arc is written,

$$x^2 = ay$$

from $x = 0$ to $x = b$, and $2b/a = d$, then the length of each arc is,

$$s = a/2 \left[d/2\sqrt{d^2 + 1} + 1/2 \ln (d + \sqrt{d^2 + 1}) \right]$$

The centroid of each arc is given by

$$\bar{x} = \frac{a^2}{12s} \left[(d^2 + 1)^{3/2} - 1 \right]$$

$$\bar{y} = \frac{a}{16} \left[\frac{b}{s} (d^2 + 1)^{3/2} - 1 \right]$$

The moments and products of inertia for each arc are:

$$Iyy = \frac{a^3 t}{64} \left[d (2d^2 + 1) \sqrt{d^2 + 1} - \ln (d + \sqrt{d^2 + 1}) \right]$$

$$Ixx = \frac{a^3 t}{1536} \left[(8d^4 + 2d^2 - 3) d\sqrt{d^2 + 1} + 3 \ln (d + \sqrt{d^2 + 1}) \right]$$

$$Ixy = \frac{a^3 t}{120} \left[(d^2 + 1)^{3/2} (3/2 d^2 - 1) + 1 \right]$$

For the entire profile, the centroid is given by

$$\bar{Y} = \frac{s_1 \bar{y}_1 + s_2 \bar{y}_2}{s_1 + s_2} \qquad \bar{X} = \frac{s_1 \bar{x}_1 - s_2 \bar{x}_2}{s_1 + s_2}$$

and the moments and products of inertia are

$$I_{\bar{X}\bar{X}} = Ixx_1 + Ixx_2 - st \bar{Y}^2$$

$$I_{\bar{Y}\bar{Y}} = Iyy_1 + Iyy_2 - st \bar{X}^2$$

$$I_{\bar{X}\bar{Y}} = Ixy_1 + Ixy_2 - st \bar{X}\bar{Y}$$

The spanwise moment on the vanes may be determined from the reaction which is known from Eq. (2b), assuming uniform loading along the span. For a

90° turn the moments are,

$$\text{for hinged ends: } M_H = \frac{s\ell^2}{4} \quad \frac{\rho W_1^2}{2}$$

$$\text{and for fixed ends: } M_F = \frac{s\ell^2}{6} \quad \frac{\rho W_1^2}{2}$$

The moment plane may be assumed to have the direction of the miter plane of the bend; hence, it makes an angle θ with the vane chord or an angle $\psi = 180^{\circ} - \theta$ with the positive direction of the x-axis. The moment plane does not pass through the center of gravity of the usual thin vane profile, but it is actually about 10 per cent ahead of the center of gravity. Assuming, however, that it does pass through the center of gravity, the maximum flexural stress is given by

$$f_s = \frac{M}{B}$$

where $B = -\dfrac{I_{\bar{X}\bar{X}} \cdot I_{\bar{Y}\bar{Y}} - I_{\bar{X}\bar{Y}}}{y\,(I_{\bar{y}\bar{y}} \sin\psi - I_{\bar{X}\bar{Y}} \cos\psi) + x\,(I_{\bar{X}\bar{X}} \cos\psi - I_{\bar{X}\bar{Y}} \sin\psi)}$

and $\underline{x}$ and $\underline{y}$ are the coordinates of the point where the maximum stress occurs.

As an example, consider the (21)300 vane used in these experiments with c = 2.83 in., t = 0.05 in., s/c = 0.5, $\theta = 105^{\circ}$, $\ell = 2$ ft and with water flowing at 20 ft per sec

$$a_1 = (0.7)^2/0.21\ c = {}^{7c}/_{3};\ a_2 = (0.3)^2/0.21\ c = {}^{3c}/_{7};$$

$$b_1 = 0.7c,\ b_2 = 0.3c;\ d_1 = 1.4,\ d_2 = 0.6;$$

$$s_1 = 0.742c,\ s_2 = 0.380c;\ \bar{x}_1 = 0.360c,\ \bar{x}_2 = 0.165c;$$

$$\bar{y}_1 = 0.073c,\ \bar{y}_2 = 0.081c;\ \bar{x} = 0.182c,\ \bar{y} = 0.076c;$$

$$Iyy_1 = 0.1256c^3t,\ Iyy_2 = 0.0132c^3t,\ Ixx_1 = 0.00695c^3t,$$

$$Ixx_2 = 0.00409c^3t,\ Ixy_1 = +\,0.02845c^3t,\ Ixy_2 = -\,0.00714c^3t;$$

$$I_{\bar{Y}\bar{Y}} = 0.101c^3t,\ I_{\bar{X}\bar{X}} = 0.0045c^3t,\ I_{\bar{X}\bar{Y}} = +\,0.00578c^3t$$

$$B = \frac{0.0455c^3t - 0.578}{9.54y - 0.431x}$$

The maximum stress occurs at the leading edge for hinged ends and is

$$f_s = \frac{0.5c\ell^2\ \rho W_1^2}{8} \Big/ \frac{0.0455c^3t - 0.578}{9.54 \cdot 0.21c + 0.431 \cdot 0.3c} =$$

$$\frac{0.133\ell^2\ \rho W_1^2}{0.0455c - 0.578/c^2} = 6280 \text{ lb per sq in.}$$

Considering that the plane of the moment is somewhat forward of the centroid of the profile, the maximum stress would be less than given above. If the vane reaction does not act along the miter line so that ψ approaches 90°, the stress is larger than that given. If vibrations take place, the peak stresses are larger, of course.

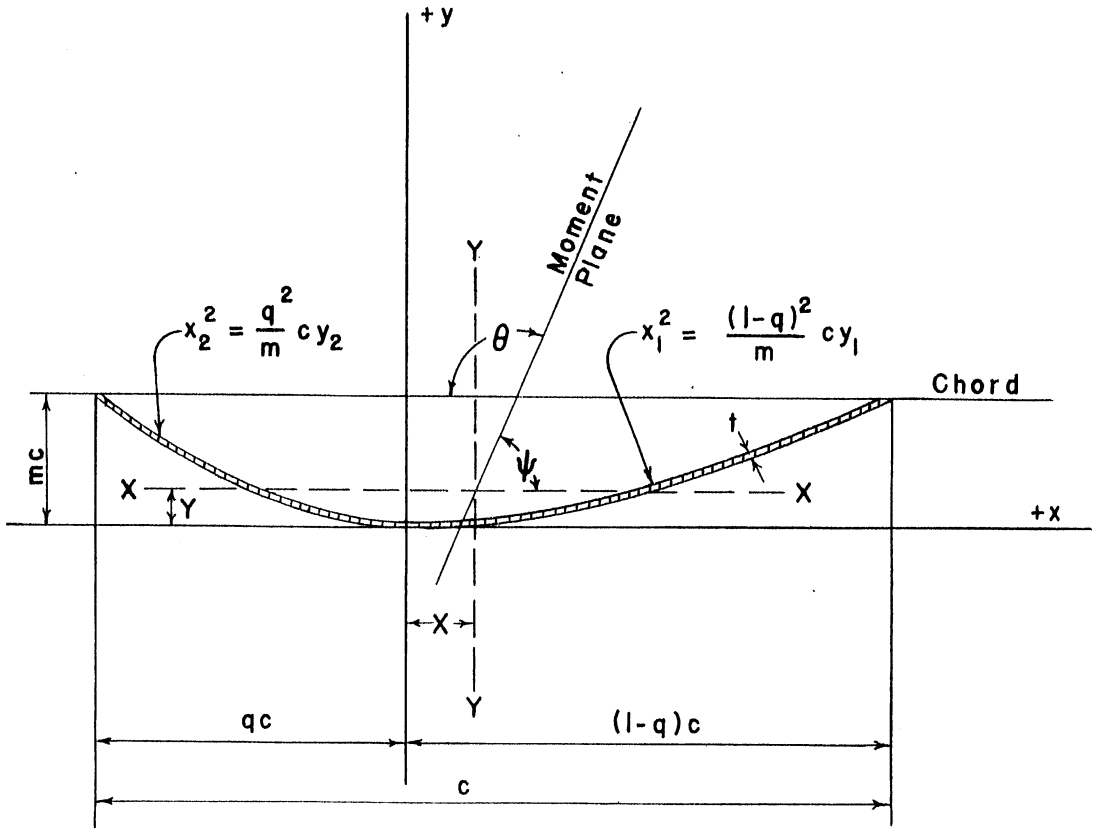

FIG. A-1

GEOMETRY OF A PARABOLIC VANE